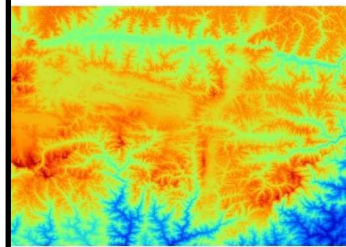


**Tectonic evolution of the Tethyan Himalaya in SE Tibet
deduced from magnetic fabric, structural,
metamorphic and paleomagnetic data**



Dissertation
zum Erlangen des Grades eines Doktors der Naturwissenschaften

der Geowissenschaftlichen Fakultät
der Eberhard Karls Universität Tübingen

**vorgelegt von
Borja Antolín Tomas
aus Zaragoza**

2010

Tag der mündlichen Prüfung: 21. 05. 2010
Dekan: Prof. Dr. Peter Grathwohl
1. Berichterstatter: Prof. Dr. Erwin Appel
2. Berichterstatter: Prof. Dr. Lothar Ratschbacher

(Kalung Massif)

Declaration of Kathmandu

- 1- *There is an urgent need for effective protection of the mountain environment and landscape.*
- 2- *The flora, fauna and natural resources of all kinds need immediate attention care and concern.*
- 3- *Actions designed to reduce the negative impact of man's activities on mountains should be encouraged.*
- 4- *The cultural heritage and the dignity of the local population are inviolable.*
- 5- *All activities designed to restore and rehabilitate the mountain world need to be encouraged.*
- 6- *Contacts between mountaineers of different regions and countries should be increasingly encouraged in the spirit of friendship, mutual respect and peace.*
- 7- *Information and education for improving the relationship between man and his environment should be available for wider and wider sections of society.*
- 8- *The use of appropriate technology for energy needs and the proper disposal of waste in the mountain areas matters of immediate concern.*
- 9- *The need for more international support- governmental as well as non-governmental to the developing mountain countries, for instance, in matters of ecological conservation.*
- 10- *The need for widening access to mountain areas in order to promote their appreciation and study should be unfettered by political considerations*

U. S. A. A. 1982

In between this study (2007) was the 25th anniversary of the Declaration of Kathmandu

Abstract

A multidisciplinary approach was carried out to elucidate the kinematic and metamorphic evolution of the Tethyan Himalayan sequence in SE-Tibet in order to contribute to the understanding of continental collision orogens as the Himalaya. Phyllosilicates preferred orientation interpreted from magnetic fabric studies, structural-field data, illite crystallinity, vitrinite reflectance and K/Ar dating were analyzed to characterize the deformation and metamorphic phases of the Triassic flysch sequence in the eastern Tethyan Himalaya. The second part of the thesis utilizes a paleomagnetic approach to determine the Miocene vertical-axis block rotation pattern in SE-Tibet and kinematic implications for the Himalayan Belt and southeastern Tibetan Plateau evolution. Additionally the paleomagnetic study was extended to the southern most area of the Tethyan Himalayan sequence within the Lingshi klippe in NW Bhutan.

The tectonometamorphic evolution of the Triassic flysch in SE-Tibet can be summarized as follows.

During the D1 phase E-W trending south facing isoclinal folds with related axial planar foliation (S1) developed. South of the locality of Qonggyai (D1 phase domain) the N-S trend and northward plunge of the magnetic lineation is in agreement with thrust emplacement towards the south (Himalayan foreland). The same studied sites indicate diagenetic to low-anchizonal metamorphism. The D1 deformation phase described here took place most probably during Eocene times. During the D2 phase continuation of N-S shortening in the flysch fold-thrust-wedge derived in a change in the fold vergence and magnetic and tectonic foliation dipping. This is generally observed in the northern studied areas east of the Cona Graben. D2 deformation is recorded through south-dipping magnetic foliation, north-vergent F2 folds and related S2 tectonic foliation. A slightly prolate magnetic ellipsoid was found in between the D1 and D2 domains recording the intersection of S1 and the subtle development of the S2 tectonic foliation. Kübler Index and vitrinite reflectance data indicate a wide range of thermal overprint from high anchizone to epizone during the D2 phase. S2 foliation development can be related to the ca. 22 Ma K/Ar ages found in the D2 domain. During the D3 phase backward propagation of the deformation led to the Great Counter backthrust generation, recorded by SSW steeply plunging magnetic lineation parallel with the stretching lineation east of Gyaca in the Great Counter backthrust zone. In the final D4 phase Middle-Late Miocene E-W extension is witnessed by ca. N-S kilometric normal faults of the Cona Graben which cross-cut all the previous structures.

Paleomagnetic analyses from Cretaceous metadykes in SE-Tibet and metasedimentary formations in NW-Bhutan indicate that the main carrier of the characteristic remanence is

pyrrhotite. The pyrrhotite component unblocks between 280-350°C in SE-Tibet and 270-325°C in NW-Bhutan, and shows reverse and normal polarities. It has a ca. constant declination in SE-Tibet through the D1 and D2 folds, and reveals best grouping at 18 % of unfolding in one site in the Lingshi klippe. Early to Middle Miocene thermal overprint of the studied metadykes and metasedimentary formations constrained by K/Ar method is related to the time of remanence acquisition. This event is younger than the D1 and at the end of D2 described in SE-Tibet. In the Lingshi klippe the pyrrhotite mean site directions show a small circle distribution likely related to the last large-scale folding event. A small circle method permits to better unravel the degree of vertical-axis rotation. Pyrrhotite components are ca. 0°, 20° and 37° clockwise rotated with respect to the Early to Middle Miocene references of stable India at the Nagarze, Qonggyai and Lingshi study areas, respectively. The rotation is related to Middle-Late Miocene strain partitioned between near-field E-W extension (with unclear influence of reactivation of older structures as strike-slip faults) and far-field eastward motion/extrusion of the Tibetan Plateau crust.

Zusammenfassung

Eine multidisziplinäre Untersuchung zur kinematischen und metamorphen Entwicklung der Tethyan Himalaya Abfolge in Süd-Ost Tibet wurde durchgeführt, um das Verständnis von Kollisionsgebirgen wie dem Himalaya zu erweitern. Die bevorzugte Orientierung von Phyllosilikaten abgeleitet von Untersuchungen der AMS, (anisotropy of magnetic susceptibility), Strukturdaten aus dem Gelände, die Kristallinität von Illiten, die Vitrinit-Reflektanz und K/Ar Datierungen wurden analysiert, um die Deformations- und metamorphe Phasen der triassischen Flysch-Abfolge im östlichen Tethyan Himalaya zu untersuchen. Der zweite Teil der vorliegenden Arbeit beinhaltet eine paläomagnetische Studie, die Aufschluss über Miozäne Blockrotationen um vertikale Achsen in Süd-Ost Tibet gibt, sowie über kinematische Auswirkungen auf die Entwicklung des Himalayas und des südöstlichen Tibetischen Plateaus. Desweiteren wurde die paläomagnetischen Untersuchungen bis zum südlichsten Bereich der Tethyan Himalaya Abfolge innerhalb der Lingshi Klippe in Nord-West Buthan ausgeweitet.

Die tektono – metamorphe Evolution des triassischen Flysches in Süd-Ost Tibet kann wie folgt zusammengefasst werden:

Während der D1-Phase entwickelten sich Ost-West verlaufende, sich nach Süden verjüngende, isoklinale Falten, sowie eine mit diesen in Bezug stehende Achsenebenenschieferung (axial plane cleavage). Südlich der Lokalität von Qonggyai (Bereich der D1-Phase) stimmen der Nord-Süd Verlauf und das nördliche Einfallen der magnetischen Lineationen mit dem Störungsversatz nach Süden (Vorland des Himalayas) überein. Die untersuchten Gebiete deuten auf eine diagenetische bis niedrig-anchizonale Metamorphose hin. Die hier beschriebene D1-Deformationsphase vollzog sich höchstwahrscheinlich während des Eozäns. Während der D2-Phase führte die Fortsetzung der Nord-Süd Verkürzung im Faltungs- und Störungsgürtel des Flysches zu einer Änderung der Falten-Vergenz und des Einfallens der magnetischen und tektonischen Foliation. Dies wurde im Allgemeinen in den nördlichen Untersuchungsgebieten östlich des Cona Grabens beobachtet. Die D2-Verformungsphase ist durch eine südlich einfallende magnetische Foliation, sowie nord-vergente F2 Falten und die damit zusammenhängende tektonische Foliation manifestiert. Ein geringfügig prolates, magnetisches Ellipsoid wurde zwischen den Bereichen der D1 und D2 Deformation bestimmt, welches die Überschneidung der S1 Foliation und der sich schleichend entwickelnden S2 Foliation darstellt. Der Kübler Index und die Reflektanz des Vitrinites deuten auf einen weiten Bereich an thermischen Überprägungen innerhalb der D2 Phase hin, der von der hochmetamorphen Anchizone bis zur unteren Epizone reicht. Die Entstehung der S2 Foliation kann mit den ca. 22 Ma K/Ar Altern, die im D2 Bereich

bestimmt wurden, verknüpft werden. Die rückwärtige Ausdehnung der Deformation während der D3-Phase führte zur Entstehung der Great Counter Backthrust, erkennbar an der steil nach SSW einfallenden magnetischen Lineation parallel zur Dehnungslineation östlich von Gyaca innerhalb der Great Counter Backthrust Zone. Die Mittel-Spät Miozäne Ausdehnung während der abschließenden D4-Phase wird durch ungefähr Nord-Süd verlaufende kilometerlange Abschiebungen des Cona Grabens angezeigt, welche alle vorherigen Strukturen durchschneiden.

Paläomagnetische Untersuchungen an den kretazischen meta-Gängen in Süd-Ost Tibet und meta-sedimentären Formationen in Nord-West Bhutan weisen darauf hin, dass der Hauptträger der Remanenz Pyrrhotite ist. Die Pyrrhotit Komponente entblockt zwischen 280 und 350 °C in Süd-Ost Tibet und zwischen 270 und 325°C in Nord-West Bhutan und zeigt reverse und normale Polaritäten. Sie hat eine ungefähr konstante Deklination in Süd-Ost Tibet entlang der D1 und D2 Falten und zeigt die beste Gruppierung bei 18 % Entfaltung innerhalb eines Gebietes der Lingshi Klippe. Früh bis Mittel Miozäne thermische Überprägungen der untersuchten meta-Gänge und meta-sedimentären Formationen wurden durch die K/Ar Datierungsmethoden eingegrenzt und stehen mit der Zeit des Remanenzserwerbs in Zusammenhang. Dieses Ereignis ist jünger als die D1-Phase und wird in Süd-Ost Tibet am Ende der D2-Phase angesiedelt. In der Lingshi Klippe zeigen die Mittelwerte der Pyrrhotit Richtungen, des untersuchten Gebietes eine Kleinkreisverteilung, welche wahrscheinlich mit dem letzten großräumigen Faltungsereignis verknüpft ist. Die Kleinkreis Methode ist besser geeignet, um den Grad der vertikalen Achsenrotation zu bestimmen. Die Pyrrhotit Komponenten sind um ungefähr 0°, 20° und 37° im Uhrzeigersinn rotiert im Bezug auf Früh bis Mittel Miozäne Referenzen von Indien bezüglich den Untersuchungsgebieten in Nagarze, Qonggyai und Lingshi. Die Rotation wird Mittel bis Spät Miozänen Deformationen zugeschrieben, aufgeteilt in lokale Ost-West Ausdehnung (mit unbekanntem Einfluss von Reaktivierungen älterer Strukturen, wie Blattverschiebungen) und regionale ostwärts Bewegung/Extrusion der Kruste des Tibetischen Plateaus.

Thesis Organization and Publications

The thesis is divided into 6 chapters. The first is an introduction which covers the goals and study framework. Chapters 2 to 5 represent four research articles, which have been published or submitted to international journals as is indicated below. Chapter 6 gives conclusions and open research questions.

List of Publications

1. Kinematic evolution of the eastern Tethyan Himalaya: Constraints from magnetic fabric and structural properties of the Triassic flysch in SE Tibet.

Antolín, B., Appel, A., Montomoli, C., Dunkl, I., Ding, L., Gloaguen, R., El Bay, R. In: J. Poblet and R. Lisle, Editors, Kinematic Evolution and Structural Styles of Fold-and-Thrust Belts. **Geological Society of London Special Publications**. (Accepted 19-11-2009)

2. Metamorphic evolution of the Tethyan Himalayan flysch in SE Tibet.

Dunkl, I., **Antolín, B.**, Wemmer, K., Rantitsch, G., Kienast, M., Montomoli, C., Ding, L., Carosi, R., Appel, E., El Bay, R., Xu, Q. and von Eynatten, H., Submitted. In: R. Gloaguen and L. Ratschbacher, Editors, Growth and Collapse of the Tibetan Plateau. **Geological Society of London Special Publications**. (In review)

3. Paleomagnetic evidence for clockwise rotation and tilting in the eastern Tethyan Himalaya (SE Tibet): Implications for the Miocene tectonic evolution of the NE Himalaya.

Antolín, B., Appel, E., Gloaguen, R., Dunkl, I., Ding, L., Montomoli, C., Liebke, U., Xu, Q. **Tectonophysics**. (In review)

4. Late orogenic deformation in the Lingshi klippe (NW Bhutan) deduced from paleomagnetic data: Consequences for extension and clockwise rotation in the eastern Himalaya

Antolín, B., Schill, E., Grujic, D., Baule, S., Quidelleur, X., Appel, E. (To be submitted).

Other publication during the PhD period

5. Indication for clockwise rotation in the Siang window south of the eastern Himalayan syntaxis and new geochronological constraints for the area.

Liebke, U., **Antolín, A.**, Appel, E., Basavaiah, N., Mikes, T., Dunkl, I., Wemmer, K. In: R. Gloaguen and L. Ratschbacher, Editors, Growth and Collapse of the Tibetan Plateau. **Geological Society of London Special Publications**. (Accepted 3-3-2010)

Own contribution to the joint publications

This thesis and the publications (see % exposed below) presented here are my own work. My supervisor, E. Appel provided scientific direction, rigorous discussion, and editorial guidance on publications 1-2-3-4. C. Montomoli provided key ideas and discussion on the structural setting in publications 1-2-3. I. Dunkl is co-author in manuscripts 1-3-4 for which he supplied discussion on the metamorphic aspects. Publication 2 is co-authored by me; I contributed to the study through laboratory work, writing, scientific discussion, artworks and plots. Manuscript 3 is co-authored by R. Gloaguen who contributed with neotectonic analyses. E. Schill and S. Baule provided me paleomagnetic data and rich comments to write publication 4. This publication is additionally co-authored by D. Grujic who provided fission track analyses and discussion on the regional setting. X. Quidelleur provided K/Ar data in publication 4.

Publication 1

Ideas: Antolín/Appel/ Montomoli

Data: 100%

Analyses: 90%

Elaboration: 95%

Publication 2

Ideas: Dunkl/Antolín/co-authors

Data: 10%

Analyses: 10%

Elaboration: 35%

Publication 3

Ideas: Antolín/Appel

Data: 90%

Analyses: 90%

Elaboration: 90%

Publication 4

Ideas: Antolín/Schill-Baule/co-authors

Data: 10%

Analyses: 10%

Elaboration: 70%

Acknowledgements

I would like to express my thanks to my academic supervisor Prof. Dr. Erwin Appel for give me this great thesis topic, revision of the ideas and manuscripts. Also thanks a lot for the opportunity to broaden my horizon at the Himalaya-Karakoram-Tibet conferences where I was able to participate and I meet people from all over the world.

Additional supervision came from Chiara Montomoli and Istvan Dunkl for the review of the publications and great cooperation during and after field work and advices, thank you very much!

The PhD project was found by Deutsche Forschungsgemeinschaft (DFG).

Great thanks go to Ding Lin for the organization of sample campaigns. Sincere thanks go to Tibetans and Chinese who helped us in SE Tibet, cooking, driving and laughing; especially to TaWa and Xu Qiang.

I am grateful to all the members of the Tuebingen geophysical working group especially to: Moti Lal Rijal for introduction in the German life style, rock magnetism advice and Sunday-momos, Dhanyavaad!

Ursina Liebke for the help during field work in 2008 in the Qonggyai valley and in the Dala granite, and for the translation of the thesis abstract into German. Vielen danke.

Zanist, Gobinda, Liu, Peter and Lorena who helped me in the magnetic measurements.

I am deeply grateful to Eva Schill and Stephanie Baule for providing me the data to write Chapter 5.

I want to give thanks to Belen Oliva and Rodolfo Carosi for scientific motivation.

Thanks to the members of the Department of Sedimentology & Environmental Geology at the University of Göttingen, Tectonophysics-Remote Sensing group at Freiberg Technical University and the Geologia-Geologia Strutturale Gruppo at the University of Pisa for the good time spent there.

I would also like to thank, Teresa Román, Antonio Casas and the people of the Structural Geology-Geophysics Department in Zaragoza University, who introduced me into the science world.

Then I am very grateful to my family and friends in Spain, who gave me always moral support, queso y jamon.

Muchas Gracias a Susana, David, Teresa, Ana, Leire, Adrian y Jesus por el apoyo brindado.

This thesis may have not been finished if I did not found very special friends in Germany “Los Tubingueros” (Tania, Caco, Ju, Giani, Juan, Ainara, Jule, Jens, Roman, Beke,...), Adi and the Juggling Club of Tuebingen, und Die Botanischer Garten.

Special thanks to Jana, who gave me lot of energy to finish the thesis during the last year.

Finally and most important I am happy to said Muchas Gracias to the two persons who insert in me this mountain addiction since I was one year old until now to go up of the Pirineos Mountains, and for all the help. They are my parents Cuca and Juan, and my brother Jorge.

Muchas Gracias a tod@s!

Table of Contents

Abstract/ Zusammenfassung	I
Thesis organization and Publications	V
Own contribution to the joint publications	VI
Acknowledgements	VII
Chapter 1: Introduction	1
1.1 Himalayan Setting	2
1.2 Previous paleomagnetic studies in the Tethyan Himalaya	4
1.3 Study area and field work	6
1.4 Thesis framework	8
Chapter 2: Kinematic evolution of the eastern Tethyan Himalaya: Constraints from magnetic fabric and structural properties of the Triassic flysch in SE Tibet	14
2.1 Abstract	14
2.2 Introduction	15
2.3 Major Himalayan tectonic elements	16
2.4 The Tethyan Himalayan Sequence, deformation and metamorphism	17
2.5 Study area: the Triassic flysch of the eastern Tethyan Himalaya	19
2.6 Structural and metamorphic data	22
2.7 AMS analysis	25
2.7.1 Magnetic mineralogy and carriers of the magnetic fabric	26
2.7.2 AMS ellipsoid: The corrected degree of anisotropy and shape parameters	30
2.7.3 Different shapes of AMS ellipsoids, definition of magnetic foliation and lineation	31
2.8 Magnetic foliation and lineation in the Triassic flysch of SE Tibet	32
2.9 Tectonic interpretation and sequence of magnetic fabric development	36
2.10 Conclusions	39

Chapter 3: Metamorphic evolution of the Tethyan Himalayan flysch in SE Tibet	45
3.1 Abstract	45
3.2 Introduction	46
3.3 Geological Setting	47
3.3.1 The Tethyan Himalayan Sequence	48
3.3.2 Mafic magmatism	48
3.3.3 Structural setting of the Tethyan Himalaya	49
3.4 Samples	50
3.5 Methods	53
3.5.1 Kübler index ('illite crystallinity')	53
3.5.2 Vitrinite reflectance	53
3.5.3 Thermobarometry	54
3.5.4 K-Ar geochronology	55
3.5.5 Zircon (U-Th)/He thermochronology	55
3.6 Results	55
3.6.1 Sheet-silicate mineralogy and Kübler index values	55
3.6.2 K-Ar ages	61
3.6.3 Vitrinite reflectance	61
3.6.4 Metamorphic pT conditions determined by Thermocalc and Perplex methods	62
3.6.5 Zircon (U-Th)/He ages	64
3.7 Discussion	66
3.7.1 Conditions and age of metamorphism of basic dykes	66
3.7.2 Low-grade metamorphism of metapelitic samples	67
3.7.3 Estimation of the maximum metamorphic temperature of metapelites by organic maturation	69
3.7.4 Greenschist-facies metamorphism at the base of THS	69
3.7.5 Post-sedimentary evolution of the Tethyan flysch in SE Tibet	69

3.8 Conclusions	72
Chapter 4: Paleomagnetic evidence for clockwise rotation and tilting in the eastern Tethyan Himalaya (SE Tibet): Implications for the Miocene tectonic evolution of the NE Himalaya	78
4.1 Abstract	78
4.2 Introduction	79
4.3 Geological setting	82
4.3.1 Boundaries and deformation of the Tethyan Himalayan sequence	82
4.3.2 Sampling and lithology of the studied area	82
4.3.3 Tectonic architecture and metamorphism in the Qonggyai valley	84
4.4 Methods	87
4.4.1 Sampling and paleomagnetic laboratory procedure	87
4.4.2 Neotectonic analysis	88
4.5 Paleomagnetic results	88
4.5.1 Magneto-mineralogical characterization	88
4.5.2 Remanence directions	90
4.6 Timing of remanence acquisition and paleomagnetic reference directions	93
4.7 Magnitude of vertical-axis rotation	94
4.8 Structures of last deformation phase and neotectonic markers	96
4.9 Discussion	99
4.9.1 Implications for eastward extrusion in SE Tibet	99
4.9.2 Implications for North Himalayan doming	100
4.10 Conclusions	102
Chapter 5: Late orogenic deformation in the Lingshi klippe (NW Bhutan) deduced from paleomagnetic data: Consequences for extension and clockwise rotation in the eastern Himalaya	107
5.1 Abstract	107

5.2 Introduction	108
5.3 Geological framework	111
5.3.1 Stratigraphy and structural anatomy of the Lingshi klippe	112
5.4 Structural investigations, finite deformation	116
5.5 Methodologies	116
5.5.1 Paleomagnetic sample treatment and analytical procedure	116
5.5.2 ^{40}K - ^{40}Ar and fission-track analytical procedures	117
5.6 Results	118
5.6.1 Magnetic mineralogy and carriers of the remanence	118
5.6.2 Pyrrhotite component: distribution and directions	123
5.6.3 K-Ar and fission-track results	124
5.7 Origin and age of the pyrrhotite component	126
5.8 Miocene clockwise vertical-axis block rotation	127
5.9 Late orogenic folding	130
5.10 Discussion: consequences for eastward extrusion	130
5.11 Conclusions	132
Chapter 6: Conclusions and open research questions	138
6.1 Kinematic and metamorphic evolution of the Tethyan Triassic flysch in SE Tibet	139
6.2 D4 phase and Paleomagnetic block rotation pattern in SE-Tibet and NW-Bhutan	140
6.3 Open research questions	141

1

Introduction

1.1 Himalayan setting

The plate tectonic collision of India into Eurasia resulted in the development of the Himalayan Belt since the Early Tertiary (ca. 55-50 Ma) (e.g., Searle, 1986; Gaetani & Garzanti, 1991; Najman et al., 2005; Liebke et al., submitted). The Himalayan orogen has a WNW-ESE length of ca. 2500 km between the Nanga Parbat (or western) syntaxis and the Namche Barwa (or eastern) syntaxis (Fig. 1a, b).

Consequence of this convergence is the actual asymmetric architecture of the orogen with a main south-vergence. Regionally it is divided into four litho-tectonic units (see details in Chapter 1-2) (Gansser, 1964; Le Fort, 1975; Hodges, 2000; Yin, 2006). These are, from top to bottom and from north to south:

1. The Tethyan Himalayan sequence (THS) is a passive margin sequence deposited on the Indian margin (e.g., Willems et al., 1996). It crops out between the south-dipping Great Counter Thrust (GCT) and the Indus-Yarlung suture zone in the north and the South Tibetan Detachment System in the south. Structurally the THS is located in the highest position within the orogen (Le Fort, 1975; Hodges, 2000).

2. The Greater Himalayan sequence (GHS) crops out between the Main Central Thrust (MCT; Heim and Gansser, 1939; Gansser, 1964) and the set of north-dipping normal faults of the South Tibetan Detachment System (STDS; e.g., Pêcher, 1991; Burchfiel et al., 1992).

3. The Lesser Himalayan Sequence (LHS) in the footwall of the MCT is made up of sediments from Proterozoic to Cambrian reaching the Paleocene age in the more eastern sectors of the belt (Stöcklin, 1980; Valdiya, 1980).

4. The Siwalik molasses in between the Main Boundary Thrust (MBT) and the Main Frontal Thrust (MFT) represent Himalayan foreland basin sediments of Miocene to Pliocene-Pleistocene age (e.g., Gansser, 1964).

The present thesis focuses on the Tethyan Himalayan sequence along two areas exposed in SE-Tibet (29.3°N-28.4°N, 90.1°E-92.8°E) (Chapters 2-3-4; Fig. 1b,c) and in NW-Bhutan (27.9°N-27.5°N, 89.3°E-89.7°E) (Chapter 5; Fig. 1b, c). The study area in NW Bhutan represents the SW continuation of the study area in SE-Tibet.

Since the Indian plate collided with the Eurasian plate three simplified mechanisms have controlled the Himalayan architecture: N-S shortening, exhumation of GHS mid-crustal rocks and E-W extension (e.g., Searle, 1996; Hodges, 2000; Yin and Harrison, 2000; Yin, 2006 for reviews). N-S shortening with associated south-vergent thrusting and folding (described in Chapter 1) dominated the first (or Eohimalayan) phase of deformation and crustal thickening in the Himalaya until Late Oligocene (Hodges, 2000). Afterwards, the second and so called Neohimalayan phase (Early Miocene-Present) was controlled by major south-verging

shortening structures (main Himalayan thrusts, MCT, MBT, MFT) which govern the present architecture of the Himalayan Belt. Additionally, the Neohimalayan phase is characterized by the extrusion of the GHS between the MCT and STDS around 23-17 Ma (Guillot et al., 2003; Godin et al., 2006). The mechanism that explains the extrusion of the GHS (e.g., channel flow model, critical taper theory; e.g., Godin et al., 2006 and references therein; Larson, 2009) has important consequences for the evolution of the Himalayan orogen and is still a major matter of debate. On the other hand the GHS has nearly lost their pre-Miocene metamorphic memory, which makes the THS an interesting unit to investigate the tectonometamorphic history of the Himalayan orogen during the earlier Eocene-Oligocene times. Furthermore, other important structures as isoclinal folds, axial-plane foliation, and the Great Counter Thrust, developed during the Neohimalayan phase in the THS but with a north-vergence opposite to the main Himalayan south-vergence. Such structures, described in Chapter 1, are additionally important to interpret the evolution of the Himalayan Belt.

The last stage in the evolution of the northern Himalaya and the southern Tibetan Plateau is characterized by E-W extension which triggered the development of N-trending kilometric grabens and half-graben structures which are extended from the central Tibetan Plateau until the northern part of the GHS in the High Himalaya. Onset of extension is still a matter of debate and has been dated from 14 Ma to 4 Ma (e.g., Blisniuk et al. 2001; Mahéo et al., 2007). Various mechanisms have been suggested for the initiation of the extension. Two of them are: combination of dextral slip-partitioning and divergent thrusting along the MFT (e.g., Armijo et al., 1989; Tapponnier et al., 2001) or thin-viscous-sheet model of the lithosphere (Houseman and England, 1996). Additionally, the Tibetan domain is governed by south-eastward and eastward movement of crustal material as indicated by GPS velocities observations and Quaternary fault slip rates (Holt et al., 2000; Zhang et al., 2004; Gan et al., 2007).

How these major deformational processes are distributed along time plays a key role for the interpretation and modelling of the uplift of the Himalaya and the Tibetan Plateau. To understand these processes, is it important to constraint how the orogenic system developed in terms of sequences of folds and thrusts (Chapter 2), metamorphic ages (Chapter 3), exhumation of mid-crustal rocks, etc., but also to identify the distribution and amount of vertical-axis block rotations and long-wavelength tiltings and to integrate them into the models of the evolution of the Himalaya-Tibetan Plateau orogen (Chapter 4-5). Paleomagnetic data is essential to restoration of the finite deformation to a pre-deformational stage (e.g., Waldhör, 1999; Pueyo, 2000; Oliva-Urcia and Pueyo, 2007) and is a robust criterion for distinguishing between kinematic types of curved mountains belts (oroclines,

progressive arcs, and primary arcs; Weil and Sussman, 2004). Furthermore, the study area witnessed E-W extension along two major grabens, the Yadong-Gulu Graben (90°E) (Chapter 5) and the Cona Graben (92°E) in SE-Tibet (Chapter 4). These graben structures have associated strike-slip faults north of the Indus-Yarlung suture (e.g., Armijo et al., 1989). To the south, in the Tethyan Himalayan sequence, these strike-slip faults are not recognized with the same clarity as in the north. These environments are propitious to experiment vertical-axis rotation related to motion along the normal faults and strike-slip faults. Even in the absence of strike-slip faults and only derived from an extensional regime vertical-axis rotation has been described before e.g. in the Basin and Range province (east central Idaho) by Janecke et al. (1991). In this way paleomagnetism can be a powerful tool to quantify block rotations.

1.2 Previous paleomagnetic studies in the Tethyan Himalaya

Klootwijk and co-authors published in 1980 some of the first paleomagnetic studies in the Tethyan Himalaya of western Nepal. Afterwards, studies have been succeeded in the western Tethyan Himalaya i.e. eastern flank of the western syntaxis (e.g., Appel et al., 1991; Klootwijk et al., 1994; Patzelt et al., 1996; Schill et al., 2003; Torsvik et al., 2009), and in the Pamirs (e.g., Waldhör et al., 2001), in the Tadjik Basin (e.g., Thomas et al., 1994) and other areas of the hinge zone and western flank of the Nanga Parbat syntaxis (Chapter 5 include a block-rotation-map of selected previous studies). A model for the Himalayan arc curvature was proposed in 1985 (Klootwijk et al., 1985) from paleomagnetic data from 11 studied localities. Notice the localities from the eastern area are located in the Lhasa block, close to the suture. This study proposed a 3-stage model for the Greater India and southern Asia convergence. The 1st stage (Latest Cretaceous/Paleocene to Early Eocene) includes initial continental indentation in the west and progressive eastward suturing. During the 2nd stage (Middle Eocene to Early Miocene) collision was accomplished by eastward extrusion of continental blocks (Tapponnier et al., 1982). Finally the 3rd stage (Late Miocene to present) witnessed intra-continental rotational underthrusting with oroclinal bending since the Late Miocene (Klootwijk et al., 1985). During the nineties formations containing ferrimagnetic pyrrhotite with a stable paleomagnetic behaviour of secondary magnetic remanences were analyzed in the western Himalaya (Appel et al., 1991, 1995). This work continued in western and central Himalaya (e.g., Schill et al., 2001, 2003; Crouzet et al., 2003) providing important constraints for the western syntaxis evolution and surrounding areas. The block rotation pattern in the western syntaxis describes a clockwise rotation in the eastern zone of the syntaxis and counterclockwise rotations in the western part since remanence acquisition after ca. 50 Ma

(e.g., Klootwijk et al., 1985; Appel et al., 1995; Klootwijk et al., 1994; Thomas et al., 1994; Schill et al., 2001; Chapter 5). Further to the east (western to central Nepal) Schill et al. (2004) obtained an increasing trend to clockwise rotations in the Tethyan Himalaya remanence directions from Hidden valley in the west (83.6°E) to Shiar valley in the east (85.1°E), for remanence acquisition ages of $\sim 30\text{-}25\text{ Ma}$ (Fig. 1b). This was interpreted as a result of a large-scale dextral shear zone associated to the eastward extrusion of the Tibetan Plateau (Schill et al., 2004). Further to the east between the Shiar valley and the study area ($86^{\circ}\text{-}89^{\circ}\text{E}$) paleomagnetic studies have been carried out in the e.g. areas of Nyalam, Khumbu, Rongbuk, Dinggye and Yadong (El Bay et al., 2008). Recently a paleomagnetic study focused on the Abor volcanic rocks of the eastern Himalayan area of Arunachal Pradesh (NE India; 95°E), showed clockwise rotated remanence directions likely related to the eastward extrusion of the Tibetan Plateau (Liebke et al., in press). However, detailed analyses on the structure of the area have to be done to verify this hypothesis.

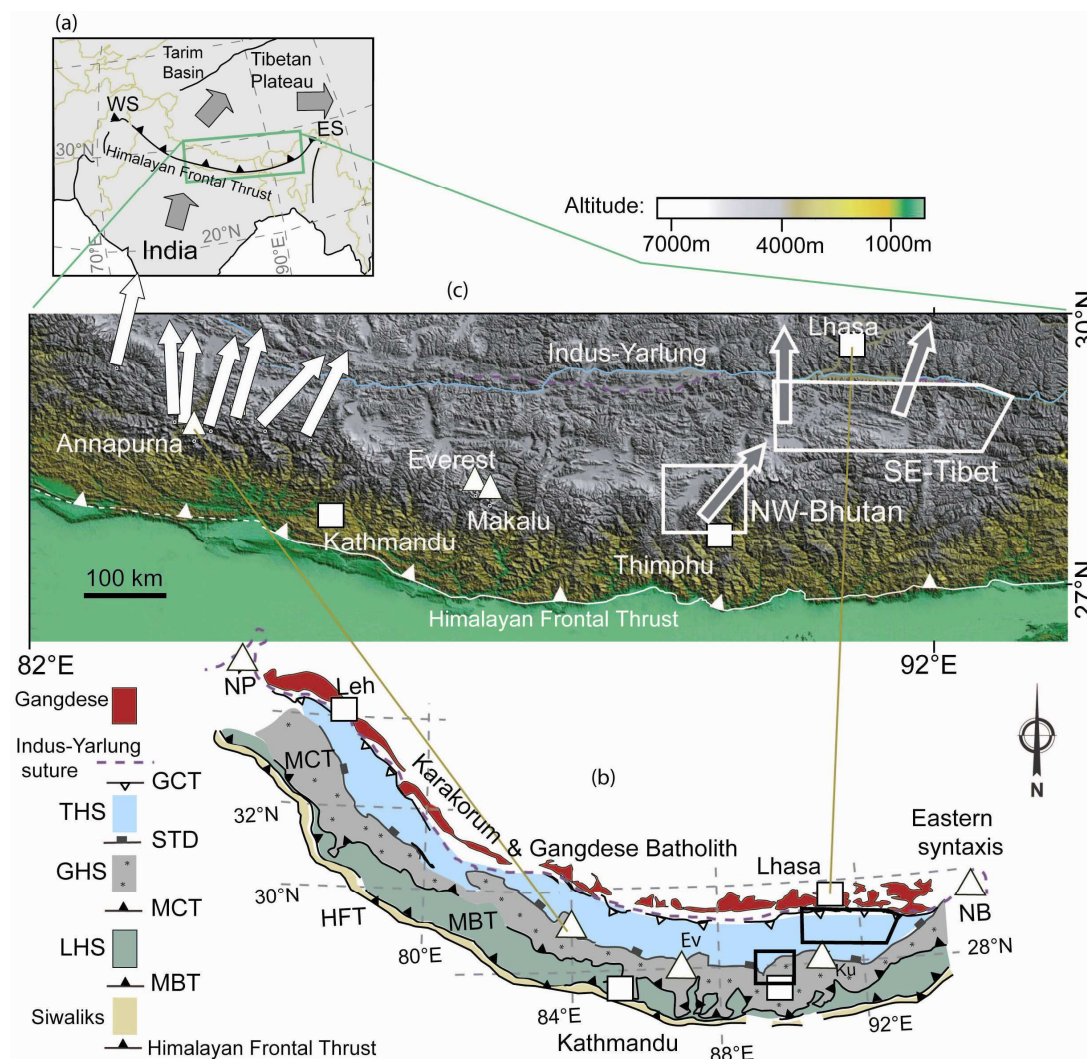


Figure 1: (a) Himalaya-Tibetan Plateau system and surrounding areas with location of the central and eastern Himalaya. Arrows are generalized GPS motions relative to Siberia (Tapponnier et al., 2001).

(b) Simplified geological map of the Himalayan Belt (Gansser, 1964; Yin, 2006). NP, Nanga Parbat; Ev, Everest; Ku, Khula Kangri and NB, Namche Barwa. GCT, Great Counter Thrust; THS, Tethyan Himalayan sequence; STDS, South Tibetan Detachment System, GHS, Greater Himalayan sequence; MCT, Main Central Thrust; LHS, Lesser Himalayan sequence; MBT, Main Boundary Thrust. (c) Digital topography (SRTM data) with published vertical-axis block rotations against stable India (white arrows; Schill et al., 2004 with references, details in Chapters 4 and 5). Grey arrows in SE-Tibet this thesis (Chapter 4) and grey arrow in NW-Bhutan from Baule, 2004 and this thesis (Chapter 5).

1.3 Study area and field work

The thesis study area is located in SE-Tibet with ca. 250 x 50 km (90-93°E/29.2-28.5°N). It is located in the Tethyan Himalaya sequence, also called Tibetan sedimentary sequence (Gansser, 1964). Its structural position within the Himalayan orogen is described in Chapter 2. Geological mapping has been done by Yu and Zheng (1979) at a scale of 1:1,000,000, and the Geological investigation brigade of Shanxi province at 1:200,000 scale (1994). Tectonometamorphic studies in the area have been focus around the suture zone, the Gangdese thrust system and the Zedong window near e.g. Zetang (e.g., Yin et al., 1994; Quidelleur et al., 1997; Aitchison et al., 2000; Harrison et al., 2000; Yin, 2006). They determined the Tertiary structural relation between Gangdese Thrust, Great Counter Thrust and the Indus-Yarlung suture west of the Cona Graben (Fig. 2). Geochemistry studies within the rocks related to the suture zone and northern parts of the Tethyan Himalaya (mélange and Triassic flysch units) were done by e.g. Dupuis et al. (2005, 2006). Attention has been also drawn on the evolution of the Miocene Yala Xiangbo north Himalayan dome (Aikman et al., 2004; Zhang et al., 2005; Aikman, 2007; Fig. 2). The study of the Eocene Dala granitoids (Fig. 2) which have major implications for the initiation of crustal thickening in the Himalaya have been noticed in Aikman et al. (2008). Furthermore petrologic studies have been carried on Cretaceous mafic dykes related to a progressive lithosphere thinning beneath eastern Gondwanaland during early Cretaceous (Zhu et al., 2008; Xu et al., 2009).

This thesis covers the structural and metamorphic evolution of the Triassic flysch area in SE-Tibet (Chapter 2-3) and the paleomagnetic study of SE-Tibet (Chapter 4). Additionally the thesis area has been extended to the south (Lingshi klippe, NW Bhutan) in Chapter 5 through a set of data sampled and preliminary analyzed by Baule (2004).

Three field work campaigns were carried out in SE-Tibet to collect field measurements and samples analyzed in Chapters 2-3-4. First field work, previous to the start of this PhD project, was carried out in 2005 to collect samples for preliminaries studies (first preliminary paleomagnetic analyses were done by R. El Bay). During the second expedition in SE-Tibet (May-June 2007) we reached the most eastern sampling areas (92.85°E; east of Gyaca) and additionally sampled in the working area of 2005 (Yamdrock lake, Puma lake, Qonggyai

valley) (Fig. 2, details in Chapter 2-3-4). Sampling was center on the Triassic flysch and additionally Cretaceous diorite dykes. A third field work in October 2008 was conducted in the Nagarze-Yamdrock lake area, the Dala granitoids and in the Qonggyai valley with collection of Cretaceous diorite dykes samples for paleomagnetism and geochronology. Additionally, 20 sites were sampled for a preliminary magnetic fabric-structural study on the Dala granitoids, and selected samples around the Yala Xiangbo north Himalayan dome for a master thesis carried out at Göttingen University (Kienast, 2009).

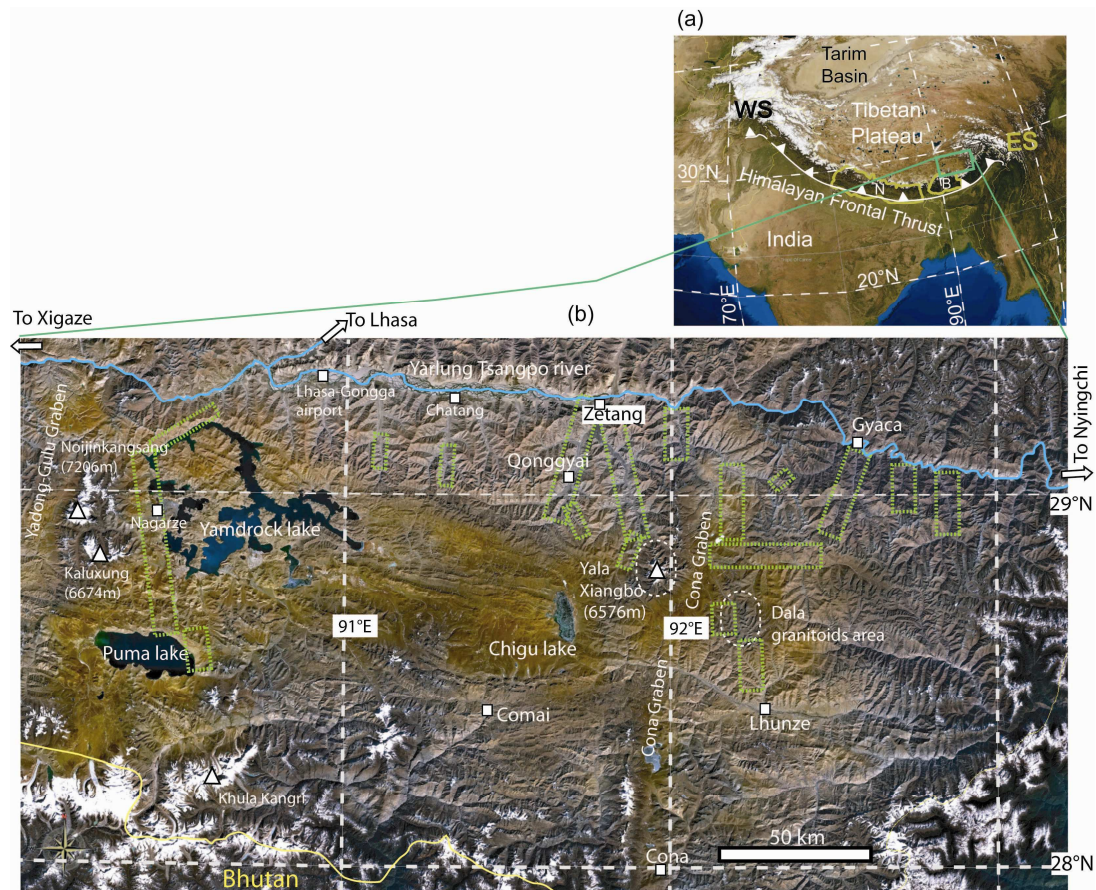


Figure 2: (a) Landsat image of the India-Eurasia collision system with location of SE-Tibet (green box). WS, Western Syntaxis; N, Nepal; B, Bhutan; ES, Eastern Syntaxis. Landsat image (NASA World Wind) of the studied profiles and areas (dashed green boxes) in SE-Tibet during this study.

1.4 Thesis framework

The present study aim to contribute to the understanding of the construction and evolution of continental collision orogens focusing in the Himalayan-Tibetan orogen and by answering three main questions:

- 1) What is the kinematic and metamorphic evolution of the eastern Tethyan Himalayan flysch?
- 2) How is the vertical-axis block rotation pattern in the eastern Tethyan Himalaya?
- 3) Which mechanism has produced the block rotation pattern? Is it oroclinal bending mechanism, eastward extrusion of the Tibetan Plateau or E-W extension?

These questions are stepwise addressed along chapters 2-3-4-5 through geological/paleomagnetic field work, anisotropy of magnetic susceptibility analyses, and paleomagnetic analyses combined with structural, geochronology and thermochronology studies. Methodologies are described in detail within each chapter.

Chapter 2 describes the deformation history of the Triassic flysch in SE-Tibet since Greater India collided with Eurasia (ca. Ypresian) until Late Miocene times. Deformation has been quantified in metapelites, slates and sandstones associated to the Triassic flysch (516 measured samples) through magnetic fabric analyses and structural analyses. Magnetic mineralogy experiments (e.g., thermomagnetic curves, high field vs low field susceptibilities) reveal that the main carriers of the anisotropy magnetic susceptibility (AMS) are phyllosilicates (illites, muscovite and chlorite). In this way we interpreted the geographical distribution of the AMS ellipsoid axes as the phyllosilicates preferred orientation (K_{\min} is ca. the pole of the foliation; e.g., Borradaile and Werner, 1994). Preferred crystallographic orientation of phyllosilicates in sheet-silicate bearing rocks reflects the strain and the degree of reorientation of platy minerals during cleavage formation in these rocks (e.g., Ramsay and Huber, 1983). Finally a 5-stage magnetic fabric evolution is proposed and integrated with the structural data, and compared with other studied areas in the Tethyan Himalaya of western Nepal, central Nepal, and south-central Tibet. However for a complete deformational history it is essential to better constraint the timing of the proposed kinematic phases. This is partially solved along Chapter 3 where the carriers of the magnetic fabric, ca. phyllosilicates (i.e. illites, muscovite and chlorite) fabric, are analyzed in terms of degree of metamorphism and age of cooling. The degree of metamorphism is measured by analyzing the organic matter maturation (vitrinite reflectance) and the “illite crystallinity” of extracted sheet-silicate fraction (< 0.2 μm , < 2 μm and 2-6 μm). The age (K/Ar dating age in < 0.2 μm , < 2 μm and 2-6 μm fractions) of the last cooling of the rocks is obtained by determining the age of cooling of the illites and muscovites below ca. $370^{\circ} \pm 50^{\circ}\text{C}$ (temperature when Ar is

considered immobile in the muscovite crystal-lattice, e.g., Wemmer, 1991; Hames and Bowring, 1994; Lister and Baldwin, 1996). Subsequently these cooling ages can be analyzed with the deformation phases to better constraint the kinematic model described in Chapter 6. In addition Chapters 2 and 3 fulfil important criterions to a correct interpretation of the posteriori studied paleomagnetic remanence and related vectors in SE Tibet (Chapter 4). These criterions (e.g., Van der Voo, 1990) are: a well-determined age of the remanence acquisition (K/Ar age, details below) and a structural control of the study area. Chapter 4 unravel the kinematic significances of the analyzed paleomagnetic data by integrate them with the obtained results from Chapters 2 and 3. Finally a block rotation pattern is described for the Qonggyai valley and Nagarze-Yamdrock lake area. In the same way Chapter 5 quantify the vertical-axis block rotations in the Lingshi klippe (NW-Bhutan) where THS sediments are surrounded by the STDS and the GHS.

Chapter 4 and 5 are interrelated through key points: presence of pyrrhotite as the main carrier of the characteristic remanence and Miocene age of the acquisition of the remanence. Pyrrhotite might be formed under metamorphic conditions by 2 main mechanisms, which depend on the degree of metamorphism. For this reason, a metamorphic control of the studied area is required when dealing with pyrrhotite remanences. First, pyrrhotite is derived from the transformation of pyrite under redox conditions and at temperatures close to the biotite isograd (ca. 400°C; Carpenter, 1974; Crouzet et al., 2003), or above 200°C in presence of carbonate and water (Lambert, 1973). A second mechanism, previously studied in the western Alps, is the production of pyrrhotite from the transformation of magnetite (e.g., Rochette, 1987; Crouzet et al., 2001). As pyrrhotite acquires a thermo-remanence at temperature <325°C, K/Ar dating (cooling down of metamorphic illites through $370^{\circ} \pm 50^{\circ}\text{C}$) is utilized to interpret the age of remanence acquisition. The origin of the pyrrhotite and their remanence in the Cretaceous diorites dykes of SE Tibet and the THS sampled rocks (shale, limestones and slates) in the Lingshi klippe can be assumed to be of thermal origin as peak metamorphic conditions underwent temperatures higher than the Curie temperature of pyrrhotite (ca. 325°C; e.g, Dekkers, 1989). K/Ar dating, structural setting, paleomagnetic fold test and the small circle distribution of the mean site directions of the pyrrhotite remanence indicate that the remanence acquisition occurred in Early to Middle Miocene times after or synchronous with the last deformation phase (Neohimalayan; Hodges, 2000). In NW Bhutan the remanence directions have been tilted after remanence acquisition due to a major long-wavelength folding event, as indicated by a small circle distribution of the mean site paleomagnetic directions. Chapter 5 utilizes Bingham statistics (1974) and a small circle

approach (e.g., Waldhör, 1999; Schill et al., 2001) to determine the block rotation prior to the last folding event.

Finally a block rotation pattern is determined for the Nagarze-Yamdrock lake area and Qonggyai valley for a remanence age of ca. 22 Ma (Chapter 4) and for the Lingshi klippe for a remanence acquisition at ca. 13 Ma (Chapter 5) (Fig. 1c). These chapters include the already published paleomagnetic results from the Himalaya in the western and central part. In addition Chapter 4 includes remote sensing analyses.

The last chapter presents the thesis summary with a linked view of the obtained results and some ideas for further investigations.

References

- Aikman, A., Harrison, T.M., Lin, D., 2004. Preliminary results from the Yala-Xiangbo Leucogranite dome, SE Tibet. 19th Himalaya-Karakoram-Tibet workshop extended abstracts. *Himalayan J. Sci.* 2, 91.
- Aikman, A.B., 2007. Tectonics of the eastern Tethyan Himalaya. PhD Thesis, The Australian National University.
- Aikman, A., Harrison, T.M., Ding, L., 2008. Evidence for Early (>44 Ma) Himalayan Crustal Thickening, Tethyan Himalaya, southeastern Tibet. *Earth Planet. Sci. Lett.* 274, 14-23.
- Aitchison, J.C., Badengzhu, Davis, A.M., Liu, J., Luo, H., Malpas, J., McDermid, I.M.C., Wu, H., Ziabrev, S., Zhou, M.F., 2000. Remnants of a Cretaceous intra-oceanic subduction system within the Yarlung-Zangbo suture (southern Tibet). *Earth Planet. Sci. Lett.* 183, 231–244.
- Appel, E., Miiller, R. and Widder, R.W., 1991. Palaeomagnetic results from the Tibetan Sedimentary Series of the Manang area (north central Nepal). *Geophys. J. Int.*, 104, 255-266.
- Appel, E., Patzelt, A., Chouker, C., 1995. Secondary paleoremanence of Tethyan sediments from the Zaskar Range (NW Himalaya). *Geophys. J. Int.* 122, 227-242.
- Armijo, R., Tapponnier, P., Tonglin, H., 1989. Late Cenozoic Right-Lateral Strike-Slip Faulting in Southern Tibet. *J. Geophys. Res.* 94, 2787-2838.
- Baule, S., 2004. Clockwise rotation and fold axes distribution in the Tethyan Himalaya of Bhutan: constraints from palaeomagnetic remanences and anisotropy of magnetic susceptibility. Master Thesis. Tübingen University.
- Bingham, C., 1974. An antipodally symmetric distribution on the sphere. *Annals of Statistics* 2, 1201-1225.
- Blisniuk, P.M., Hacker, B.R., Glodny, J., Ratschbacher, L., Bi, S., Wu, Z., McWilliams, M.O., Calvert, A., 2001. Extension in central Tibet since at least 13.5 Myr. *Nature* 412, 628-632.
- Burchfiel, B., Zhiliang, C., Hodges, K.V., Yuping, L., Royden, L.H., Changrong, D. Jiene, X., 1992., The South Tibetan detachment system, Himalaya orogen: extension contemporaneous with and parallel to shortening in a collisional mountain belt. *Geol. Soc. Am. Spec. Pap.* 269, 1-41.
- Borradaile, G.J., Werner, T., 1994. Magnetic anisotropy of some phyllosilicates. *Tectonophysics*, 235, 223-248.
- Carpenter, R., 1974. Pyrrhotite isograd in Southeastern Tennessee and Southwestern North Carolina, *Geol. Soc. Am. Bull.* 85, 451-456.
- Crouzet, C., Stang, H., Appel, E., Schill, E., Gautam, P., 2001. Detailed analysis of successive pTRMs carried by pyrrhotite in Himalayan metacarbonates: an example from Hidden Valley Central Nepal. *Geophys. J. Int.* 146, 607-618.
- Crouzet, C., Gautam, P., Schill, E., Appel, E., 2003. Multicomponent magnetization in Western Dolpo (Tethyan Himalaya, Nepal): implications for tectonic motions. *Tectonophysics*. 377, 179–196.
- Dekkers, M.J., 1989. Magnetic properties of natural pyrrhotite. II. High- and low-temperature behaviour of Jrs and TRM as a function of grain size. *Phys. Earth Planet. Inter.* 57, 266–283.

- Dupuis, C., Hébert, R., Dubois-Coté, V., Wang, C.S., Li, Y.L., Li, Z.J., 2005. Petrology and geochemistry of mafic rocks from mélange and flysch units adjacent to the Yarlung Zangbo Suture Zone, southern Tibet. *Chem. Geo.* 214, 287-308.
- Dupuis, C., Hébert, R., Dubois-Coté, V., Guilmette, C., Wang, C.S., Li, Z.J. 2006. Geochemistry of sedimentary rocks from mélange and flysch units south of the Yarlung Zangbo suture zone, southern Tibet. *J. Asian Earth Sci.* 26, 489-508.
- El Bay, R., Appel, E., Carosi, R., Ding, L., Dunkl, I., Gloaguen, R., Montomoli, C., Paudel, L. and Wauschkuhn, B. 2008. Kinematics of the crust in southern Tibet and Higher Himalayan Crystalline –a paleomagnetic approach. 23rd Himalaya-Karakoram-Tibet workshop extended abstracts. *Himalayan J. Sci.* 5, 22.
- Gaetani, M., Garzanti, E., 1991. Multicyclic history of the northern Indian continental margin (northwestern Himalaya). *AAPG Bull.* 75, 1427–1446.
- Gan, W., Zhang, P., Shen, Z-K., Niu, Z., Wang, M., Wan, Y., Zhou, D., Cheng, J., 2007. Present-day crustal motion within the Tibetan Plateau inferred from GPS measurements. *J. Geophys. Res.* 112, B08416.
- Gansser, A., 1964. *Geology of the Himalaya*. Wiley-Interscience, New York. 289 pp.
- Godin, L., Grujic, D., Law, R.D., Searle, M.P., 2006. Channel flow, extrusion and exhumation in continental collision zones: an introduction. In: R.D. Law, M.P. Searle, L. Godin, (Eds.), *Channel Flow, Ductile Extrusion and Exhumation in Continental Collision Zones*. *Geol. Soc. London Spec. Publ.* 268, 1-23.
- Guillot S., Garzanti, G., Baratoux D., Marquer D., Maheo, G., de Sigoyer J., 2003. Reconstructing the total shortening history of the NW Himalaya, *Geochem., Geophys., Geosyst.* 4.
- Hames, W.E., Bowring, S.A., 1994. An empirical evaluation of the argon diffusion geometry in muscovite. *EPSL.* 124, 161–169.
- Harrison, T.M., Yin, A., Grove, M., Lovera, O.M., 2000. The Zedong Window: A record of superposed Tertiary convergence in southeastern Tibet. *J. Geophys. Res.* 105, 19,211-19,320.
- Heim, A., Gansser, A., 1939. Central Himalaya. *Geological Observations of the Swiss Expedition 1936. Mémoires de la Société Helvétique des Sciences Naturelles*, 7/31, 1-245.
- Hodges, K.V., 2000. Tectonics of the Himalaya and southern Tibet from two perspectives. *Geol. Soc. Amer. Bull.* 112, 324-350.
- Holt, W.E., Chamot-Rooke, N., Le Pichon, X., Haines, A.J., Shen-Tu, B., Ren, J., 2000. Velocity field in Asia inferred from Quaternary fault slip rates and Global Positioning System observations. *J. Geophys. Res.* 105, 19185–19209.
- Houseman, G., England, P.C., 1996. A lithospheric thickening model for the Indo-Asian collision, in *Tectonic Evolution of Asia*, In: Yin, A., Harrison, T.M. (Eds.), *Tectonics of Asia*. Rubey Symposium volume. Cambridge University Press. 3-17.
- Janecke, S.U., Geissman, J.W., Bruhn, R.L., 1991, Localized rotation during Paleogene extension in east-central Idaho: paleomagnetic and geologic evidence. *Tectonics.* 10, 403-432.
- Kienast, M., 2009. Master Thesis. Thermochronological and Thermobarometric Investigations in the area of the Yala Xiangbo dome, SE Tibet.
- Klootwijk, C.T., Bingham, D.K., 1980. The extent of Greater India, III. Palaeomagnetic data from the Tibetan Series, Thakkhola region, Nepal Himalaya. *EPSL.* 51, 381-405.
- Klootwijk, C.T., Conaghan, P., Powell, C., 1985. The Himalayan Arc: large-scale continental subduction, oroclinal bending and back-arc spreading. *EPSL.* 75, 167-183.
- Klootwijk, C.T., Conaghan, P.J., Nazirullah, R., de Jong, K.A., 1994. Further paleomagnetic data from Chitral (Eastern Hindukush): evidence for an early India– Asia contact. *Tectonophysics.* 237, 1 – 25.
- Lambert, I.B., 1973. Post-depositional availability of sulphur and metals and formation of secondary textures and structures in stratiform sedimentary sulfide deposits. *J. Geol. Soc. Aus.* 20, 205-215.
- Larson, K., 2009. The Tectonometamorphic evolution of the Greater Himalayan Sequence as exposed in Central Nepal and adjacent South-Central Tibet. PhD Thesis, Queen’s University, Canada.
- Le Fort, P. 1975. Himalayas, the collided range. Present knowledge of the continental arc. *Am. J. Sci.* 275-A. 1-44.
- Liebke, U., Antolin, A., Appel, E., Basavaiah, N., Mikes, T., Dunkl, I., Wemmer, K., (in press). Indication for clockwise rotation in the Siang window south of the eastern Himalayan syntaxis and new geochronological constraints for the area. In: Gloaguen, R., Ratschbacher, L., (Eds.), *Growth and Collapse of the Tibetan Plateau*. *Geol. Soc. London Spec. Publ.*

- Liebke, U., Appel, E., Neumann, U., Antolin, B., Ding, L., Xu, Q., (submitted). Position of the Lhasa terrane prior to India-Asia collision derived from palaeomagnetic inclinations of 53 Ma old dykes of the Linzhou Basin: constraints on the age of collision and post-collisional shortening within the Tibetan Plateau. *Geophys. J. Int.*
- Lister, G.S., Baldwin, S.L., 1996. Modelling the effect of arbitrary P-T-t histories on argon diffusion in minerals using the MacArgon program for the Apple Macintosh. *Tectonophysics*, 253, 83-109.
- Mahéo, G., Leloup, P.H., Valli, F., Lacassin, R., Arnaud, N., Paquette, J.-L., Fernandez, A., Haibing, L., Farley, K.A., Tapponnier, P., 2007. Post 4 Ma initiation of normal faulting in southern Tibet. Constraints from the Kung Co half graben. *EPSL*. 256, 233-243.
- Najman, Y., Carter, A., Oliver, G., Garzanti, E., 2005. Provenance of Eocene foreland basin sediments, Nepal: Constraints to the timing and diachroneity of early Himalayan orogenesis. *Geology*. 33, 309-312.
- Oliva-Urcia, B., Pueyo, E.L., 2007. Rotational basement kinematics deduced from remagnetized cover rocks (Internal Sierras, southwestern Pyrenees). *Tectonics*. 26, TC4014.
- Pan, G., Ding, J., Yao, D., Wang, L., 2004. Geological map of Qinghai-Xizang (Tibet) Plateau and Adjacent Areas (1:1,500,000). Chengdu Institute of Geology and Mineral Resources, China Geological Survey. Chengdu Cartographic Publishing House.
- Patzelt, A., Li, H., Wang, J., Appel, E., 1996. Paleomagnetism of Cretaceous to Tertiary sediments from southern Tibet: evidence for the extent of the northern margin of India prior to the collision with Eurasia. *Tectonophysics*. 259, 259-284.
- Pêcher, A., 1991. The contact between the higher Himalayan crystalline sediments and the Tibetan sedimentary series: Miocene large-scale dextral shearing. *Tectonics*. 10, 587-598.
- Pueyo, E., 2000. Rotaciones paleomagneticas en sistemas de cabalgamientos. Tipos, causas, significado y aplicaciones (ejemplos de las Sierras Exteriores y Cuenca de Jaca, Pirineo Aragónés). PhD Thesis. University of Zaragoza.
- Quidelleur, X., Grove, M., Lovera, O.M., Harrison, T.M., Yin, A., 1997. Thermal evolution and slip history of the Renbu-Zedong Thrust, southeastern Tibet. *J. Geophys. Res.* 102, 2659-2679.
- Ramsay, J.G., Huber, M.I., 1983. *The Techniques of Modern Structural Geology. Volume 1: Strain Analysis.* Academic Press, London.
- Rochette, P., 1987. Metamorphic control of the magnetic mineralogy of black shales in the Swiss Alps: toward the use of "magnetic isograds". *EPSL*. 84, 1015-1020.
- Schill, E., Appel, E., Zeh, O., Singh, V.K., Gautam, P., 2001. Coupling of late-orogenic tectonics and secondary pyrrhotite remanences: Towards a separation of different rotation processes and quantification of rotational underthrusting in the western Himalayas (N-India). *Tectonophysics*. 337, 1-21.
- Schill, E., Appel, E., Godin, L., Crouzet, C., Gautam, P., Regmi, K., 2003. Record of deformation by secondary magnetic remanences and magnetic anisotropy in the Nar/Phu valley (central Himalaya). *Tectonophysics*. 377, 197-209.
- Schill, E., Appel, E., Crouzet, C., Gautam, P., Wehland, F., Staiger, M., 2004. Oroclinal bending versus regional significant clockwise rotations in the Himalayan arc-Constrains from secondary pyrrhotite remanences. In: Sussman, A.J. and Weil, A.B. (Eds.), *Orogenic Curvature: Integrating Paleomagnetic and Structural Analyses.* Spec. Pap. Geol. Soc. Am. 383, 73-85.
- Searle, M., 1986. Structural evolution and sequence of thrusting in the High Himalayan, Tibetan-Tethys and Indus suture zones of Zaskar and Ladakh, Western Himalaya. *J. Structural Geol.* 8, 923-936.
- Searle, M.P., 1996. Cooling history, Erosion, Exhumation and Kinematics of the Himalaya - Karakoram -Tibet orogenic belt. In: Yin, A., Harrison, T.M. (Eds.), *Tectonics of Asia.* Rubey Symposium volume. Cambridge University Press. 110-137.
- Stöcklin, J. 1980. Geology of Nepal and its regional frame. *J. Geol. Soc. London.*, 137, 1-34.
- Tapponnier, P., Peltzer, G., Le Dain, A.Y., Armijo, R and Cobbold, P., 1982. Propagating extrusion tectonics in Asia: New insights from simple experiments with plasticine. *Geology*. 10, 611-616.
- Tapponnier, P., Zhiqin, X., Roger, F., Meyer, B., Arnaud, N., Wittlinger, G., Jingsui, Y., 2001. Oblique Stepwise Rise and Growth of the Tibet Plateau. *Science*. 294, 1671-1677.
- Taylor, M., Yin, A., Ryerson, J.F., Kapp, P., Ding, L., 2003. Conjugate strike-slip faulting along the Bangong-Nujiang suture zone accommodates coeval east-west extension and north-south shortening in the interior of the Tibetan Plateau. *Tectonics*. 22(4), 1044.

- Thomas, J.C., Chauvin, A., Gapais, D., Cobbold, P.R., Bazhenov, M.L., Perroud, H., Burtman, V.S., 1994. Paleomagnetic evidence for Cenozoic block rotation in the Tadjik depression (Central Asia). *J. Geophys. Res.* 99, 15141– 15160.
- Torsvik, T.H., Paulsen, T.S., Hughes, N.C., Myrow, P.M., Ganerød, M., 2009. The Tethyan Himalaya: palaeogeographical and tectonic constraints from Ordovician palaeomagnetic data. *J. Geol. Soc.* 166-4, 679-687.
- Valdiya, K.S. 1980. *Geology of the Kumaun Lesser Himalaya*. Dehra Dun, Wadia Institute of Himalayan Geology.
- Van der Voo, R.B., 1990. The reliability of paleomagnetic data. *Tectonophysics*. 184, 1– 9.
- Waldhör, M., 1999. The small circle reconstruction in palaeomagnetism and its application to palaeomagnetic data from the Pamirs. PhD Thesis. Tübingen University.
- Waldhör, M., Appel, E., Frisch, W., Patzelt, A., 2001. Paleomagnetic investigation in the Pamirs and its tectonic implications. *J. Asian Earth Sci.* 19, 429-451.
- Weil, A.B., Sussman, A.J., 2004. Classifying curved orogens based on timing relationships between structural development and vertical-axis rotations. In Sussman, A.J., Weil, A.B. (Eds.), *Orogenic Curvature: Integrating Paleomagnetic and Structural Analyses*. *Spec. Pap. Geol. Soc. Am.* 383, 1-15.
- Wemmer, K., 1991. K/Ar-Altersdatierungsmöglichkeiten für retrograde Deformationsprozesse im spröden und duktilen Bereich - Beispiele aus der KTB-Vorbohrung (Oberpfalz) und dem Bereich der Insubrischen Linie (N-Italien). PhD Thesis. Göttinger Arbeiten zur Geologie und Paläontologie, 51.
- Willems, H., Zhou, Z., Zhang, B., Gräfe, K. U., 1996. Stratigraphy of the Upper Cretaceous and Lower Tertiary strata in the Tethyan Himalayas of Tibet (Tingri area, China). *Geol. Rundsch.* 85, 723-754.
- Yin, A., 2006. Cenozoic evolution of the Himalayan Orogen as constrained by along strike variations of structural geometry, exhumation history, and foreland sedimentation. 2006. *Earth-Science Rev.* 76, 1-131.
- Yin, A., Harrison, T.M., Ryerson, F.J., Wenji, C., Kidd, W., Copeland, P. 1994. Tertiary structural evolution of the Gangdese thrust system, southeastern Tibet. *J. Geophys. Res.* 99, 18,175-18,201.
- Yu, Z., Zheng, A., 1979. *Geologic Map of the Lhasa region at a scale of 1:1,000,000*. Geol. Publ. House, Beijing.
- Zhang, P.Z., Shen, Z., Wang, M., Gan, W., Bürgmann, R., Molnar, P., Wang, Q., Niu, Z., Sun, J., Wu, J., Hanrong, S., Xinzhao, Y., 2004. Continuous deformation of the Tibetan Plateau from global positioning system data. *Geology.* 32, 809–812.
- Zhang, B., Zhang, J., Guo, L., Wang, W., 2005. Microstructural and deformational studies on mylonite in the detachment faults of Yalashangbo dome, North Himalayan domes zone. *Prog. Nat. Sci.* 15, 11, 1005-1013.
- Zhu, D., Mo, X., Pan, G., Zhao, Z., Dong, G., Shi, Y., Liao, Z., Wang, L., Zhou, C., 2008. Petrogenesis of the earliest Early Cretaceous mafic rocks from the Cona area of the eastern Tethyan Himalaya in south Tibet: Interaction between the incubating Kerguelen plume and the eastern Greater India lithosphere? *Lithos.* 100, 147-173.
- Xu X., Ding L., Xu Q., Cai F., Zhang Q., Zhang L., Lai Q., 2009. Tectonics implications of the Ultramafic Dykes in Southeastern Tibet. *Chinese J. Geol.* 44, 1012-1024 (in Chinese with English abstract).

World Wide Web references

- Digital topography, SRTM data, is from the Consortium for Spatial Information (CGIAR/CSI): <http://srtm.csi.cgiar.org>
- NASA World Wind, Landsat images: <http://worldwind.arc.nasa.gov/java/>

2

Kinematic evolution of the eastern Tethyan Himalaya: Constraints from magnetic fabric and structural properties of the Triassic flysch in SE Tibet

2.1 Abstract

Anisotropy of magnetic susceptibility (AMS) combined with structural analysis are used in this work with the aim to characterize the tectonic evolution of the Triassic flysch within the eastern Tethyan Himalaya Thrust Belt in SE Tibet. The attitude of the magnetic foliation and lineation are concordant with the planar and linear structures of tectonic origin defined by the preferred orientation of the iron-bearing silicates. Two different tectonic domains can be defined. The southern domain is controlled by the Eohimalayan tectonic foliation (S1) recorded in the magnetic foliation which trends E-W and dips to the north. The northern domain is dominated by the Neohimalayan magnetic foliation with WNW-ESE strike and dips to the south opposite to the vergence of the main structures. A slightly prolate magnetic ellipsoid has been found in between the two domains recording the intersection of S1 and the subtle development of the S2 tectonic foliation. Hinterland propagation of the deformation lead to the Great Counter backthrust generation, pointed out by the SSW steeply plunging magnetic lineation. Furthermore different orientations of magnetic foliation may indicate an Early Miocene $\sim 20^\circ$ clockwise vertical-axis rotation.

2.2 Introduction

The collision of India into Eurasia resulted in large-scale shortening of “Greater India” and the consequent development of the Himalayan chain in the Early Tertiary (*c.* 55-50 Ma) (e.g. Searle 1986; Gaetani & Garzanti 1991; Patzelt *et al.* 1996; Najman *et al.* 2005). The Tibetan Plateau and its bordering orogenic mountain belts like the Himalaya provide one of the best natural laboratories to study continental collision processes. The Himalayan orogen has a length of *c.* 2500 km between the Nanga Parbat and the Namche Barwa peaks. These extreme points are geologically called Western and Eastern Syntaxis respectively (Fig. 1a, b).

The present study is focused in a key area of the eastern Himalayan belt in SE Tibet, close to the Eastern syntaxis, where the structural style changes from frontal collision along the Himalaya to dextral shear between Indian and Asian plates as indicated by GPS observations and Quaternary fault slip rates (Holt *et al.* 1991). Furthermore the study area belongs to the Tethyan Himalaya which represents the carapace to mid-crustal rocks whose exhumation mechanism is under discussion (e.g. Godin *et al.* 2006, Kellett & Godin 2009). To better understand the processes we focus our study in the Triassic flysch of the Tethyan Himalaya in order to obtain better constraints on the kinematic evolution and structural style of folds and thrusts since the India-Asia collision. In the remote area of SE Tibet a very long (*c.* 80 km) and continuous section of Triassic flysch of Tethyan Himalaya crops out perpendicular to the main E-W trend of the belt, where little work has been done until now (Fig. 1b, c).

The present work combines the analysis of anisotropy of magnetic susceptibility (AMS) and structural data. The usefulness of AMS has been widely proved for studying deformation in weakly deformed rocks like mudstones or granites with an incipient deformation (e.g. Borradaile & Tarling 1981; Tarling & Hrouda 1993; Bouchez 1997; Borradaile & Jackson 2004; Román-Berdiel *et al.* 2004). Moreover in deformed rocks, with a dominant paramagnetic signal of the tensor, AMS can be a reliable and fast tool for quantifying the preferred orientation of elongated particles or structural elements or crystallographic alignment of minerals (e.g. Hirt *et al.*, 1988; Averbuch *et al.* 1992; Parés & van der Pluijm 2002; Oliva-Urcia *et al.* 2009). The study of AMS in slightly deformed rocks has been recently emphasized by Burmeister *et al.* (2009) and it seems that it is able to highlight strain distributions more efficiently than measurements techniques of finite strain analyses.

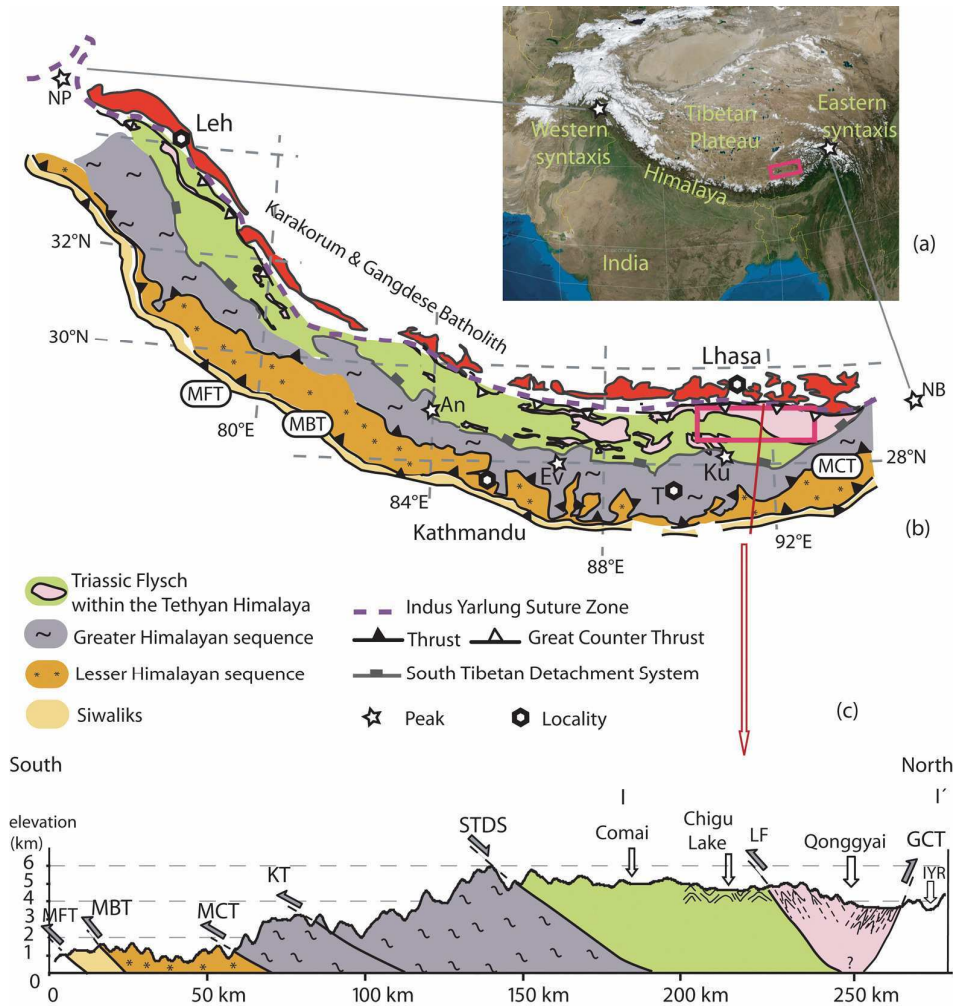


Figure 1: (a) Satellite image of the Himalayan-Tibetan orogen and surrounding area. (b) Geological sketch map of the Himalayan chain after Steck (2003), Pan *et al.* (2004) and Yin (2006). A rectangle shows the location of the studied area. MFT, Main Frontal Thrust; MBT, Main Boundary Thrust; MCT, Main Central Thrust; NP, Nanga Parbat; An, Annapurna; E, Everest; Ku, Khula Kangri; NB, Namche Barwa; T, Timphu. (c) Simplified cross-section of the eastern Himalayas; location in Fig. 1b; topographic profile from DEM data. STDS, South Tibetan Detachment System; LF, Lhunze Fault; GCT, Great Counter Thrust and IYR, Indus-Yarlung River. MFT, MBT, MCT, KT (Kakhtang thrust) and STDS attitude from Grujic *et al.* (2002) and McQuarrie *et al.* (2008); Tethyan Himalayan (I-I') features from Fig. 3 (this study).

2.3 Major Himalayan tectonic elements

The Himalayan belt is the result of the complex superposition of two main tectonic and metamorphic phases: the Eohimalayan phase related to the first stages of the collision (Middle Eocene to Late Oligocene) and the Neohimalayan phase responsible for the main structure of the orogen (Early Miocene to present) (Hodges *et al.* 2000; Fig. 2). Looking at the major Neohimalayan tectonic elements the Himalaya can be divided into four litho-tectonic units (Fig. 1b, c) (Gansser, 1964; Le Fort 1975; Hodges 2000; Yin 2006). These are, from bottom to top and from south to north:

1. The Siwalik molasses in the footwall of the Main Boundary Thrust (MBT) made up of Himalayan foreland basin sediments of Miocene to Pliocene-Pleistocene age (Gansser 1964) (Fig. 1b, c).

2. The Lesser Himalayan Sequence (LHS) in the footwall of the Main Central Thrust (MCT) (Fig. 1b; c), consisting of sediments from Proterozoic to Cambrian reaching the Paleocene age in the more eastern sectors of the belt (Stöcklin 1980; Valdiya 1980). Sediments were deposited in a proximal position on the Indian shelf and deformed by thrusts and folds under very low-grade metamorphic conditions (Colchen *et al.* 1986; Hodges 2000).

3. The Greater Himalayan sequence (GHS) cropping out between the MCT and the set of north-dipping normal faults of the South Tibetan Detachment System (STDS) (Pêcher 1991; Burchfiel *et al.* 1992). It represents the metamorphic core of the Himalayas with high grade metasediments and meta-igneous rocks (Le Fort 1975; Grujic *et al.* 2002). Leucogranitic intrusions are common in the contact zone with the STDS, e.g. the Manaslu granite (e.g. Guillot *et al.* 1993). The contemporaneous activity of the MCT and the STDS, confined between 23-17 Ma (Godin *et al.* 2006) led to the exhumation of the GHS (Fig. 1b, c; Fig. 2).

4. The Tethyan Himalaya sequence (THS) is a typical passive margin sequence deposited on the Indian passive margin. It crops out between the south-dipping Great Counter Thrust (GCT) in the north and the STDS in the south (Fig. 1b, c). The Great Counter Thrust is a south-dipping thrust system (Heim & Gansser 1939; Searle 1986; Ratschbacher *et al.* 1994; Ding *et al.* 2005) which can be detected along the entire Himalaya from Zaskar to east of Gyaca (Fig. 1). North of the Great Counter Thrust the Indus Yarlung Suture Zone (IYSZ) marks the contact with the southern margin of Eurasia represented by the Lhasa Block. Moreover the Tethyan Himalayan sequences are affected by an Oligocene-Miocene discontinuous belt of metamorphic rocks and leucogranitic bodies named the North Himalayan gneiss domes (e.g. Lee *et al.* 2000; Hodges 2000).

2.4 The Tethyan Himalayan Sequence, deformation and metamorphism

The Tethyan Himalayan Sequence crops out along *c.* 150 km between the South Tibetan Detachment System and the Indus Yarlung Suture Zone with approximately the same width from Annapurna to the East of Khula Kangri (Fig. 1b). The Tethyan Himalaya is built up of a continuous sedimentary sequence ranging from Cambro-Ordovician to Eocene and deposited on the passive northern margin of the Indian continent (Fuchs 1967; Willems *et al.* 1996; Garzanti 1999, Dupuis *et al.* 2006). The central Tethyan Himalaya can be divided in two sub-zones which are separated by the Gyrong-Kangmar thrust (Liu 1992; Liu & Einsele 1994; Willems *et al.* 1996). The southern sub-zone is formed by slightly metamorphosed carbonate

platforms and the northern sub-zone is defined by clastic sediments indicating the separation of the Indian plate from Gondwana and the following abyssal sedimentation conditions (Gaetani & Garzanti 1991; Brookfield 1993; Liu & Einsele 1994; Willems *et al.* 1996).

The sequence has experienced a complex structural history (see figure 2 for correlation of tectonic features in the Tethyan Himalaya). Godin (2003) defined five main phases of deformation, in the south Tethyan Himalaya in central Nepal, which can be partially or completely recognized along strike of the THS (Fig. 2). The first phase (D1) is defined by south-vergent small-scale folds (F1) with related low-grade axial planar foliation (S1) (e.g. Godin 2003; Carosi *et al.* 2007; Fig. 2). The D2 phase is characterized by large asymmetrical north-vergent megascopic backfolds (Kellett & Godin 2009) and a penetrative axial plane foliation (S2) defined by the preferred orientation of biotite, muscovite and elongated quartz grains in pelitic layers (Godin 2003, Carosi *et al.* 2007; Fig. 2). Crouzet *et al.* (2007) found K/Ar ages around 30-25 Ma interpreted as ages of recrystallized K-white micas newly formed during metamorphism and D2 in central Nepal. Moreover secondary pyrrhotite remanences show that F2 folding took place about 35-32 Ma (Appel *et al.* 1991; Crouzet *et al.* 2001; Schill *et al.* 2003). The third phase is related to the development of the South Tibetan Detachment system at *c.* 23-17 Ma for the whole belt (Godin *et al.* 2006 and references therein; Fig. 2). In the eastern Himalaya near Khula Kangri (Fig. 1b), Edwards & Harrison (1997) found an age < 12.5 Ma for the STDS development. D4 deformation phase is characterized by SW-NE shortening recorded in post-peak metamorphic F4 kink folds associated with a regional crenulation cleavage S4 and SW directed thrusts (Godin 2003). Since at least the late Miocene (*c.* 8 Ma) E-W extension affected the Tethyan Himalaya sequence (D5 phase; Fig. 2) giving rise to N-S Graben structures, e.g. the Takkhola Graben in central Himalaya and the Cona Graben in the eastern Himalaya (Armijo *et al.* 1986; Garzzone *et al.* 2003). The Tethyan Himalaya sequence experienced low-grade metamorphic conditions (Garzanti *et al.* 1994; Crouzet *et al.* 2007; Aikman *et al.* 2008; Dunkl *et al.* 2008) characterized by peak palaeotemperatures ranging from 250°C to 450°C (Crouzet *et al.* 2007). The age of the metamorphism decreases from the west to the east Himalaya ranging from 44-47 Ma in Zaskar to 30-25 Ma in central Himalaya (Bonhomme & Garzanti 1991; Crouzet *et al.* 2007).

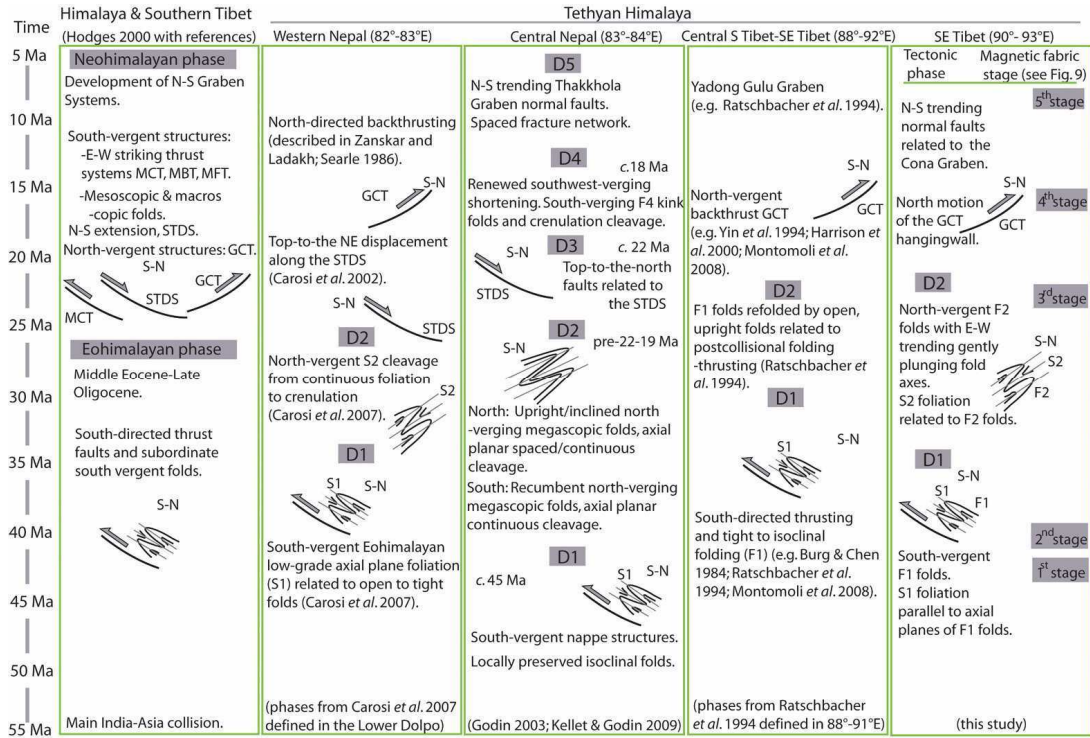


Figure 2: Simplified synthesis of main deformation events in the Tethyan Himalaya from west to east. Left column refers to previous synthesis proposed by Hodges (2000) including general Himalayan events.

2.5 Study area: the Triassic flysch of the eastern Tethyan Himalaya

The present study is focused on the Triassic flysch of the Tethyan Himalaya with a sedimentation age of Middle Triassic to early Jurassic (Chang 1984; Pan *et al.* 2004). Our work is concentrated in an area geographically located south of the Yarlung Tsangpo River that extends from Nagarze in the west as far as east of Gyaca (Fig. 3). Here the flysch consists of turbidites and carbonate flysch (Dupuis *et al.* 2005) and it is represented by black shales interbedded with sandstone/siltstone and locally some limestone. The organic-rich pelitic lithologies always contain early diagenetic pyrite crystals. The sequence is intruded by mafic dykes and contains small ultramafic intrusions. The dominant structures are folds and imbricate thrusts involving the whole passive continental margin sequence of the Tethyan Himalaya (Yin & Harrison 2000; Aikman *et al.* 2008).

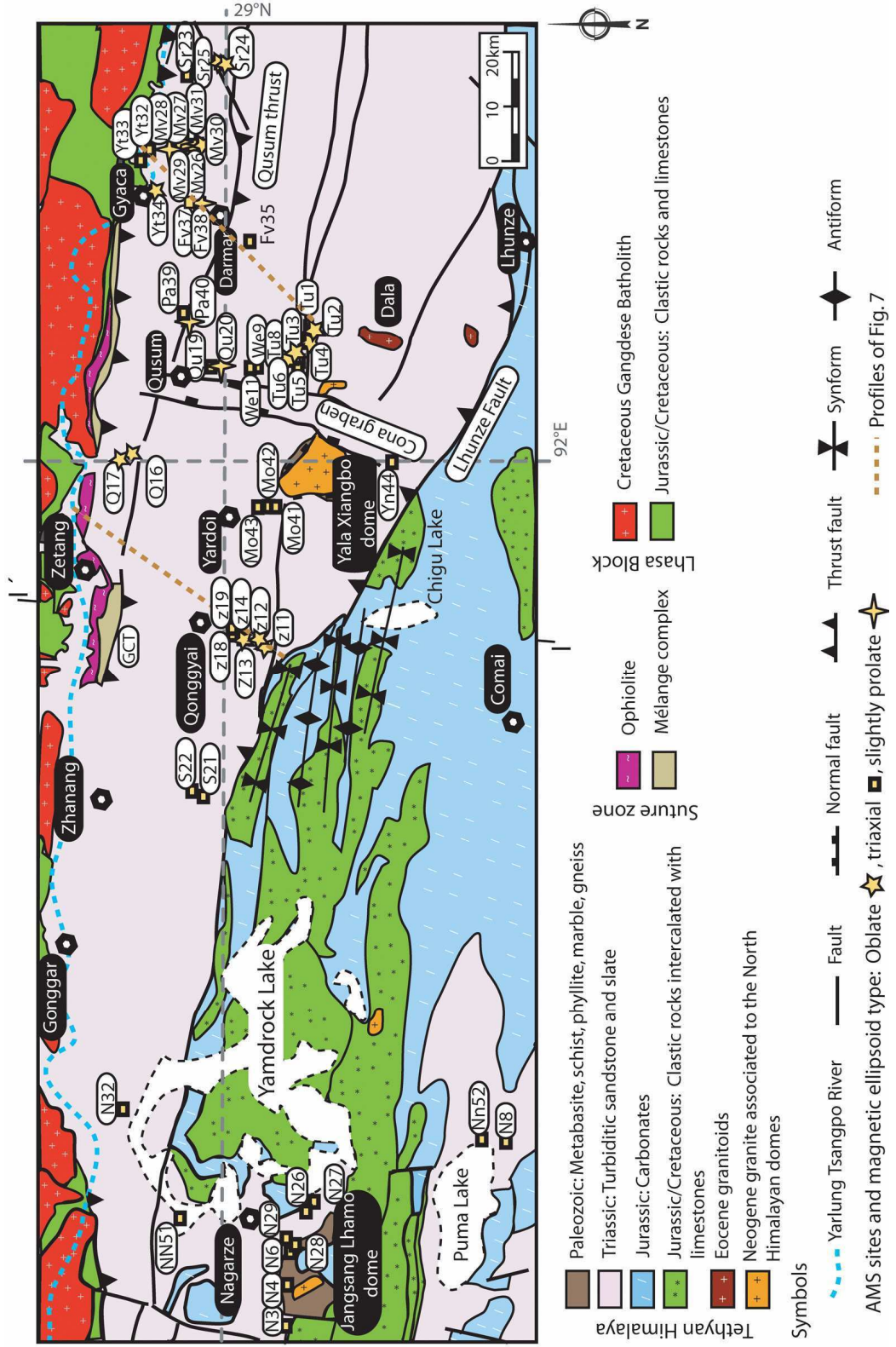
In the north the Great Counter Thrust separates the Triassic flysch from the mélangé complex and the Cretaceous clastic rocks (Fig. 3). The mélangé complex (constituted by cherts, shales, marbles, andesites, diorites, mafic and ultramafic bodies, limestones and phyllites) has been deposited on the growing Neo-Tethys ocean floor and incorporated in a subduction complex mélangé (Searle *et al.* 1987). The Cretaceous clastic rocks were deposited in the active palaeomargin of the Indus Yarlung Suture Zone (Harrison *et al.* 2000; Pan *et al.* 2004; Dupuis *et al.* 2005). In the eastern Himalaya the Renbu-Zedong Thrust (Yin *et al.* 1994;

Harrison *et al.* 2000) has been correlated with the Great Counter Thrust. The Great Counter Thrust in the Ringbung area is dated by K/Ar in a phyllite as 17.5 Ma old (Ratschbacher *et al.* 1994). This age coincides with the interval of activity from 18 Ma to 10 Ma of the Great Counter Thrust in the Zedong area dated by Ar/Ar analyses on K-feldspar analysis (Quidelleur *et al.* 1997; Harrison *et al.*, 2000).

Towards the south the Triassic flysch is in contact with the Upper Jurassic (continental clastic rocks, marls and marine limestones) and Cretaceous clastic rocks which represent the platform sequence of the Indian passive margin (e.g. Liu & Einsele, 1996). The southern contact between the Triassic flysch and the Jurassic-Cretaceous rocks (Fig. 3) is marked by the Lhunze Fault which is likely comparable with the E-W trending and N-dipping Gyrong-Kangmar thrust cropping out around 50 km west of the Yadong Gulu Graben (Chen *et al.* 1990; Liu 1992; Yin 2006; Aikman *et al.* 2008).

Two kinds of intrusions have affected the Triassic flysch in the study area: the Dala granitoids of Eocene age (Aikman *et al.* 2008) and the Neogene North Himalayan gneiss domes (Fig. 3). The latter are represented by the Mt. Jangsang Lhamo south of Nagarze and the Yala Xiangbo south of Qusum (Fig. 3). Preliminary thermochronological data indicate that the Yala Xiangbo leucogranite was emplaced at *c.* 18 Ma, and cooled through the muscovite closure window at *c.* 13.5 Ma (Aikman *et al.* 2004; Zhang *et al.* 2005). The Neogene domes have been interpreted as metamorphic core complex owing to the fact that the granites are surrounded by detachment faults and shear zones (e.g. Zhang *et al.* 2005). Afterwards the E-W Neogene extension played a key role in the deformation of the eastern Tethyan Himalaya giving rise to the NNE-SSW Cona Graben that can be followed from the north of the Indus Yarlung Suture Zone as far as the South Tibetan Detachment System, with approximately 210 km length and 8 km width (Fig. 3). The Cona Graben is the easternmost graben that crosses the Tethyan Himalaya and GPS velocities have indicated no significant (0.3 ± 0.9 mm/yr) fault opening at present-day (Gan *et al.* 2007).

Figure 3: Simplified geological map of SE Tibet. Modified from Pan *et al.* (2004), Yin (2006) and Aikman *et al.* (2008). The studied sites are marked in function of the type of AMS ellipsoid. Line I-I' indicates the cross section in Fig. 1c. Dashed orange lines indicate the two cross sections of Fig. 7.



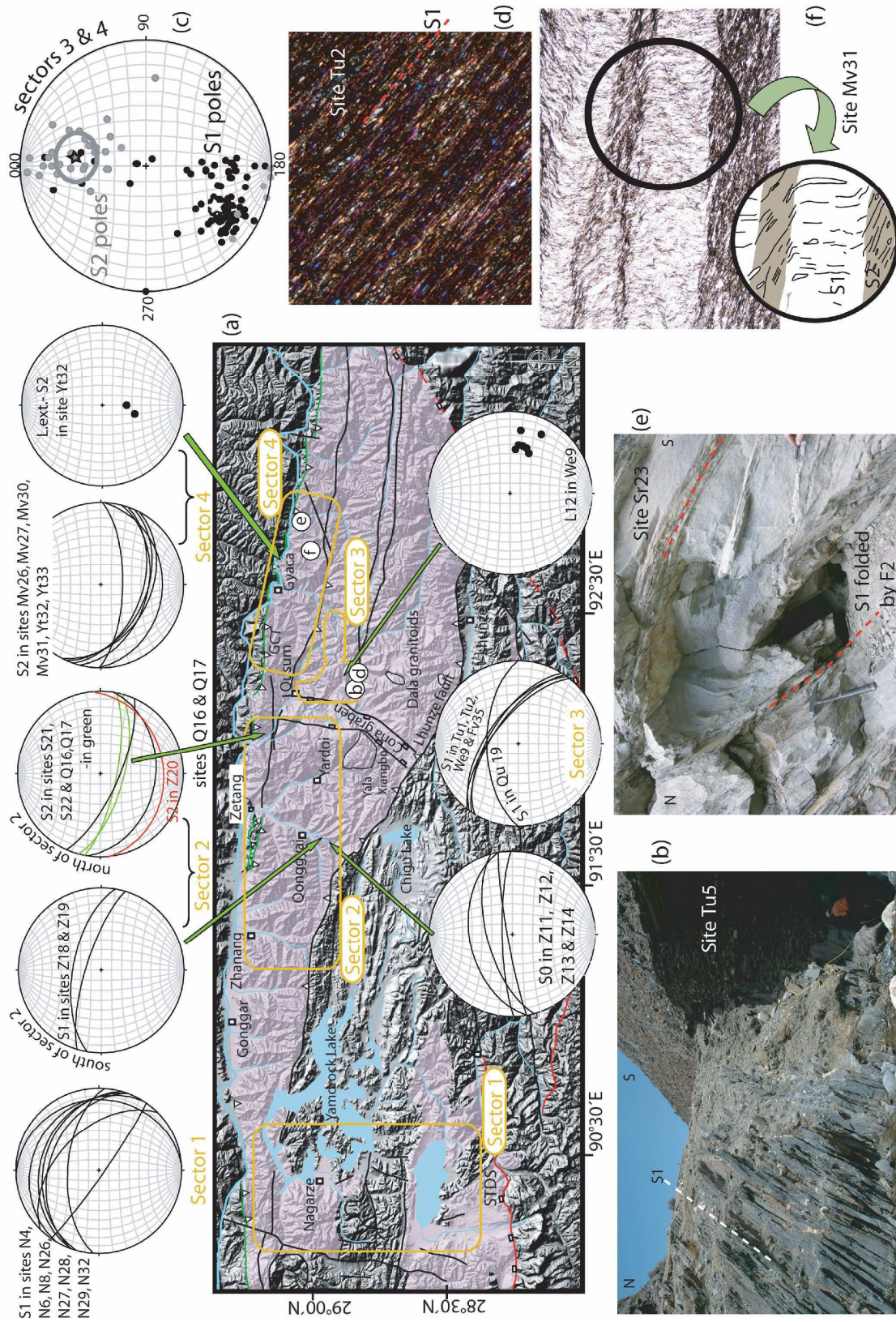
2.6 Structural and metamorphic data

A polyphase tectonic history has been recognized in the study area characterized by two main tectonic phases named hereafter D1 and D2 (see Fig. 2 for correlation between Tethyan Himalayan deformation phases). During the first D1 tectonic phase, referred to the Eohimalayan event (Hodges 2000), metric to kilometric asymmetrical F1 folds developed. F1 folds face to the south and their axes trend ENE-WSW. Parallel to axial planes of F1 folds, a S1 axial plane foliation can be recognized (see stereograms of sector 1, south of sector 2 and sector 3 in Fig. 4a). In the southern parts of the studied area S1 is the dominant planar structure in the field (Fig. 4b). In the Nagarze area (sector 1; Fig. 4a) the mean vector of the S1 poles trends 220° and plunges 70° ($\alpha_{95}=22^\circ$; $k=4.9$) and in the Qonggyai valley (south of Zetang in sector 2; Fig. 4a) the S1 pole mean vector trends 182° and plunges 30° ($\alpha_{95}=24^\circ$; $k=13.8$; Fig. 4a). East of the Cona Graben, in sector 3, S1 poles mean vector trends 210° and plunges 35° ($\alpha_{95}=5.6^\circ$; $k=7.3$; Fig. 4c). S1 is a low grade foliation and microstructural observations show that moving from south to north, S1 foliation varies from a disjunctive spaced stylolitic cleavage with no dynamic recrystallization to a fine continuous foliation (Montomoli *et al.* 2008) marked by synkinematic recrystallization of very fine-grained phyllosilicates (Fig. 4d). Object lineations, trending NW-SE, are well represented by strain fringes, mainly composed of quartz around pyrite crystals. D1 deformation occurred in diagenetic or lower anchizonal conditions probably in Paleogene times (Dunkl *et al.* 2008).

A later D2 deformation phase is superimposed on D1 structures (Fig. 2). D2 is represented by a weak crenulation cleavage in the southern portions but moving towards the GCT it gives rise to decimetre to decametre-scale F2 folds (Fig. 4e). F2 folds have E-W trending gently plunging axes and verge to the north. Associated with F2 folds a S2 foliation was generated. Axial plane foliation S2 strikes WNW-ESE with moderate dips towards the south (see stereograms north of sector 2 and sector 4 in Fig. 4a). Equal area projection of S2 poles of sector 4 show a grouping ($\alpha_{95}=14.6^\circ$; $k=3.2$; Fig. 4c) with a mean vector trending 007° and plunging 43° (Fig. 4a & c). Foliation S2 varies from a discrete zonal crenulation with well defined cleavage domains near the Qusum Thrust (Fig. 4f) to a fine continuous foliation in a more strained area in the vicinity of the Great Counter Thrust, where S2 is the most visible structural element in the outcrop. In some cases, in the more northern areas S2 is associated with the dynamic recrystallization of illite-sericite (Montomoli *et al.* 2008). East of the Cona Graben the WNW-ESE trending thrust fault with south to south-southwest dip described in Yin *et al.* (2006), that we name the Qusum Thrust, represents the boundary between S1 and S2 foliations.

Top-to-the-N or NE brittle-ductile shear zones are developed in the overturned limbs of F2 folds with kinematic indicators such as C-S fabric (Berthè et al. 1979). On C surfaces stretching lineations strike N-S and plunge gently to the south (Montomoli *et al.* 2008; see Fig. 4a stereogram with stretching lineation within S2 at site Yt32). D2 took place at higher anchizonal to greenschist facies conditions in Miocene times and the process culminated around 24 Ma as Dunkl *et al.* (2008) have shown.

Figure 4: (a) SRTM topography overlapped with the Triassic flysch (pink color) and the structural elements of Fig. 3. The orange rectangles show the sectors described in the structural and magnetic fabric sections; b, d, e and f letters correspond to the position of the outcrop and thin section images. Lower-hemisphere, equal-area stereogram of the general trend of tectonic foliations per site and stretching lineation (L.ext.) within S2 foliation from site Yt32 and intersection lineations of foliation S1 and S2 (L12) in site We9. (b) Outcrop view of site Tu5, dashed line shows S1 foliation. (c) Lower-hemisphere, equal-area stereogram of the poles of S1 and S2 tectonic foliations of sector 3 and 4, stars indicate mean vectors. (d) Photomicrograph of S1 foliation developed in the slates of the site Tu2 (field of view 5 mm). (e) Example of F2 fold in site Sr23. (f) Thin section photomicrograph from the slates of the site Mv31 and geological interpretation; both S1 and S2 foliations are recognizable (field of view 7 mm).



2.7 AMS analysis

AMS was measured in 516 cylindrical rock specimens with a standard size of 2.5 cm diameter and 2.1 cm length. Samples were collected from 53 sites distributed along north-south valleys between Yamdrock lake and east of Gyaca (Fig. 3), with an average of 10 cores at each site. A portable gasoline powered rock drill machine was used and cores were oriented in situ with a magnetic compass. The study of AMS was carried out with an AGICO KLY-2 Kappabridge at Tuebingen University. The AMS ellipsoid was determined from 15 different directional measurements. The results can be characterized by the bulk susceptibility (K_m) given as arithmetic mean of the three principal axes of the AMS ellipsoid: $K_m = 1/3(K_{max} + K_{int} + K_{min})$ and the orientations and magnitudes of the $K_{max} > K_{int} > K_{min}$ axes of the AMS ellipsoid. The statistical procedure to obtain the directional data was based on tensor analysis by Jelinek (1977), using the program anisoft42 developed by Chadima and Jelinek (last version of 2008). The mean values for areas were calculated by Fisher statistics (Fisher *et al.* 1987) with the program Stereogram v1.2 (Allmendiger 2002-2003). In numerous tectonic and AMS studies it has been shown that in rocks where iron-rich silicates control magnetic susceptibility the cluster of minimum axes of the magnetic ellipsoid (K_{min}) is related to the magnetic foliation because the minimum susceptibility axis is nearly perpendicular to the basal cleavage of phyllosilicates crystals (e.g. Kneen 1976; Borradaile & Werner 1994; Martín-Hernández & Hirt 2003). A cluster of maximum axes (K_{max}) or magnetic lineation can reflect either the extension direction, the intersection of two competing subfabrics (because the maximum susceptibility axis is the intersection axis between the phyllosilicates crystals), or an orientation in between (Borradaile & Tarling 1981; Housen *et al.* 1993; Parés *et al.* 1999; Parés & van der Pluijm 2002; Soto *et al.* 2003). Furthermore Jelinek's method gives different scalar parameters which are very useful to describe the magnetic fabrics: the corrected anisotropy degree (P') can be related to the intensity of the preferred orientation of minerals in rocks in which the susceptibility is mainly carried by paramagnetic minerals. The shape parameter (T) indicates the form of the magnetic ellipsoid. T can range from -1 (prolate ellipsoid) to 1 (oblate ellipsoid). The magnetic foliation parameter ($F = K_{int}/K_{min}$) and magnetic lineation parameter ($L = K_{max}/K_{int}$) can be plotted in a Flinn type plot (Flinn, 1962) normally used in structural geology. We used also Jelinek's elliptical confidence angles as markers of the quality of AMS data (Jelinek, 1977).

2.7.1 Magnetic mineralogy and carriers of the magnetic fabric

The determination of the minerals that contribute to the anisotropy of magnetic susceptibility is an essential step in order to understand the origin of the magnetic fabric and their structural interpretation. In the following we predominantly utilize median values and quartiles for concentration-dependent parameters because these are more representative than mean values and standard deviation in data sets with some significant outliers.

The bulk susceptibility median of the 53 studied sites is 232×10^{-6} SI (1st quartile= 187×10^{-6} SI, 3rd quartile= 372×10^{-6} SI, mean= 334×10^{-6} SI and STD= 314×10^{-6} SI) (Table 1; Fig. 5a). Around 89 % of the sites show a low bulk susceptibility median $< 500 \times 10^{-6}$ SI typical for rocks where the magnetic fabric is usually controlled by the crystal lattice orientation of the paramagnetic fraction (Rochette 1987). Similar values of magnetic susceptibility have been found in other studies where paramagnetic minerals controlled the AMS ellipsoid (e.g. Tarling & Hrouda 1993). Sites N6, Tu5, Tu6 and Mv30 have higher values ($K_m > 800 \times 10^{-6}$ SI) probably related to a significant contribution of the ferro(i)magnetic fraction to the total magnetic susceptibility and they will be analysed separately. Natural Remanent Magnetization (NRM) was measured in 10 samples per site with a 2G RF-SQUID magnetometer. The NRM median is low, 0.4 mA/m (1st quartile= 0.26 mA/m, 3rd quartile= 1.4 mA/m, mean= 10.8 mA/m and STD= 43.3 mA/m) (Table 1). Around 72 % of the sites give median values of NRM < 1 mA/m and there is no correlation of K_m and NRM ($R^2=0.12$) likely indicating a low content of ferro(i)magnetic minerals (Fig. 5a). A similar analysis was carried out on 41 samples from 24 sites, looking at the relation between the K_m and saturation isothermal remanent magnetization (SIRM) at 2.4 T (SIRM imparted by a MMPM9 pulse magnetizer). Also for SIRM and K_m no significant dependence was found. Variation of magnetic susceptibility was measured for 14 sites between -196 °C and room temperature using a low temperature unit attached to a KLY-3 Kappabridge (AGICO). The measured thermomagnetic curves, after free furnace correction, show a temperature dependence of susceptibility following the Curie Law (Nagata 1961) characteristic for paramagnetic minerals (Fig. 5b). Moreover variation of magnetic susceptibility was measured for 7 sites between room temperature and 700 °C using a high temperature unit attached to a KLY-3 Kappabridge (AGICO). The measured thermomagnetic curves, after free furnace correction, show no presence of pyrrhotite and a minor contribution of magnetite indicated by decay around 580 °C.

In thin sections and in outcrop views we observed pyrite crystals inside the slates. Pyrite influence on the total magnetic susceptibility is small but it is an important source for the creation of pyrrhotite during the metamorphism (Rochette 1987; Borradaile & Sarvas 1990;

Crouzet *et al.* 2001). The main decay of intensity of the SIRM around 325°C indicates the presence of pyrrhotite in all the studied samples (Fig. 5c). IRM acquisition in a direct field up to a maximum of 1.8 T shows near saturation at 0.3 T suggesting that the pyrrhotite grains are in a rather low coercive multidomain state. It is also noted that in site Yt32 additional magnetite was observed by its Curie temperature around 580 °C.

The aforementioned results were further examined quantitatively by means of hysteresis properties. Hysteresis properties were measured in 28 sites with an Alternating Gradient Force Magnetometer AGFM 2900 (Princeton Measurements Corp.). The maximum applied field was 800mT in which the ferro(i)magnetic phase is fully saturated. All samples show a straight line at high fields due to the intrinsic high field susceptibility of the paramagnetic minerals (Borradaile & Werner 1994). The ferro(i)magnetic component shows a low coercivity ($H_c < 10$ mT) confirming the presence of a very low coercive MD pyrrhotite or some contribution of magnetite (Fig. 5d). In order to quantify the paramagnetic and ferro(i)magnetic contribution to the total magnetic susceptibility we calculated the bulk specific susceptibility of the paramagnetic fraction from the slope of the hysteresis loop at high fields and compared it with the total bulk specific susceptibility at low fields of the same sample as was previously done by other authors (e.g. Richter & van der Pluijm 1994). The values obtained in 11 samples from different homogeneously distributed sites indicate that in five samples (sites Pa40, Fv38, N3, Qu20, Sr24) the ferro(i)magnetic contribution is less than 30 % and in six samples (sites Fv 37, Z13, Yt33, Mo42, Tu4, Tu5) the ferro(i)magnetic contribution to the total magnetic susceptibility is in between 30% and 60% (Fig. 5e). However, one has to be cautious with these results as they are based on very small samples and thus reliability of upscaling is dependent on the homogeneity of the rocks.

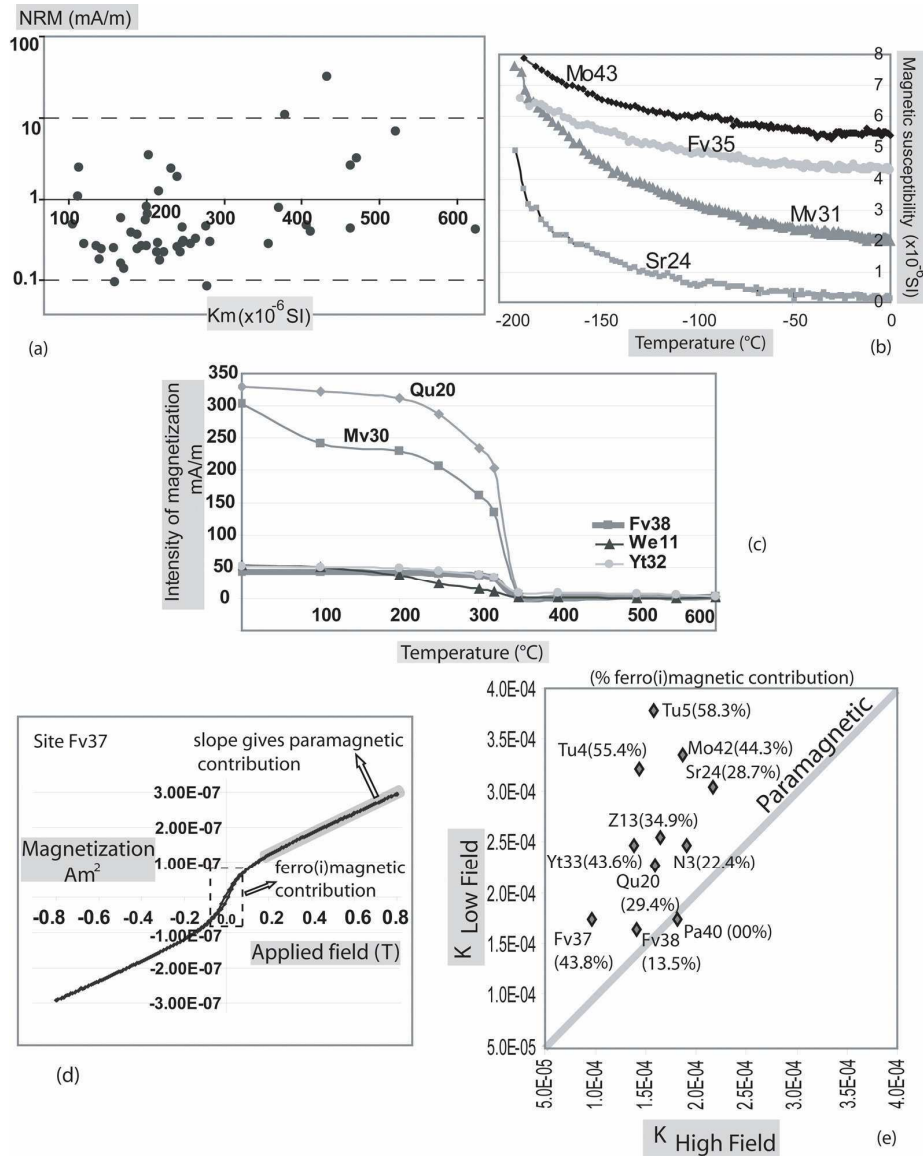


Figure 5: Magnetic mineralogy analysis. (a) Km versus NRM plot without sites Tu5, Tu6, Mv30 and N6 with important ferro(i)magnetic contribution, see discussion in the text. (b) Curves of magnetic susceptibility versus the temperature. (c) Thermal demagnetization curves of the SIRM. (d) Hysteresis curve from site Fv37. (e) High field bulk magnetic susceptibility versus low field bulk magnetic susceptibility essays.

Consequently all these results in conjunction with the well defined magnetic foliation parallel to the tectonic foliation plane and the fact that P' values are characteristic of rocks governed by phyllosilicates (Fig. 6a) point out that a predominating paramagnetic control of the total anisotropy of magnetic susceptibility can be expected in most sampled sites. For this reason the geographical distribution of the axes of the ellipsoid of magnetic susceptibility can be interpreted in terms of the preferred orientation of the phyllosilicates in relation to their structural location. However, there might be also some small contribution from subordinate

pyrrhotite or magnetite mainly in sites Tu5, Tu6, Mv30 and N6 which have not been included in the scalar parameter plots and in the tectonic interpretation. Although these four sites show K_{\min} axis nearly perpendicular to the tectonic foliation (Table 1 & Fig. 4a) as in the sites controlled by the paramagnetic mineral fraction, may be related to a coaxiality of magnetic fabrics and petrofabrics, as was previously noted by Borradaile & Sarvas (1990) in the slates west of Atikokan (Canada).

Site	NRM (mA/m)	n	AMS type	Km (*10E-6 SI)	Kmax (T/P)	CA	Kmin (T/P)	CA	P'	T
Tu1	28.44±21.10	16	2	432.8±372.8	114/30	26/6	215/18	15/6	1.56	0.65
Tu2	0.35±0.18	12	2	180.4±50.6	314/20	60/11	217/17	15/8	1.23	0.82
Tu3	64.18±115.6	8	1	463.0±797.1	121/17	36/6	223/35	8/4	1.41	0.74
Tu4	0.33±0.28	11	1	239.5±39.7	310/10	31/8	215/27	14/7	1.28	0.94
Tu5	349.6±269.6	10	2	1395.0±1079.0	345/44	30/18	212/35	22/10	2.12	0.44
Tu6	98.85±121	10	2	1304±1079.0	342/47	22/12	210/31	14/7	2.08	0.59
Tu8	11.95±14.48	10	1	239.7±38.3	310/18	19/6	215/14	36/17	1.24	0.60
We9	9.04±12.23	10	2	470.7±198.7	113/22	12/6	217/31	17/6	1.30	0.43
We11	23.63±58.19	10	1	623.5±467.0	082/33	13/5	207/42	7/5	1.54	0.61
Qu19	0.29±0.11	11	2	246.8±23.8	284/9	14/5	187/34	9/3	1.17	0.30
Qu20	0.78±0.63	9	3	214.4±15.8	280/9	19/14	166/67	27/11	1.16	-0.13
Sr23	0.34±0.36	9	2	243.7±99.3	277/11	12/4	014/33	12/5	1.15	0.61
Sr24	0.58±0.37	7	1	166.8±45.1	103/15	81/17	003/33	19/7	1.15	0.59
Sr25	0.84±1.09	10	1	105.3±38.8	124/19	39/7	019/38	8/6	1.17	0.70
Mv26	0.61±0.25	9	1	199.7±73.1	140/12	49/13	031/57	30/18	1.21	0.30
Mv27	0.49±0.15	7	3	276.5±27.5	262/29	8/6	004/19	34/5	1.16	0.09
Mv28	0.33±0.18	9	1	357.1±83.4	141/65	34/15	032/9	15/12	1.26	0.58
Mv29	0.45±0.24	13	3	411.6±69.0	271/9	12/10	179/13	36/7	1.18	0.14
Mv30	157.7±184.80	13	1	1684±1521.0	167/44	48/11	014/43	13/6	2.35	0.39
Mv31	22.56±28.78	10	3	520.7±477.8	285/14	9/4	188/25	47/9	1.46	-0.07
Yt32	0.54±0.91	9	2	282.1±42.2	193/70	10/4	003/20	11/4	1.18	0.61
Yt33	0.49±0.30	10	2	246.2±23.5	189/64	24/16	030/24	23/15	1.37	0.85
Yt34	23.97±35.00	9	1	377.8±277.2	109/24	56/7	006/26	8/5	1.38	0.40
Fv35	1.66±1.29	10	2	216.1±51.0	122/7	33/5	216/28	7/5	1.16	0.54
Fv37	0.01±0.05	7	2	160.0±20.9	149/48	20/4	024/27	7/4	1.28	0.70
Fv38	0.47±0.55	11	3	119.6±27.6	281/2	14/6	015/68	22/6	1.15	0.43
Pa39	0.30±0.14	10	2	247.3±105.4	091/36	28/15	190/13	19/14	1.28	0.58
Pa40	0.13±0.06	11	3	171.6±43.9	283/6	15/6	125/83	39/10	1.23	0.49
N3	10.20±18.34	14	1	370.0±277.0	298/3	13/4	095/86	5/3	1.20	0.44
N4	45.64±106.60	11	1	203.0±178.0	332/8	4/3	161/82	6/2	1.33	0.50
N6	216.70±357.90	14	2	857±702.0	344/13	4/2	198/75	3/1	2.29	0.02
N8	1.13±2.35	9	1	264.0±38.5	298/14	25/1	143/74	7/2	1.15	0.61
N26	3.08±2.12	12	2	232.0±38.4	331/50	12/6	177/37	10/3	1.15	0.65
N27	1.22±1.45	11	2	112.0±28.5	297/66	6/3	205/1	8/3	1.17	0.68
N28	3.03±3.11	10	2	113.0±14.5	329/33	8/5	215/32	7/3	1.17	0.63
N29	0.96±0.55	9	2	200.0±75.1	356/33	16/7	210/52	13/7	1.07	0.27
N32	0.35±0.32	9	1	189.0±30.5	123/24	58/28	220/15	30/17	1.07	0.31
Nn51	0.08±0.04	5	2	278.0±20.1	164/54	19/2	339/36	5/3	1.12	0.56
Nn52	1.84±3.14	10	2	406.0±77.4	339/30	10/4	211/47	20/3	1.12	-0.09
Q16	0.29±0.22	10	1	167.0±40.0	253/51	22/3	011/20	5/3	1.21	0.83
Q17	0.36±0.43	7	1	140.0±64.3	248/53	38/5	010/22	9/6	1.14	0.59
S21	0.26±0.16	5	2	142.0±17.5	219/22	11/1	350/58	15/2	1.05	0.37
S22	0.36±0.23	8	2	189.0±12.6	228/78	9/8	007/10	10/6	1.08	0.41
Z11	0.21±0.08	10	1	213.0±16.5	083/4	24/5	175/17	7/2	1.08	0.65
Z12	1.73±3.32	11	1	194.0±25.6	285/29	30/7	179/27	19/12	1.20	0.80
Z13	0.23±0.29	11	2	223.0±23.3	012/47	7/3	173/41	17/2	1.21	0.83
Z14	1.04±0.95	10	1	202.0±46.9	081/12	21/7	174/16	8/6	1.11	0.79
Z18	0.27±0.25	12	2	136.0±45.2	056/55	18/5	185/23	7/1	1.09	0.45
Z19	0.29±0.20	12	2	158.0±16.7	015/69	5/4	189/21	7/4	1.10	0.29
Mo41	3.40±5.74	9	2	463.0±291.0	348/40	11/3	160/50	6/3	1.07	-0.07
Mo42	0.28±0.16	9	2	257.0±22.9	005/43	10/5	157/44	10/3	1.19	0.68
Mo43	0.26±0.36	10	2	218.0±36.9	340/46	10/5	147/44	6/4	1.17	0.65
Yn44	0.27±0.04	7	2	201.0±10.3	279/16	11/3	169/50	10/4	1.07	0.28

Table 1: NRM ; natural remanent magnetization mean (mA/m). STD: Standard deviation. AMS data (Jelinek's statistics, 1977): n, number of measured samples; Km, Bulk magnetic susceptibility ($\times 10^{-6}$ SI); K_{\max} and K_{\min} mean (trend/plunge) with the 95 % confidence angle (CA). P' , corrected degree of anisotropy; T, shape parameter.

2.7.2 AMS ellipsoid: The corrected degree of anisotropy and shape parameters

The corrected degree of anisotropy (P') in the slates of SE Tibet is in the range of P' characteristic for slates where the main carriers of the AMS are phyllosilicates (Tarling & Hrouda 1993; Parés *et al.* 2002). The sites show a median value of 1.18 (1st quartile= 1.14; 3rd quartile= 1.27; Mean= 1.28, STD= 0.30) (Fig. 6a & Table 1). Moreover these values are similar to the crystalline anisotropies of chlorite (P' = 1.15-1.19) or muscovite (P' = 1.15-1.27) (values of P' given by Martín-Hernández & Hirt 2003 and Borradaile & Werner 1994 respectively). In order to detect the dependence of the corrected degree of anisotropy on the rock composition (iron content) we studied the relation between the corrected degree of anisotropy and Km at site scale and regional scale. Only two sites (We9 and Sr23) indicate dependence of the corrected degree of anisotropy on the magnetic susceptibility at site scale. The plot of Km vs P' mean site values indicates no correlation between the magnetic susceptibility (iron content) and the degree of anisotropy ($R^2=0.37$; Fig. 6a). These data corroborate the magnetic mineralogy analysis suggesting that the phyllosilicates predominantly control the AMS signal.

The shape of the magnetic ellipsoid is oblate in 92 % of the sites; only sites N6, Qu20, Nn52 and Mo41 show a slightly prolate ellipsoid. The shape parameter mean is 0.5 (STD= 0.26) suggesting the dominance of a planar fabric controlled by the foliation (Fig. 6b & Table 1). Likewise the F parameter (F mean= 1.18, STD= 0.16) and the L parameter (L mean= 1.06, STD= 0.08) distribution in the Flinn diagram confirms the control of the foliation (Fig. 6b).

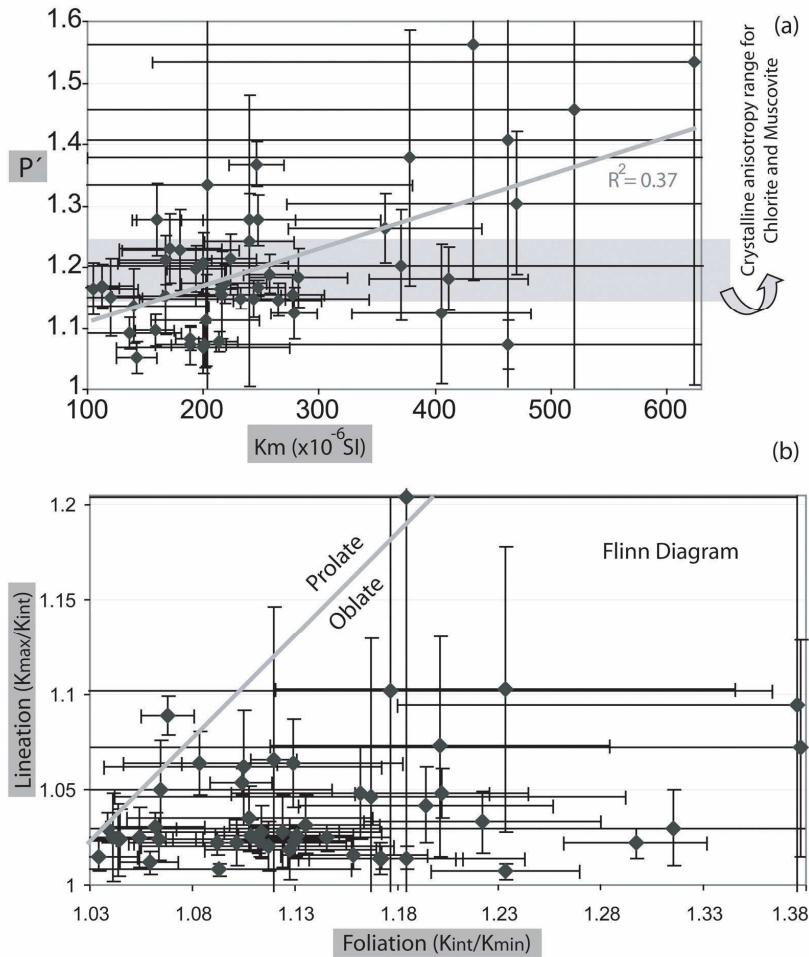


Figure 6: AMS scalar parameters plots. (a) K_m versus P' . (b) Flinn diagram.

2.7.3 Different shapes of AMS ellipsoids, definition of magnetic foliation and lineation

Equal area plots of the principal AMS axes show three typical shapes of AMS ellipsoids (Figs. 3, 7 & Table 1). The first type is an oblate ellipsoid with a cluster of K_{min} perpendicular to the foliation plane and K_{max} and K_{int} distributed along the foliation plane (e.g. site Q16 in Fig. 7a). The fact that K_{max} is not grouped prevents the definition of the magnetic lineation (e.g. Pueyo *et al.* 2004). The second type and most common one shows a triaxial ellipsoid with all three axes well grouped; K_{min} axes are perpendicular to the foliation plane and K_{max} axes represent different structural elements. They can be parallel to the F1 or F2 fold axes, related to the intersection of S1 and S2 as previously documented Housen *et al.* (1993) (e.g. see Fig. 4a intersection lineation of S1 and S2, L12, in site We9 is nearly parallel to K_{max} orientation of We9; Table 1) or parallel to the stretching lineation (e.g. site Yt32 in Fig. 7b). The third type presents a slightly prolate ellipsoid characterized by a semicircle distribution of K_{min} axes and a cluster of K_{max} axes, magnetic lineation, which is related the intersection lineation of S1 and S2 foliations as can be seen in the site Qu20 in Fig. 7b. How these

ellipsoids are spatially distributed in the studied area as well as the orientation and relation with the structural elements is discussed below.

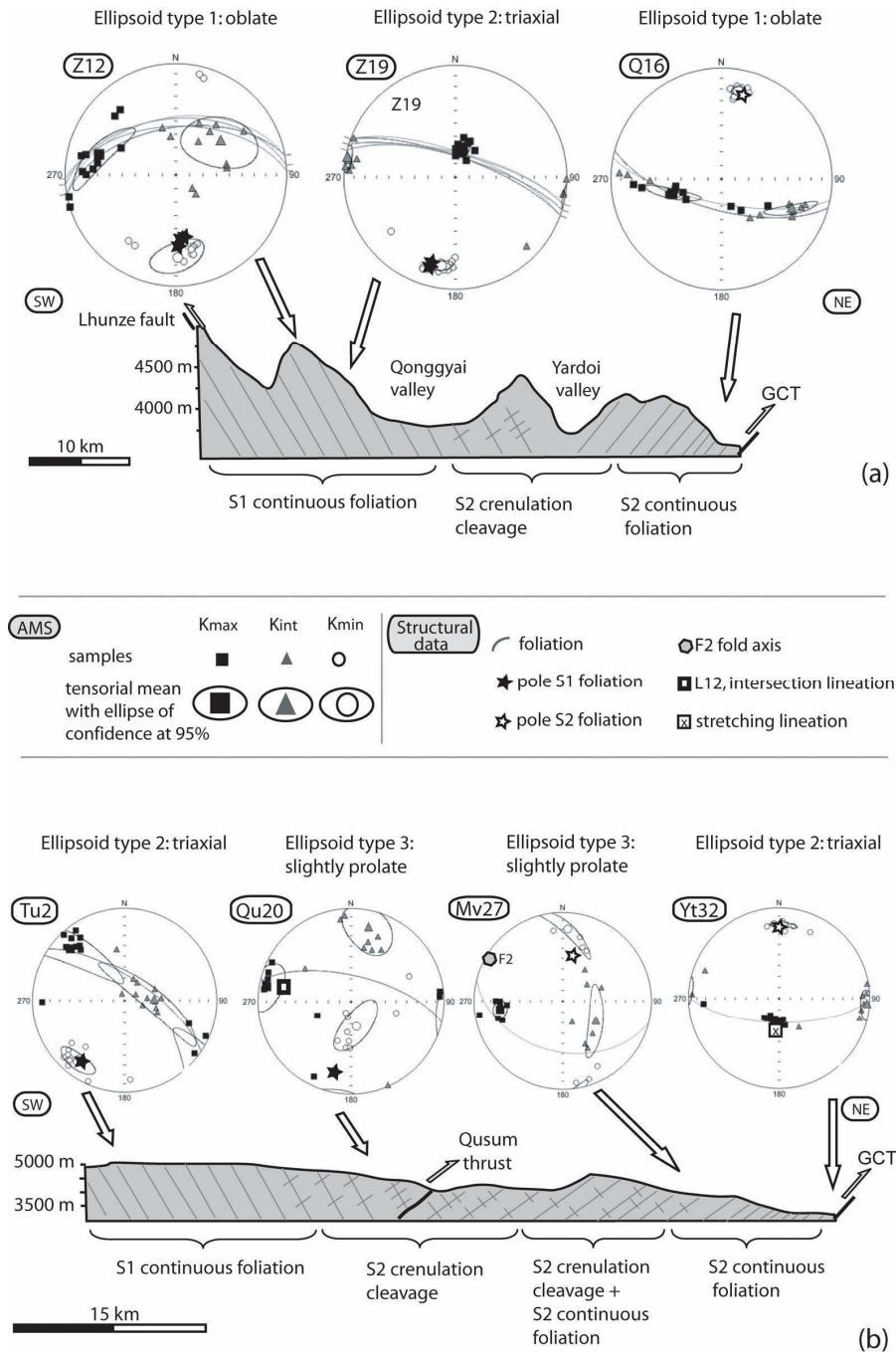


Figure 7: Types of AMS ellipsoids within two simplified cross sections indicated in Fig. 3 with the schematic stages of cleavage development. (a) Cross section from the Lhunze fault to the Great Counter thrust along the Qonggyai valley. (b) Cross section crossing sectors 3 and 4.

2.8 Magnetic foliation and lineation in the Triassic flysch of SE Tibet

Four sectors like in the structural section have been distinguished in order to understand the relation between the magnetic fabric and the structural data (Fig. 8).

Sector 1 mainly corresponds to the Nagarze area which is located east of the Yadong Gulu Graben and in the vicinity of the Jangsang Lhamo North Himalayan gneiss dome (Figs. 4 & 8). These nine sites show a triaxial magnetic ellipsoid described above. Magnetic foliation strikes WNW-ESE with moderate dips towards the north and parallel to S1 tectonic foliation (Fig. 8a). It is also noted that the dip varies from very gentle angles beside the Jangsang Lhamo Dome to near vertical moving to the east. Magnetic lineation has a NNW-SSE trend and north-northwest plunge approximately parallel to gneiss dome elongation (Fig. 8b). Like the magnetic foliation the plunge values of the magnetic lineation increase from the Jangsang Lhamo dome to the east. Furthermore two sites were drilled in the east side of the Puma Lake and approximately 40 km north of the South Tibetan Detachment System (Fig. 3; sites N7 and N8). These two sites have directions and plunges of the magnetic lineation and foliation that follow the general trend of the magnetic axes at Nagarze.

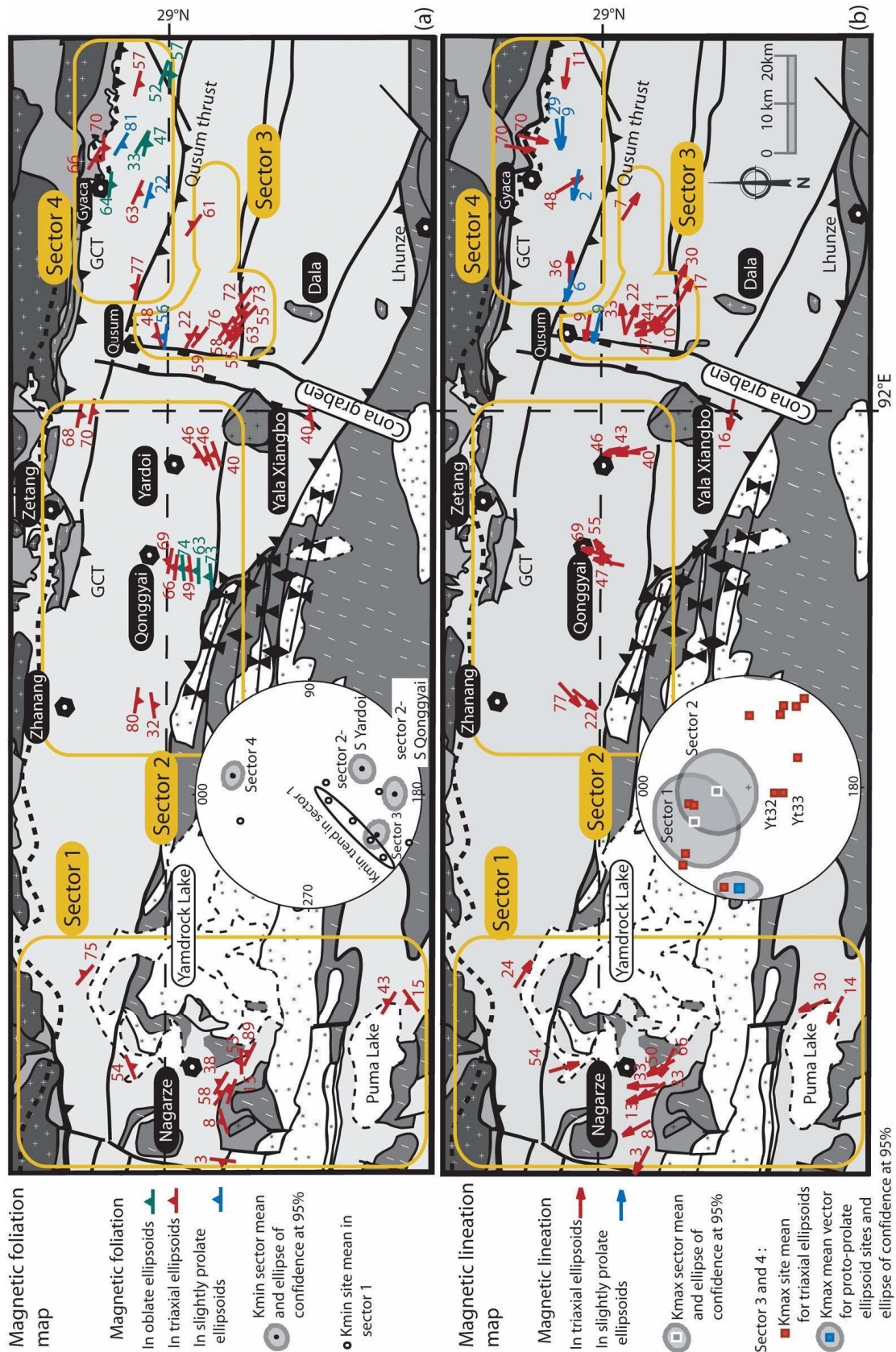
Sector 2 covers the valleys south of Zhanang and Zetang towards Yala Xiangbo dome (Figs. 4 & 8). Sites S21 and S22 in the Zhanang valley present triaxial magnetic ellipsoids with magnetic foliation trending E-W with moderate dip to the south parallel to S2 tectonic foliation. Magnetic lineation trends NNE-SSW with plunge towards the south-southwest. The Qonggyai profile (location in Fig. 3) presents AMS ellipsoids that change from oblate in the south to triaxial in the central part and magnetic foliation strikes E-W and dips to the north analog to tectonic foliation S1 (Fig. 7a site Z12). The magnetic lineation contained in the magnetic foliation and S1, trends NNE-SSW with moderate north-northeast plunge (K_{\max} mean vector=028/59, $\alpha_{95}=26.7^\circ$, $k=33.5$) (Fig. 7a site Z19). Northwest of Yala Xiangbo and south of Yardoï three sites describe triaxial ellipsoids and magnetic foliation striking SW-NE with moderate dip values towards the northwest. The cluster of K_{\max} values describes a magnetic lineation trending NNW-SSE with 43° plunge towards the north-northwest (Fig. 8b). Moving towards Zetang and the Great Counter Thrust the AMS ellipsoid is oblate (sites Q16 and Q17) and magnetic foliation strikes WNW-ESE but with southward dip similar to S2 tectonic foliation (Figs. 7a site Q16 & 8a). From these results we can define two domains within sector 2 with opposite dip of the magnetic foliation and tectonic foliation (Figs. 7a & 8a).

Sector 3 lies geographically between north of the Dala pass and Qusum. Tectonically this area is east of the Cona Graben and south of the Qusum Thrust. Eastward of the Yala Xiangbo (sites Tu and We) AMS ellipsoids are triaxial, the magnetic foliation has a NW-SE strike and dips about 60° to the northeast parallel to S1 (Fig. 7a site Tu2). The magnetic lineation trends NW-SE and plunges to the northwest and southeast. Moving to the north the magnetic foliation changes to E-W strike and the magnetic lineation becomes E-W with a

gentle plunge to the east parallel to the intersection of S1 and S2 tectonic foliations. In the proximity of the Qusum Thrust and the S2 domain, the magnetic ellipsoid switches to be more prolate (e.g. $T = -0.13$ in site Qu20). Here magnetic lineation trends E-W with almost horizontal plunge, parallel to the intersection of S1 and S2 tectonic foliations (Fig. 7b site Qu20 & Fig. 8b).

Sector 4 is located between the Great Counter Thrust and the Qusum Thrust where S2 is the main tectonic foliation. The southern and central parts present AMS ellipsoids which are slightly prolate (sites Mv27, Mv29, Fv38, Pa40) or oblate AMS ellipsoids (Fig. 7b site Mv27). The magnetic foliation reflected in the oblate ellipsoids (sites Sr24, Sr25, Mv26, Mv28, Mv30 & Yt34) has WNW-ESE strike and south-southwest dips parallel to S2 tectonic foliation. The slightly prolate ellipsoids present magnetic lineations with E-W direction and gentle plunges towards the west and are parallel to the F2 fold axes and the lineation defined by the intersection of S1 and S2 foliation. Towards the north, close to the Great Counter Thrust and the Indus Yarlung Suture Zone (sites Sr23, Yt32 & Yt33), ellipsoids turn to triaxial shape. Magnetic foliation trends W-E with steep dips towards the south and the magnetic lineation trends N-S with a 67° plunge to the south (sites Yt32 & Yt33), parallel to the stretching lineation and perpendicular to the Great Counter Thrust surface (Fig. 7b site Yt32 & Fig. 8a & b).

Figure 8: (a) Magnetic foliation map and lower-hemisphere, equal-area stereogram with the K_{\min} mean vector for sector 2 south of Yardoi, sector 2 south of Qonggyai, sector 3, sector 4 and scattered distribution of single sites K_{\min} mean vector of sector 1. (b) Magnetic lineation map and lower-hemisphere, equal-area stereogram of K_{\max} mean vector for sector 1 and 2, and K_{\max} mean vector for sites within sectors 3 and 4. Both maps follow the same map legend of Fig. 3 with grey scale colors.



2.9 Tectonic interpretation and sequence of magnetic fabric development

Magnetic foliation and lineation in the slates of the Triassic flysch are the result of a complex sum of tectonic and metamorphic phases from the India-Asia collision until present. We suggest a 5-stage-evolution of the magnetic fabric supported by the structural properties to constraint the kinematic evolution of the eastern Tethyan Himalaya. Magnetic foliation and lineation have been analysed referred to their present-day orientation (see Fig. 9 for kinematic model proposed here and Fig. 2 to comparison with other kinematic models previously proposed):

1st Stage

During the Eohimalayan or D1 phase (Middle Eocene-Late Oligocene; Hodges 2000; Fig. 2) the collision of India and Asia produced the development of E-W trending south facing isoclinal folds with related axial planar foliation (S1). This is shown south of Qonggyai (sector 2; Fig. 4a & Fig. 8a) by well grouping K_{\min} directions and K_{\max} and K_{int} axes scattered within the tectonic S1 foliation plane (Fig. 9a).

2nd Stage

Near the locality of Qonggyai where D1 phase governs the orientation of the structures, the magnetic lineation is interpreted as the direction of stretching lineation of the phyllosilicates, under the prevailing stress field, during thrust sheet emplacement as has been described in other thrust structures (Oliva-Urcia *et al.* 2009). The plunge of the magnetic lineation indicates thrust emplacement towards the S-SW (Himalayan foreland) (Fig. 9b) in agreement with the south-directed displacement along the Lhunze fault, 15 km south of the studied sites (Aikman *et al.* 2008). Detailed structural and thermochronological analysis should be carried on the Lhunze Fault to closely constraint the timing and local and regional importance of this fault.

3rd Stage

Continuous deformation in the flysch thrust-wedge produced a change in the fold vergence around 20 km south of the Indus Yarlung Suture Zone and the Gangdese granite. This north-vergent deformation starts with the incipient development of the north-vergent F2 folds and related S2 crenulation cleavage (Fig. 2). This switch of vergence in the structures is recorded in the magnetic fabric by a subtle prolate ellipsoid with K_{\min} axes distributed in a semicircle (Figs. 7b sites Qu20, Mv27; Fig. 9c). This stage of magnetic fabric is similar to the stage of pencil cleavage (e.g. Borradaile & Tarling 1981; Housen *et al.* 1993; Parés *et al.* 1999) characterized by the incipient development of a new planar feature, in our case the foliation S2. This composite fabric reflects a combination of the S1 and the younger S2 foliation with K_{\max} axes strikingly E-W with gentle plunge, parallel to the intersection lineation between S1

and S2 (L12). The reason for this parallelism is that this direction is the intersection axis between the iron sheet silicates (Parés *et al.* 1999). As the foliation S2 becomes pervasive it transposes the older S1 and K_{\min} cluster parallel to the pole of S2 tectonic foliation. K_{\max} and K_{int} axes are distributed in a girdle that coincides with the S2 foliation plane. The time interval for the S2 foliation development can be related to the *c.* 24 Ma K/Ar ages found in illites (Dunkl *et al.* 2008), which we relate to an authigenic origin linked to the formation of the foliation S2. As deformation increases K_{\max} and K_{\min} axes become tightly clustered (triaxial ellipsoid) and magnetic lineation trends E-W parallel to F2 axes and the intersection lineation of S1 and S2 foliations (e.g. Fig 8b sites Fv35 and Sr23).

4th Stage

Continuation of backward deformation towards higher structural levels was probably responsible for the formation of the north-directed Great Counter backthrust around 18 Ma to 10 Ma (Quidelleur *et al.* 1997; Harrison *et al.* 2000; Fig. 2) which placed the Triassic flysch over the mélangé complex or the Cretaceous rocks. This event is reflected in the N-S direction and 67° southward plunge of the magnetic lineation that is strikingly coincident with the stretching lineation in sites Yt32 and Yt33. The magnetic lineation is the expression of the strain undergone by the hangingwall of the Great Counter backthrust during its emplacement (Fig. 9d).

5th Stage

From a more speculative point of view the 5th stage suggests two possible processes, which during the Middle Miocene resulted in the change of the E-W trend of the Eohimalayan magnetic foliation preserved in the Qonggyai valley to the NW-SE trend of the post-Eohimalayan magnetic foliation near Nagarze (sector 1) and east of the Cona Graben (sectors 3 and 4). The first possibility is an approximately 20° clockwise rotation of the magnetic foliation related to vertical-axis rotations during the eastward extrusion of the Tibetan plateau (Tapponnier *et al.* 1982). Schill *et al.* (2004) also reported clockwise rotation in the central Tethyan Himalaya based on secondary remanence directions which were probably acquired during the last metamorphic cooling in Late Oligocene or Early Miocene times. Gan *et al.* (2007) describe a NE trend of GPS velocities in SE Tibet. Their data furthermore indicate that the GPS velocity east of the Cona Graben is more eastward directed which implies a clockwise rotation of this area relative to the adjacent area in the west. The second possibility can be associated with the doming of the North Himalayan domes. The magnetic foliation around the Yala Xiangbo describes a slight bend that is parallel to the contact of the dome with the flysch and in Nagarze area the inclination of the magnetic foliation and lineation decreases towards east of the flank of the Jangsang Lhamo dome. These two facts can suggest

that the Triassic flysch had passively accommodated the doming around 18-13.5 Ma (Aikman *et al.* 2004) producing block rotations and tilting of the neighbouring structural elements.

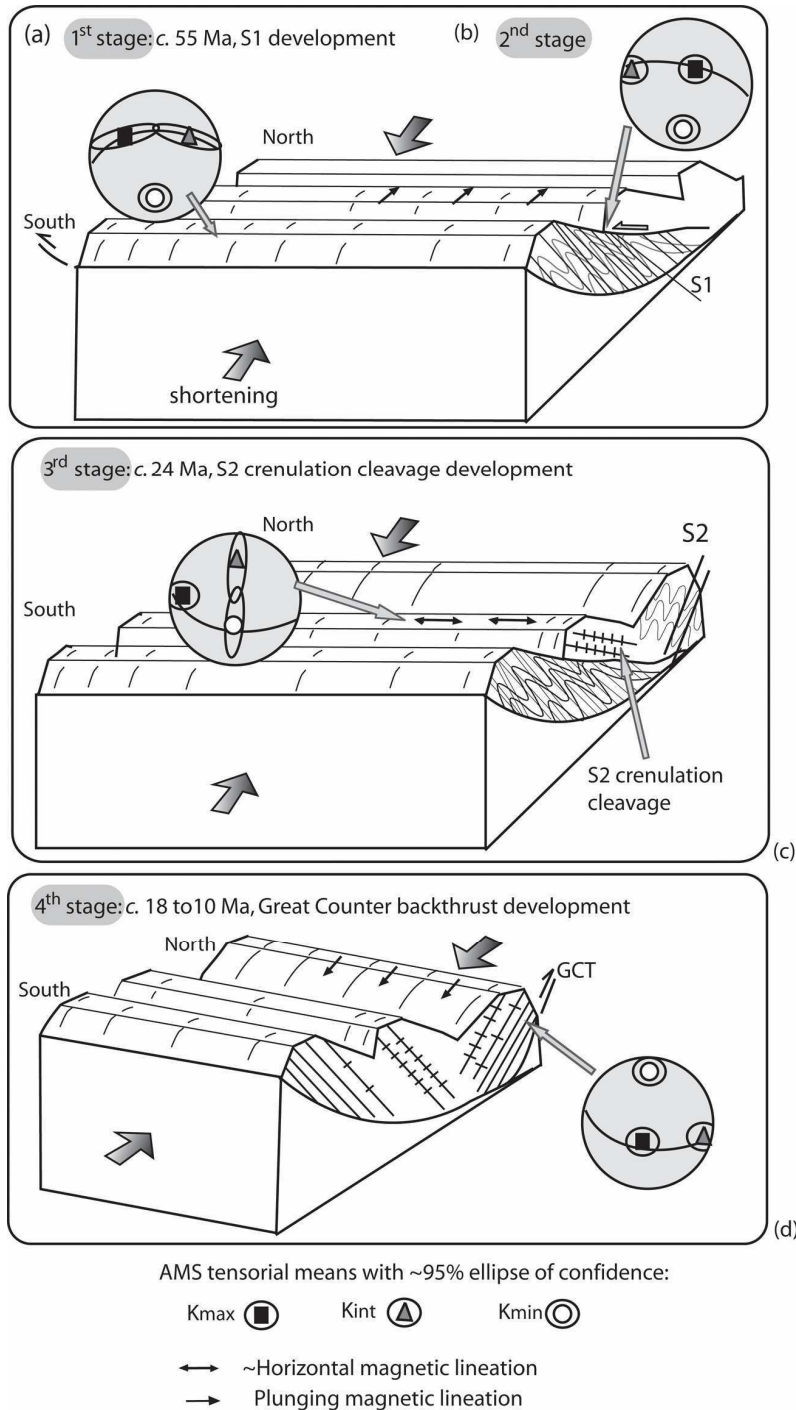


Figure 9: Block diagrams showing the successive stages of the magnetic fabric evolution and the kinematics of the Triassic flysch in the eastern Tethyan Himalaya: (a) 1st stage, (b) 2nd stage, (c) 3rd stage and (d) 4th stage.

2.10 Conclusions

The AMS and structural data collected in the Triassic flysch of the Tethyan Himalaya indicate that the magnetic fabric is an indicator of progressive deformation when the original foliation is overprinted, and allow us to reconstruct the fabric and tectonic evolution processes in SE Tibet.

In the studied slates magnetic susceptibility is predominantly carried by the paramagnetic fraction. This is shown by temperature dependence of the susceptibility following the $\sim 1/T$ Curie law, the comparison between the high field versus the low field susceptibilities and the parallelism between tectonic and magnetic foliation.

AMS provides quantitative information about the orientation of phyllosilicates alignment and the degree and shape of the AMS ellipsoid. Directions of stretching and intersection of the two foliations have been detected even when it is difficult to identify them in the field or only possible to measure them with extensive time consumption. AMS combined with structural studies allow to gain a deeper structural insight on the evolution of the Triassic flysch within the eastern Tethyan Himalaya. Two different tectonic domains can be defined. East of the Cona graben these domains are separated by the Qusum Thrust. The southern domain is structurally dominated by E-W striking and north dipping magnetic foliation parallel to the Eohimalayan S1 tectonic foliation in accordance with the characteristic south vergence of the orogen. North of the Qusum Thrust “backward” deformation is reflected in the magnetic foliation and tectonic S2 foliation which have WNW-ESE direction and dips to the south, opposite to the main vergence of the Himalayan system. In between the two domains an intermediate magnetic fabric is found where the incipient S2 foliation overlaps the S1 foliation and K_{\max} cluster roughly parallel to the intersection of S1 and S2 tectonic foliations. K/Ar age of *c.* 24 Ma (Dunkl *et al.* 2008) have been related to new micas with an authigenic origin linked to the formation of the S2 foliation. The two domains described in this study are the result of D1 and D2 deformation phases which can be observed in other N-S sections along the fold-thrust belt (Fig. 2), indicating no major changes in deformation features along E-W strike of the Tethyan Himalaya.

Magnetic lineation is interpreted as the transport direction of thrust structures in two locations within the study area. Near Qonggyai we identified a north-northeast plunging magnetic lineation that is related to the phyllosilicates elongation direction, and could be the expression of the strain caused in the footwall of the Lhunze basement thrust. Close to the Yarlung Tsangpo, the magnetic lineation shows N-S trend and steep south plunge, and recorded the transport direction of the Neohimalayan Great Counter backthrust about 18 Ma to 10 Ma (Quidelleur *et al.* 1997; Harrison *et al.* 2000) synchronous with the activity on the MCT and STDS (Yin *et al.* 1994).

Different orientations of magnetic foliations may indicate a Middle Miocene *c.* 20° clockwise vertical-axis rotation. This result would be in accordance with clockwise block rotations in the central Himalaya observed in secondary remanence directions (Schill *et al.* 2004) and present GPS velocities (e.g. Gan *et al.* 2007) that point out large-scale dextral shearing caused by the eastward extrusion of the Tibetan Plateau. Likewise intrusion and exhumation of the North Himalayan domes can have induced block rotations and tilting of the adjacent tectonic elements. However these hypotheses need additional structural and palaeomagnetic analyses to be verified.

The authors thank the German Research Foundation (DFG) for financial support; Institute of Tibetan Plateau Research (ITP) and the Chinese Academy of Sciences (CAS) for logistic support. We thank Taba, Puchum, Nobu, and Xu Qiang for helping us during the field work. The authors are grateful to Zanist Hama-Aziz and Liu Yang for support in the magnetic measurements. We wish to thank B. Oliva-Urcia and R. Carosi for constructive comments. We deeply acknowledge the revisions from E. Pueyo, B. Housen, J. Poblet and R. Lisle which helped to improve the first version of the manuscript.

References

- Aikman, A., Harrison, T.M. & Ding, L. 2004. Preliminary results from the Yala-Xiangbo Leucogranite dome, SE Tibet. *Himalaya Journal of Sciences*, 2, 91.
- Aikman, A., Harrison, T.M. & Ding, L. 2008. Evidence for Early (>44 Ma) Himalayan Crustal Thickening, Tethyan Himalaya, southeastern Tibet. *Earth and Planetary Science Letters*, 274, 14-23.
- Appel, E., Müller, R., Widder, R.W. 1991. Palaeomagnetic results from the Tibetan Sedimentary Series of the Manang area (north central Nepal). *Geophysical Journal International*, 104, 255-266.
- Armijo, R., Tapponnier, P., Mercier, J.L. & Tonglin, H. 1986. Quaternary extension in southern Tibet: field observations and tectonic implications. *Journal of Geophysical Research*, 91, 13803-13872.
- Averbuch, O., Frizon de Lamotte, D. & Kissel, C. 1992. Magnetic fabric as a structural indicator of the deformation path within a fold-thrust structure: a test case from the Corbières (NE Pyrenees, France). *Journal of Structural Geology*, 14, 461-474.
- Berthé, D., Choukroune, P. & Jegouzo, P. 1979. Orthogneiss, mylonite and non coaxial deformation of granites: the example of the South Armorican Shear Zone. *Journal of Structural Geology*, 1, 31-42.
- Bonhomme, M. & Garzanti, E. 1991. Age of metamorphism in the Zaskar Tethys Himalaya (India). *Géologie Alpine*, 16, 15-16.
- Bouchez, J.L. 1997. Granite is never isotropic: an introduction to AMS studies of granitic rocks. In: Bouchez, J.L., Hutton, D.H.W. & Stephen, W.E. (eds) *Granite: From Segregation of Melt to Emplacement Fabrics*. Kluwer Academic Publishers, 95-112.
- Borradaile, G.J. & Tarling, D.H. 1981. The influence of deformation mechanism on magnetic fabrics in weakly deformed rocks. *Tectonophysics*, 77, 151-168.
- Borradaile, G.J. & Sarvas, P. 1990. Magnetic susceptibility fabrics in slates: structural, mineralogical and lithological influences. *Tectonophysics*, 172, 215-222.
- Borradaile, G.J. & Werner, T. 1994. Magnetic anisotropy of some phyllosilicates. *Tectonophysics*, 235, 223-248.
- Borradaile, G.J. & Jackson, M. 2004. Anisotropy of magnetic susceptibility (AMS): magnetic petrofabric of deformed rocks. In: Martín-Fernández, F., Lüneburg, C.M., Aubourg, C. & Jackson, M. (eds) *Magnetic Fabric: Methods and Applications*. Geological Society, London, Special Publications, 238, 299-360.
- Brookfield, M. 1993. The Himalayan passive margin from Precambrian to Cretaceous. *Sedimentary Geology*, 84, 1-35.
- Burchfiel, B.C., Zhiliang, C., Hodges, K.V., Yuping, L., Royden, L.H., Changrong, D. & Jiene, X. 1992. The South Tibetan detachment system, Himalaya orogen: extension contemporaneous with

- and parallel to shortening in a collisional mountain belt. Geological Society of America, Special Papers, 269.
- Burg, J.P. & Chen, G.M. 1984. Tectonics and structural zonation of southern Tibet, China. *Nature*, 311, 219-223.
- Burmeister, K.C., Harrison, M.J., Marshak, S., Ferré, E.C., Bannister, R.A. & Kodama, K.P. 2009. Comparison of Fry strain ellipse and AMS ellipsoid trends to tectonic fabric trends in very low-strain sandstone of the Appalachian fold-thrust belt. *Journal of Structural Geology*, doi: 10.1016/j.jsg.2009.03.010.
- Carosi, R., Montomoli, C. & Visonà, D. 2002. Is there any detachment in the Lower Dolpo (western Nepal)? *Comptes Rendus Geoscience*, 334, 933-940.
- Carosi, R., Montomoli, C. & Visonà, D. 2007. A structural transect in the Lower Dolpo: Insights on the tectonic evolution of Western Nepal. *Journal of Asian Earth Sciences*, 29, 407-423, doi: 10.1016/j.jseaes.2006.05.001.
- Chang, C. 1984. Les caractéristiques tectoniques et l'évolution de la zone de suture du Yarlung-Zangbo. In: Mercier, J.L. & Li, G.C. (eds) *Mission Franco-Chinoise Au Tibet 1980: Étude Géologique Et Géophysique De La Croûte Terrestre Et Du Manteau Supérieur Du Tibet Et De L'Himalaya*. Editions du Centre National de la Recherche Scientifique, Paris, France, 341-350.
- Chen, Z., Liu, Y., Hodges, K.V., Burchfiel, B.C., Royden, L.H. & Deng, C. 1990. The Kangmar dome: A metamorphic core complex in southern Xizang (Tibet). *Science*, 250, 1552-1556.
- Colchen, M., Le Fort, P. & Pêcher, A. 1986. *Annapurna-Manaslu-Ganesh Himal notice de la carte géologique au 1/200.000 (bilingual edition, French-English)*. Centre National de la Recherche Scientifique, Paris.
- Crouzet, C., Stang, H., Appel, E., Schill, E. & Gautam, P. 2001. Detailed analysis of successive pTRMs carried by pyrrhotite in Himalayan metacarbonates: an example from Hidden Valley Central Nepal. *Geophysical Journal International*, 146, 607-618.
- Crouzet, C., Dunkl, I., Paudel, L., Arkai, P., Rainer, T.M., Balogh, K. & Appel, E. 2007. Temperature and age constraints on the metamorphism of the Tethyan Himalaya in Central Nepal: A multidisciplinary approach. *Journal of Asian Earth Sciences*, 30, 113-130, doi:10.1016/j.jseaes.2006.07.014.
- Ding, L., Kapp, P. & Wan, X. 2005. Paleocene-Eocene record of ophiolite obduction and initial India-Asia collision, south central Tibet. *Tectonics*, 24, TC3001, doi:10.1029/2004TC001729.
- Dunkl, I., Lin, D., Montomoli, C., Wemmer, K., Rantisch, G., Antolin, B., El Bay, R. & Appel, E. 2008. Diagenetic and metamorphic overprint and deformation history of Permo-Triassic Tethyan sediments, SE Tibet. *Himalayan Journal of Sciences*, 5, 49.
- Dupuis, C., Hébert, R., Dubois-Coté, V., Wang, C.S., Li, Y.L. & Li, Z.J. 2005. Petrology and geochemistry of mafic rocks from mélange and flysch units adjacent to the Yarlung Zangbo Suture Zone, southern Tibet. *Chemical Geology*, 214, 287-308.
- Dupuis, C., Hébert, R., Dubois-Coté, V., Guilmette, C., Wang, C.S. & Li, Z.J. 2006. Geochemistry of sedimentary rocks from mélange and flysch units south of the Yarlung Zangbo suture zone, southern Tibet. *Journal of Asian Earth Sciences*, 26, 489-508.
- Edwards, M.A. & Harrison, T.M. 1997. When did the roof collapse? Late Miocene north-south extension in the high Himalaya revealed by Th-Pb monazite dating of the Khula Kangri granite. *Geology*, 25, 543-546.
- Fisher, N.I., Lewis, T. & Embleton, B.J.J. 1987. *Statistical analysis of spherical data*. Cambridge University Press, Cambridge.
- Flinn, D. 1962. On folding during three-dimensional progressive deformation. *Quarterly Journal of the Geological Society of London*, 118, 385-433.
- Fuchs, G. 1967. *Zum Bau des Himalaya*. Österreichische Akademie der Wissenschaften, Mathematisch-Naturwissenschaftliche Klasse, Denkschriften, 113, 1-211.
- Gaetani, M. & Garzanti, E. 1991. Multicyclic history of the northern Indian continental margin (northwestern Himalaya). *American Association of Petroleum Geologists, Bulletin*, 75, 1427-1446.
- Gan, W., Zhang, P., Shen, Z.-K., Niu, Z., Wang, M., Wan, Y., Zhou, D. & Cheng, J. 2007. Present-day crustal motion within the Tibetan Plateau inferred from GPS measurements. *Journal of Geophysical Research*, 112, B08416, doi: 10.1029/2005JB004120.
- Gansser, A. 1964. *Geology of the Himalayas*. Wiley Interscience, London.
- Garzanti, E. 1999. Stratigraphy and sedimentary history of the Nepal Tethys Himalaya passive margin. *Journal of Asian Earth Sciences*, 17, 805-827.

- Garzanti, E., Gorza, M., Martellini, L. & Nicora, A. 1994. Transition from diagenesis to metamorphism in the Paleozoic to Mesozoic succession of the Dolpo-Manang synclinorium and Thakkola graben (Nepal Tethys Himalaya). *Eclogae Geologicae Helveticae*, 87, 613-632.
- Garzione, C.N., DeCelles, P.G., Hodkinson, D.G., Ojha, T.P. & Upreti, B.N. 2003. East-west extension and Miocene environmental change in the southern Tibetan plateau: Thakkhola graben, central Nepal. *Geological Society of America Bulletin*, 115, 3-20.
- Godin, L. 2003. Structural evolution of the Tethyan sedimentary sequence in the Annapurna area, central Nepal Himalaya. *Journal of Asian Earth Sciences*, 22, 307-328.
- Godin, L., Grujic, D., Law, R.D. & Searle, M.P. 2006. Channel flow, extrusion and exhumation in continental collision zones: an introduction. In: Law, R.D., Searle, M.P. & Godin, L. (eds) *Channel Flow, Ductile Extrusion and Exhumation in Continental Collision Zones*. Geological Society, London, Special Publications, 268, 1-23.
- Grasemann, B. & Vannay, J.-C. 1999. Flow controlled inverted metamorphism in shear zones. *Journal of Structural Geology*, 21, 743-750.
- Grujic, D., Hollister, L. & Parrish, R.R. 2002. Himalayan metamorphic sequence as an orogenic channel: insight from Bhutan. *Earth and Planetary Science Letters*, 198, 177-191.
- Guillot, S., Pêcher, A., Rochette, P. & LeFort, P. 1993. The emplacement of the Manaslu granite of central Nepal: field and magnetic susceptibility constraints. In: Treloar, P.J. & Searle, M.P. (eds) *Himalayan tectonics*. Geological Society, London, Special Publications, 74, 413-428.
- Harrison, T.M., Yin, A., Grove, M. & Lovera, O.M. 2000. The Zedong Window: A record of superposed Tertiary convergence in southeastern Tibet. *Journal of Geophysical Research*, 105, 19,211-19,320.
- Heim, A. & Gansser, A. 1939. Central Himalaya. *Geological Observations of the Swiss Expedition 1936. Mémoires de la Société Helvétique des Sciences Naturelles*, 7/31, 1-245.
- Hirt, A.M., Lowrie, W., Clendenen, W.S. & Kligfield, R. 1988. The correlation of magnetic anisotropy with strain in the Chelmsford Formation of the Sudbury Basin, Ontario. *Tectonophysics*, 145, 177-189.
- Hodges, K.V. 2000. Tectonics of the Himalaya and southern Tibet from two perspectives. *Geological Society of America Bulletin*, 112, 324-350.
- Holt, W.E., Ni J.F., Wallace, T.C. & Haines, A.J. 1991. The Active Tectonics of the Eastern Himalayan Syntaxis and Surrounding Regions. *Journal of Geophysical Research*, 96 (B9), 14,595-14,632.
- Housen, B.A., Richter, C. & van der Pluijm, B.A. 1993. Composite magnetic anisotropy fabrics: experiments, numerical models, and implications for the quantification of rock fabrics. *Tectonophysics*, 220, 1-12.
- Jelinek, V. 1977. The statistical theory of measuring anisotropy of magnetic susceptibility of rocks and its application. *Geofyzika Brno*.
- Kellett, D.A & Godin, L. 2009. Pre-Miocene deformation of the Himalayan superstructure, Hidden valley, central Nepal. *Journal of the Geological Society, London*, 166, 261-275.
- Kneen, S. 1976. The relationship between the magnetic and strain fabrics of some haematite-bearing Welsh slates. *Earth and Planetary Science Letters*, 31, 413-416.
- Lee, J., Hacker, B.R., Dinklage, W.S., Wang, Y., Gans, P., Calvert, A., Wan, J.L., Chen, W.J., Blythe, A.E. & McClelland, W. 2000. Evolution of the Kangmar Dome, southern Tibet: Structural, petrologic, and thermochronologic constraints. *Tectonics*, 19, 872-895.
- Le Fort, P. 1975. Himalayas, the collided range. Present knowledge of the continental arc. *American Journal of Science*, 275-A. 1-44.
- Liu, G. 1992. Permian to Eocene sediments and Indian passive margin evolution in the Tibetan Himalayas. *Tübinger Geowissenschaftliche, A 13*, 1-268.
- Liu, G & Einsele, G. 1994. Sedimentary history of the Tethyan basin in the Tibetan Himalayas. *Geologische Rundschau*, 83, 32-61.
- Liu, G & Einsele, G. 1996. Various types of olistostromes in a closing ocean basin, Tethyan Himalaya (Cretaceous, Tibet). *Sedimentary Geology*, 104, 203-226.
- Martín-Hernández, F. & Hirt, A. M. 2003. The anisotropy of magnetic susceptibility in biotite, muscovite and chlorite single crystals. *Tectonophysics*, 337, 13-28.
- McQuarrie, N., Robinson, D., Long, S., Tobgay, T., Grujic, D., Gehrels, G., Ducea M. 2008. Preliminary stratigraphic and structural architecture of Bhutan: Implications for the along strike architecture of the Himalayan system. *Earth and Planetary Science Letters*, 272, 105-117.

- Montomoli, C., Appel, E., Antolin, B., Dunkl, I., El Bay, R., Lin, D. & Gloaguen, R. 2008. Polyphase deformation history of the "Tibetan Sedimentary Sequence" in the Himalaya chain (South-East Tibet). *Himalayan Journal of Sciences*, 5, 91.
- Nagata, T. 1961. *Rock Magnetism*. Maruzen, Tokyo.
- Najman, Y., Carter, A., Oliver, G. & Garzanti, E. 2005. Provenance of Eocene foreland basin sediments, Nepal: Constraints to the timing and diachroneity of early Himalayan orogenesis. *Geology*, 33, 309-312.
- Oliva-Urcia, B., Larrasoana J.C., Pueyo, E.L., Gil, A., Mata, P., Parés, J.M., Schleicher, A.M. & Pueyo, O. 2009. Disentangling magnetic subfabrics and their link to deformation processes in cleaved sedimentary rocks from the Internal Sierras (west central Pyrenees, Spain). *Journal of Structural Geology*, 31, 163-176.
- Pan, G., Ding, J., Yao, D. & Wang, L. 2004. Geological map of Qinghai-Xizang (Tibet) Plateau and Adjacent Areas (1:1,500,000). Chengdu Institute of Geology and Mineral Resources, China Geological Survey. Chengdu Cartographic Publishing House.
- Parés, J.M. & van der Pluijm, B. 2002. Evaluating magnetic lineations (AMS) in deformed rocks. *Tectonophysics*, 350, 283-298.
- Parés, J.M., van der Pluijm, B.A. & Dinarès-Turell, J. 1999. Evolution of magnetic fabric during incipient deformation of mudrocks (Pyrenees, northern Spain). *Tectonophysics*, 307, 1-14.
- Patzelt, A., Li, H., Wang, J. & Appel, E. 1996. Paleomagnetism of Cretaceous to Tertiary sediments from southern Tibet: evidence for the extent of the northern margin of India prior to the collision with Eurasia. *Tectonophysics*, 259, 259-284.
- Pêcher, A. 1991. The contact between the higher Himalayan crystalline sediments and the Tibetan sedimentary series: Miocene large-scale dextral shearing. *Tectonics*, 10, 587-598.
- Pueyo, E.L., Román-Berdiel, T., Bouchez, J.L., Casas, A.M. & Larrasoana, J.C. 2004. In: Martín-Fernández, F., Lüneburg, C.M., Aubourg, C. & Jackson, M. (eds) *Magnetic Fabric: Methods and Applications*. Geological Society, London, Special Publications, 238, 395-420.
- Quidelleur, X., Grove, M., Lovera, O.M., Harrison, T.M. & Yin, A. 1997. Thermal evolution and slip history of the Renbu-Zedong Thrust, southeastern Tibet. *Journal of Geophysical Research*, 102, 2659-2679.
- Ratschbacher, L., Frisch, W., Liu, G., Chen, C. 1994. Distributed deformation in southern and western Tibet during and after the India-Asia collision. *Journal of Geophysical Research*, 99, 19,917-19,945.
- Richter, C. & van der Pluijm, B.A. 1994. Separation of paramagnetic and ferrimagnetic susceptibilities using low temperature magnetic susceptibilities and comparison with high field methods. *Physics of the Earth and Planetary Interiors*, 51, 113-123.
- Rochette, P. 1987. Metamorphic control of the magnetic mineralogy of black shales in the Swiss Alps: toward the use of "magnetic isograds". *Earth and Planetary Science Letters*, 84, 1015-1020.
- Román-Berdiel, T., Casas, A.M., Oliva-Urcia, B., Pueyo, E. & Rillo, C. 2004. The main Variscan deformation event in the Pyrenees: new data from the structural study of the Bielsa granite. *Journal of Structural Geology*, 17, 1337-1346.
- Schill, E., Appel, E., Godin, L., Crouzet, C., Gautam, P. & Regmi, K. 2003. Record of deformation by secondary magnetic remanences and magnetic anisotropy in the Nar/Phu valley (central Himalaya). *Tectonophysics*, 377, 197-209.
- Schill, E., Appel, E., Crouzet, C., Gautam, P., Wehland, F. & Staiger, M. 2004. Oroclinal bending versus regional significant clockwise rotations in the Himalayan arc-Constrains from secondary pyrrhotite remanences. In: Sussman, A.J. & Weil, A.B. (eds) *Orogenic Curvature: Integrating Paleomagnetic and Structural Analyses*. Geological Society of America Special Paper, 383, 73-85.
- Searle, M. 1986. Structural evolution and sequence of thrusting in the High Himalayan, Tibetan-Tethys and Indus suture zones of Zaskar and Ladakh, Western Himalaya. *Journal of Structural Geology*, 8, 923-936.
- Soto, R., Mattei, M. & Casas, A.M. 2003. Relationship between AMS and folding in an area of superimposed folding (Cotiella-Bóixols nappe, Southern Pyrenees). *Geodinamica Acta*, 16, 171-185.
- Steck, A. 2003. Geological Map of the NW Himalaya. *Eclogae Geologicae Helvetiae*, 96 (2), 147-U13.
- Stöcklin, J. 1980. Geology of Nepal and its regional frame. *Journal of the Geological Society*, London, 137, 1-34.

- Tapponnier, P., Peltzer, G., Le Dain, A.Y., Armijo, R & Cobbold, P. 1982. Propagating extrusion tectonics in Asia: New insights from simple experiments with plasticine. *Geology*, 10, 611-616.
- Tarling, D.H. & Hrouda, F. 1993. *The Magnetic Anisotropy of Rocks*. Chapman and Hall, London.
- Valdiya, K.S. 1980. *Geology of the Kumaun Lesser Himalaya*. Dehra Dun, Wadia Institute of Himalayan Geology.
- Willems, H., Zhou, Z., Zhang, B., Gräfe, K. U. 1996. Stratigraphy of the Upper Cretaceous and Lower Tertiary strata in the Tethyan Himalayas of Tibet (Tingri area, China). *Geologische Rundschau*, 85, 723-754.
- Yin, A. 2006. Cenozoic evolution of the Himalayan Orogen as constrained by along strike variations of structural geometry, exhumation history, and foreland sedimentation. 2006. *Earth-Science Reviews*, 76, 1-131.
- Yin, A. & Harrison, T.M. 2000. Geologic evolution of the Himalayan-Tibetan orogen. *Annual Review of Earth and Planetary Sciences*, 28, 211-280.
- Yin, A., Harrison, T.M., Ryerson, F.J., Wenji, C., Kidd, W. & Copeland, P. 1994. Tertiary structural evolution of the Gangdese thrust system, southeastern Tibet. *Journal of Geophysical Research*, 99, 18,175-18,201.
- Zhang, B., Zhang, J., Guo, L. & Wang, W. 2005. Microstructural and deformational studies on mylonite in the detachment faults of Yalashangbo dome, North Himalayan domes zone. *Progress in Natural Science*, 15, 11, 1005-1013.

3

Metamorphic evolution of the Tethyan Himalayan flysch in SE Tibet

3.1 Abstract

The metamorphic conditions and the age of thermal overprint were determined in metapelites, metaarenites and metabasites of the Tethyan Himalayan Sequence (THS) in SE Tibet by using Kübler Index and vitrinite reflectance data and applying, thermobarometrical (Thermocalc and Perplex) and geochronological (illite/muscovite K-Ar and zircon (U-Th)/He chronology) methods. The multiple folded thrust pile experienced a four-stage tectonothermal overprint with peak conditions varying locally between the diagenetic stage (*c.* 170 °C) and the amphibolite facies (*c.* 600 °C at 10 kbar). Burial diagenesis and heating due to Early Cretaceous dyke emplacement generated the first growth of illite in the metapelites. During the Himalayan collision (*c.* 44 Ma) some tectonic blocks of the THS were buried tectonically to deeper crustal level and experienced greenschist to amphibolite facies metamorphism (D1). Later, during Oligocene to Miocene times the entire THS was probably continuously deformed and underwent anchi- to epizonal metamorphic conditions (D2). This period terminated at *c.* 24-22 Ma. The base of the THS was metamorphosed close to the north Himalayan metamorphic domes in Miocene times (*c.* 13 Ma). The post-metamorphic cooling below *c.* 180 °C lasted until Late Miocene and took place heterochronously.

3.2 Introduction

The northward drift of Greater India during the Cenozoic resulted in the closure of the Tethys sea, the initiation of the India-Asia collision in the Paleocene and the subsequent uplift of the Himalayan Range (c. 55-50 Ma; e.g. Gaetani & Garzanti 1991; Patzelt *et al.* 1996; Najman *et al.* 2005). The Himalayan arc forms an active WNW-ESE asymmetric fold and thrust belt with a main southward vergence (Fig. 1a, b). The northern member of the Himalaya is the Tethyan Himalayan Sequence (THS) which is located in the highest structural position within the orogen (Le Fort 1975; Hodges 2000; Fig. 1a, b). For that reason the rocks forming the THS have probably better preserved the early tectonothermal evolution of the Himalayan orogen than other tectonometamorphic units, like the Greater Himalayan mid-crustal rocks which have nearly lost their pre-climax memory during metamorphism around 23-17 Ma (Guillot *et al.* 1994; Harrison *et al.* 1997; Searle & Godin 2003; Godin 2006).

The THS can be traced along the 2500 km of the Himalayan arc between the Nanga Parbat syntaxis in the west and the Namche Barwa syntaxis in the east (Fig. 1). The Cambrian to Eocene sequence is composed of very variable lithologies, derived from different sedimentary facies zones of the former passive continental margin of the Indian plate (e.g. Brookfield 1993; Willems *et al.* 1996; Garzanti 1999). Some tectonic domains are altered only diagenetically and usually low-grade metamorphism was not exceeded (e.g. Fuchs 1967; Hodges *et al.* 1996; Crouzet *et al.* 2007).

The aim of this study is to constrain the tectonothermal evolution of the THS from metamorphic and geochronological data. In the study area (Fig. 1b) few metamorphic and geochronological studies have been done so far. The present study focuses on north-south profiles along 250 km between Nagarze in the west (90°20'E) and Gyaca in the east (92°50'E) (Fig. 2). The studied profiles are distributed along valleys south of the Indus-Yarlung River. From west to east the main studied valleys are given by the name of the major localities (length of the profile in brackets): Nagarze (85 km), Zetang (45 km), Qusum (70 km) and Gyaca (17 km).

Kübler Index (KI) for 'illite crystallinity', vitrinite reflectance data, and K-Ar dating of micron and sub-micron fractions of illite are used to constrain the degree and age of metamorphism on metapelites, slates and sandstones of the Triassic flysch, the dominant sequence of the eastern THS. Thermobarometric methods (Thermocalc and Perplex, Holland & Powell 1998 and Connolly & Petrinin 2002, respectively) were applied on Triassic slates and metamorphosed basic dyke rocks, which experienced a greenschist to amphibolite facies overprint.

3.3 Geological Setting

The major tectonic elements in the Himalayan Range are from south to north, the Himalaya Frontal Thrust (HFT), the Main Boundary Thrust (MBT), the Main Central Thrust (MCT), the South Tibetan Detachment System (STDS), the Great Counter Thrust (GCT) and the Indus Yarlung Suture Zone (IYSZ; Fig. 1b, c; Hodges 2000; Upreti 2001 and references therein; Yin 2006). These structural elements divide the Himalaya into 3 main units traceable along the entire mountain belt. The Lesser Himalayan sequence between MBT and MCT is composed of Proterozoic to Cambrian sediments deposited on the proximal Indian shelf. Paleocene sediments are found in the eastern part of the belt (Stöcklin 1980; Valdiya 1980). This sequence was deformed by thrust and folds under very low-grade metamorphic conditions (Le Fort 1975; De Celles *et al.* 2001; Robinson *et al.* 2003; Paudel & Arita 2006). The Greater Himalayan Sequence (GHS) in the hangingwall of the north dipping MCT consists of high grade meta-sediments, meta-igneous rocks (Le Fort 1971; Pêcher 1975; Grujic *et al.* 2002; Searle & Godin 2003) and leucogranitic intrusions in the footwall of the STDS (e.g. Guillot *et al.* 1993; Searle & Godin 2003). The uppermost unit, the Tethyan Himalayan Sequence is bordered by STDS and GCT and forms the cover of the Greater Himalayan Sequence. The middle part of the THS is characterized by the outcrop of the North Himalayan gneiss domes which core is formed by leucogranite bodies of Early Miocene age (e.g. Lee *et al.* 2000; Leech 2008).

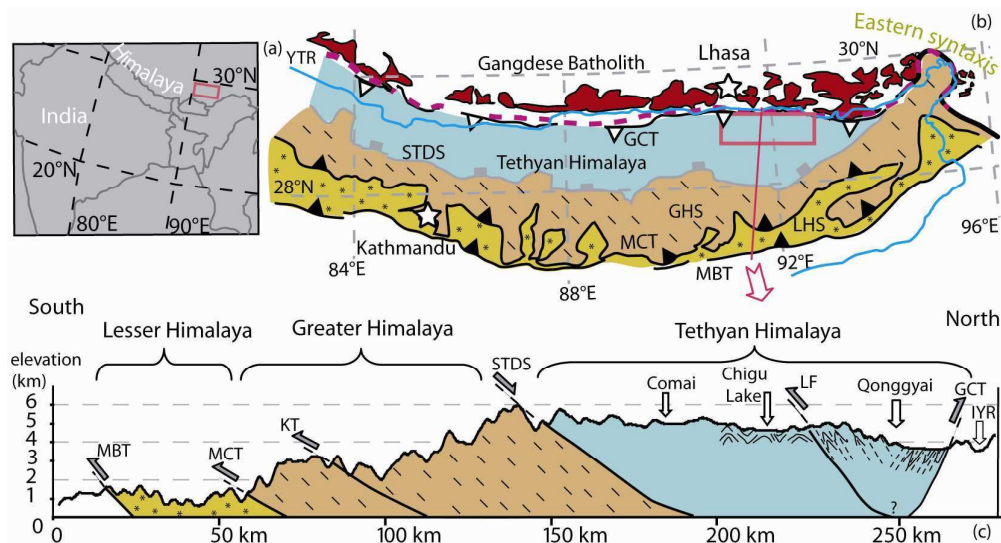


Figure 1: (a) Position of the study area in SE Tibet (red box). (b) Major structural units of Central and Eastern Himalayas. The study area (red box, see Fig. 2) situated close to the eastern termination of Tethyan Himalayan Sequence. Violet dashed line shows the Indus-Yarlung suture zone; YTR: Yarlung Tsangpo River; GCT: Great Counter Thrust; STDS: South Tibetan Detachment System; GHS: Greater Himalayan Sequence; MCT: Main Central Thrust; LHS: Lesser Himalayan Sequence; MBT: Main Boundary Thrust (simplified after Pan *et al.* 2004; Yin 2006). (c) Schematic cross section along the red line in Fig. 1b. KT: Kakhtang thrust, STDS attitude from Grujic *et al.* 2002 (and

references therein), McQuarrie *et al.* 2008. Structures in the northern Tethyan Himalaya from Antolín *et al.* (in press).

3.3.1 The Tethyan Himalayan Sequence

The Tethyan Himalayan Sequence involves a Cambro-Ordovician to Eocene pile that crops out along *c.* 150 km between STDS and IYSZ (Fig. 1; Brookfield 1993; Pan *et al.* 2004), deposited on the passive northern margin of the Indian continent (Fuchs 1967; Willems *et al.* 1996; Garzanti 1999). The Gyrong-Kangmar thrust in south-central Tibet divides the Tethyan Himalaya into two sub-units (Liu 1992; Liu & Einsele 1994). The southern sub-unit, north of the STDS, is formed by more than 13 km thick Cambrian to Eocene carbonates of the former passive margin, whereas the northern sub-unit is composed of Cretaceous clastic sediments recording the separation of the Indian plate from Gondwana and the drift to abyssal conditions (Willems *et al.* 1996). Towards the east, in SE Tibet, Lhunze fault (Fig. 2) separates the passive paleomargin into two sub-units (Aikman *et al.* 2008). South of it, the Tethyan sediments are composed of Cretaceous clastic rocks, Jurassic-Cretaceous marine clastic rocks intercalated with intermediate-basic volcanic rocks, and marine limestones in the hangingwall of the STDS (Fig. 2; Pan *et al.* 2004). The sub-domain north of the Lhunze fault is built up by turbiditic sandstones and slates -subsequently called flysch- deposited in an abyssal and bathyal environment between Middle Triassic and Early Jurassic (Mercier *et al.* 1984; Pan *et al.* 2004; Dupuis *et al.* 2005). In the north the flysch is juxtaposed against rocks of the active palaeomargin (Lhasa block), ophiolites related to the IYSZ and the *mélange* complex. This contact is traceable from the western to the eastern Himalaya and is differentiated by the Great Counter Thrust (Fig. 1a; Heim & Gansser 1939; Ratschbacher *et al.* 1994; Yin *et al.* 1994; Quidelleur *et al.* 1997). The *mélange* complex (limestones, cherts, marbles, shales, phyllites, andesites, diorites, mafic and ultramafic bodies) deposited on the growing Neo-Tethys ocean floor (e.g. Searle *et al.* 1986). The southern border of the Lhasa block is made up of Cretaceous clastic rocks and the Gangdese granite (Yin *et al.* 1994; Harrison *et al.* 2000; Pan *et al.* 2004). Ophiolites are widespread distributed along the suture and related to a supra-subduction environment (Ding *et al.* 2005; Dupuis *et al.* 2005, 2006).

3.3.2 Mafic magmatism

SE Tibet the Tethyan flysch sequence is penetrated by basalt, diabase, gabbroic diabase, diorite, olivine websterite and lherzolite dikes (Zhu *et al.* 2008; Xu *et al.* 2009). The silica content ranges from 43 to 55 %. The thickness of the dykes is variable; it ranges from a few meters to *c.* 100 m. The texture and the typical crystal size are also very variable from fine

grained, nearly aphanitic to very coarse-grained holocrystalline. In the ultramafic members poikilitic or cumulate textures are typical. According to zircon SHRIMP U/Pb geochronology the dykes intruded 145 to 130 Ma ago (Xu *et al.* 2009). Some of the magmatic bodies and typically their interior parts show well preserved magmatic textures, but in many occurrences the dykes are strongly deformed and transformed to chlorite or amphibole schists. The dykes form usually dissected boudins; the margins and the contact aureoles of the dykes are mainly detached or altered to banded, chaotic, mica-rich zones.

3.3.3 Structural setting of the Tethyan Himalaya

The entire Tethyan sequence has been folded and imbricated during four main tectonic stages. In the southern sector of the study area the first tectonic phase (D1), referable to the Eohimalayan phase (Hodges 2000), is the main deformation phase. It is related to the Middle Eocene to Late Oligocene collision of India with Asia and characterized by top-to-the-south thrust faults and south-vergent folds (F1) with a related axial plane foliation S1 (e.g. Burg and Chen 1984; Ratschbacher *et al.* 1994, Carosi *et al.*, 2007; Aikman *et al.* 2008; Montomoli *et al.* 2008). D2, the Neohimalayan stage of Hodges (2000), is characterized by north-facing F2 folds and related S2 axial plane cleavage (e.g. Carosi *et al.* 2007; Montomoli *et al.* 2008; Kellett & Godin 2009). Antolín *et al.* (in press) estimated the W-E to WNW-ESE orientated and south-dipping preferred orientation of the S2 axial plane foliation within the Triassic flysch of the study area. Godin (2003) utilizing crosscutting relationships of the different structural elements, and U-Pb geochronology dated D2 fold structures as developed during the Oligocene. In central Nepal Crouzet *et al.* (2007) found K-Ar ages of newly formed illite *c.* 30-25 Ma related to the D2 tectonic phase. Afterwards during the course of the D3 phase, the synchronous activity of the STDS and the MCT along the Himalayan arc resulted in the exhumation of mid-crustal rocks of the GHS at *c.* 23-17 Ma ago (Godin *et al.* 2006 with references). By Th-Pb ion microprobe dating on monazite grains from the Khula Kangri granite, the age of activity of the STDS was dated to be younger than 12.5 Ma in the Eastern Himalaya (Fig. 2; Edwards & Harrison 1997). Whereas the displacement along the MCT in the western Arunachal Pradesh was dated to be *c.* 10 Ma by U-Th ion microprobe dating of monazite inclusions in synkinematic garnets (Yin 2006). During this time interval, the northern part of the Tethyan Himalaya was thrust along the GCT to the north at about 17 Ma in the south-central Tibet (Rinbung area) and between 18-10 Ma near Zetang (Ratschbacher *et al.* 1994; Harrison *et al.* 2000 respectively). The D4 phase took place during Miocene times when orogen parallel (E-W) extension triggered N-S-trending normal faults in

form of graben structures crosscutting the Lhasa block and the Tethyan Himalaya. The study area is bounded to the west by the Yadong Gulu Graben and is dissected by the Cona Graben at longitude c. 92°E (Fig. 2; Armijo *et al.* 1986; Garzione *et al.* 2003).

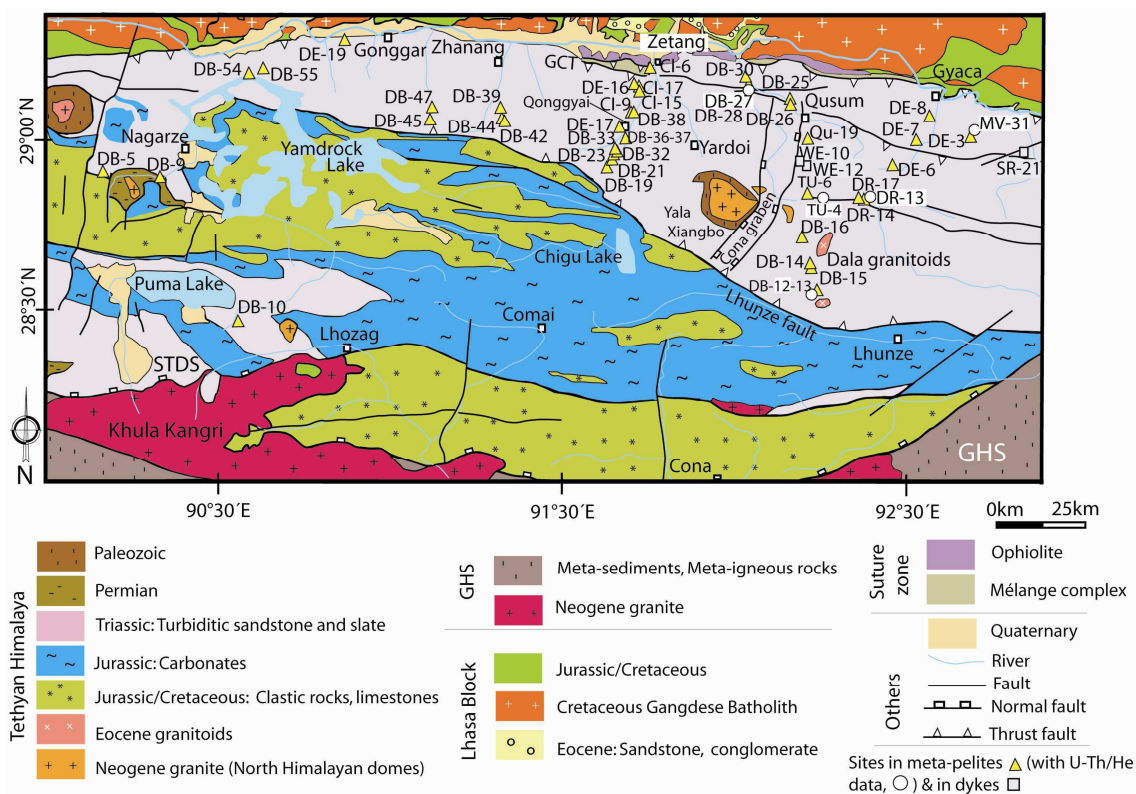


Figure 2: Simplified geological map of SE Tibet (after Pan *et al.* 2004; Yin, 2006; Aikman *et al.* 2008; Antolín *et al.* in press).

3.4 Samples

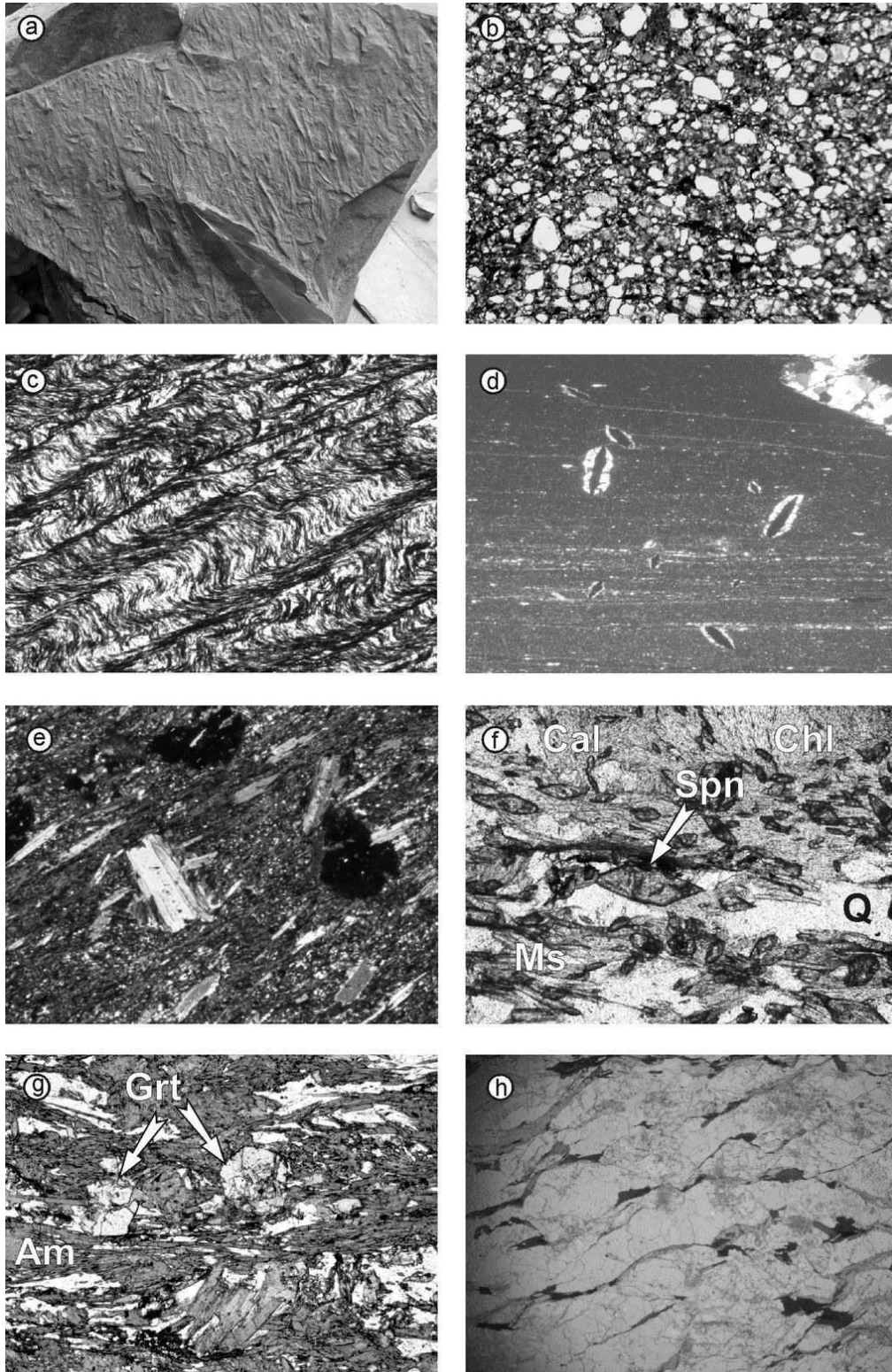
The study area is situated south and south-east of Lhasa along a 250 km long stripe, where the Tethyan sediments form the widest belt in the Himalayan chain (Fig. 1b). Sampling was performed during four field campaigns between 2005 and 2008. The field work had three goals: (a) sampling for anisotropy of magnetic susceptibility and paleomagnetic investigations (details in Antolín *et al.* in press) (b) sampling for geothermobarometry and geochronology and (c) collecting structural field observations and oriented samples for microstructural survey of the studied flysch profiles (details in Montomoli *et al.* 2008). 203 samples were collected from pelites and arenites of the Triassic flysch sequence and from the basaltic-dioritic dykes and greenschists formed from these magmatite bodies.

The metapelites are typically dark gray to black; TOC content ranges from 2 to 4 wt% and sulphur content from 0.01 to 0.3 wt% in the < 63 μm fraction. They are rich in early diagenetic pyrite cubes with crystal size sometimes exceeding 2 cm. Sandstone layers are

widespread in the sequence; they are usually gray, well-sorted quartz-litharenites, with some wackes and red quartzites. The deformation of the flysch assemblage varies strongly along N-S profiles (e.g. Montomoli *et al.* 2008, Antolín *et al.* in press) and the post-sedimentary overprint ranges from the diagenetic stage to greenschist and amphibolite facies. Thus, microscopic textures and mineral assemblages of samples from different structural domains vary from purely sediment to completely re-crystallized schists (see Fig. 3 a-d).

The mafic-intermediate magmatites usually form several meters wide dykes or house-sized, dissected boudins. They experienced a very variable degree of deformation; in the internal zones of the coarsest gabbro and diorite bodies even primary mafic minerals are well preserved, but the margins of the magmatic bodies commonly show transformation to chlorite-muscovite schist. In tectonic units where the degree of metamorphism is high, the entire volume of the magmatites is transformed to greenschist or amphibole-garnet schist and penetrative ductile deformation is widespread (see Fig. 3 e & f).

Figure 3: Macroscopic images and microphotographs demonstrating the characteristic textures and the mineral assemblages of the Tethyan (meta)flysch sequence. (a) Bottom-view of the bedding surface of a sandstone layer from the less deformed, southernmost zone of the sequence, which experienced only diagenetic overprint (site DB-19). Width of image is c. 15 cm. (b) Microphotograph of the sandstone layer of photo a). The texture elements are sedimentary in character, the detrital components are not oriented and deformed, the pressure solution is hardly detectable. Width of image is 4.3 mm. (c) Typical, crenulated texture of the low-grade metapelites. Width of image is 4.3 mm. (d) In thermal aureole of the leucogranite intrusions of the Yala Xiangbo dome rutile crystals were grown in the metapelites. Width of image is 4.3 mm. (e) Schist-parallel and unoriented growth of millimeter sized muscovite crystals in a metamorphosed dyke. Width of image is 4.3 mm. (f) The typical mineral assemblage of the greenschist-facies metamorphosed dykes: chlorite > calcite ~ quartz > sphene ~ albite. Width of image is 1.1 mm. (g) Amphibol-garnet schist (site SR-21). Width of image is 4.3 mm. (h): Microphotograph showing the deformation of Dala granite. The bands of biotite were formed in a partly-crystallized, semi-ductile state of granite. Width of image is 8 mm).



3.5 Methods

3.5.1 Kübler index ('illite crystallinity')

For Kübler index (KI) estimation and K-Ar dating the fractions $< 0.2 \mu\text{m}$, $< 2 \mu\text{m}$, and $2\text{-}6 \mu\text{m}$ nominal size from fine grained, pelitic-silty samples were separated. Samples with visible detritic mica flakes were excluded. After crushing the samples to *c.* 1 cm size, only homogeneous, fine-grained rock fragments, completely free of limonite staining and calcite or quartz veins were selected. The hand-picked aliquots were crushed and ground in a ring mill (vibration mill equipped by hard metal inlays) for 10 to 20 seconds, sieved and splitted into two parts. The $< 63 \mu\text{m}$ fractions were used to extract the illite-rich fractions of $< 2 \mu\text{m}$ by settling in Atterberg cylinders. A second aliquot of $< 2 \mu\text{m}$ fraction was used to separate the fraction $< 0.2 \mu\text{m}$ by an ultra-centrifuge. Due to the coarse crystal size of newly grown mica, it was not possible to produce a sufficient amount of $< 0.2 \mu\text{m}$ fraction in samples with a relatively high degree of metamorphism. From these samples the < 2 and $2\text{-}6 \mu\text{m}$ fractions were investigated only. The mineralogical composition of all fine aliquots was examined by X-ray diffraction. The KI is the half height peak width of the $10\text{-}\text{\AA}$ illite peak (Kübler, 1990). Digital measurement of KI was carried out by step scan (301 points, $7\text{-}10^\circ 2\Theta$, scan step $0.010^\circ 2\Theta$, integration time 4 seconds, receiving slit 0.1 mm, automatic divergence slit) on a Philips PW 1800 diffractometer. The KI values were calculated by the IDEFIX computer program developed at the Geoscience Centre of the University of Göttingen by D. Friedrich and was rewritten to FORTRAN by K. Ullemeyer (Geomar, Kiel) in 2005.

The measurements were carried out in 'air dry' and 'glycolated' state of the size fractions in order to detect and quantify the expandable layers of smectite type minerals. All samples were investigated in duplicates; the KI-values are given in $\Delta^{\circ}2\Theta$ as the averages of the two measurements. The anchizone is limited by 0.25 and $0.42 \Delta^{\circ}2\theta$, respectively as suggested by Kübler (1967, 1968, 1990). These boundaries were settled by an interlaboratory standardization program (see e.g. Warr and Rice 1994, Árkai *et al.* 2007, Kisch *et al.* 2004).

3.5.2 Vitrinite reflectance

Apparent maximum and minimum vitrinite reflectance (R_{max} , R_{min}) was measured on polished sections cut perpendicular to the foliation using polarized light. Random reflectance (R_r) was measured on sections cut perpendicular to foliation using plane polarized light. The measurements were carried out at wavelength of 546 nm. Reflection was recorded on fine-dispersed vitrinite particles characterized by elongated shape, smooth surface and strong bireflectance, without any traces of oxidation and/or re-deposition.

3.5.3 Thermobarometry

Petrographic thin sections were polished, carbon coated and analyzed using a JEOL JXA 8900 electron microprobe. A tungsten filament was used as electron source; the acceleration voltage for quantitative, wave length dispersive, spot analyses and line scans was set to 15 kV. The beam current was adjusted to 15 nA with a beam diameter of 5 μm . The count time for the peak position for each element was 15 seconds. The lower and upper background was measured for 5 seconds each. A Phi-Rho Z matrix correction was applied on all measurements (Armstrong, 1991). The following phases were used as standards for the analyzed elements: olivine_SC, albite, sanidine, TiO_2 , hematite, anorthite, wollastonite, rhodonite, Cr_2O_3 and NiO.

The pressure and temperature (pT) conditions calculated with Thermocalc (Holland & Powell 1998 and Powell & Holland 2006) were obtained using the average pT mode or *avpT*. The PC Version 3.32 of Thermocalc with the internally consistent dataset tc-ds55s, obtained from the Thermocalc resource page was used (<http://www.metamorph.geo.uni-mainz.de/thermocalc/index.html>). The input data, selected electron microprobe spot analyses, was recalculated using the program AX, by T. J. B. Holland (<http://rock.esc.cam.ac.uk/astaff/holland/index.html>), to convert the mineral compositions into chemical activities. After each run of Thermocalc the activities of the phases were iteratively recalculated with AX. This was done until achieving a best fit between the pT results of Thermocalc and the calculation conditions for AX. The crucial σ_{fit} value of the *avpT* mode of Thermocalc (Powell & Holland, 2006) was observed during the calculations. The quoted pT values are within the σ_{fit} range. The pT determinations with Thermocalc were done for samples WE-12 and Sr-21-a.

The computer program Perplex (Connolly & Petrinin 2002 and Connolly 2005) was applied to construct a phase diagram section or pseudosections (Powell & Holland 2008) of sample SR-21-a. The pseudosection was utilized to plot the garnet composition isopleths of the four garnet endmembers (almandine, pyrope, grossularite and spessartine). The necessary chemical information was obtained with a whole rock XRF analyses as well as electron microprobe spot analyses of garnet cores. The intersection of four isopleths yields the range of pT conditions during the initial growth period of the garnets. This approach is discussed by J. A. D. Connolly on the Perplex resource page (http://www.perplex.ethz.ch/perplex_pseudosection.html).

3.5.4 K-Ar geochronology

The argon isotopic composition was measured in a pyrex glass extraction and purification line coupled to a VG 1200 C noble gas mass spectrometer operating in static mode. The amount of radiogenic ^{40}Ar is determined by isotope dilution method using a highly enriched ^{38}Ar spike from Schumacher, Bern (Schumacher 1975). The spike is calibrated against the biotite standard HD-B1 (Fuhrmann *et al.* 1987). The age calculations are based on the constants recommended by the IUGS quoted in Steiger & Jäger (1977). Potassium is determined in duplicate by Eppendorf Elex 63/61 flame photometer. The samples are dissolved in a mixture of HF and HNO₃ according to the technique of Heinrichs & Herrmann (1990). CsCl and LiCl are added as an ionisation buffer and internal standard, respectively. The analytical error for the K-Ar age calculations is given on a 95% confidence level (2 σ). Details of argon and potassium analyses are given in Wemmer (1991).

3.5.5 Zircon (U-Th)/He thermochronology

Zircon crystals were concentrated by standard mineral separation processes (crushing, sieving, gravity and magnetic separation). For zircon (U-Th)/He chronology single crystal aliquots were dated; only intact, euhedral crystals with minor inclusions were selected. The shape parameters were determined and archived by multiple microphotographs and used for the correction of alpha ejection (Farley *et al.* 1996). The crystals were wrapped in *c.* 1x1 mm-sized platinum capsules and degassed in high vacuum by heating with an infrared diode laser. The extracted gas was purified using a SAES Ti-Zr getter at 450 °C. The chemically inert noble gases and a minor amount of other rest gases were then expanded into a Hiden triple-filter quadrupole mass spectrometer equipped with a positive ion counting detector. Crystals were checked for degassing of He by sequential reheating and He measurement. Following degassing, samples were retrieved from the gas extraction line, spiked with calibrated ^{230}Th and ^{233}U solutions and dissolved in pressurized teflon bombs using distilled 48% HF + 65% HNO₃ in five days at 220 °C. Spiked solutions were analyzed by isotope dilution method using a Perkin Elmer Elan DRC II ICP-MS equipped with an APEX micro-flow nebulizer.

3.6 Results

3.6.1 Sheet-silicate mineralogy and Kübler index values

The studied grain size fractions are composed mainly of illite/muscovite, chlorite, paragonite, quartz and minor albite. Kaolinite, smectite and carbonates were not detected. The illite/chlorite ratios are typically high (ideal for KI determination and for K-Ar

geochronology, see DB-47 in Fig. 4), but in some samples chlorite is the dominant sheet silicate (CE-6E in Fig. 4). In some samples we found some discrepancy between the crystallinity state of illite/muscovite and chlorite, although the correlations of Kübler and Árkai indices are usually very good (e.g. Árkai 1991; Potel 2007). In these cases we assume that the origin of the two mineral species is different, i.e. illite/muscovite crystals are mainly well-crystallized and detrital in origin, while the chlorite is newly-formed at low pT conditions.

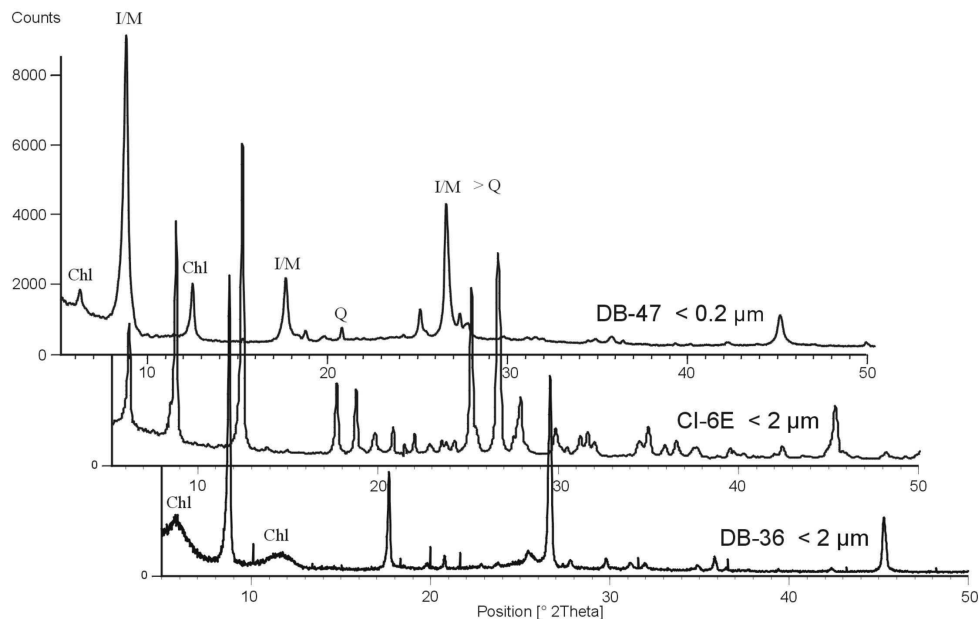


Figure 4: XRD patterns of oriented, air-dried $< 2 \mu\text{m}$ and $< 0.2 \mu\text{m}$ fractions demonstrating the characteristic mineralogical composition of the analysed samples. I/M = illite/muscovite, Chl = chlorite, Q = quartz. DB-47: A typical metapelite sample, the dominant component is illite/muscovite and the amounts of Q and Chl are subordinate. CI-6E: A rare and less optimal composition, as chlorite is more abundant than illite. DB-36: Beyond the well crystallized illite the chlorite peaks are very diffuse.

Paragonite is also present in several samples (Fig. 5a). Deconvolution experiments performed on the double-peak white mica XRD patterns (using FITYK, Wojdyr 2007) suggest that K-Na 'mixed layer phases' are present (Livi *et al.* 1997; Árkai *et al.* 2003).

The KI values are dominantly indicate anchizonal to epizonal overprint, only one sample is in the diagenetic zone (Table 1; Fig. 6a). The good correlation between the air-dried and glycolized samples indicates that there are practically no expandable smectite layers in the majority of the samples (the only exception is sample DB-19; see Fig. 5b). This property of the crystal lattice is important for the evaluation of K-Ar ages (see below).

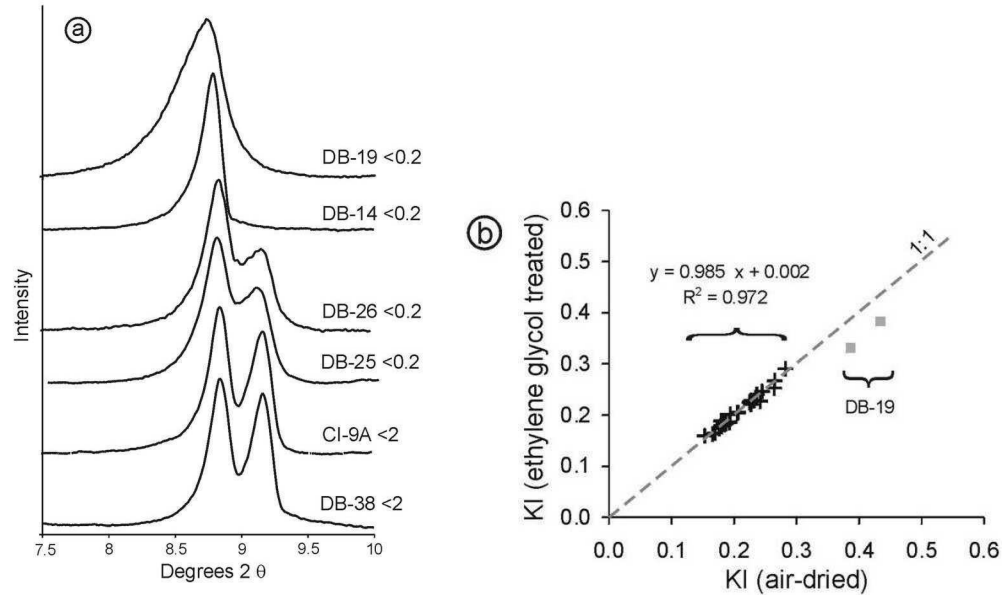


Figure 5: (a) Diagnostic sections of XRD patterns showing badly and well crystallized illite (samples DB-19 and DB-14, respectively) and the paragonite-bearing samples (two peaks). (b) Plot of Kübler Index (KI) measured on air dried versus KI measured on ethylene glycol treated samples. For the correlation coefficient and regression parameters only the values below 0.38 were considered. The 2σ error bars of the presented values are smaller than the symbols.

Sample	Long. [°]	Lat. [°]	Fraction [µm]	Kübler Index		K-Ar					
				air dry	glyc.	< 0.2 µm		< 2 µm		2-6 µm	
					$[\Delta \cdot 2\theta]$	[Ma]	±2s	[Ma]	±2s	[Ma]	±2s
DB-1	89.6575	28.4848	<0.2	0.193	0.187	35.6	1.0				
			<2	0.193	0.186			34.6	0.7		
DB-5	90.1567	28.8988	<6	0.153	0.160						
DB-9	90.3183	28.8850	<6	0.205							
DB-14	92.2190	28.6208	<0.2	0.179	0.179	35.0	1.1				
			<2	0.170	0.165			37.9	0.9		
DB-19	91.6215	28.9048	<0.2	0.434	0.383	88.7	1.5				
			<2	0.387	0.331			106.5	3.3		
DB-21	91.6362	28.9271	<0.2	0.242	0.227	55.7	1.0				
			<2	0.207	0.205			60.1	0.8		
DB-23	91.6419	28.9333	<2	0.199				61.61	0.905		
			2-6	0.179	0.176					73.0	1.0
DB-25	92.1574	29.1036	<0.2	0.509	0.528	23.4	1.9				
			<2	0.228	0.229			32.2	1.6		
DB-26	92.1574	29.1036	<0.2	0.232	0.228	31.6	2.2				
			<2	0.185	0.182			33.0	1.5		
DB-32	91.6496	28.9522	<0.2	0.227	0.221	46.8	1.4				
			<2	0.205	0.205			71.8	1.9		
DB-36	91.6764	28.9881	<0.2	0.194	0.201	32.8	1.0				
			<2	0.166	0.163			33.8	0.6		
DB-38	91.6950	29.0650	<0.2	0.184	0.183	24.2	1.2				
			<2	0.180	0.189			22.0	1.1		
DB-44	91.3174	29.0537	<0.2	0.245	0.246	74.9	1.2				
			<2	0.225	0.225			82.7	2.4		
DB-45	91.1048	29.0483	<0.2	0.265	0.267	77.8	1.5				
			<2	0.237	0.241			86.6	1.1		
DB-47	91.1116	29.0857	<0.2	0.282	0.291	79.0	0.9				
			<2	0.265	0.253			90.4	1		
DB-55	90.6353	29.1977	<0.2	0.205	0.204	62.2	1.3				
			<2	0.183	0.184			63.6	0.8		
CI-6E	91.7515	29.1947	<0.2	0.187	0.184	49.0	1.8				
			<2	0.177	0.174			56.6	0.8		
CI-9A	91.7045	29.0730	<0.2	0.185		25.7	0.9				
			<2	0.187				30.0	1.4		
DE3	92.68549	28.99237	<2	0.173							
			2-6	0.165	0.161					21.7	0.4
DE7	92.5367	28.99006	<2	0.172	0.176						
DE8a	92.56647	29.05447	2-6	0.160	0.168					22.0	0.8
DE19	90.8410	29.2836	<0.2	0.171	0.172						
DR14	92.38454	28.81682	<2	0.171	0.215			27.6	0.9		
			2-6	0.160	0.157					34.4	0.8
DR17	92.3736	28.81771	<2	0.153							
			2-6	0.150	0.152						
QU19	92.21065	28.98917	<2	0.160	0.200			48.3	1.1		
			2-6	0.174	0.160					51.6	0.8
TU6b	92.21517	28.83353	<2	0.165				13.9	0.7		
			2-6	0.148	0.149					14.2	0.5

Table 1: Geographical coordinates of the sampled sites. Sheet-silicate analyzed fraction. Illite Kübler Index (KI) data in air dry and glycolated (glyc.) state of the size fractions. K/Ar age of the three analyzed fractions with respective 95% confidence level ($2s = 2\sigma$). Italics in the columns of Kübler Index indicate that paragonite is also present among the sheet-silicates. In some cases it was not possible to express the KI.

Sample	Fraction [μm]	K2O [Wt. %]	40 Ar * [nl/g] STP	40 Ar * [%]	Age [Ma]	2s-Error [Ma]
Illite-rich fractions from (meta)pelitic samples from the Tethyan flysch						
DB-1	<2	4.93	5.56	50.3	34.6	0.7
DB-1	<0.2	4.81	5.57	54.3	35.6	1.0
DB-14	<2	7.11	8.79	54.7	37.9	0.9
DB-14	<0.2	6.75	7.69	47.0	35.0	1.1
DB-19	<2	6.09	21.56	94.4	106.5	3.3
DB-19	<0.2	6.47	18.98	94.0	88.7	1.5
DB-21	<2	6.44	12.70	87.6	60.1	0.8
DB-21	<0.2	6.32	11.53	86.5	55.7	1.0
DB23	<2	5.17	10.45	83.9	61.6	0.9
DB23	2-6	4.18	10.04	76.3	73.0	1.0
DB-25	<2	3.44	3.61	19.6	32.2	1.6
DB-25	<0.2	3.63	2.76	12.9	23.4	1.9
DB-26	<2	3.65	3.92	23.1	33.0	1.5
DB-26	<0.2	3.58	3.67	21.8	31.6	2.2
DB-32	<2	3.81	9.00	79.5	71.8	1.9
DB-32	<0.2	5.61	8.58	72.9	46.8	1.4
DB-36	<2	6.49	7.15	56.0	33.8	0.6
DB-36	<0.2	6.07	6.48	52.0	32.8	1.0
DB-38	<2	5.24	3.74	31.0	22.0	1.1
DB-38	<0.2	4.34	3.40	27.7	24.2	1.2
DB-44	<2	5.32	14.53	89.0	82.7	2.4
DB-44	<0.2	5.42	13.36	85.1	74.9	1.2
DB-45	<2	5.51	15.76	91.7	86.6	1.1
DB-45	<0.2	5.67	14.55	90.4	77.8	1.5
DB-47	<2	5.65	16.90	90.6	90.4	1.0
DB-47	<0.2	6.08	15.82	88.5	79.0	0.9
DB-55	<2	6.05	12.63	82.1	63.6	0.8
DB-55	<0.2	5.92	12.07	82.5	62.2	1.3
CI-6E	<2	4.83	8.96	82.8	56.6	0.8
CI-6E	<0.2	4.89	7.83	71.2	49.0	1.8
CI-9A	<2	4.27	4.17	45.7	30.0	1.4
CI-9A	<0.2	4.56	3.80	42.7	25.7	0.9
DE3	2-6	6.52	4.60	76.7	21.7	0.4
DE8a	2-6	2.91	2.07	30.1	22.0	0.8
DR14	<2	5.92	5.31	33.2	27.6	0.9
DR14	2-6	5.15	5.77	45.4	34.4	0.8
QU19	<2	6.04	9.53	44.7	48.3	1.1
QU19	2-6	5.14	8.67	64.3	51.6	0.8
TU6b	<2	5.24	2.36	19.1	13.9	0.7
TU6b	2-6	3.86	1.77	28.4	14.2	0.5
Coarse muscovite of the greenschist (meta-basalt)						
WE-12	125-250	7.57	10.90	96.8	44.1	0.5
WE-10A	125-250	8.52	12.16	98.4	43.7	0.6

Table 2: K/Ar ages of illite fractions of fine grained (meta)pelitic members of Tethyan flysch and of coarse muscovites formed in meta-basalt rocks. For each sample potassium content (K2O) and the proportion of radiogenic argon (Ar) is shown. K/Ar age (Ma) is given with respective 95% confidence level ($2s = 2\sigma$).

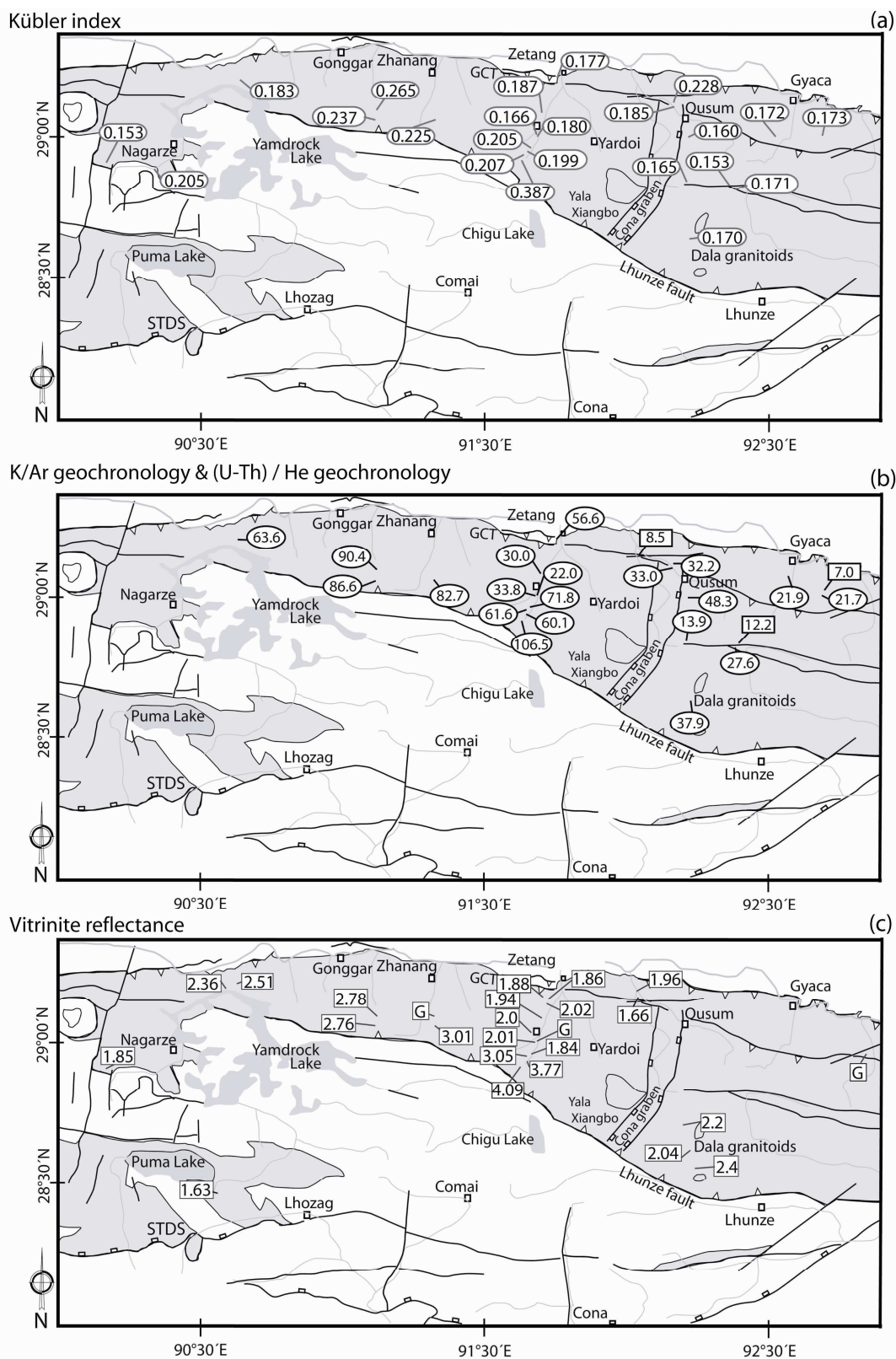


Figure 6: Areal distribution of metamorphic and geochronological results in SE Tibet. Gray area: Triassic flysch. (a) Kübler Index (fraction < 2 μ m), (b) K-Ar ages of illite fractions < 2 μ m (in ellipses) and (U-Th)/He ages (in rectangles), (c) vitrinite reflectance. G: graphite particles recorded in the organic matter. Uncertainties of the plotted values and analytical details are in Tables 1 to 5.

3.6.2 K-Ar ages

The lack of smectite interlayers in the dated samples indicates that the proportion of exchangeable cations is low (i.e. crystals are closed for cation migration). Thus, we do not need to count some unpredictable Ar diffusion processes due to a non-illitic lattice.

The illite/muscovite K-Ar ages range between 106 Ma and 14 Ma (see Table 2, Fig. 6b). The potassium-oxide content is in each case below the stoichiometric composition of muscovite and varies between 3.4 and 7.1 wt%. The proportion of radiometric argon shows an even wider scatter between 13 and 98 %. These two parameters correlate well (Fig. 7). The samples group according to the sheet-silicate assemblage. The illite-rich samples show the highest K content and the highest proportion of radiogenic argon. The chlorite bearing fractions contain less K and Ar*, and the paragonite-bearing samples are characterized by the smallest values. Figure 7 indicates mixing between K-bearing and K-free phases and shows high amounts of atmospheric argon in paragonite and chlorite.

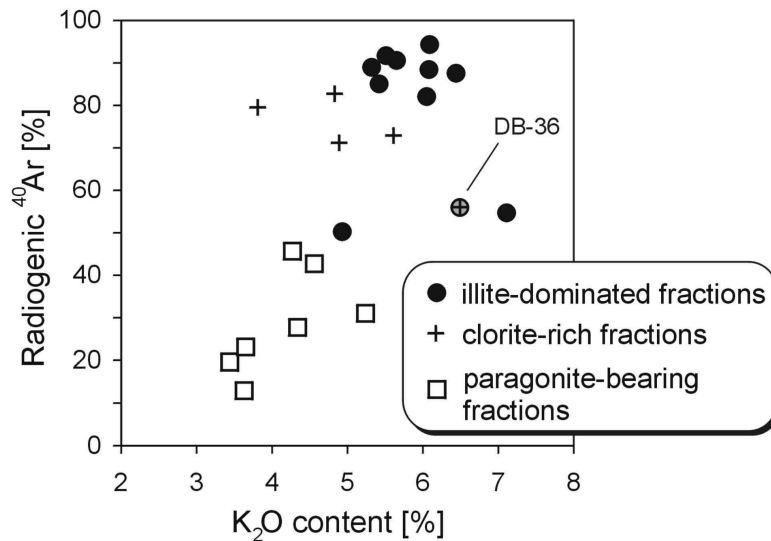


Figure 7: Plot of potassium content versus the proportion of radiogenic argon and the mineralogy of the dated sheet-silicate rich fractions. The 2σ error bars of the presented values are smaller than the symbols. The DB-36 sample contains the badly crystallized chlorite (see Fig. 4).

3.6.3 Vitrinite reflectance

Vitrinite reflectance values range from 1.6 to 4.1 % (highest R_{max} value = 10.4 %; Table 3), the areal distribution of the measured R_o values in the study area is presented in Figure 6c.

Sample	Long. [°]	Lat. [°]	Elev. [m]	Ro [%]	sd	Rmax [%]	sd	Rmin [%]	sd	N
DB-1	89.6575	28.4848	4329	1.98	0.27					50
DB-3	89.6640	28.4967	4341	2.01	0.29					22
DB-5	90.1567	28.8988	4957	1.85	0.30					19
DB-10	90.5334	28.4597	5128	1.63	0.16					24
DB-13	92.2446	28.5411	4373	2.40	0.19					39
DB-15	92.2190	28.6208	5030	2.04	0.33					14
DB-16	92.1906	28.7015	4844	2.20	0.26					16
DB-19	91.6215	28.9048	4139	4.09	0.24					30
DB-21	91.6362	28.9271	4025	3.77	0.21					30
DB-23	91.6419	28.9333	4040	3.05	0.31					50
DB-28	92.0433	29.1454		1.66	0.27					22
DB-30	92.0321	29.1714	3614	1.96	0.25					19
DB-32	91.6496	28.9522	3970	1.84	0.24					6
DB-33	91.6564	28.9649	3939	2.01	0.30					5
DB-42	91.3024	29.0303	4092	3.01	1.59					8
DB-45	91.1048	29.0483	4129	2.76	0.36					50
DB-47	91.1116	29.0857	3953	2.78	0.28					50
DB-54	90.5926	29.1888	4502	2.36	0.26					50
DB-55	90.6353	29.1977	4685	2.51	0.22					50
CI-9B	91.7045	29.0730	3693	1.94	0.21					22
CI-17M	91.7210	29.1487	3634	1.86	0.25					30
CI-15B	91.7107	29.1275	3648	2.02	0.18					5
DE-16C	91.7210	29.1487	3634	1.88	0.21					30
DE-17B	91.6671	29.0150	3846	2.00	0.21					30
Graphite bearing samples										
DB-37	91.6794	29.0099	3812			10.4	0.98	1.19	0.38	26
DB-39	91.3100	29.0874	3655			9.85	0.84	1.43	0.73	18
DB-39	91.3100	29.0874	3655	graphite particles						
SR-21a	92.85992	28.95235	3389	graphite						

Table 3: Vitrinite reflectance values (Ro) measured on (meta)pelitic samples of SE Tibet. Sd, standard deviation.

3.6.4 Metamorphic pT conditions determined by Thermocalc and Perplex methods

Thermobarometric analyses were performed on two metamorphosed dykes collected in the NE part of the study area (WE and SR sites; see Fig. 2). The mineral paragenesis of samples WE-12 and SR-21a are [Ms, Chl, Carb, Q, /Ep] and [Amp, Grt, Ep, Chl, Fsp, Q, /Carb], respectively, see Figs. 3e and 3g. Mineralogical and textural evidence indicate the absence of retrograde transformation or complex deformation.

Site WE-12: For Thermocalc 19 of a total of 74 spot analyses performed on sample WE-12 were selected. Table 4 shows the averages of the selected analyses for the Thermocalc computations as well as the cations per formula unit. The calculations of the cations per formula unit were done with AX. For the calculations the CO₂-fraction of the fluid-phase was set to 10%. The obtained pT results for sample WE-12 are T = 474 ± 35 °C & P = 6.4 ± 1.6 kbar ($\sigma_{\text{fit}} = 1.64$). Even though the 2 σ error for the temperature is quoted as 35 °C (Thermocalc output) it should be treated as the minimum error of 50 °C as stated in Powell & Holland (2008). The reason for that is the wide range of possible error sources of thermobarometric calculations (Kohn & Spear 1991; Powell & Holland 1994).

Site SR-21a: Thermocalc evaluations of sample SR-21-a were performed on mineral assemblages in the vicinity of garnets. According to the microstructural observations the Grt-Fsp-Chl-Am assemblage is in equilibrium. In the surroundings of 8 selected garnet crystals a total of 122 spot analyses were done. The garnet analyses performed on the rims of the grains were used to identify the metamorphic conditions with Thermocalc (Spear 1995). The garnet compositions determined in the cores of the crystals were the base for the Perplex method. The results of two data sets yielding the most reliable Thermocalc results having the smallest 2σ errors (see Table 5) are shown below.

The Thermocalc results for assemblage #1 are:

$$\begin{aligned} T &= 531 \text{ }^\circ\text{C}, \quad 2\sigma = 13 \text{ }^\circ\text{C} \\ P &= 9.4 \text{ kbar}, \quad 2\sigma = 1.0 \text{ kbar} \quad \sigma_{\text{fit}} = 0.87 \end{aligned}$$

For assemblage #2 the results are as follows:

$$\begin{aligned} T &= 511 \text{ }^\circ\text{C}, \quad 2\sigma = 12 \text{ }^\circ\text{C} \\ P &= 10.0 \text{ kbar}, \quad 2\sigma = 0.9 \text{ kbar} \quad \sigma_{\text{fit}} = 0.48 \end{aligned}$$

The reported $2s$ errors are underestimating the real uncertainty, thus in the following we prefer to use the above stated minimum of $50 \text{ }^\circ\text{C}$ and 1 kbar respectively.

For the Perplex calculations 10 spot analyses of garnet cores, with weight percent totals between 99.5 % and 101 %, were selected and averaged (Table 4). The Perplex garnet isopleths for sample SR-21-a are depicted in Figure 8. The pT result for this sample lies at $T = 600 \pm 50 \text{ }^\circ\text{C}$ & $P = 7.4 \pm 1.5 \text{ kbar}$.

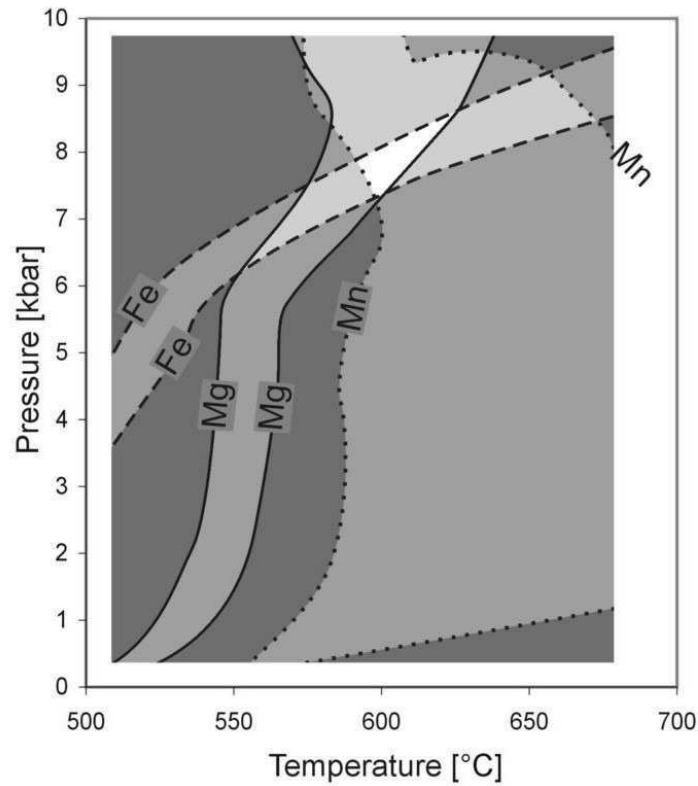


Figure 8: Metamorphic pressure and temperature conditions (white area) of amphibole-garnet schist of SR 21 site determined by PERPLEX method. Paired garnet isopleths demarcate the stability field of garnet that is in equilibrium with the bulk rock chemistry and mineral paragenesis. The lines show the ± 1 s.d. of the chemical compositions determined in the cores of the garnet crystals by multiple electron microprobe analyses (see Tab. 5).

3.6.5 Zircon (U-Th)/He ages

Zircon helium ages and analytical details are listed in Table 5 and the dated localities are plotted in Fig. 6b. The amounts of actinide elements for all single crystal measurements are at least 20 times higher than the limit of detection. The ages are slightly different in the samples, but cluster in the Late Miocene (12.2. to 7 Ma).

WE-12

mineral	SiO ₂	TiO ₂	Al ₂ O ₃	Cr ₂ O ₃	Fe ₂ O ₃	FeO	MnO	MgO	CaO	Na ₂ O	K ₂ O
Ms	46.33	0.17	35.44	0.00	0.00	1.04	0.01	0.73	0.03	1.09	9.01
Chl	24.61	0.04	23.47	0.08	0.00	26.18	0.31	13.12	0.01	0.01	0.01
Carb	0.02	0.01	0.01	0.01	0.00	1.23	0.75	0.56	59.04	0.01	0.02
Ep	38.49	0.08	25.29	0.01	10.08	0.61	0.03	0.01	23.70	0.00	0.01
mineral											
Ms	3.10	0.01	2.80	0.00	0.00	0.06	0.00	0.07	0.00	0.14	0.77
Chl	2.60	0.00	2.92	0.01	0.00	2.31	0.03	2.06	0.00	0.00	0.00
Carb	0.00	0.00	0.00	0.00	0.00	0.03	0.02	0.03	1.92	0.00	0.00
Ep	3.02	0.01	2.34	0.00	0.60	0.04	0.00	0.00	1.99	0.00	0.00

SR-21a: compositios used for Thermocalc

Assemblage #1	SiO ₂	TiO ₂	Al ₂ O ₃	Cr ₂ O ₃	Fe ₂ O ₃	FeO	MnO	MgO	CaO	Na ₂ O	K ₂ O
Grt	38.15	0.10	20.97	0.00	0.00	27.01	2.93	1.72	9.79	0.02	0.00
Fsp	66.34	0.00	21.32	0.00	0.27	0.00	0.03	0.00	2.10	10.50	0.03
Chl	25.66	0.06	19.93	0.07	0.27	28.94	0.44	12.65	0.03	0.00	0.01
Am	45.08	0.42	14.31	0.03	0.27	17.14	0.24	8.73	9.66	2.43	0.11
Assemblage #2											
Grt	37.58	0.09	20.46	0.03	0.10	27.09	3.13	1.77	8.97	0.02	0.00
Fsp	68.31	0.00	19.75	0.01	0.00	0.00	0.00	0.00	0.24	11.67	0.04
Chl	24.85	0.04	18.83	0.00	0.00	28.40	0.42	12.86	0.02	0.01	0.01
Am	45.63	0.32	11.51	0.04	3.30	12.87	0.17	10.38	10.01	2.02	0.14
Assemblage #1	Si	Ti	Al	Cr	Fe3	Fe2	Mn	Mg	Ca	Na	K
Grt	3.02	0.01	1.96	0.00	0.00	1.79	0.20	0.20	0.83	0.00	0.00
Fsp	2.90	0.00	1.10	0.00	0.01	0.00	0.00	0.00	0.10	0.89	0.00
Chl	2.75	0.01	2.52	0.01	0.02	2.60	0.04	2.02	0.00	0.00	0.00
Am	6.61	0.05	2.48	0.00	0.03	2.10	0.03	1.91	1.52	0.69	0.02
Assemblage #2											
Grt	3.02	0.01	1.94	0.00	0.01	1.82	0.21	0.21	0.77	0.00	0.00
Fsp	2.98	0.00	1.02	0.00	0.00	0.01	0.00	0.00	0.01	0.99	0.00
Chl	2.75	0.00	2.46	0.00	0.00	2.63	0.04	2.12	0.00	0.00	0.00
Am	6.77	0.04	2.01	0.01	0.37	1.60	0.02	2.30	1.59	0.58	0.03

SR-21a: average garnet core composition used for Perplex

mineral	SiO ₂	TiO ₂	Al ₂ O ₃	Cr ₂ O ₃	Fe ₂ O ₃	FeO	MnO	MgO	CaO	Na ₂ O	K ₂ O
Grt	37.90	0.13	20.56	0.03	0.15	26.90	3.96	1.65	9.14	0.00	0.00
	Si	Ti	Al	Cr	Fe3	Fe2	Mn	Mg	Ca	Na	K
Grt	3.02	0.01	1.93	0.00	0.01	1.79	0.27	0.20	0.78	0.00	0.00

Table 4: Average chemical and cation composition of the mineral phases used for thermobarometry. Oxygen numbers used for cation numbers are: MS: 11, Chl: 14, Carb: 6, Ep: 12.5, Grt: 12, Fsp:8 Amph: 23.

Sample	aliq.	He		U238		Th232		Sm		Ejection correct. (Ft)	Uncorr. He-age [Ma]	Ft-Corr. He-age [Ma]	1s [Ma]	Sample		
		vol. [ncc]	s.e. [ncc]	mass [ng]	s.e. [ng]	mass [ng]	s.e. [ng]	Th/U ratio	mass [ng]					s.e. [ng]	unweighted aver. (1 s.e.)	
DB-27	#1	2.661	0.045	3.048	0.055	1.195	0.029	0.39	0.028	0.002	0.70	6.6	9.5	0.2		
	#2	0.981	0.017	1.125	0.020	0.538	0.013	0.48	0.052	0.003	0.76	6.5	8.5	0.2		
	#3	0.781	0.014	0.890	0.016	0.718	0.017	0.81	0.065	0.004	0.80	6.1	7.6	0.2	8.5	0.5
DR13	#1	2.591	0.044	2.048	0.037	0.765	0.018	0.37	0.031	0.002	0.78	9.6	12.4	0.3		
	#2	5.782	0.096	4.092	0.074	2.234	0.054	0.55	0.052	0.003	0.80	10.4	13.0	0.3		
	#3	2.193	0.037	1.945	0.035	0.406	0.010	0.21	0.028	0.002	0.79	8.9	11.2	0.3	12.2	0.5
MV31c	#1	0.633	0.012	1.043	0.019	0.196	0.005	0.19	0.004	0.000	0.74	4.8	6.5	0.2		
	#2	1.582	0.027	2.234	0.040	0.523	0.013	0.23	0.016	0.004	0.73	5.6	7.6	0.2	7.0	0.4

Table 5: Results of zircon (U-Th)/He geochronology

3.7 Discussion

Low-grade pelites potentially contain detrital grains, which carry a signal of the crystallization conditions and K-Ar age of white mica from the source region of the sediment (Hower *et al.* 1963; Hurley *et al.* 1963). The distinction of the inherited and newly formed generations in bulk aliquots (grain size fractions) is difficult. However, white micas formed in basic and intermediate magmatic rocks are exclusively metamorphic in origin. Therefore these white micas are free of any inherited signals and their K-Ar age reflects the age of metamorphism. Thus, we will discuss separately the results yielded by metapelitic and metabasic formations.

3.7.1 Conditions and age of metamorphism of basic dykes

Thermobarometric analyses indicate greenschist facies and amphibolite facies metamorphism for the WE and SR sites, respectively. The key observation for the amphibole schist is the difference in the calculated pressures using Thermocalc and Perplex method. The pressures of the garnet rim assemblages calculated by Thermocalc are at least 2 kbar higher than the pressure conditions of the garnet core obtained by Perplex method. This indicates prograde metamorphism for the time of garnet growth.

The greenschists of the WE sites contain well developed white mica crystals (Fig. 3e) and no magmatic relicts. White mica does not occur in mafic magmatic rocks and the structure and texture of this folded greenschist does not show any relict, magmatic element. Therefore, the muscovites are completely metamorphic in origin. The K-Ar ages are 43.7 and 44.1 Ma. Noticeable is the high percentage of radiogenic argon (Table 2). The two samples were collected in *c.* 1 km distance from two distinct metamagmatite bodies of different chemistry and deformation degree. We interpret these ages as the formation age of the muscovites, thus, the age of greenschist facies metamorphism that took place in a part of the THS east of the Yala Xiangbo dome. These ages are very close to the emplacement age of the Dala granite (44.1±1.2 Ma, U-Pb zircon dating; Aikman *et al.* 2008) that is located 25 km SE of the sampled metabasic dyke. At this location the Dala granite intruded into a lower structural level and experienced some near-solidus deformation (Fig. 3h) that occurred simultaneously or soon after the emplacement. Similar *c.* 44 Ma ages were measured by different methods in different structural levels giving a significant bench-mark for the Paleogene (D1 or Eohimalayan) tectonic event in the eastern THS.

At the evaluation of the thermobarometric data of the amphibole-garnet schist of SR site it is important to point out that the studied site is far from the metamorphic domes (> 60 km to

Yala Xiangbo dome), thus the immediate heating from the lower structural unit is not probable. We assume that the amphibolite facies metamorphism was co-genetic with the *c.* 44 Ma old greenschist facies event detected at the WE sites, mentioned above.

3.7.2 Low-grade metamorphism of metapelitic samples

The geothermometrical and geochronological data from sub-greenschist facies pelitic lithologies are not as well constrained as the results measured on orthometamorphic formations of higher pT conditions (like the data discussed above). Anchi- and epizonal conditions result in only incomplete, disequilibrium phase transformations. This fact is supported by field observations. The metapelitic samples show a very variable intensity of white-mica growth within one outcrop. The mica growth process is strongly controlled by the lithology: in silty and sandy protoliths the neof ormation of white mica is in a more advanced state than in the neighbouring pelitic lithologies. We assume that three major factors are responsible for this difference: (i) the high permeability of the arenitic lithologies, (ii) the local liberation of potassium and increase of K^+ activity during decomposition of feldspar grains and lithic fragments in arenites, and (iii) the presence of dispersed organic material in pelitic lithologies probably embedded the silicate phases and reduced the diffusivity.

Figure 6 presents the results obtained on metapelitic samples projected on the schematic geological map of the study area. The sample sites with the highest metamorphic degree are related to tectonic slices derived from the deeper part of the THS situated close to the Yala Xiangbo dome (e.g. site TU-6). For the proper understanding of the evolution of the studied THS area we have to evaluate the KI data in concert with the argon geochronology. In epi- and anchizonal overprinted areas the mineral transformation is usually incomplete and the individual crystallinity and age data typically show just apparent values, which are actually points along mixing or transformation curves. The interpretation of individual data is difficult and can result in misleading conclusions. Thus, we do not force a specific interpretation of a single sample or sample site, but rather prefer to process the data in bulk with the purpose of identifying the major epochs of the thermal evolution for the entire eastern THS.

The KI values are controlled by the ratio of detrital and newly formed illite. The newly formed / detrital ratio usually increases towards finer size fractions. Using two fractions the finer one is richer in newly formed sheet silicates and always indicates a value closer to the conditions of the latest metamorphic event (Reuter 1987; Clauer & Chaudhuri 1999). The same is true for the K-Ar ages of these size fractions. The detrital grains carry an old age signal, while the newly grown population is always younger (Hower et al. 1963;

Hurley et al. 1963). By combining the KI with the K-Ar ages the newly formed / detrital ratio can be estimated especially if the initial detrital age is known.

The Kübler Index measured on different size fractions and the corresponding K-Ar ages of the metapelites in SE Tibet are plotted on Fig. 9. The plot shows clear trends. The older K-Ar ages are measured in samples having a lower degree of illite crystallinity. With increasing crystallinity the argon ages are getting younger. The $< 0.2 \mu\text{m}$ fractions - being rich in newly formed illite - show less ordered illite structures and younger K-Ar ages than the $< 2 \mu\text{m}$ fractions. The distances between the projection points of the two size fractions become smaller with increasing metamorphic degree. For samples showing the youngest argon ages the two fractions give indistinguishable results. We assume that in these cases both size fractions are dominated by the newly formed white mica. This convergence indicates equilibrium conditions and these ages (c. 24-22 Ma) are considered as the cessation of illite growth. These sites are structurally controlled by the D2 phase and the backthrust development along GCT. For this reason the new growth of illites at c. 24-22 Ma are most likely related to the development of the S2 foliation (Montomoli *et al.*, 2008; Antolín *et al.* in press).

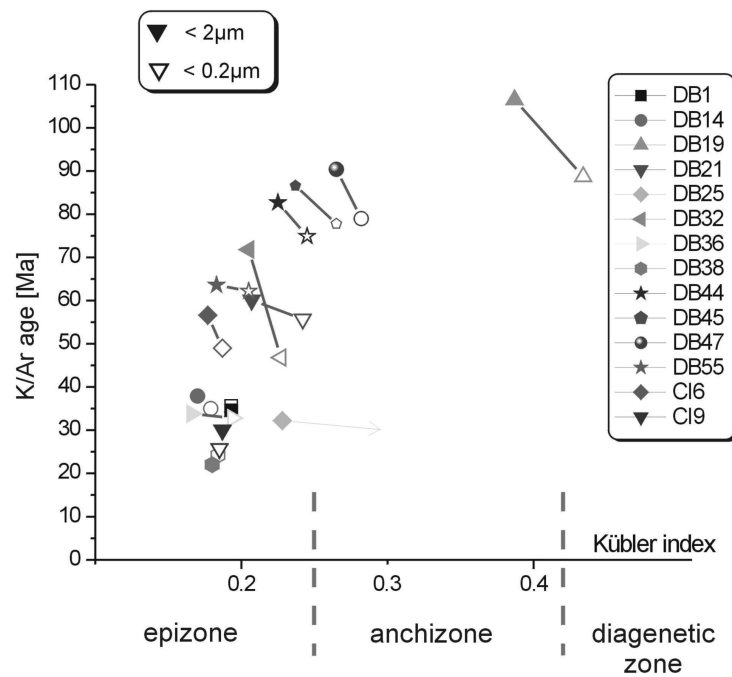


Figure 9: Plot of Kübler Index vs. K-Ar age measured on the same fraction. Note that $< 0.2 \mu\text{m}$ fractions show smaller degree of illite crystallinity and younger K-Ar age compared to $< 2 \mu\text{m}$ fractions.

3.7.3 Estimation of the maximum metamorphic temperature of metapelites by organic maturation

The vitrinite reflectance cannot be converted immediately to temperature, because the transformation of organic material is a kinetic process (Barker & Pawliewicz 1986; Sweeney & Burnham 1990). Peak temperature estimation for the Triassic flysch was performed by means of three different algorithms, assuming different effective heating times (Fig. 11). For the selection of the most reliable curve we have to consider the effective heating time. The above outlined K-Ar ages indicate that the final metamorphism of the Triassic flysch took place in Oligo-Miocene time, thus we exclude both long-lasting maximum temperature conditions as well as a shock-heating process. The most probable duration of the maximum temperature is between *c.* 5 and 15 Ma. Thus, we use the Bostick (1979) and the Sweeney and Burnham (1990) algorithms assuming 10 Ma effective heating time to estimate the range of maximum temperature (Fig. 11). Considering this conversion, the lowest vitrinite reflectance values (around $R_o=1.65\%$) indicate *c.* 170-185 °C maximum temperature. Typical reflectance values around $R_o=2\%$ to 3% indicate *c.* 180-200 °C and 225-235 °C maximum temperatures, respectively. Above *c.* 4 % reflectance the transformation of R_o values to temperature is not properly calibrated (see e.g. Judik *et al.* 2008), thus for the estimation of maximum metamorphic temperature of the Triassic flysch we have to use the inorganic mineral phases of the metamorphosed dikes of the sequence (see above).

3.7.4 Greenschist-facies metamorphism at the base of THS

The sample set of site TU-6 was collected close to the detachment of the Yala Xiangbo dome, from a zone that was intruded by thin leucogranitic and aplitic dykes parallel to the S1 foliation of the metapelites. The dykes have only weakly developed chilled margins. This sample site represents a deep structural level of the THS. Newly grown, well developed muscovite crystals dominate the micro-texture and KI indicates a highly crystalline lattice of the white mica. The muscovite K-Ar ages are the youngest in the studied sample set (14.2 - 13.9 Ma; Fig. 6b). This age range is close to the *c.* 13.5 Ma muscovite K-Ar age reported from the Yala Xiangbo dome by Aikman *et al.* (2004).

3.7.5 Post-sedimentary evolution of the Tethyan flysch in SE Tibet

The evolution of the region is rather complex, therefore we compiled the known thermal and tectonic events and the assumed mineral transformations and illite forming periods to better understand the evolution of the eastern Tethyan Himalayan Sequence (Fig. 10).

The burial history is reconstructed from the subsidence curve of Jadoul *et al.* (1998) estimating the minimum amount of burial of the Triassic flysch. In their study the sedimentary sequence was interpreted as a near-shore facies assemblage, thus the thickness of the total Mesozoic pile may be significantly more in our study area. Therefore in the assumed depth of at least 4 to 5 km the burial diagenesis can already generate new clay mineral assemblages (Meunier & Velde 2004), thus we consider the sedimentary burial as the first illite-forming epoch (Fig. 10).

The oldest argon ages of the coarsest size fractions, dominated by detrital mica are much younger than the typical Precambrian mica ages of the basement rock of the Indian continent, which was presumably the source area of the sediment (Gaetani & Garzanti 1991). They are even younger than the *c.* 250 to 210 Ma age of sedimentation. On the other hand the oldest detrital (mixed) ages are older than the Eocene (*c.* 44 Ma) greenschist facies metamorphic event detected in the metabasic rocks. The lack of pre-Mid Cretaceous detrital mica ages indicates that there was a post-sedimentary reset older than the Cenozoic collision of THS. The most plausible candidate for the post-Triassic, pre-Eocene thermal reset of the Ar age of detrital mica grains is the high heat flow during Early Cretaceous magmatism of the region probably created by the Kerguelen plume (Zhu *et al.* 2008; Xu *et al.* 2009). We assume that at that time a significant part of the THS was in anchi- and epizonal conditions and the emplacement of the dykes and their hydrothermal aureole triggered the formation of white mica in the pelites (Fig. 10).

During Eocene times the THS experiences locally greenschist and probably also amphibolite facies metamorphism. This metamorphic event was related to the Himalayan collision. A part of our data measured on metapelites shows very weak overprint, thus several tectonic blocks -mainly in the southern part of the THS- occupied only shallow depths during the Eocene subduction (Fig. 10).

During Oligo-Miocene times the ongoing shortening resulted in deformation mainly in the northern zones of the THS. The formation of illite is common, but the intensity of the deformation and the mineral growth is very variable. The pT conditions were usually not sufficient for a complete reset. The majority of the KI and K-Ar data from the THS reflect disequilibrium conditions and actually mark a mixing line between pre-Neogene and Neogene events. After the Oligo-Miocene stacking (D2 tectonic phase) the pile of the Tethyan Himalaya was penetrated by the Yala Xiangbo dome and associated leucogranitic dykes (TU-6 site) reaching greenschist facies conditions. The youngest K-Ar ages are around 14 Ma and they were measured on samples from the deeper part of the sequence, probably close to the

basal detachment. However, this overprint was local, because a significant part of the THS shows only partial reset and low crystallinity of the newly grown illite. This indicates that the maximum thermal overprint during Miocene times did not exceed anchizone conditions (see e.g. Fig. 9).

In Figure 10 the dashed line represents the tectonic blocks, which experienced the lowest degree of transformation. On the other hand the ZHe ages assign a minimum temperature for the THS for the Miocene. The obtained ZHe cooling ages derived from the late and complete reset of zircons between 12 and 7 prove that the currently exposed level of the THS situated deeper than the *c.* 180 °C isotherm until Late Miocene.

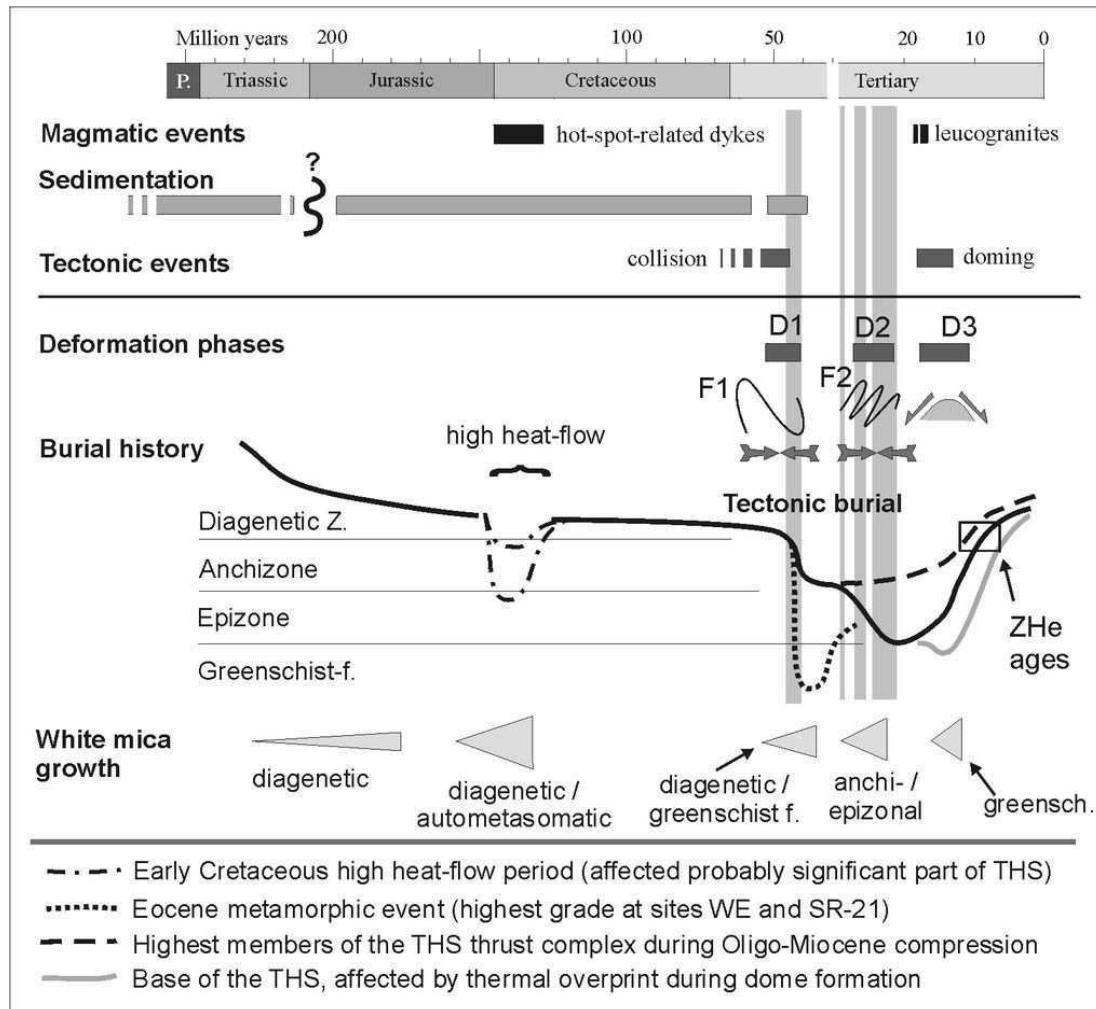


Figure 10: Synopsis of the tectonothermal evolution of the Tethyan Himalayan flysch in SE Tibet. Time intervals emphasized by grey vertical lines are the major deformation periods dated as *c.* 44 Ma and an Oligo-Miocene one, which terminated at *c.* 24-22 Ma. Different processes were resulted in white mica growth, which took place in more periods, both in diagenetic and in metamorphic conditions.

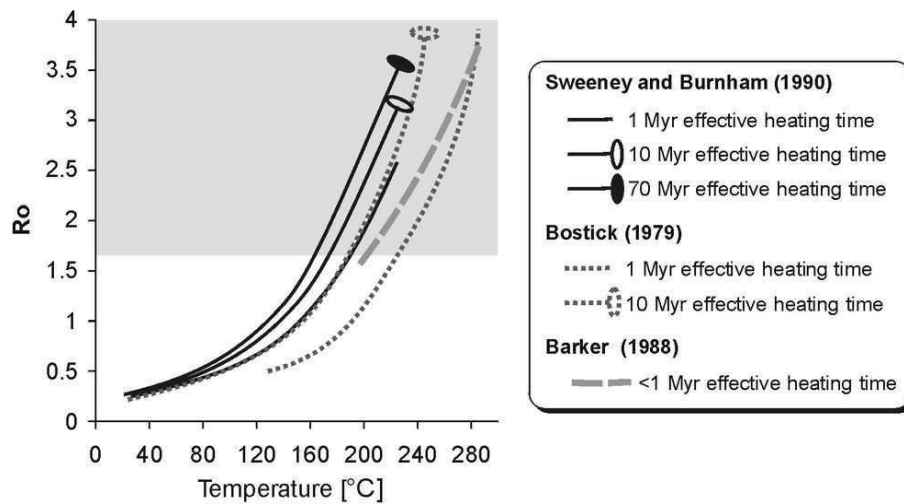


Figure 11: Estimation of palaeotemperature from vitrinite reflectance values. Three different algorithms were used for conversion assuming different effective heating times. Gray belt represents the vitrinite reflectance values (except the graphitized samples). Evaluation is in the text.

3.8 Conclusions

The different tectonic blocks of the THS in SE Tibet experienced a thermal overprint between c. 170 °C and 600 °C.

The Tethyan Triassic flysch sequence registers four tectonothermal events.

1. *Early Cretaceous*. Its direct dating is not possible, nevertheless from the hot-spot related magmatism penetrating the region and from the missing pre-Mid Cretaceous illite/muscovite argon ages we assume a period of increased heat flow and illite formation in the metapelites.
2. *Eocene (c. 44 Ma)*. The early Himalayan granites (Dala granitoids) intruded during or slightly before the greenschist and locally even amphibolite facies metamorphism. Maximum temperature and pressure conditions of c. 600 °C and 7.8 kbar indicate that a part of the THS was subducted to mid-crustal levels.
3. *Oligo-Miocene (terminated at c. 22 Ma)*. The different tectonic blocks of the THS experienced sub-greenschist facies metamorphism with a wide range of deformation and thermal overprint. We assume that this process was associated to a long-lasting shortening which probably terminated c. 22 Ma ago. This N-S shortening phase can be correlated to the D2 tectonic phase (Godin, 2003; Kellet & Godin, 2009; Antolín *et al.* in press) or to the Neohimalayan phase described in Hodges (2000).
4. *Miocene (between c. 18 and 13 Ma)*. The very base of the TH sequence in the surroundings of the Yala Xiangbo dome experienced greenschist-facies overprint. The formation of white micas or the cooling below their argon closure temperature took place around 13 Ma ago

caused by the emplacement and exhumation of the Yala Xiangbo dome (Aikman *et al.* 2004; Zhang *et al.* 2005).

Zircon (U-Th)/He ages indicate that the post-metamorphic cooling history lasted until Late Miocene times. The final cooling was not coeval in the whole THS, the northern zones experienced a later cooling probably induced by the exhumation of the hangingwall of the north-vergent Great Counter Thrust along its backthrust plane. The existing ages on the activity of MCT and STDS (see Godin *et al.* 2006) and GCT (Yin *et al.* 1994; Ratschbacher *et al.* 1994; Harrison *et al.* 2000) suggest that these three tectonic elements were active during the same time interval.

As detected in many sampling sites, the lithology of the protolith has an important role on the development of metamorphic minerals. The growth of white mica and garnet was hindered by high organic content and low permeability in the metapelites, while the meta-arenitic lithologies always contain much coarser and well-developed metamorphic minerals. Consequently, textures and sometimes even the paragenesis of meta-arenites and meta-tuffs indicate higher metamorphic conditions than the adjacent metapelites.

The authors are grateful for the aid during fieldwork to our Tibetan drivers Puchum, Tawa, Nobu (Lhasa), and to the Chinese students Xu Xiaoxia, Xu Qiang and Zhang Qinghai (Beijing) who partly joined the field work. Many thanks for careful sample preparation to U. Grunewald and I. Ottenbacher (Göttingen). This work was funded by the German Research Foundation (DFG) and is part of the Priority Programme "Tibetan Plateau: Formation, Climate, Ecosystems (TiP)".

References

- Aikman, A., Harrison, T. M. & Lin, D. 2004. Preliminary results from the Yala-Xiangbo Leucogranite dome, SE Tibet. *Himalaya Journal of Sciences*, **2**, 91.
- Aikman, A., Harrison, T. M. & Lin, D. 2008. Evidence for Early (>44 Ma) Himalayan Crustal Thickening, Tethyan Himalaya, southeastern Tibet. *Earth and Planetary Science Letters*, **274**, 14-23.
- Antolín, B., Apell, E., Montomoli, C., Dunkl, I., Ding, L., Gloaguen R. & El Bay, R. In press. Kinematic evolution of the eastern Tethyan Himalaya: Constraints from magnetic fabric and structural properties of the Triassic flysch in SE Tibet. In: Poblet, J. & Lisle, R. (eds) *Kinematic Evolution and Structural Styles of Fold-and-Thrust Belts*. Geological Society, London, Special Publications.
- Árkai, P. 1991. Chlorite crystallinity: an empirical approach and correlation with illite crystallinity, coal rank and mineral facies as exemplified by Palaeozoic and Mesozoic rocks of northeast Hungary. *Journal of Metamorphic Geology*, **9**, 723 - 734.
- Árkai, P., Sassi, F. P. & Desmons, J. 2007. Very low- to low-grade metamorphic rocks. In: Fettes, D. & Desmons, J. (eds) *Metamorphic Rocks: A Classification and Glossary of Terms: Recommendations of the International Union of Geological Sciences Subcommission on the Systematics of Metamorphic Rocks*. Cambridge University Press, Cambridge, UK, 36–42.
- Árkai, P., Faryad, S. W., Vidal, O. and Balogh, K. 2003. Very low-grade metamorphism of sedimentary rocks of the Meliata unit, Western Carpathians, Slovakia: implications of phyllosilicate characteristics. *International Journal of Earth Sciences*, **92**, 68–85.
- Armijo, R., Tapponnier, P., Mercier, J.L. & Tonglin, H. 1986. Quaternary extension in southern Tibet: field observations and tectonic implications. *Journal of Geophysical Research*, **91**, 13803-13872.

- Armstrong, J. T. 1991. Quantitative elemental analysis of individual microparticles with electron beam instruments. In: Heinrich, K. F. J. & Newbury, D.E. (eds) *Electron Probe Quantification*. Plenum, New York, 261–315.
- Barker, C. E. 1988. Geothermics of petroleum systems: Implications of the stabilization of kerogen thermal maturation after a geologically brief heating duration at peak temperature. In: Magoon, L.B. (ed.) *Petroleum systems of the United States*, U.S. Geological Survey Bulletin 1870, 26–29.
- Barker, C. E. & Pawlewicz, M. J. 1986. The correlation of vitrinite reflectance with maximum temperature in humic organic matter. In: Buntebarth, G. & Stegena, L. (eds) *Lecture notes in Earth Sciences*, Paleogeothermics, 5, 79-93, Springer Verlag.
- Bonhomme, M. & Garzanti, E. 1991. Age of metamorphism in the Zaskar Tethys Himalaya (India). *Géologie Alpine*, 16, 15-16.
- Bostick, N. H. 1979. Microscopic measurement of the level of catagenesis of solid organic matter in sedimentary rocks to aid exploration for petroleum and to determine former burial temperatures - A review. In: Scholle, P. A. & Schluger, P. R., (eds) *Aspects of Diagenesis*, Society of Economic Paleontologists and Mineralogists Special Publication 26, 17–44, Tulsa, Oklahoma.
- Brookfield, M. 1993. The Himalayan passive margin from Precambrian to Cretaceous. *Sedimentary Geology*, 84, 1-35.
- Burg, J.P. & Chen, G.M. 1984. Tectonics and structural zonation of southern Tibet, China. *Nature*, 311, 219-223.
- Carosi, R., Montomoli, C. & Visonà, D. 2007. A structural transect in the Lower Dolpo: Insights on the tectonic evolution of Western Nepal. *Journal of Asian Earth Sciences*, 29, 407-423, doi: 10.1016/j.jseaes.2006.05.001.
- Clauer, N. & Chaudhuri, S., 1999, Isotopic dating of very low-grade metasedimentary and metavolcanic rocks: techniques and methods, In: Frey, M. & Robinson, D. (eds) *Low-grade Metamorphism*, 202-226, Blackwell.
- Connolly, J. A. D. & Pettrini, K. 2002. An automated strategy for calculation of phase diagram sections and retrieval of rock properties as a function of physical conditions. *Journal of metamorphic Geology*, 20, 697-708.
- Connolly, J. A. D. 2005. Computation of phase equilibria by linear programming: A tool for geodynamic modeling and its application to subduction zone decarbonation. *Earth and Planetary Science Letters*, 236, 524-541.
- Crouzet, C., Dunkl, I., Paudel, L., Arkai, P., Rainer, T. M., Balogh, K. & Appel, E. 2007. Temperature and age constraints on the metamorphism of the Tethyan Himalaya in Central Nepal: A multidisciplinary approach. *Journal of Asian Earth Sciences*, 30, 113-130, doi:10.1016/j.jseaes.2006.07.014.
- DeCelles, P. G., Robinson, D. M., Quade, J., Ojha, T. P., Garzione, C. N., Copeland, P. 2001. Stratigraphy, structure and tectonic evolution of the Himalayan fold-thrust belt in western Nepal. *Tectonics*, 20, 487-509.
- Ding, L., Kapp, P. & Wan, X. 2005. Paleocene-Eocene record of ophiolite obduction and initial India-Asia collision, south central Tibet. *Tectonics*, 24, TC3001, doi:10.1029/2004TC001729.
- Dupuis, C., Hébert, R., Dubois-Coté, V., Wang, C. S., Li, Y. L. & Li, Z. J. 2005. Petrology and geochemistry of mafic rocks from mélange and flysch units adjacent to the Yarlung Zangbo Suture Zone, southern Tibet. *Chemical Geology*, 214, 287-308.
- Dupuis, C., Hébert, R., Dubois-Coté, V., Guilmette, C., Wang, C. S. & Li, Z. J. 2006. Geochemistry of sedimentary rocks from mélange and flysch units south of the Yarlung Zangbo suture zone, southern Tibet. *Journal of Asian Earth Sciences*, 26, 489-508.
- Edwards, M.A. & Harrison, T.M. 1997. When did the roof collapse? Late Miocene north-south extension in the high Himalaya revealed by Th-Pb monazite dating of the Khula Kangri granite. *Geology*, 25, 543-546.
- Farley, K. A., Wolf, R. A. & Silver, L. T. 1996. The effects of long alpha-stopping distance on (U-Th)/He ages. *Geochimica Cosmochimica Acta*, 60, 4223-4229.
- Fuchs, G. 1967. *Zum Bau des Himalaya*. Österreichische Akademie der Wissenschaften, Mathematisch-Naturwissenschaftliche Klasse, Denkschriften, 113, 1-211.
- Fuhrmann, U., Lippolt, H. J. & Hess, J. C. 1987. Examination of some proposed K-Ar standards: ⁴⁰Ar/³⁹Ar analyses and conventional K-Ar-Data. *Chemical Geology*, 66, 41-51.

- Gaetani, M & Garzanti, E. 1991. Multicyclic history of the northern Indian continental margin (northwestern Himalaya). *American Association of Petroleum Geologists, Bulletin*, 75, 1427–1446.
- Garzanti, E. 1999. Stratigraphy and sedimentary history of the Nepal Tethys Himalaya passive margin. *Journal of Asian Earth Sciences*, 17, 805-827.
- Garzione, C. N., DeCelles, P. G., Hodkinson, D. G., Ojha, T. P. & Upreti, B. N. 2003. East-west extension and Miocene environmental change in the southern Tibetan plateau: Thakkhola graben, central Nepal. *Geological Society of America Bulletin*, 115, 3-20.
- Godin, L. 2003. Structural evolution of the Tethyan sedimentary sequence in the Annapurna area, central Nepal Himalaya. *Journal of Asian Earth Sciences*, 22, 307-328.
- Godin, L., Grujic, D., Law, R. D. & Searle, M. P. 2006. Channel flow, extrusion and exhumation in continental collision zones: an introduction. In: Law, R. D., Searle, M. P. & Godin, L. (eds) *Channel Flow, Ductile Extrusion and Exhumation in Continental Collision Zones*. Geological Society, London, Special Publications, 268, 1-23.
- Grujic, D., Lincoln, S., Hollister, L. S. & Parrish, R. R. 2002. Himalayan metamorphic sequence as an orogenic channel: insight from Bhutan. *Earth and Planetary Science Letters*, 198, 177-191.
- Guillot, S., Pêcher, A., Rochette, P. & LeFort, P. 1993. The emplacement of the Manaslu granite of central Nepal: field and magnetic susceptibility constraints. In: Treloar, P.J. & Searle, M.P. (eds) *Himalayan tectonics*. Geological Society, London, Special Publications, 74, 413-428.
- Harrison, T. M., Ryerson, F. J., Le Fort, P., Yin, A., Lovera, O. M. & Catlos, E. J. 1997. A late Miocene-Pliocene origin for the Central Himalayan inverted metamorphism. *Earth and Planetary Science Letters*, 146, E1-E8.
- Harrison, T.M., Yin, A., Grove, M. & Lovera, O.M. 2000. The Zedong Window: A record of superposed Tertiary convergence in southeastern Tibet. *Journal of Geophysical Research*, 105, 19,211-19,320.
- Heim, A. & Gansser, A. 1939. *Central Himalaya. Geological Observations of the Swiss Expedition 1936*. Mémoires de la Société Helvétique des Sciences Naturelles, 7/31, 1-245.
- Heinrichs, H. & Herrmann, A. G. 1990. *Praktikum der Analytischen Geochemie*. 669 p., Springer Verlag.
- Hodges, K.V., Parrish, R. R. & Searle, M. P. 1996. Tectonic evolution of the central Annapurna Range, Nepalese Himalayas. *Tectonics*, 15, 1264-1291.
- Hodges, K.V. 2000. Tectonics of the Himalaya and southern Tibet from two perspectives. *Geological Society of America Bulletin*, 112, 324-350.
- Holland, T. J. B. & Powell, R. 1998. An internally-consistent thermodynamic dataset for phases of petrological interest. *Journal of Metamorphic Geology*, 16, 309-344.
- Hower, J., Hurley, P. M., Pinson, W. H., & Fairbairn, H. W. 1963. The dependence of K-Ar age on the mineralogy of various particle size ranges in a shale. *Geochimica et Cosmochimica Acta*, 27, 405-410.
- Hurley, P. M., Hunt, J. M., Pinson, W. H. & Fairbairn, H. W. 1963. K-Ar age values on the clay fractions in dated shales. *Geochimica Cosmochimica Acta*, 27, 279-284.
- Jadoul F., Berra F. & Garzanti E. 1998. The Tethys Himalayan passive margin from Late Triassic to Early Cretaceous (South Tibet). *Journal of Asian Earth Sciences*, 16, 173-198.
- Judik, K., Rantitsch, G., Rainer, Th. M., Árkai, P. & Tomljenović, B. 2008. Organic metamorphism in metasedimentary rocks from Mt. Medvednica (Croatia). *Swiss Journal of Geosciences*, 101, 605-616.
- Kellett, D. A & Godin, L. 2009. Pre-Miocene deformation of the Himalayan superstructure, Hidden valley, central Nepal. *Journal of the Geological Society, London*, 166, 261-275.
- Kisch, H. J., Árkai, P. & Brime, C. 2004. On the calibration of the illite Kübler index (illite “crystallinity”). *Schweizerische Mineralogische und Petrographische Mitteilungen*, 84, 323–331.
- Kohn, M. J. & Spear, F. S. 1991. Error propagation for barometers: 1. Accuracy and precision of experimentally located end-member reactions. *American Mineralogist*, 76, 128-137.
- Kübler, B. 1967. La cristallinité de l’illite et les zones tout à fait supérieures du métamorphisme. *Étages Tectoniques*, 105–122.
- Kübler, B. 1968. Evaluation quantitative du mtamorphisme par la cristallinité de l’illite. *Bulletin du Centre de Recherches, Pau SNPA*, 2, 385–397.

- Kübler, B. 1990. "Cristallinité" de l'illite et mixed-layers: brève révision. *Schweizerische Mineralogische und Petrographische Mitteilungen*, 70, 89–93.
- Le Fort, P. 1975. Himalayas, the collided range. Present knowledge of the continental arc. *American Journal of Science*, 275-A. 1-44.
- Le Fort, P. 1971. *Les formations cristallophyliennes de la Thakkhola. Recherches géologiques dans l'Himalaya du Népal, région del Thakkhola*. E'dition du CNRS Paris.
- Lee, J., Hacker, B. R., Dinklage, W. S., Wang, Y., Gans, P., Calvert, A., Wan, J. L., Chen, W.J., Blythe, A.E. & McClelland, W. 2000. Evolution of the Kangmar Dome, southern Tibet: Structural, petrologic, and thermochronologic constraints. *Tectonics*, 19, 872-895.
- Leech M. L. 2008. Does the Karakoram fault interrupt mid-crustal channel flow in the western Himalaya?. *Earth and Planetary Science Letters*, 276, 314-322.
- Liu, G. 1992. *Permian to Eocene sediments and Indian passive margin evolution in the Tibetan Himalayas*. Tübinger Geowissenschaftliche, A 13.
- Liu, G & Einsele, G. 1994. Sedimentary history of the Tethyan basin in the Tibetan Himalayas. *Geologische Rundschau*, 83, 32-61.
- Liu, G & Einsele, G. 1996. Various types of olistostromes in a closing ocean basin, Tethyan Himalaya (Cretaceous, Tibet). *Sedimentary Geology*, 104, 203-226.
- Livi, K. J. T., Veblen, D. R., Ferry, J. M. & Frey, M. 1997. Evolution of 2:1 layered silicates in low-grade metamorphosed Liassic shales of Central Switzerland. *Journal of Metamorphic Geology*, 15, 323–344.
- McQuarrie, N., Robinson, D., Long, S., Tobgay, T., Grujic, D., Gehrels, G., Ducea M. 2008. Preliminary stratigraphic and structural architecture of Bhutan: Implications for the along strike architecture of the Himalayan system. *Earth and Planetary Science Letters*, 272, 105-117.
- Mercier, J. L *et al.* 1984. La collision Inde-Asie côté Tibet. In: Mercier, J. L. & Li, G.C. (eds) *Mission Franco-Chinoise Au Tibet 1980: Étude Géologique Et Géophysique De La Croûte Terrestre Et Du Manteau Supérieur Du Tibet Et De L'Himalaya*. Editions du Centre National de la Recherche Scientifique, Paris, France, 341-350. 29.
- Meunier, A. & Velde, B. 2004. Illite: origins, evolution and metamorphism. 286 ., Springer.
- Montomoli, C., Appel, E., Antolin, B., Dunkl, I., El Bay, R., Lin, D. & Gloaguen, R. 2008. Polyphase deformation history of the "Tibetan Sedimentary Sequence" in the Himalaya chain (South-East Tibet). *Himalayan Journal of Sciences*, 5, 91.
- Najman, Y., Carter, A., Oliver, G. & Garzanti, E. 2005. Provenance of Eocene foreland basin sediments, Nepal: Constraints to the timing and diachroneity of early Himalayan orogenesis. *Geology*, 33, 309-312.
- Pan, G., Ding, J., Yao, D. & Wang, L. 2004. *Geological map of Qinghai-Xizang (Tibet) Plateau and Adjacent Areas (1:1,500,000)*. Chengdu Institute of Geology and Mineral Resources, China Geological Survey. Chengdu Cartographic Publishing House.
- Patzelt, A., Li, H., Wang, J. & Appel, E. 1996. Paleomagnetism of Cretaceous to Tertiary sediments from southern Tibet: evidence for the extent of the northern margin of India prior to the collision with Eurasia. *Tectonophysics*, 259, 259-284.
- Pêcher, A. 1975. The Main Central Thrust of the Nepal Himalaya and the related metamorphism in the Modi Khola cross-section (Annapurna Range). *Himalayan Geology* 5. 115–131.
- Paudel L. P. & Arita K. 2006. Thermal evolution of the Lesser Himalaya, central Nepal: Insights from K-white micas compositional variation. *Gondwana Research*, 9, 409-425.
- Potel, S. 2007. Very low-grade metamorphic study in the pre-Late Cretaceous terranes of New Caledonia (southwest Pacific Ocean). *Island Arc*, 16, 291–305.
- Powell, R. & Holland, T. J. B. 1994. Optimal geothermometry and geobarometry. *American Mineralogist*, 79, 120-130.
- Powell, R. & Holland, T. J. B. 2006. Course Notes for "THERMOCALC Short Course" - Sao Paulo, Brazil, on CD-ROM.
- Powell, R. & Holland, T. J. B. 2008. On Thermobarometry. *Journal of metamorphic Geology*, 26, 155-179.
- Quidelleur, X., Grove, M., Lovera, O. M., Harrison, T. M. & Yin, A. 1997. Thermal evolution and slip history of the Renbu-Zedong Thrust, southeastern Tibet. *Journal of Geophysical Research*, 102, 2659-2679.

- Ratschbacher, L., Frisch, W., Liu, G., Chen, C. 1994. Distributed deformation in southern and western Tibet during and after the India-Asia collision. *Journal of Geophysical Research*, 99, 19,917-19,945.
- Reuter, A. 1987. Implications of K-Ar ages of whole-rock and grain-size fractions of metapelites and intercalated metatuffs within an anchizonal terrane. *Contribution to Mineralogy and Petrology*, 97, 105-115.
- Robinson, D. M., De Celles, P. G., Garziona, C. N., Pearson, O. N., Harrison, T. M., Catlos, E. J. 2003. Kinematic model for the Main Central thrust in Nepal. *Geology*, 31, 339-362.
- Schumacher, E. 1975. Herstellung von 99,9997% ^{38}Ar für die $^{40}\text{K}/^{40}\text{Ar}$ Geo-chronologie. *Geochronologia Chimia*, 24, 441-442.
- Searle, M. 1986. Structural evolution and sequence of thrusting in the High Himalayan, Tibetan-Tethys and Indus suture zones of Zaskar and Ladakh, Western Himalaya. *Journal of Structural Geology*, 8, 923-936.
- Searle, M. P. & Godin, L. 2003. The south Tibetan detachment and the Manaslu leucogranite: A structural reinterpretation and restoration of the Annapurna-Manaslu Himalaya, Nepal. *Journal of Geology*, 111, 505-523.
- Spear, F. S. 1995. *Metamorphic Phase Equilibria and Pressure-Temperature-Time Paths*. Mineralogical Society of America, Washington, D.C., 1-799.
- Steiger, R. H. & Jäger, E. 1977. Subcommittee on Geochronology: Convention on the Use of Decay Constants in Geo- and Cosmochronology. *Earth and Planetary Science Letters*, 36, 359-362.
- Stöcklin, J. 1980. Geology of Nepal and its regional frame. *Journal of the Geological Society, London*, 137, 1-34.
- Sweeney, J. J. & Burnham, A. K. 1990. Evaluation of a simple model of vitrinite reflectance based on chemical kinetics. *Bulletin American Association of Petroleum Geologists*, 74, 1559-1570.
- Upreti, B. N. 2001. Stratigraphy, structure, and tectonic evolution of the Himalayan fold-thrust belt in western Nepal. *Tectonics*, 20, 487-509.
- Valdiya, K.S. 1980. *Geology of the Kumaun Lesser Himalaya*. Dehra Dun, Wadia Institute of Himalayan Geology.
- Warr L. N. & Rice A. H. N. 1994. Interlaboratory standardisation and calibration of clay mineral crystallinity and crystallite size data. *Journal of Metamorphic Geology*, 12, 141-152.
- Wemmer K. 1991. *K/Ar-Altersdatierungsmöglichkeiten für retrograde Deformationsprozesse im spröden und duktilen Bereich - Beispiele aus der KTB-Vorbohrung (Oberpfalz) und dem Bereich der Insubrischen Linie (N-Italien)*. Göttinger Arbeiten zur Geologie und Paläontologie, 51.
- Willems, H., Zhou, Z., Zhang, B., Gräfe, K. U. 1996. Stratigraphy of the Upper Cretaceous and Lower Tertiary strata in the Tethyan Himalayas of Tibet (Tingri area, China). *Geologische Rundschau*, 85, 723-754.
- Wojdyr, M. 2007. FITYK: A curve fitting and data analysis program. World Wide Web address: <http://www.unipress.waw.pl/fityk/>
- Yin, A. 2006. Cenozoic tectonic evolution of the Himalayan orogen as constrained by along-strike variation of structural geometry, exhumation history, and foreland sedimentation. *Earth-Science Reviews*, 76, 1-131.
- Yin, A., Harrison, T. M., Ryerson, F. J., Wenji, C., Kidd, W. & Copeland, P. 1994. Tertiary structural evolution of the Gangdese thrust system, southeastern Tibet. *Journal of Geophysical Research*, 99, 18,175-18,201.
- Xu, X., Ding, L., Qiang, X., Fulong, C., Qinghai, Z., Liyun, Z., Qingzhou, L. 2009. Tectonic implications of the Ultramafic Dykes in Southeastern Tibet. *Chinese Journal of Geology*, 44 (3), 1012-1024.
- Zhang, B., Zhang, J., Guo, L. & Wang, W. 2005. Microstructural and deformational studies on mylonite in the detachment faults of Yalashangbo dome, North Himalayan domes zone. *Progress in Natural Science*, 15, 11, 1005-1013.
- Zhu, D., Mo, X., Pan, G., Zhao, Z., Dong, G., Shi, Y., Liao, Z., Wang, L., Zhou, C. 2008. Petrogenesis of the earliest Early Cretaceous mafic rocks from the Cona area of the eastern Tethyan Himalaya in south Tibet: Interaction between the incubating Kerguelen plume and the eastern Greater India lithosphere? *Lithos*, 100, 147-173.

4

Paleomagnetic evidence for clockwise rotation and tilting in the eastern Tethyan Himalaya (SE Tibet): Implications for the Miocene tectonic evolution of the NE Himalaya

4.1 Abstract

Crustal movement around and away from the Namche Barwa syntaxis is indicated in the Asian velocity field inferred from GPS data and Quaternary fault slip rates. Nevertheless, there is limited field-based control on the rotational history of the north-eastern Himalayan arc. Exploring the poly-phase nature of deformation, within the Cretaceous diorite dykes and the Triassic flysch, in the eastern Tethyan Himalaya (90°-92°E), combined with new remote sensing data and the existing thermo-geochronological data allow us to unravel the kinematic relationship between our new paleomagnetic remanence vectors and the deformation phases. Magneto-mineralogical analyses in the Cretaceous diorite dykes indicate that the characteristic remanent magnetization is mainly carried by pyrrhotite. The approximate constant declination values within the double vergent flysch pile in the Qonggyai valley and the ~22 Ma K-Ar age of the last metamorphic event suggest that the remanence is post-Eohimalayan folding and likely of thermo-remanent origin. Calculated vertical-axis rotations in Nagarze and Qonggyai areas indicate a trend from no apparent rotation in the west to 20° clockwise rotation in the east with respect to the Indian plate. This result can be kinematically related to the Middle to Late-Miocene southeast extrusion of SE Tibet. Furthermore the observed pattern of tilting around horizontal axis may reflect concealed North Himalayan doming.

4.2 Introduction

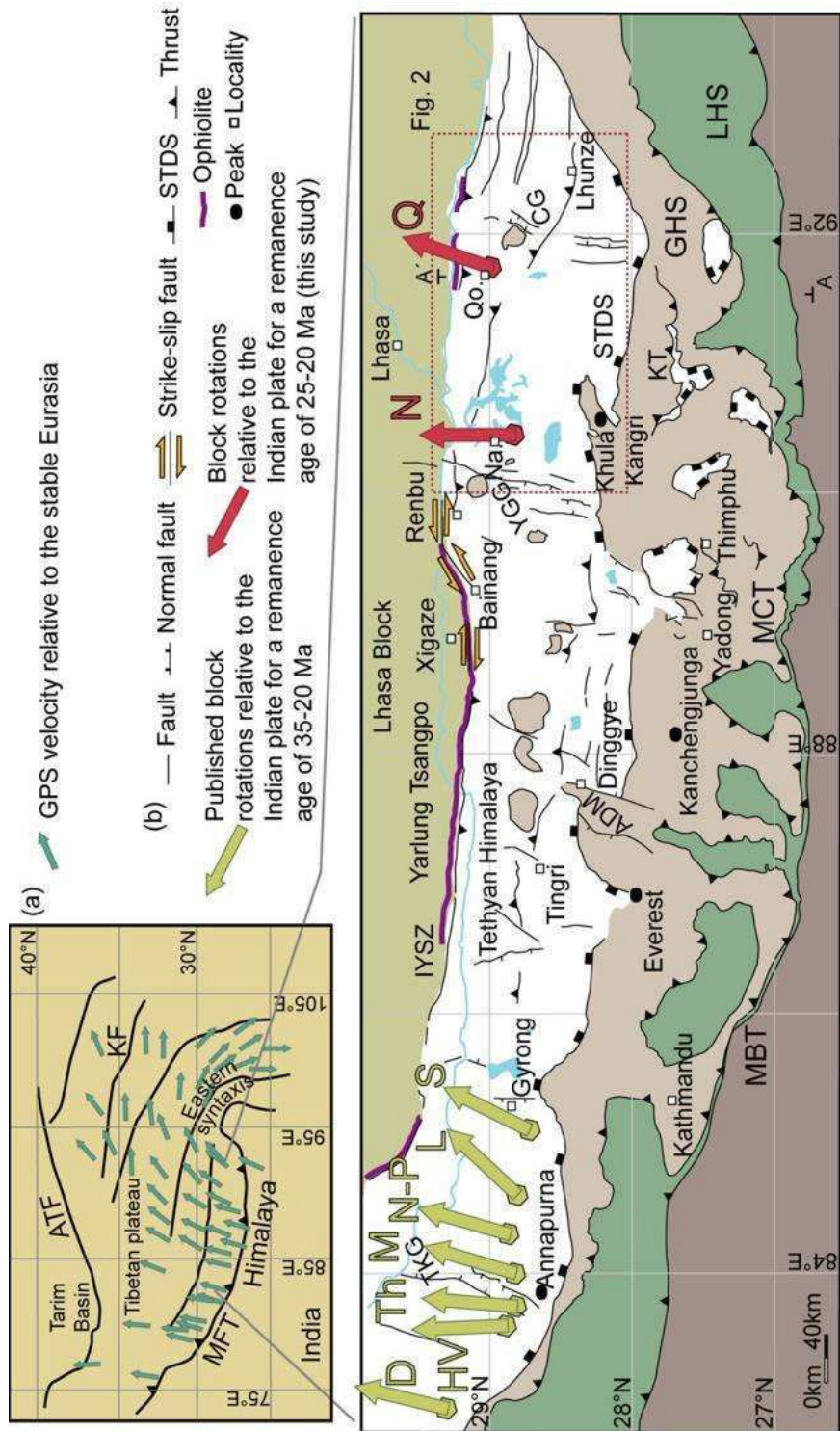
The indentation of the Indian plate into the Eurasian plate and ongoing north-south convergence of both continents resulted in large-scale shortening of Greater India (Ali and Aitchison, 2005) and the rise of the Himalayan belt around ~55 Ma (e.g. Gaetani and Garzanti, 1991; Guillot et al., 2003; Liebke et al., submitted). Since these two tectonic plates collided three simplified mechanisms have controlled the Himalayan architecture: N-S shortening, N-S extension and orogen-parallel extension (Searle, 1996; Hodges, 2000; Yin and Harrison, 2000 for reviews). How these end members processes are partitioned along time plays a key role for the interpretation and modeling of the uplift of the Himalaya and the Tibetan plateau.

The present study focuses on SE Tibet, a cornerstone area in the kinematic evolution of the Himalaya-Tibet system because of its structural position in between two tectonic domains: the Himalayan domain, controlled by N-S shortening and E-W extension (since Middle Miocene; e.g. Armijo et al., 1986; Jessup et al., 2008), and the Tibetan domain governed by ESE-WNW extension and southeastward and eastward movement of crustal material (since Middle Miocene, e.g. Tapponnier et al., 1982; Royden et al., 1997; Zhang et al., 2004). The far east of southern Tibet, close to the eastern Himalayan syntaxis, is a region where the indentation of India presently creates strong lateral inhomogeneity of deformation (Armijo et al., 1989; Royden et al., 1997; Holt et al., 2000). Eastward motion is evident by GPS velocities which indicate motion around and away from the eastern syntaxis (e.g. Gan et al., 2007; Fig. 1a). However, there is currently limited field-based studies on the rotational history of the eastern Himalayan arc (Li and Yin, 2008), which can be utilized to constrain the mechanisms that have controlled part of the kinematic evolution of the eastern Himalayan Belt and SE part of the Tibetan plateau. The present study utilizes new measured paleomagnetic remanence directions, widely proved as a powerful tool in distinguishing between different kinematic models of deformation in orogens (Weil and Sussman, 2004), e.g. Apalachian mountains (Eldredge et al., 1985), Pyrenees belt (Oliva-Urcia and Pueyo, 2007); Patagonian orocline (Maffione et al., 2009). In the Himalayan orogen paleomagnetism has been applied to quantify vertical-axis block rotations in the western Himalaya reflecting the indentation of India into Eurasia and the development of the western syntaxis. The block rotation pattern in the western syntaxis describes a clockwise rotation in the eastern zone of the syntaxis and counterclockwise rotations in the western part since remanence acquisition at ~50-40 Ma (Klootwijk et al., 1985; Appel et al., 1995; Schill et al., 2001). These results have been utilized to interpret the mechanism of the formation of the Nanga Parbat Haramosh syntaxis as pure-bending, also called oroclinal bending (Schill and Holt, 2004). Further to the

east (western to central Nepal) Schill et al. (2004) obtained an increasing trend to clockwise rotations in the Tethyan Himalaya remanence directions from Hidden valley in the west (83.6°E) to Shiar valley in the east (85.1°E), for remanence acquisition ages ~30-25 Ma (Fig. 1b). This was interpreted as a result of a large-scale dextral shear zone associated to the eastward extrusion of the Tibetan plateau (Schill et al., 2004). Further to the east between the Shiar valley and the study area there are no paleomagnetic data published until present.

In this paper, we report new paleomagnetic results from the Cretaceous diorite dykes widely exposed within the Triassic flysch in the eastern Tethyan Himalaya (90°-92°E). These are combined with structural data, remote sensing analysis and the existing K-Ar geochronology, Kübler Index (illite crystallinity) and vitrinite reflectance data from the Triassic flysch. Outcome from these sources provide vertical-axis block rotations and tilt around horizontal axis to constraint the Miocene kinematic evolution and deformation mechanisms in the NE Himalayan region.

Figure 1: (a) selected and slightly generalized GPS velocity field relative to stable Eurasia (after Gan et al., 2007). MFT, Main Frontal Thrust; KF, Kunlun Fault; ATF, Altyn Tagh Fault. (b) simplified geological map of the central and eastern Himalaya (after Lee et al., 2000; Pan et al., 2004; Kellett et al., 2009) with the published paleomagnetic block rotations in the Tethyan Himalaya (Schill et al., 2004 and references therein): D, Dolpo ; HV, Hidden valley; Th, Thakkhola; M, Manang; N-P, Nar/Phu; L, Larkya; S, Shiar. Paleomagnetic block rotations calculated in this study: N, Nagarze and Q, Qonggyai. TKG, Thakkhola Graben; IYSZ, Indus Yarlung suture zone; ADM, Ama Drime Massif; YGG, Yadong-Gulu Graben; Na, Nagarze; Qo, Qonggyai; CG, Cona Graben; STDS, South Tibetan Detachment System; KT, Kakhtang thrust; GHS, Greater Himalayan sequence; MCT, Main Central Thrust; LHS, Lesser Himalayan sequence; MBT, Main Boundary Thrust. Sense of strike slip-faults close to the IYSZ: South of Xigaze and in Bainang (Ratschbacher et al., 1994) and in Renbu (Yin et al., 1994).



4.3 Geological setting

4.3.1 Boundaries and deformation of the Tethyan Himalayan sequence

The study area is located in the eastern Tethyan Himalayan sequence (THS) in SE Tibet, between the north dipping normal faults of the South Tibetan Detachment System (STDS) (e.g. Pêcher et al., 1991; Burchfiel et al., 1992; Carosi et al., 1998) and the Indus Yarlung Suture zone (IYSZ) (Gansser, 1964; Fig.1b). The THS is the cover of the Greater Himalayan sequence (GHS) which has been probably exhumed during contemporaneous normal-sense ductile shearing along the STDS and the south-vergent thrusting on the Main Central Thrust (MCT) (Burchfiel et al., 1992; Grujic et al., 2002) at about 24-12 Ma for the whole Himalaya (Godin et al., 2006 and references therein).

The IYSZ is complexly affected by the development of the Gangdese Thrust system, the Great Counter Thrust (GCT) and locally strike-slip and normal fault systems (Yin et al., 1994; Harrison et al., 2000; Ding et al., 2005).

The THS represents a ~150 km wide zone comprising a stratigraphic record of sedimentation at the northern continental margin of India from Paleozoic to Eocene times (Gaetani and Garzanti, 1991; Willems et al., 1996). Despite differences between studies along different profiles, five main and common events have controlled the actual view of the structure in the THS. In geochronological order these are south-verging isoclinal folds with related axial plane foliation (Eocene to Early Oligocene; e.g. Burg and Chen, 1984; Ratschbacher et al., 1994; Hodges, 2000), north-vergent folds with axial plane foliation (Oligocene to Early Miocene; Godin, 2003; Montomoli et al., 2008; Kellett and Godin, 2009), top-to-the NE displacement along the STDS and north-vergent backthrusting activity on the GCT (Middle Miocene; e.g. Harrison et al., 2000; Carosi et al., 2002; Dunkl et al., submitted), exhumation of the North Himalayan domes (Miocene; see Leech, 2008 for an updated review), N-S normal faults and seven major N-S-trending graben structures related to E-W extension (Late Miocene; e.g. Armijo et al., 1986; Searle, 1996; Garzzone et al., 2003; Jessup et al., 2008; Fig. 1b).

4.3.2 Sampling and lithology of the studied area

We collected paleomagnetic samples from 30 sites in SE Tibet along two N-S profiles of about 30 km from 29°10'N to 28°54'N and separated by 130 km in E-W direction. One transect is located in Nagarze-Yamdrock Lake area (90°19'E) with 10 sites and the other in the Qonggyai valley (91°40'E) with 20 sites (Fig. 2a). The studied rocks are diorite, diabase and dolerite dykes intruded in the Triassic flysch. These dykes were sampled 15 km south of the IYSZ and 85-100 km north of STDS. The thickness of the dykes ranges from one meter to

~100 m. The texture and the typical crystal size are very variable, changing from very coarse-grained holocrystalline to fine grained, nearly aphanitic. In the ultramafic members poikilitic or cumulate textures are typical. Some of the magmatic bodies and typically their interior parts show well conserved magmatic textures, but in many outcrops the dykes are strongly deformed and transformed to chlorite or amphibole schists. The margins and contact aureoles of the dykes are mainly altered to banded, chaotic and mica-rich zones (Dunkl et al., submitted). Close to Nagarze SHRIMP U-Pb dating of mafic dykes indicate emplacement age of 135-133 Ma (Zhu et al., 2008; Xu et al., 2009). Genesis of the studied dykes has been related to a progressive lithosphere thinning beneath eastern Gondwanaland during early Cretaceous (Zhu et al., 2008). The dykes are generally deformed within the flysch and have been affected by the main regional tectonic events above described.

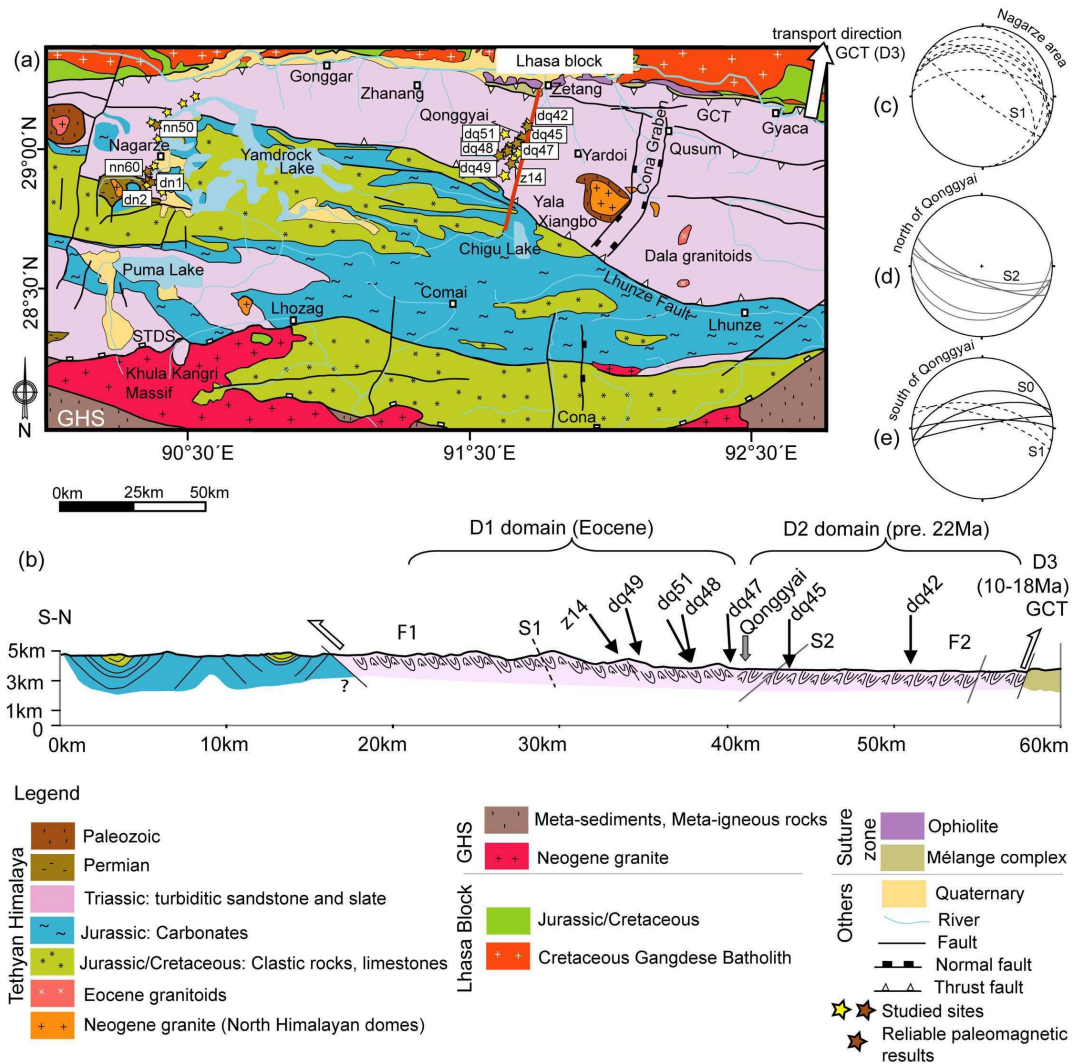


Figure 2: (a) lithotectonic map of the study area in SE Tibet after Harrison et al., (2000); Pan et al., (2004) and Aikman et al., (2008). (b) cross section along the Qonggyai valley transect after map of Pan et al., (2004); Aikman et al., (2008) and data from Montomoli et al., (2008) and Antolín et al., (in press). GCT, Great Counter Thrust. STDS, South Tibetan Detachment System; GHS, Greater Himalayan sequence. (c) equal-area lower-hemisphere stereogram of S1 foliation measured in

Nagarze and Yamdrock lake area. (d) stereogram with S2 foliation measured north of Qonggyai and east of Zetang. (e) stereogram with S0 and S1 foliation measured south of Qonggyai.

4.3.3 Tectonic architecture and metamorphism in the Qonggyai valley

The Qonggyai valley exposes the Triassic flysch and diorite dykes along ca. 40 km between the south dipping GCT in the north and the Lhunze fault in the south (Fig. 2a,b). The GCT system brings the Triassic flysch over the mélangé complex, ophiolites and Cretaceous sediments of Eurasian affinity (e.g., Yin et al., 1994; Harrison et al., 2000; Dupuis et al., 2006). The Lhunze fault trends from NW-SE to E-W and dips to the N (Aikman et al., 2008), separating the Triassic flysch (hangingwall) from the Cretaceous and Upper Jurassic rocks (footwall). The flysch sediments, turbiditic sandstones and slates, were deposited in an abyssal and bathyal environment between Middle Triassic and Early Jurassic (Dupuis et al., 2006). South of the Lhunze fault the Cretaceous clastic rocks, limestones and Upper Jurassic continental clastic rocks, marls and marine limestones represent the platform sequence of the Indian passive margin (Fig. 2a) (Liu and Einsele, 1994; Pan et al., 2004).

The flysch pile within these two thrusts describes a double vergent wedge derived from the multi-phase tectonic history of the Tethyan Himalaya. The southern portion, approximately between the Lhunze fault and Qonggyai is dominated by D1 structures typically of Eohimalayan age (Hodges, 2000). It is characterized by E-W isoclinal F1 folds and related axial planar foliation S1 trending E-W with dip to the N (Montomoli et al., 2008) (Figs. 2b,c,e and 3a). Figure 3b show a decametric folded diorite dyke (F1 fold) parallel to the Triassic flysch F1 folds (Fig. 3c). Stretching lineation, obtained from anisotropy of magnetic susceptibility data, south of Qonggyai trend SSW-NNE with intermediate plunges to the N and has been related to southward motion of flysch slices along thrust planes towards the Himalayan foreland in consonance with the main southward vergence of the orogen (Antolín et al., in press). Locally S1 can occur steeply dipping toward the S as in the area around Qonggyai village, due to the development of later collapse folds with sub-horizontal axial plane. Figure 3d,g show S1 foliation in the margin of a dyke parallel to the foliation of the neighboring slates (site dq47 in Fig. 2a,b). Moving to the north the flysch is characterized by north-vergent F2 decametric folds and microfolds which deform the S1 foliation (Montomoli et al., 2008). Approaching the GCT the flysch structure is controlled by S2 foliation trending E-W and dipping to the south, caused by hinterland propagation of the deformation (D2 deformation phase; Figs. 2d and 3a). K-Ar isotope radiogenic ages in newly grown illites near site dq45, within the D2 domain, show ~22 Ma cooling ages which have been related to peak metamorphism during D2 phase (Dunkl et al., 2008; Antolín et al., in press). During D2 the Triassic flysch and diorite dykes underwent anchi- to epizonal metamorphic conditions, as

indicated Kübler Index values (Dunkl et al., submitted). Continuation of backward deformation towards higher structural levels was probably responsible for the formation of the north-directed GCT around 18 Ma to 10 Ma (D3 phase; Fig. 3a) (Yin et al., 1994; Harrison et al., 2000; Antolín et al., in press).

The Yala Xiangbo North Himalayan dome (Fig. 2a) was emplaced at ca. 18 Ma and cooled at ca. 13.5 Ma (Aikman et al., 2004). Finally orogen parallel extension (E-W) dominates the orogen architecture, which trigger kilometer-scale N-trending normal faults during the Pliocene; D4 phase (e.g. Armijo et al., 1986; Fig. 3a). The study area is bounded to the west by the Yadong Gulu Graben (90°E) and is cross-cut by the easternmost Himalayan Graben, the Cona Graben at ~92°E (Figs. 1b and 2a; Armijo et al., 1986; Garzzone et al., 2003). GPS velocities indicate no significant (0.3 ± 0.9 mm/yr) fault opening at present-day in the Cona Graben and 2.0 ± 0.6 mm/yr opening rate in the Yadong-Gulu Graben (Gan et al., 2007).

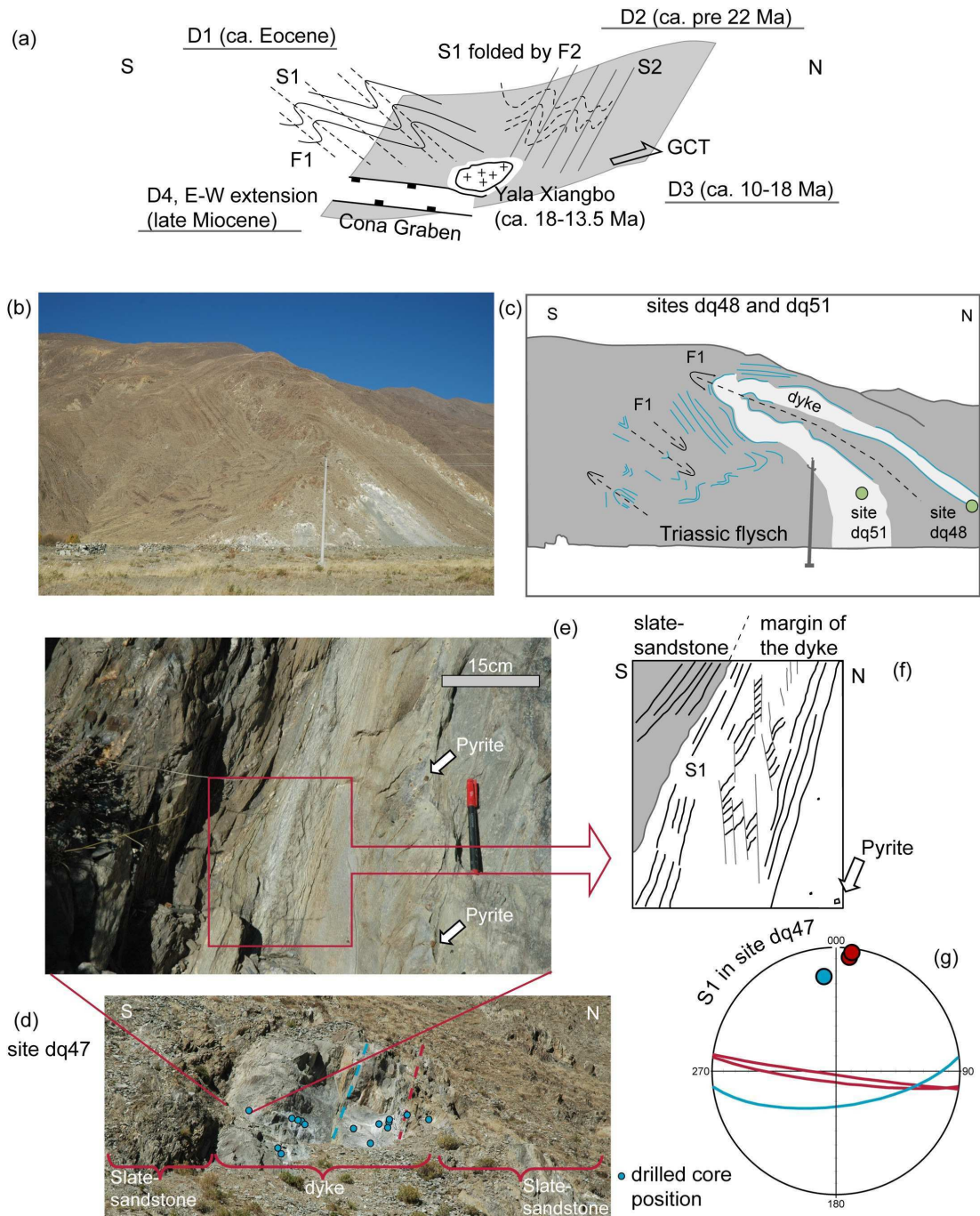


Figure 3: (a) Sketch of structural relationship between deformation phases within the Triassic flysch. (b) and (c) picture and interpretation of F1 folds close to sites dq48 and dq51. (d) Studied site dq47. (e) and (f) picture of the contact between dyke and flysch and interpretation of the foliation developed in the margin of the dyke. (g) Equal-area lower-hemisphere stereogram of S1 foliation in site dq47.

4.4 Methods

4.4.1 Sampling and paleomagnetic laboratory procedure

In general 10 cores with 2.5 cm in diameter were taken from each site using a portable gasoline powered drill; orientation was done by a magnetic compass. The cores were cut into specimens of standard size (2.2 cm length). Sampling was focused in the margin of the dykes where sulphure migration from the neighboring slates could increase the original sulphure content of the dyke and result in the formation of pyrrhotite. Two sites (dq48, dq51) were drilled within the limbs of a decametric isoclinal fold deformed within the Triassic flysch (Fig. 3c). Foliation attitudes in the neighboring flysch and at the margin of the dykes allow tectonic correction of some of the sites.

Rock magnetic experiments were elaborated to determine the nature of the carrier of characteristic remanence magnetization (ChRM): Low and high temperature thermomagnetic curves using a CS3 unit coupled with a Kappabridge KLY-3 (AGICO), acquisition curves of isothermal remanent magnetization (IRM) in a stepwise increasing DC field up to 1.9 T at room temperature using an MMPM9 pulse magnetizer (Magnetic Measurements) and stepwise thermal demagnetization of the saturation IRM (SIRM). Furthermore in 3 selected samples we performed low-temperature measurements down to 5 °K in a zero field environment using a Magnetic Properties Measurement System (MPMS) -XL7 magnetometer (Quantum Design Ltd.).

Demagnetization procedures were first performed on pilot specimens (two samples per site). Alternating field stepwise demagnetization (AfD) of natural remanent magnetization (NRM) was performed using an automatic degausser (2G600) coupled to a three-axis SQUID magnetometer (RF SQUID 760 R, 2G Enterprises). This magnetometer was also used to measure the magnetization remaining after each step of heating. Stepwise thermal demagnetization (ThD) of NRM and SIRM were performed utilizing a thermal specimen demagnetizer, model TD-48SC (ASC Scientific). Susceptibility was monitored after each step of ThD to control changes in the magnetic mineralogy using a Kappabridge KLY-2 (AGICO). After comparison of the two methods, ThD was chosen for demagnetization of the bulk samples. AfD did not reach complete demagnetization and furthermore ThD showed more stable demagnetization behavior. ChRM directions for each sample were computed using principal component analysis (Kirschvink, 1980). Sites means were determined by Fisher statistics (1953) and small circle method after Waldhör et al. (2001, 2006). All magnetic measurements were done in the paleomagnetic laboratory at the University of Tübingen except MPMS measurements which were carried out at University of Bremen.

4.4.2 Neotectonic analysis

Rivers flowing along bedrock channels are the primary non-glacial mechanism of incision. The rate at which channels incise sets the rate at which the rest of the landscape evolves, and hence may control the response time of such landscapes to tectonic forcing (e.g. Jackson et al., 1996; Gloaguen et al., 2008). The drainage network is extracted from SRTM v.4 data by calculating flow directions at all points using the D8 algorithm. Stream longitudinal profiles are identified and selected based upon least cost path analyses. We compute paths of least down slope resistance (i.e. the downstream flow path) and Strahler's stream order. Incision maps, i.e. the local relief within a moving window, provide useful information for the determination of neotectonic features (e.g. Käbner et al., 2008). The spatial organisation of a river system and its space filling properties (e.g. dendritic, orthogonal) can be strongly controlled by tectonics (e.g. Jackson et al., 2002; Gloaguen et al., 2007). Their analysis provides first hand clues to characterize tectonic forcing on landscape formation (e.g. Burbank et al., 1996; Shahzad et al., 2009). Analysis of basin asymmetry can provide important map-scale data for neotectonic assessment, allowing the delineation of geomorphic domains of stream migration that may be related to tilting fault blocks or developing folds (e.g., Cox et al., 2001). As streams respond to uplift or subsidence by migrating laterally in a down-tilt direction, a record of this migration is preserved as a preferential direction of transverse asymmetry of the drainage basins of the tilting region. This technique produces a vector field (T-factors) of spatially averaged directions of basin asymmetry (inferring lateral stream migration), and areas showing preferred directions of stream migration can be evaluated in terms of ground tilting. A semi-automated method of analysis which delivers the T-factor morphometric index from a Digital Elevation Model (DEM) has been implemented on MATLAB (Shahzad and Gloaguen, submitted). From these vector data, different spatial domains will be drawn, showing areas of basins displaying potentially different directions of asymmetry.

4.5 Paleomagnetic results

4.5.1 Magneto-mineralogical characterization

Rock powder samples from 11 sites, two from Nagarze and 9 from Qonggyai were analysed for susceptibility versus temperature. Low-temperature curves down to -196 °C show temperature dependence following the Curie Law (Nagata, 1961) below -100 °C, indicating small contribution of paramagnetic minerals to the total magnetic susceptibility signal. Low-temperature curves down to 5 °K carried out in the MPMS did not show Morin transition of hematite at ~260 °K, Verwey transition of magnetite at ~120 °K, or pyrrhotite transition at

30-34°K (Rochette et al., 1990; Fig. 4a). High-temperature curves indicate that magnetic susceptibility is predominantly controlled by the existence of pyrrhotite pointed out by a Hopkinson peak followed by a marked drop of susceptibility around the Curie temperature of pyrrhotite at ca. 325 °C (Fig. 4b, dq47 and dn5). At higher temperature > 400 °C a rise in magnetic susceptibility indicates the new formation of magnetite due to heating. Some samples indicate also a contribution of initial magnetite indicated by a decay of susceptibility around the Curie temperature of magnetite ca. 580 °C (Fig. 4b, dq42).

IRM starts to saturate from 300-500 mT until 1 T when saturation is almost reached (Fig. 4c). Such saturation fields are clearly higher than expected for magnetite (max. 300mT) and typical for pyrrhotite. Thermal demagnetization of SIRM is mainly achieved around the Curie temperature of pyrrhotite (325 °C) in all the studied samples and afterwards a minor decay at around 580 °C indicates a small contribution of magnetite (Fig. 4d).

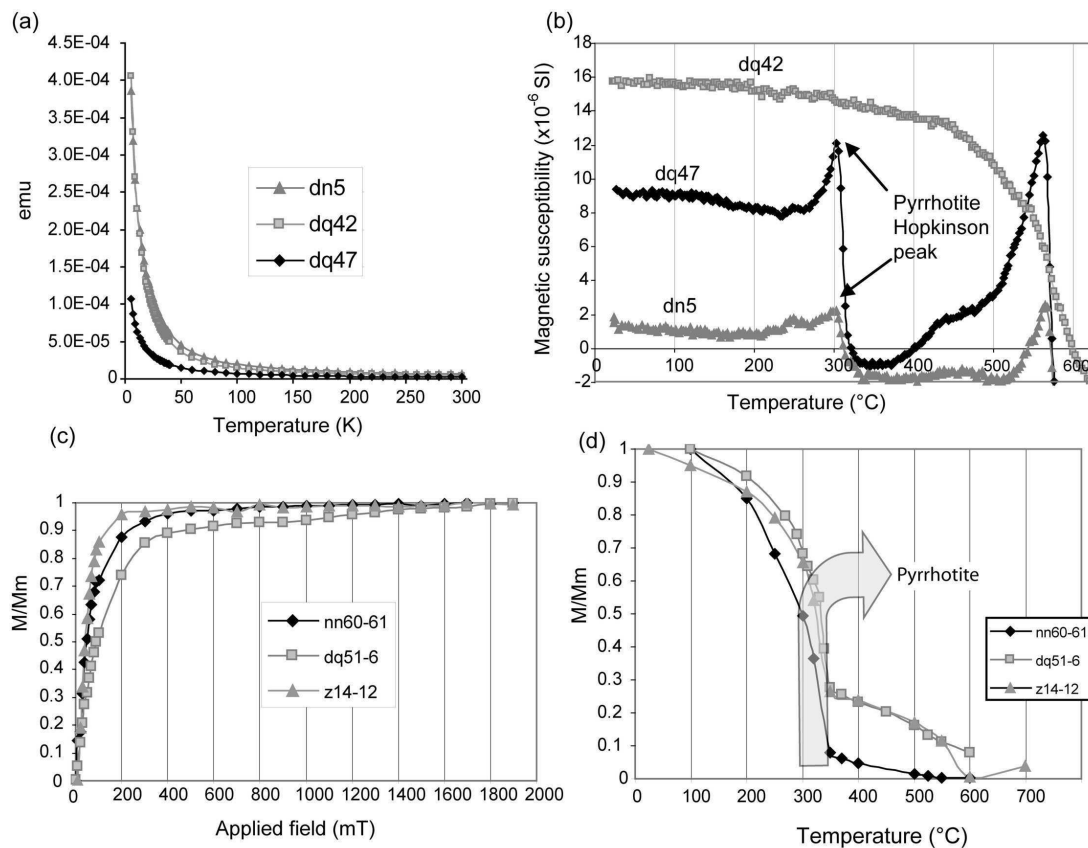


Figure 4: Magnetic mineralogy experiments. (a) MPMS low-temperature curves. (b) High-temperature curves of magnetic susceptibility versus temperature. (c) Stepwise IRM acquisition. (d) Thermal demagnetization of SIRM (pyrrhotite unblocking indicated).

These results confirm the existence of pyrrhotite as the major ferro(i)magnetic phase in the studied dykes. Surprisingly despite the clear existence of pyrrhotite in e.g. high-temperature curves and thermal demagnetization of SIRM there is no low temperature transition observed

at 30-34 °K in the MPMS analyses. Occurrence of pyrrhotite as a remanence carrier within the Tethyan Himalaya has been widely demonstrated in low-grade metacarbonates of the western and central Himalaya providing stable and meaningful remanence directions (Rochette et al., 1990; Appel et al., 1995; Schill et al., 2004).

Measured magnetic susceptibility after each step of heating during thermal demagnetization indicates no significant changes of the magnetic susceptibility below the Curie temperature of pyrrhotite. Some of the samples exhibit an increase of the magnetic susceptibility above 400 °C, likely indicating the transformation of the initial pyrrhotite and pyrite into magnetite as previously pointed out by Crouzet et al. (2001).

4.5.2 Remanence directions

Thermal demagnetization with detailed stepwise heating around the Curie temperature of pyrrhotite (10 °C steps from 270 °C to 350 °C) was performed in order to determine the pyrrhotite component. About 50 % of the studied sites show no stable components. For the other sites common rock magnetic properties and sufficiently clear demagnetization behavior permit to separate a stable component in most of the samples within the pyrrhotite unblocking temperature range from 280 °C to 350 °C (Fig. 5).

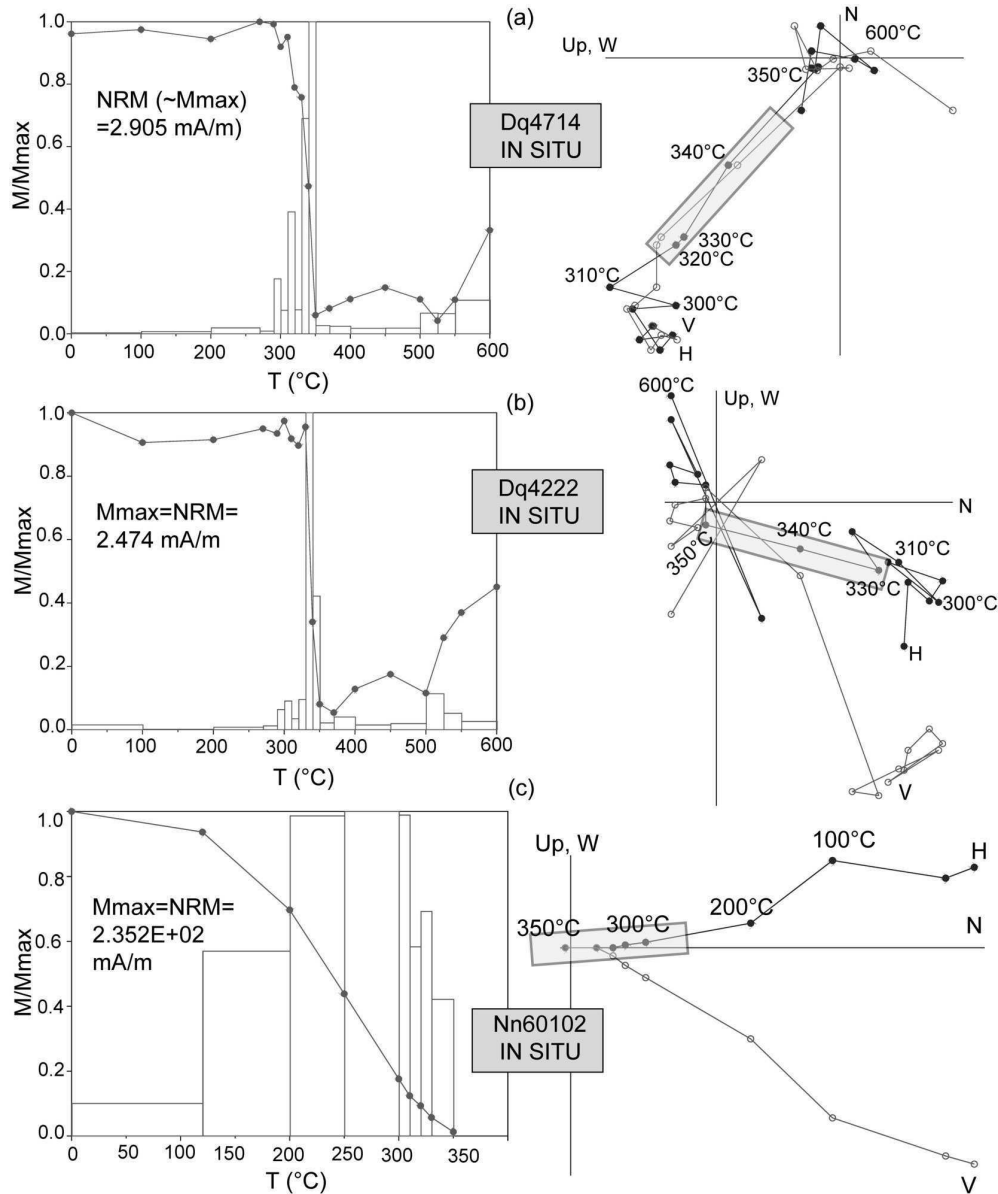


Figure 5: Thermal demagnetization of NRM for representative specimens from sites dq47 (a), dq42 (b) and nn60 (c). Intensity curves (left) and orthogonal Zijderveld plots (right) are shown; the main unblocking range is indicated.

In total 11 sites, 7 in Qonggyai valley and 4 in Nagarze area, show a consistent demagnetization behavior and reliable components could be extracted from the Zijderveld diagrams. Remanence directions show normal and reverse polarity. In some of the sites several components can be isolated in the range of the unblocking temperature of pyrrhotite and in most of the cases they show similar (anti-parallel) directions.

In Qonggyai valley 7 sites, equally distributed along the profile, indicate the presence of one stable pyrrhotite component; reliable directions were obtained for a significant number of samples ($n = 73$) (Figs. 2a and 5a,b). The site means directions have $6.6 < \alpha_{95} < 22.1$ and $k > 10$ (except in site dq51, $k = 5.2$) indicating good grouping of the intra-site remanence

directions (Table 1, Fig. 6a). This component shows an approximate constant declination of ca. 019° (geographic coordinate system; normal polarity) along 30 km of the double vergent flysch wedge as can be seen in the stereogram of the site mean vectors and in the density plot of ChRM directions of all specimens (Fig. 6a,b,c). Inclination values are ranging from 50° to 10° (Table 1, Fig. 6a). No significant changes in declinations have been detected along the two different structural domains, the southern domain controlled by F1 folds and S1 foliation (Eocene to Early-Oligocene) with south vergence and the northern domain governed by F2 folds and S2 foliation with north vergence (Oligocene to Early-Miocene) (Fig. 6a,c).

In Nagarze area the demagnetization behavior is similar as in Qonggyai valley and 4 sites (28 samples) exhibit pyrrhotite unicomponents (Figs. 2a and 5c). The specimen directions within sites are more scattered than in the Qonggyai valley, but the 4 sites show similar site mean declinations (Table 1, Fig. 6d,e). The directional maxima in the density plot appears at declination 001° (Fig. 6d,e). Inclinations show lower values than in Qonggyai valley ranging from 30° to 6° (Table 1, Fig. 6d).

Sites	Geographic coordinates		S. D.	n	Polarity		In situ		k	α_{95} (°)	$\alpha_{95}/\cos I$ (°)	Rot. at 20 Ma		Rot. at 25 Ma	
	Latitude °N	Longitude °E			norm./rev.	D	I	Act.90 (°)				B. & C. 02 (°)	Act.90 (°)	B. & C. 02 (°)	
dq42	29.0860	91.7048	D2	13/20	13/0	14.9	50.7	22.5	8.9	14.1	13.0	9.4	13.5	13.8	
dq45	29.0450	91.6875	D2	7/18	7/0	19.6	37.4	22.0	13.1	16.5	17.7	14.1	18.2	18.5	
dq47	29.0261	91.6704	D1	17/31	0/17	32.1	24.1	20.0	8.2	9.0	30.2	26.6	30.7	31.0	
dq48	28.9971	91.6335	D1	7/24	3/4	16.3	15.9	10.9	19.2	19.9	14.4	10.8	14.9	15.2	
dq49	28.9783	91.6068	D1	6/18	6/0	7.9	17.3	30.7	12.3	12.9	6.0	2.4	6.5	6.8	
dq51	28.9954	91.6340	D1	11/25	5/6	11.7	10.8	5.2	22.1	22.5	9.8	6.2	10.3	10.6	
z14	28.9494	91.6485	D1	12/12	8/4	13.8	23.8	44.8	6.6	7.2	11.9	5.7	12.4	10.1	
nn50	29.0925	90.3929	D1	12/20	9/3	1.1	30.1	18.4	10.4	12.0	-0.8	-4.4	-0.3	0.0	
nn60	28.9202	90.4808	D1	8/16	6/2	3.5	17.8	10.6	17.9	18.7	1.6	-2.0	2.1	2.4	
dn1+dn2	28.8832	90.3729	D1	8/19	2/6	0.8	5.4	16.6	14.0	14.1	-1.1	-4.7	-0.6	-0.3	

Table 1: Statistical parameters for the pyrrhotite component. S.D, structural domain; D1, domain controlled by D1 deformation phase; D2, domain controlled by D2 deformation phase. n, number of specimens measured/number of specimens included in statistics. norm./rev., normal/reverse polarities. D and I, declination and inclination in geographic coordinates. k, precision parameter. α_{95} , 95% confidence angle. Rot., rotation angle calculated from the expected direction obtained in the APWPs of Act.99 (Acton, 1999) and B. & C. 02 (Besse and Courtillot, 2002).

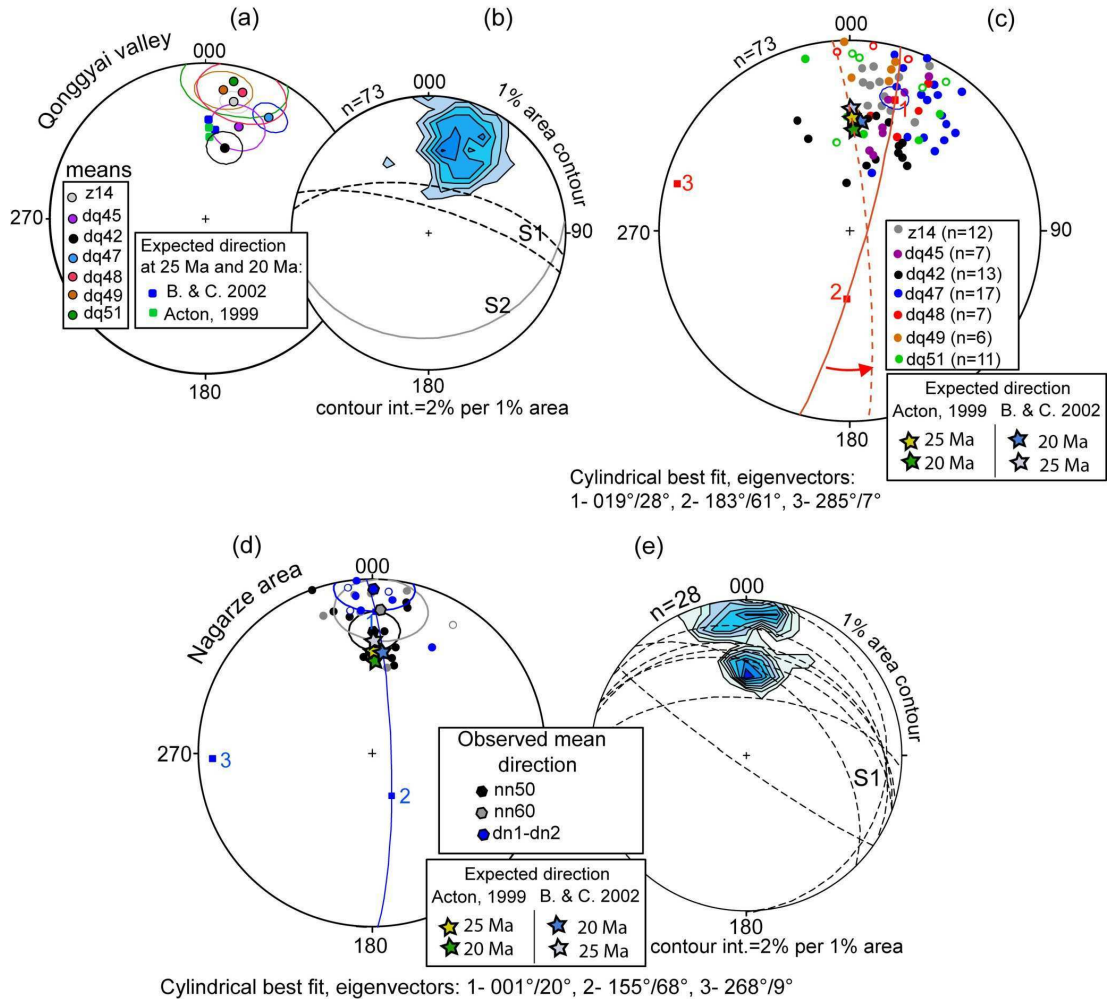


Figure 6: Paleomagnetic results in the Qonggyai valley and Nagarze area (all stereograms are in equal-area projection). (a) Mean site directions in Qonggyai valley and expected directions from the APWPs of Acton (1999) and Besse and Courtillot (2002). (b) Density plot stereogram of single specimen ChRM components and general trend of S1 and S2 foliation. (c) Individual ChRM components with cylindrical best fit; open (solid) circles are projected in the upper (lower) hemisphere. (d) Observed in situ mean directions in Nagarze (hexagons); single specimen directions, open (solid) circles are projected in the upper (lower) hemisphere; expected directions from the two APWPs and cylindrical best fit. (e) Density plot stereogram of single specimen ChRM components and S1 foliation planes.

4.6 Timing of remanence acquisition and paleomagnetic reference directions

Peak metamorphic conditions are crucial for the formation of pyrrhotite and secondary remanence acquisition. Metamorphic ages (K-Ar) from newly grown illites in the Triassic flysch along the Qonggyai valley indicate that the last metamorphic peak was at ~22 Ma, associated to the end of the D2 tectonic phase (Dunkl et al., 2008). Illite Kübler Index in the Triassic flysch of Qonggyai valley ranges from 0.17 to 0.39 and vitrinite reflectance values vary from 1.84 % to graphite grade (for details see Dunkl et al., submitted). Near Qonggyai town vitrinite reflectance values indicate the highest level of maturation reaching graphite stage ($R_{max} \sim 9\%$), and the dykes have been transformed to greenschist. Paleotemperature

estimates from these values yield maximum temperatures between 200 °C and lower greenschist facies (biotite-in ca. 450 °C; Dunkl et al., submitted). Thus we suppose a thermo-remanent origin of the pyrrhotite remanence related to the Early-Miocene temperature climax. Alternatively the origin of the pyrrhotite remanence can be related to Miocene granitic bodies cropping out in the core of the North Himalayan domes (e.g. Hodges, 2000; Lee et al., 2000), producing local thermo-metamorphism in the Triassic sediments. In the study area two Neogene granitoids outcrop in Nagarze area and one SE of Qonggyai within the Yala Xiangbo North Himalayan dome (Fig. 2a). The Yala Xiangbo dome was emplaced at ~18 Ma, and cooled through the muscovite closure window at ~13.5 Ma (Aikman et al., 2004).

Sulphur provenance for pyrrhotite formation is supposed to come from the organic material of the pelites during diagenesis and metamorphism. Pyrrhotite could also be formed by the transformation of pyrite or magnetite (Crouzet et al., 2003 with references). Pyrite is widely present in the margin of the dykes and small amounts of magnetite have also been found after magnetic mineralogy analysis which could mark this transformation.

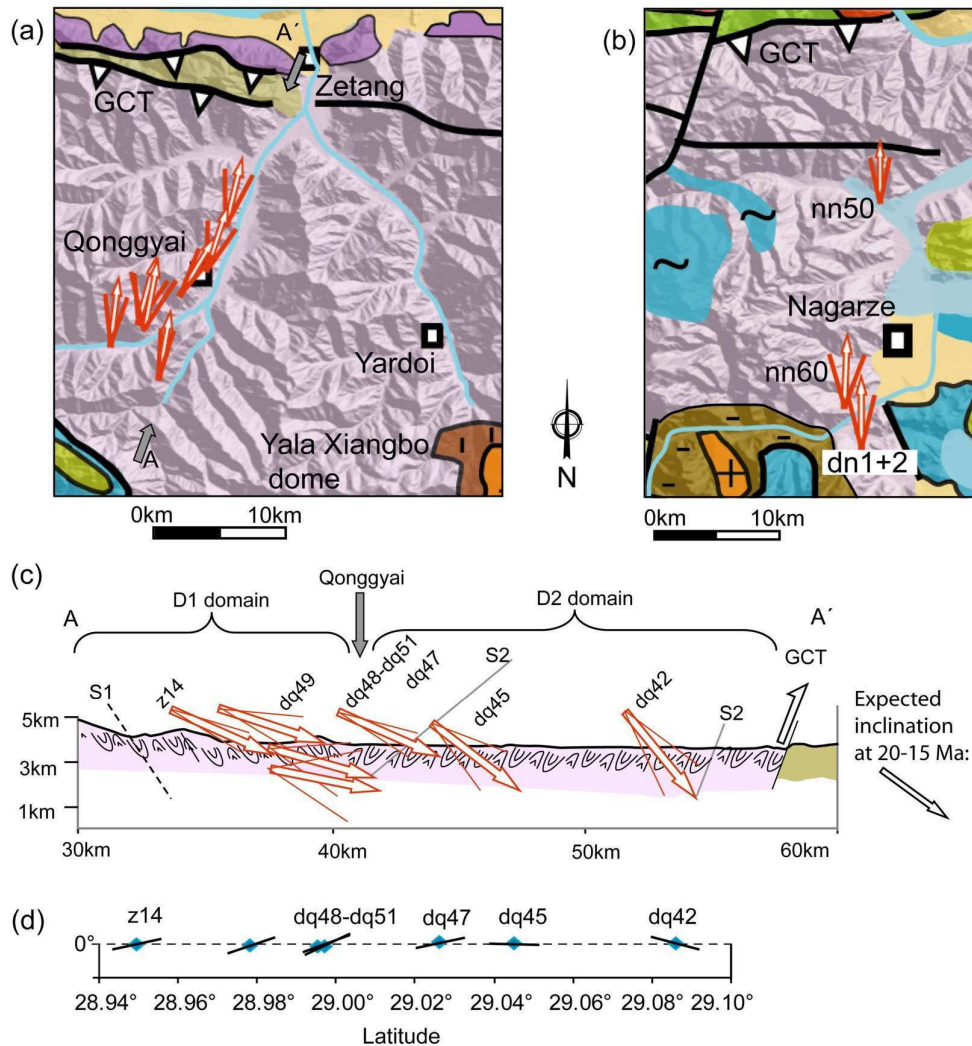
Due to the absence of significant dip variability among sites within the D1 or D2 domains (Fig. 2b), a non-significant fold test has been found. However similar values of declination of the ChRM contained in pyrrhotite unicomponents (Fig. 6a,b,c) within the two different vergence tectonic domains along the Qonggyai valley indicate that the remanence acquisition was post-folding F1 folds of Eohimalayan age and likely post F2 folds and S2 foliation or synchronous with the last pulses of the D2 tectonic phase (~22 Ma). To quantify the amount of vertical-axis rotation and tilting around a horizontal-axis since remanence acquisition, we calculated the expected remanence direction at 20 and 25 Ma from the apparent polar wander paths (APWP) of stable India (Acton, 1999; Besse and Courtillot, 2002) centered in the study area. The reference directions of the two APWP differ 3.7° for 20 Ma and 0.3° for 25 Ma and provide a high-quality reference point. Moreover the reference inclination has been calibrated taking into account 4.5 mm/yr velocity of the northward drift of India-Asia since 25 Ma (Guillot et al., 2003) which yields 30° and 36° of inclination at 25 Ma and 20-15 Ma respectively.

4.7 Magnitude of vertical-axis rotation

As a first approximation for vertical-axis rotation in the area the mean of the pyrrhotite components for the 11 sites were compared with the expected direction at 25 Ma and 20 Ma from the two APWP (Table 1) (e.g. expected declination and inclination at 25 Ma are D/I= 001°/36°; Besse and Courtillot, 2002). The seven sites in the Qonggyai profile indicate a

consistent trend of clockwise rotation ranging from 7° (site dq49) to 31° (site dq47) at 25 Ma (Fig. 7a). On the other hand different inclination values of the site mean directions are reflecting tilting around horizontal axes (Fig. 7c,d). The Different inclination values and quite constant declination values of the site mean remanence vectors and single specimens ChRM directions result in a distribution along a small circle which can be well fitted using cylindrical best fit (Bingham analysis; Bingham, 1974). Directions are distributed within a small circle with an eigenvector 1 of 019° (Fig. 6c). A posteriori the angle of block rotation can be obtained when the small-circle is rotated around a vertical-axis until the expected remanence direction is lying on the small-circle (Fig. 6c). This method is a solid approach to calculate vertical-axis block rotations when the remanences are distributed on a small circle as previously noticed by Waldhör et al. (2001, 2006). From this small-circle method an 18° clockwise block rotation can be calculated for an expected remanence age of 25 Ma in the Qonggyai area. If the observed remanence directions are compared with an expected remanence acquisition age at 20 Ma a clockwise rotation of 17° and 14° will be obtained using APWPs Acton (1990) and Besse and Courtillot (2002), respectively (Figs. 6c and 1b). If the secondary remanence acquisition age occurred at ~ 15 Ma related to the contact metamorphism around the Yala Xiangbo dome, a clockwise rotation of 18° - 15° is obtained. In Nagarze area we obtained block rotation data at 3 points, site nn50, site nn60 and site dn1-dn2 (dn1 and dn2 sites were unified because their closer position). The mean site remanence directions indicate a lack of vertical-axis block rotations with respect to stable India for a remanence acquisition age of 25-20 Ma (Figs. 7b and 1b). The same result is obtained when the 28 ChRM directions from individual specimens are fitted into a small circle. Eigenvector 1 of the cylindrical best fit is 001° which is equal to the expected direction (Fig. 6d).

Figure 7: Vertical axis block rotations and tilt around horizontal-axis. (a) Geological map overlapped with digital topography; arrows indicate angle of rotation versus stable India at 25 Ma in Qonggyai valley; cones show the confidence angle $\alpha_{95}/\cos I$. (b) geological map overlapped with digital topography; arrows indicate angle of rotation versus stable India at 25 Ma in Nagarze area, cones represent confidence angles $\alpha_{95}/\cos I$. (c) cross section along Qonggyai valley with observed inclinations from in situ mean directions of pyrrhotite components; black arrow show expected inclination (averaged from APWPs of Acton, 1999 and Besse and Courtillot, 2002). (d) tilt around horizontal-axis values in the Qonggyai profile.



4.8 Structures of last deformation phase and neotectonic markers

The area is structurally dominated by two sets of structures that control the surface processes. The analysis at 11 sites of tectonic markers witnessing the last deformation stage (D4) indicates the existence of E-W strike-slip faults while the sub N-trending structures are extensional faults (Fig. 8a). These structures cross-cut GCT, STDS and Yala Xiangbo dome and therefore must be Late-Miocene to present. These structures are most probably coeval as has been previously described in the Bangong-Nujiang suture zone (e.g. Armijo et al., 1989; Taylor et al., 2003). The paleostress analysis based on the inversion of fault striae, tension gashes and elongated quartz fibers indicates a regional $N020^\circ$ compression (P-axis) in agreement with present-day kinematics (e.g. Wang et al., 2001). The grain of the relief is marked by large ca. E-W trending faults, mainly the reactivation of older structures, such as the Yarlung Tsangpo suture, numerous sub N-trending faults of smaller extent and the 200 km long Cona Graben system (Fig. 8a; Armijo et al., 1989; Pan et al., 2004). These rifts are

en-echelon and have a slight signature on the topography. Nonetheless, their traces can be determined with accuracy on a slope map and an incision map (Fig. 8a,b).

The ongoing deformation is attested by the strong river disequilibrium reflected e.g. in the Yarlung Tsangpo river longitudinal profile characteristic of river piracy (Fig. 8c). The knick-point K is located on the West Cona Graben shoulder (Fig. 8a). The shape of the strongly disequilibrated profile suggests that the E-W extension and the induced subsidence derived in a topographic gradient and a deepening of the base level of the river Yarlung Tsangpo. In turn, it triggered an increased westward incision of the Yarlung Tsangpo and allowed the capture of a river previously flowing westward. This recent connection is attested by the angles between tributaries and the main river (Yarlung Tsangpo). In the west of the Cona Graben, the tributaries to the Yarlung Tsangpo flow westwards and connect to the main river with an acute angle pointing west.

The drainage system is largely controlled by the D4 structures. In a 50 km, E-W band centered by the Yarlung Tsangpo river, the rivers have an orthogonal pattern. Outside this band, the drainage network is dominantly sub-dendritic. The drainage system of Yarlung Tsangpo area is characterized by N-S elongated and pear-shaped watersheds and is bounded to the South by a NNW-SSE zone of N120 elongated watersheds parallel to the Lhunze fault (Fig. 8d,e). The southern segment of the Cona Graben system is characterized by N-S rectangular elongated watersheds (Fig. 8e). The basin asymmetries of the area indicate that the Yarlung Tsangpo area is dominated by E-W river offsets while the Cona Graben zones are mostly displaying N-S river offsets. The drainage system is indubitably under strong and active tectonic forcing. The basins forming the Cona Graben are dextrally offset on the slope, vertical dissection and incision maps and appear partially rotated. The Cona Graben southern segment, south of the Lhunze fault, is oriented N-S while the middle segment is oriented N015°-020° (Fig. 8). Although, scarce our data suggest that the offsets occur along reactivated structures showing right-lateral transtensional markers in the field. Additional structural field work focused in the three different segments of the Cona Graben and in the Lhunze fault and Yarlung Tsangpo suture are needed to better constraint their neotectonic importance.

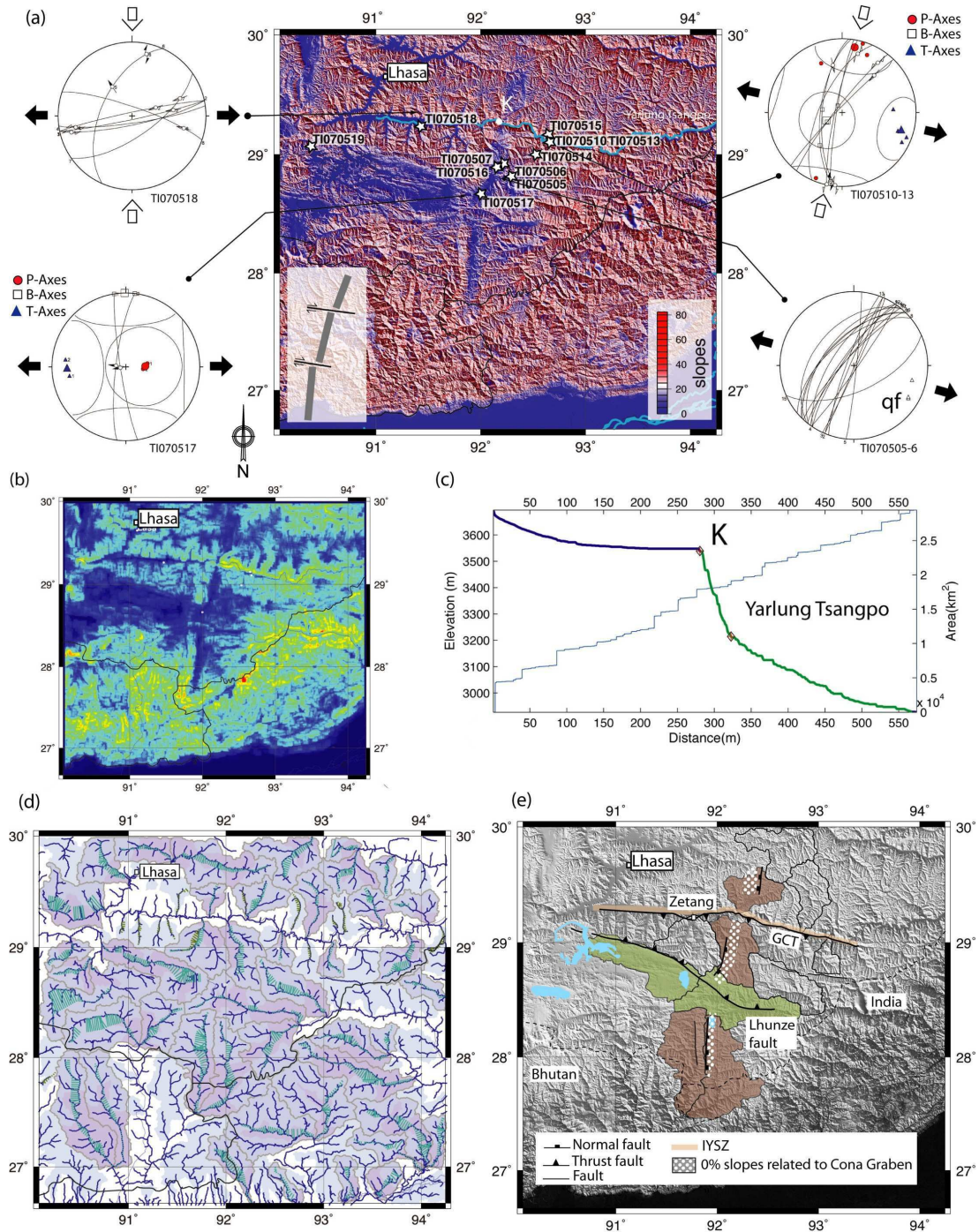


Figure 8: D4 structures and geomorphological analysis. (a) Slope map draped on a shaded relief based on SRTM v.4 data. The numbers represent site locations where neotectonic markers were measured. Four representative structural analyses of D4 strain markers such as fault striae and tension gashes are displayed on the sides (black arrows: assumed maximum horizontal extensional stress direction, white arrows: assumed maximum horizontal compressive stress direction, qf: quartz fibers). In the right down part sketch of the Cona Graben en-echelon system (see text for further explanations). The light blue line represents the Yarlung Tsangpo river which profile is plotted in C. K is a major knick-point. (b) Incision map (local relief within 3 km). (c) Longitudinal profile of the Yarlung Tsangpo river in the study area and its contributing area. (d) Drainage system (dark blue lines represent the rivers of Strahler orders greater than 1, light blue shapes represent watersheds with Strahler order 2, gray contour shapes represent watersheds with Strahler order 3, the turquoise lines display the amount of offset between the main watershed rivers and the watershed symmetry axis). (e) Digital topography with the GCT, IYSZ, Lhunze fault and Cona Graben structures. Watersheds

associated to the Lhunze fault in green color, watersheds associated to the Cona Graben in brown color.

4.9 Discussion

4.9.1 Implications for eastward extrusion in SE Tibet

Taking into account that the remanence was acquired between 23-14 Ma the rotation angle can be interpreted in terms of vertical-axis block rotation related to slip along the ramp of the Great Counter Thrust (18-10 Ma; Harrison et al., 2000) or associated to movements along strike-slip faults linked to the E-W Late Miocene extension in the Himalaya and eastward extrusion of the Tibetan plateau (e.g. Royden et al., 1997; Tapponnier et al., 2001).

Taking into account that the movement of the hangingwall along the frontal ramp of the GCT was most probably frontal, and north-directed as indicated by stretching lineation values (N-S trend and 70° plunge towards the south; Montomoli et al., 2008; Antolín et al., in press) in the thrust zone, perpendicular to the thrust plane, block rotation are not expected by this process (Fig. 2a; for details about thrust ramp geometries and paleomagnetic vectors see Pueyo et al., 2003). However, our results fit well with the combined Quaternary strain rates and GPS velocity field (Fig. 1; Holt et al., 2000; Zhang et al., 2004). Rotation rates obtained from the GPS velocity field relative to Eurasia reflect a similar pattern with increasing clockwise rotation from the Nagarze-Yamdrock area towards Qonggyai valley and the eastern syntaxis (Royden et al., 1997; Holt et al., 2000; Gan et al., 2007). Furthermore our neotectonic analyses are in agreement with the paleomagnetic results as witnessed by the en-echelon Graben system and the dextrally offset basins.

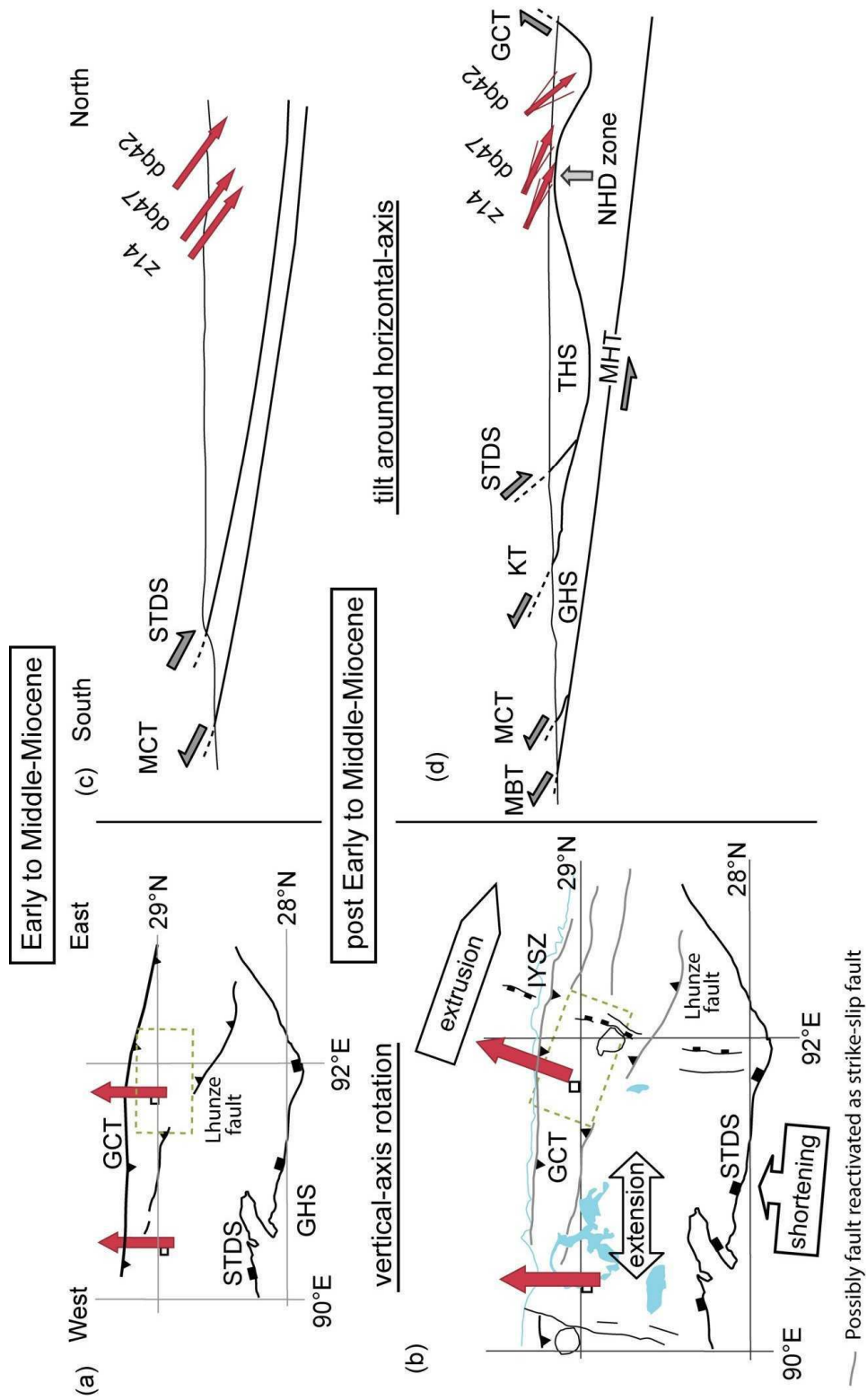
These data together point out that the paleomagnetic remanence vectors in Nagarze (~90°E) are the result of the dominant northward indentation of India and in Qonggyai (~92°E) they have been 20° clockwise rotated due to SE extrusion of the southern part of the Tibetan plateau around the eastern syntaxis (Namche Barwa) (Fig. 9a,b). Vertical-axis clockwise rotation probably occurs as the result of displacements along E-W right-lateral strike-slip faults with similar slip sense as the Karakorum-Indus-Yarlung Tsangpo fault system and the Jiali fault system (Armijo et al., 1989; Ratschbacher et al., 1994; Van der Woerd et al., 2009). These faults are kinematically linked with the E-W extension controlled by the sub N-trending south Tibetan Grabens (Taylor et al., 2003; Fig. 9a,b). The south Tibetan Grabens may have been active since around 14-8 Ma on the central and southern Tibetan plateau (Blisniuk et al., 2001; Harrison et al., 1995). Early Pliocene ages have been also described in the Kung Co half-Graben (86.5°E) close to Tingri (Mahéo et al., 2007) and associated to the onset of E-W extension. Furthermore reactivation of pre-existing weak structural zones as the IYSZ and the Lhunze fault might have played a significant role in the accommodation of E-

W (or orogen-parallel) extension and eastward extrusion of the Tibetan plateau (Jessup et al., 2008; this study).

4.9.2 Implications for North Himalayan doming

Relatively to the expected inclination at 20-15 Ma the observed inclinations in Qonggyai valley reflect a N-S pattern of tilt around horizontal axis indicating 15° tilting in site dq42, no tilting in site dq45 and back-tilting south of it (Fig. 7c, d). In Yamdrock Lake and Nagarze area an increasing degree of back-tilting can be observed from N to S approaching the Neogene leucogranite intrusion south of Nagarze. Taking into account that the sites in Qonggyai valley are 40km WNW of the Yala Xiangbo dome and following the E-W lineament of the others North Himalayan domes, the tilt pattern can be interpreted as concealed doming. This is supported by the vitrinite reflectance values along the Qonggyai valley which indicate a maximum temperature and peak in the degree of metamorphism close to Qonggyai town which can be related to the roof of a deep-seated and not completely developed dome. This zone may have risen in Middle and Late Miocene times (Grujic et al., 2002), tilting and back-tilting the paleomagnetic vectors in the Qonggyai valley and close to Nagarze town around an E-W horizontal axis (eigenvector 3 of the cylindrical best fit; Fig. 6c,d) coincident with the lineament of the outcropping domes. Figure 9c,d sketch the supposed scenario for the observed inclination values.

Figure 9: Miocene kinematic model for the eastern Tethyan Himalaya. (a) Expected orientation of the paleomagnetic reference direction in the study area in Early and Middle-Miocene times within the structural frame (tectonic maps are simplified from Fig. 2 and Fig. 8). (b) Clockwise rotation of the pyrrhotite remanence directions in Qonggyai valley related to the strain partitioning and eastward extrusion of the Tibetan plateau. (c) Geodynamic scenario in Early and Middle-Miocene times with the expected inclination of the paleomagnetic vectors (schematic, interpretative, evolutionary cross-sections along A-A' in Fig. 1b, slightly modified from Grujic et al., 2002). (d) Rise of the North Himalayan dome (NHD) zone in Middle and Late Miocene times could have induced tilting and back-tilting of the remanence vectors.



4.10 Conclusions

The paleomagnetic data presented here allow us to separate a stable post-folding magnetization component in the Cretaceous diorite dykes emplaced in the Triassic turbiditic sediments, demagnetized in the pyrrhotite unblocking Curie temperature. Pyrrhotite occurrence is supported by a Hopkinson peak and decay at 325 °C in high-temperature susceptibility curves, SIRM saturation field values > 300mT, and a sharp decrease of remanent magnetization at ~325 °C during thermal demagnetization of the SIRM. A small contribution of magnetite is additionally present. The secondary character of the ChRM can be asserted by several facts: (i) in situ mean declinations are approximately constant in the Qonggyai valley, despite of the double vergence of folds and related axial planar foliation, south-vergent in the southern domain and north-vergent in the northern domain. (ii) Thermochronological data in the Triassic flysch indicating that a peak metamorphism above the Curie temperature of pyrrhotite was reached for the last time between 22 Ma and 14 Ma at the end of D2 tectonic phase (Aikman et al., 2004; Dunkl et al., 2008). Therefore the magnetization is of thermoremanent origin and can be evaluated as a record of the Early Miocene field.

Remanence vectors from Nagarze-Yamdrock Lake area and Qonggyai valley indicate a transition from no rotation in the west to ~20° clockwise rotation in the east against stable India since Early to Middle-Miocene. This rotation can be explained by the strong strain partitioning between E-W strike-slip faulting and E-W extension reflected in the en-echelon Cona Graben system, the drainage system and the watersheds shape and distribution. At regional scale our results represent a field support for the clockwise rotation of the southeastern corner of the Tibetan plateau around the eastern syntaxis during the eastward extrusion of the Tibetan plateau (Armijo et al., 1989; Royden et al., 1997; Tapponnier et al., 2001).

Tilting and back-tilting of the paleomagnetic remanence vectors around a horizontal-axis may reflect risen of the North Himalayan dome zone in Middle Miocene times.

Acknowledgements

The authors are grateful for the aid during fieldwork to Tawa. We thank G. Ojha, P. Branscheid and L. Bello for assistance during paleomagnetic measurements. We thank the paleomagnetic laboratory at Bremen University and T. Frederichs for MPMS analysis. Stereographic projections were produced with Allmendinger's "Stereonet for Windows v.1.2". This research was supported by grants from the Chinese NSF (40625008 to Ding), CAS (KZCX2-YW-Q09-03 to Ding), National Basic Research Program of China (2009CB421000 to Ding) and by funding from the German Science Foundation (DFG) in the frame of project Ap 34/26-1, 2 and Ap 34/33-1 which is part of the Priority Programme 1372 "Tibetan Plateau: Formation, Climate, Ecosystems (TiP)".

References

- Acton, G.D., 1999. Apparent polar wander of India since the Cretaceous with implications for regional tectonics and true polar wander. In T. Radhakrishna and J.D.A. Piper, Editors, *The Indian subcontinent and Gondwana; a paleomagnetic and rock magnetic perspective: Memoir-Geological Society of India*. 44, 129-175.
- Aikman, A., Harrison, T.M., Lin, D., 2004. Preliminary results from the Yala-Xiangbo Leucogranite dome, SE Tibet. 19th Himalaya-Karakoram-Tibet workshop extended abstracts. *Himalayan J. Sci.* 2, 91.
- Aikman, A., Harrison, T.M., Ding, L., 2008. Evidence for Early (>44 Ma) Himalayan Crustal Thickening, Tethyan Himalaya, southeastern Tibet. *Earth Planet. Sci. Lett.* 274, 14-23.
- Antolín, B., Appel, E., Montomoli, C., Dunkl, I., Ding, L., Gloaguen R., El Bay, R. In press. Kinematic evolution of the eastern Tethyan Himalaya: Constraints from magnetic fabric and structural properties of the Triassic flysch in SE Tibet. In: J. Poblet and R. Lisle, Editors, *Kinematic Evolution and Structural Styles of Fold-and-Thrust Belts*, Geol. Soc. London Spec. Publ.
- Ali, J.R., Aitchison, J.C., 2005. Greater India. *Earth Sci. Revs* 72, 169-188.
- Appel, E., Patzelt, A., Chouker, C., 1995. Secondary paleoremanence of Tethyan sediments from the Zaskar Range (NW Himalaya). *Geophys. J. Int.* 122, 227-242.
- Armijo, R., Tapponnier, P., Mercier, J.L., Tonglin, H., 1986. Quaternary extension in southern Tibet: field observations and tectonic implications. *J. Geophys. Res.* 91 (nB14), 13803-13872.
- Armijo, R., Tapponnier, P., Tonglin, H., 1989. Late Cenozoic Right-Lateral Strike-Slip Faulting in Southern Tibet. *J. Geophys. Res.* 94, 2787-2838.
- Besse, J., Courtillot, V., 2002. Apparent and true polar wander and the geometry of the geomagnetic field over the last 200 Myr. *J. Geophys. Res.* 107 (B11), 2300. doi: 10.1029/2000jb000050.
- Bingham, C., 1974. An antipodally symmetric distribution on the sphere. *Annals of Statistics* 2, 1201-1225.
- Blisniuk, P.M., Hacker, B.R., Glodny, J., Ratschbacher, L., Bi, S., Wu, Z., McWilliams, M.O., Calvert, A., 2001. Extension in central Tibet since at least 13.5 Myr. *Nature* 412, 628-632.
- Burbank, D., Meigs, A., Brozovi, N., 1996. Interactions of growing folds and coeval depositional Systems. *Basin Res.* 8, 199-223.
- Burchfiel, B., Zhiliang, C., Hodges, K.V., Yuping, L., Royden, L.H., Changrong, D. Jiene, X., 1992. The South Tibetan detachment system, Himalaya orogen: extension contemporaneous with and parallel to shortening in a collisional mountain belt. *Geol. Soc. Am. Spec. Pap.* 269, 1-41.
- Burg, J.P., Chen, G.M., 1984. Tectonics and structural zonation of southern Tibet, China. *Nature* 311, 219-223.
- Carosi R., Lombardo, B., Molli, G., Musumeci, G., Pertusati, P., 1998. The South Tibetan Detachment system in the Rongbuk valley, Everest region. Deformation features and geological implications. *J. Asian Earth Sci.* 16, 299-311.
- Carosi, R., Montomoli, C., Visonà, D., 2002. Is there any detachment in the Lower Dolpo (western Nepal)? *Comptes Rendus Geoscience* 334, 933-940.
- Cox, R.T., Van Arsdale, R.B., Harris J.B., 2001, Identification of possible Quaternary deformation in the northeastern Mississippi Embayment using quantitative geomorphic analysis of drainage-basin asymmetry. *Geol. Soc. Am. Bull.* 113, 615-624.
- Crouzet, C., Stang, H., Appel, E., Schill, E., Gautam, P., 2001. Detailed analysis of successive pTRMs carried by pyrrhotite in Himalayan metacarbonates: an example from Hidden Valley Central Nepal. *Geophys. J. Int.* 146, 607-618.
- Ding, L., Kapp, P., Wan, X., 2005. Paleocene-Eocene record of ophiolite obduction and initial India-Asia collision, south central Tibet. *Tectonics* 24, TC3001, doi:10.1029/2004TC001729.
- Dunkl, I., Lin, D., Montomoli, C., Wemmer, K., Rantisch, G., Antolín, B., El Bay, R. Appel, E., 2008. Diagenetic and metamorphic overprint and deformation history of Permo-Triassic Tethyan sediments, SE Tibet. 23th Himalaya-Karakoram-Tibet workshop extended abstracts. *Himalayan J. Sci.* 5, 49.
- Dunkl, I., Antolín, B., Wemmer, K., Rantitsch, G., Kienast, M., Montomoli, C., Ding, L., Carosi, R., Appel, E., El Bay, R., Xu, Q. and von Eynatten, H., Submitted. Metamorphic evolution of the Tethyan Himalayan flysch in SE Tibet. In: R. Gloaguen and L. Ratschbacher, Editors, *Growth and Collapse of the Tibetan Plateau*, Geol. Soc. London Spec. Publ.

- Dupuis, C., Hébert, R., Dubois-Coté, V., Guilmette, C., Wang, C.S., Li, Z.J., 2006. Geochemistry of sedimentary rocks from mélange and flysch units south of the Yarlung Zangbo suture zone, southern Tibet. *J. Asian Earth Sci.* 26, 489-508.
- Eldredge, S., Bachtadse, V., Van der Voo, R., 1985. Paleomagnetism and the orocline hypothesis. *Tectonophysics* 119, 153-179.
- Fisher, R.A., 1953. Dispersion on a sphere. *Proc. R. Soc. London.* 217, 295-305.
- Gaetani, M., Garzanti, E., 1991. Multicyclic history of the northern Indian continental margin (northwestern Himalaya). *AAPG Bull.* 75, 1427-1446.
- Gan, W., Zhang, P., Shen, Z-K., Niu, Z., Wang, M., Wan, Y., Zhou, D., Cheng, J., 2007. Present-day crustal motion within the Tibetan Plateau inferred from GPS measurements. *J. Geophys. Res.* 112, B08416, doi: 10.1029/2005JB004120.
- Gansser, A., 1964. *Geology of the Himalaya*. Wiley-Interscience, New York. 289 pp.
- Garzzone, C.N., DeCelles, P.G., Hodkinson, D.G., Ojha, T.P., Upreti, B.N., 2003. East-west extension and Miocene environmental change in the southern Tibetan plateau: Thakkhola graben, central Nepal. *Geol. Soc. Amer. Bull.* 115, 3-20.
- Gloaguen, R., Marpu, P.R., Niemeyer, I., 2007. Automatic extraction of faults and fractal analysis from remote sensing data. *Nonlinear Proc. Geoph.* 14 (2), 131-138
- Gloaguen, R., Käbner, A., Wobbe, F., Shahzad, F., Mahmood, A., 2008. Remote Sensing Analysis of Crustal Deformation using River Networks. *Geoscience and Remote Sensing Symposium. IGARSS 2008. IEEE International (2008).* 4, 1- 4.
- Godin, L., 2003. Structural evolution of the Tethyan sedimentary sequence in the Annapurna area, central Nepal Himalaya. *J. Asian Earth Sci.* 22, 307-328.
- Godin, L., Grujic, D., Law, R.D., Searle, M.P., 2006. Channel flow, extrusion and exhumation in continental collision zones: an introduction. In: R.D. Law, M.P. Searle, L. Godin, Editors, *Channel Flow, Ductile Extrusion and Exhumation in Continental Collision Zones*, *Geol. Soc. London Spec. Publ.* 268, 1-23.
- Grujic, D., Hollister, L.S., Parrish, R.R., 2002. Himalayan metamorphic sequence as an orogenic channel: insight from Bhutan. *Earth Planet. Sci. Lett.* 198, 177-191.
- Guillot S., Garzanti, G., Baratoux D., Marquer D., Maheo, G., de Sigoyer J., 2003. Reconstructing the total shortening history of the NW Himalaya, *Geochem., Geophys., Geosyst.* 4. doi: 10.1029/2002GC000484.
- Harrison, T.M., Copeland, P., Kidd, W.S.F., Lovera, O.M., 1995. Activation of the Nyainqen-tanghla shear zone: Implications for uplift of the southern Tibetan Plateau. *Tectonics* 14, 658-676.
- Harrison, T.M., Yin, A., Grove, M., Lovera, O.M., 2000. The Zedong Window: A record of superposed Tertiary convergence in southeastern Tibet. *J. Geophys. Res.* 105, 19,211-19,320.
- Hodges, K.V., 2000. Tectonics of the Himalaya and southern Tibet from two perspectives. *Geol. Soc. Amer. Bull.* 112, 324-350.
- Holt, W.E., Chamot-Rooke, N., Le Pichon, X., Haines, A.J., Shen-Tu, B., Ren, J., 2000, Velocity field in Asia inferred from Quaternary fault slip rates and Global Positioning System observations: *J. Geophys. Res.* 105, 19185-19209.
- Jackson, J., Norris, R., Youngson, J., 1996. The structural evolution of fault and fold systems in central Otago, New Zealand: Evidence revealed by drainage patterns. *J. Struct. Geol.* 18, 217-234.
- Jackson, J., Ritz, J.F., Siame, L., Raisbeck, G., Yiou, F., Norris, R. J., Youngson, J.H., Bennett, E., 2002. Fault growth and landscape development rates in Otago, New Zealand, using in situ cosmogenic ¹⁰Be. *Earth Planet. Sci. Lett.* 195, 185-193.
- Jessup, M.J., Newell, D.L., Cottle, J.M., Berger, A.L., Spotila, J.A., 2008. Orogen-parallel extension and exhumation enhanced by focused denudation in the Arun River gorge, Ama Drime Massif, Tibet-Nepal. *Geology* 36, 587-590.
- Käbner, A., Gloaguen, R., Stanek, K.-P. 2008. Remote sensing analysis of recent tectonics in the Eger Rift (Czech Republic). *International Geoscience and Remote Sensing Symposium (IGARSS)*, 1636-1639.
- Kellett, D.A., Godin, L., 2009. Pre-Miocene deformation of the Himalayan superstructure, Hidden valley, central Nepal. *J. Geol. Soc. London* 166, 261-275.
- Kellett, D.A., Grujic, D., Erdmann, S., 2009. Miocene structural reorganization of the South Tibetan detachment, eastern Himalaya: Implications for continental collision. *Lithosphere* 1, 5, 259-281.
- Kirschvink, J.L., 1980. The least-squares line and plane and the analysis of palaeomagnetic data. *Geophys. J. R. Astron. Soc.* 62, 699-718.

- Klootwijk, C.T., Bingham, D.K., 1980. The extent of Greater India, III. Palaeomagnetic data from the Tibetan Series, Thakkhola region, Nepal Himalaya. *Earth Planet. Sci. Lett.* 51, 381-405.
- Klootwijk, C.T., Conaghan, P., Powell, C., 1985. The Himalayan Arc: large-scale continental subduction, oroclinal bending and back-arc spreading. *Earth Planet. Sci. Lett.* 75, 167-183.
- Leech, M. L., 2008. Does the Karakoram fault interrupt mid-crustal channel flow in the western Himalaya?. *Earth Planet. Sci. Lett.* 276, 314-322.
- Lee, J., Hacker, B.R., Dinklage, W.S., Wang, Y., Gans, P., Calvert, A., Wan, J.L., Chen, W.J., Blythe, A.E., McClelland, W., 2000. Evolution of the Kangmar Dome, southern Tibet: Structural, petrologic, and thermochronologic constraints. *Tectonics* 19, 872-895.
- Li, D., Yin, A., 2008. Orogen-parallel, active left-slip faults in the Eastern Himalaya: Implications for the growth mechanism of the Himalayan Arc. *Earth Planet. Sci. Lett.* 274, 258-267.
- Liebke, U., Appel, E., Neumann, U., Antolin, B., Ding, L, Xu, Q., Submitted. Position of the Lhasa terrane prior to India-Asia collision derived from palaeomagnetic inclinations of 53 Ma old dykes of the Linzhou Basin: constraints on the age of collision and post-collisional shortening within the Tibetan Plateau. *Geophys. J. Int.*
- Liu, G., Einsele, G., 1994. Sedimentary history of the Tethyan basin in the Tibetan Himalayas. *Geol. Rundsch.* 83, 32-61.
- Maffione, M., Speranza, F., Faccenna, C., Rosello, E., Paleomagnetic evidence for a pre-early Eocene (~50 Ma) bending of the Patagonian orocline (Tierra del Fuego, Argentina): Paleogeographic and tectonic implications, *Earth Planet. Sci. Lett.* (2009), doi: 10.1016/j.epsl.2009.11.015.
- Mahéo, G., Leloup, P.H., Valli, F., Lacassin, R., Arnaud, N., Paquette, J.-L., Fernandez, A., Haibing, L., Farley, K.A., Tapponnier, P., 2007. Post 4 Ma initiation of normal faulting in southern Tibet. Constraints from the Kung Co half graben. *Earth Planet. Sci. Lett.* 256, 233-243.
- Montomoli, C., Appel, E., Antolín, B., Dunkl, I., El Bay, R., Lin, D., Gloaguen, R., 2008. Polyphase deformation history of the “Tibetan Sedimentary Sequence” in the Himalaya chain (South-East Tibet). 23th Himalaya-Karakoram-Tibet workshop extended abstracts. *Himalayan J. Sci.* 5, 91.
- Nagata, T. 1961. *Rock Magnetism*, 2nd edition, Maruzen, Tokyo, pp. 350.
- Oliva-Urcia, B., Pueyo, E.L., 2007. Rotational basement kinematics deduced from remagnetized cover rocks (Internal Sierras, southwestern Pyrenees). *Tectonics* 26, TC4014.
- Pan, G., Ding, J., Yao, D., Wang, L., 2004. Geological map of Qinghai-Xizang (Tibet) Plateau and Adjacent Areas (1:1,500,000). Chengdu Institute of Geology and Mineral Resources, China Geological Survey. Chengdu Cartographic Publishing House.
- Pêcher, A., Bouchez, J.L., Le Fort, P., 1991. Miocene dextral shearing between Himalaya and Tibet. *Geology* 19, 683-685.
- Pueyo, E.L., Pocoví, A., Parés, J.M., Millán, H., Larrasoána, J.C., 2003. Thrust ramp geometry and spurious rotations of paleomagnetic vectors. *Stud. Geophys. Geod.* 47, 331-357.
- Ratschbacher, L., Frisch, W., Liu, G., Chen, C., 1994. Distributed deformation in southern and western Tibet during and after the India-Asia collision. *J. Geophys. Res.- Solid Earth* 99, 19917-19945.
- Rochette, P., Fillion, G., Mattéi, J.L., Dekkers, M.J., 1990. Magnetic transition at 30-34 Kelvin in pyrrhotite: insight into widespread occurrence of this mineral in rocks. *Earth Planet. Sci. Lett.* 98, 319-328.
- Royden, L.H., Burchfiel, B.H., King R.W., Wang, E., Chen, Z., Shen, F., Liu, Y., 1997. Surface Deformation and Lower Crustal Flow in Eastern Tibet. *Science* 276, 788-790.
- Schill, E., Appel, E., Zeh, O., Singh, V.K., Gautam, P., 2001. Coupling of late-orogenic tectonics and secondary pyrrhotite remanences: Towards a separation of different rotation processes and quantification of rotational underthrusting in the western Himalayas (N-India). *Tectonophysics* 337, 1-21.
- Schill, E. and Holt, W.E., 2004. 20 Ma of lateral mass transfer around the western Himalayan syntaxis. Extended abstracts: 19th Himalaya-Karakoram-Tibet Workshop, Niseko, Japan. 19th Himalaya-Karakoram-Tibet workshop extended abstracts. *Himalayan J. Sci.* 2, 4, 244-245.
- Schill, E., Appel, E., Crouzet, C., Gautam, P., Wehland, F., Staiger, M., 2004. Oroclinal bending versus regional significant clockwise rotations in the Himalayan arc-Constrains from secondary pyrrhotite remanences. In: Sussman, A.J. and Weil, A.B. (Eds.), *Orogenic Curvature: Integrating Paleomagnetic and Structural Analyses*. *Spec. Pap. Geol. Soc. Am.* 383, 73-85.

- Searle, M.P., 1996. Cooling history, Erosion, Exhumation and Kinematics of the Himalaya - Karakoram - Tibet orogenic belt. In: Yin, A., Harrison, T.M. (Eds.), *Tectonics of Asia*. Rubey Symposium volume, Los Angeles. pp. 110-137.
- Shahzad, F., Mahmood, S.A., Gloaguen, R., 2009. Drainage network and lineament analysis: An approach for Potwar Plateau (Northern Pakistan). *J. Mount. Sci.* 6 (1), 14-24.
- Shahzad, F., Gloaguen, R., Drainage network and lineament analysis. TecDEM, a Matlab Toolbox, Submitted to *Computer and Geosciences*.
- Tapponnier, P., Peltzer, G., Le Dain, A.Y., Armijo, R and Cobbold, P., 1982. Propagating extrusion tectonics in Asia: New insights from simple experiments with plasticine. *Geology* 10, 611-616.
- Tapponnier, P., Zhiqin, X., Roger, F., Meyer, B., Arnaud, N., Wittlinger, G., Jingsui, Y., 2001. Oblique Stepwise Rise and Growth of the Tibet Plateau. *Science* 294, 1671-1677.
- Taylor, M., Yin, A., Ryerson, J.F., Kapp, P., Ding, L., 2003. Conjugate strike-slip faulting along the Bangong-Nujiang suture zone accommodates coeval east-west extension and north-south shortening in the interior of the Tibetan Plateau. *Tectonics*, 22(4), 1044, doi:10.1029/2002TC001361, 2003.
- Van der Woerd, J., Leloup, Ph.-H., Liu-Zeng, J., Lacassin, R., Tapponnier, P., 2009. A comment on "Orogen-parallel, active left-slip faults in the eastern Himalaya: Implications for the growth mechanism of the Himalayan arc" by Li and Yin (*Earth Planet. Sci. Lett.* 278 (2008) 258-267. *Earth Planet. Sci. Lett.* 285, 217-222.
- Waldhör, M., Appel, E., Frisch, W., Patzelt, A., 2001. Paleomagnetic investigation in the Pamirs and its tectonic implications. *J. Asian Earth Sci.* 19, 429-451.
- Waldhör, M., Appel, E., 2006. Intersections of remanence small circles: new tools to improve data processing and interpretation in palaeomagnetism. *Geophys. J. Int.* 166, 33-45.
- Wang, Q., Zhang P.Z., Freymueller J.T., Bilham, R., Kristine K.M., Lai, X., You, X., Niu, Z., Wu, J., Li, Y., Liu, J., Yang, Z., Chen, Q., 2001. Present-Day Crustal Deformation in China Constrained by Global Positioning System Measurements. *Science*. 294, 574-577.
- Weil, A.B., Sussman, A.J., 2004. Classifying curved orogens based on timing relationships between structural development and vertical-axis rotations. In Sussman, A.J. and Weil, A.B. (Eds.), *Orogenic Curvature: Integrating Paleomagnetic and Structural Analyses*. *Spec. Pap. Geol. Soc. Am.* 383, 1-15.
- Willems, H., Zhou, Z., Zhang, B., Gräfe, K. U., 1996. Stratigraphy of the Upper Cretaceous and Lower Tertiary strata in the Tethyan Himalayas of Tibet (Tingri area, China). *Geol. Rundsch.* 85, 723-754.
- Yin, A., Harrison, T.M., Ryerson, F.J., Wenji, C., Kidd, W., Copeland, P., 1994. Tertiary structural evolution of the Gangdese thrust system, southeastern Tibet. *J. Geophys. Res.* 99, 18.175-18.201.
- Yin, A., Harrison, T.M., 2000. Geologic evolution of the Himalayan-Tibetan orogen. *Ann. Rev. Earth Planet. Sci.* 28, 211 -280.
- Zhang, P.Z., Shen, Z., Wang, M., Gan, W., Bürgmann, R., Molnar, P., Wang, Q., Niu, Z., Sun, J., Wu, J., Hanrong, S., Xinzhaoy, Y., 2004. Continuous deformation of the Tibetan Plateau from global positioning system data. *Geology* 32, 809-812.
- Zhu, D., Mo, X., Pan, G., Zhao, Z., Dong, G., Shi, Y., Liao, Z., Wang, L., Zhou, C., 2008. Petrogenesis of the earliest Early Cretaceous mafic rocks from the Cona area of the eastern Tethyan Himalaya in south Tibet: Interaction between the incubating Kerguelen plume and the eastern Greater India lithosphere?. *Lithos* 100, 147-173.
- Xu X., Ding L., Xu Q., Cai F., Zhang Q., Zhang L., Lai Q., 2009. Tectonics implications of the Ultramafic Dykes in Southeastern Tibet. *Chinese J. Geol.* 44, 1012-1024 (in Chinese with English abstract).

World Wide Web references

Digital topography, SRTM data, is from the Consortium for Spatial Information (CGIAR/CSI): <http://srtm.csi.cgiar.org>

5

Late orogenic deformation in the Lingshi klippe (NW Bhutan) deduced from paleomagnetic data: Consequences for extension and clockwise rotation in the eastern Himalaya

5.1 Abstract

A paleomagnetic, structural and geochronological approach permits to unravel the Miocene kinematic evolution of the Lingshi klippe (NW Bhutan). The structural study and K-Ar dating provides new data to define a new large synclinal fold within the core of the Lingshi klippe identifying Cretaceous sediments associated with the nucleus of the fold. Magnetic mineralogy analysis reveals pyrrhotite as the main carrier of the characteristic remanence magnetization in the Chekha formation and Tethyan Himalayan rocks. The remanence is of secondary and thermal origin as indicated by fold test and ~13 Ma K-Ar ages related to the last metamorphic peak. A small circle reconstruction method permits to disentangling the remanence directions from the superimposed folding and rotational event, to finally determine 37°.6 clockwise rotation after ~13 Ma prior or synchronous with the last-orogenic folding. This vertical-axis rotation might witness near-field imprint of E-W extension of the upper-crust along the NNE trending faults of the Yadong cross structure, and possibly developed as a response to far-field tectonic stresses generated by the SE motion of the SE Tibetan plateau.

5.2 Introduction

To comprehend the formation of continental collisional orogens as the Himalaya, it is important to constraint how the orogenic system develops in terms of e.g., sequences of thrusts, exhumation of midcrustal rocks and GPS velocities. Paleomagnetism can contribute to decipher the development of vertical-axis block rotations and long-wavelength tiltings. Previous paleomagnetic studies in the western Himalayan orogen (76°E-80°E) (e.g., Klootwijk et al., 1985; Appel et al., 1995; Schill et al., 2002a; Schill et al., 2003), indicate that the orogen curvature in the western syntaxis region is formed by oroclinal bending mechanism since Oligocene (Fig. 1a, b; Schill and Holt, 2004). In the central Himalaya paleomagnetic vectors indicate an eastward increase in the degree of clockwise block rotation since 30-20 Ma from 2.3° counterclockwise at 83.6°E to 26.5° clockwise at 85.1°E (Fig. 1c; Schill et al., 2004, and references therein). Paleomagnetic data in the eastern Tethyan Himalaya indicate a lack of rotation at 90°E and 20° clockwise rotation at 92°E since ca. 22 Ma (Fig. 1a; Antolín et al., submitted). Oligocene to Early-Miocene clockwise rotations from the central and eastern domains have been interpreted as a regional imprint of the eastward extrusion of the Tibetan plateau (e.g., Schill et al., 2004; Antolín et al., submitted), first recognized by Tapponnier et al. (1982). However the eastern Himalaya has not been analyzed in such detail as the western part. A detailed paleomagnetic control of the central and eastern Himalaya is indispensable previous to analyze when the arc curvature of this part of the orogen was acquired and which mechanism has produced it. For instance a homogeneously and dense net of distributed paleomagnetic vectors along the entire fold-thrust belt is required prior to apply the “oroclinal bending test” (Eldredge et al., 1985; Weil and Van der Voo, 2002). In addition, the GPS velocity field indicates present-day eastward motion of the upper-crust towards the eastern syntaxis (Fig. 1a; Gan et al., 2007) which mechanism and time of onset is still a matter of debate, and which have major implications for the evolution of the Himalaya-Tibetan plateau system. In the present study we focus on the eastern Himalayan area of NW Bhutan (Fig. 1c, d).

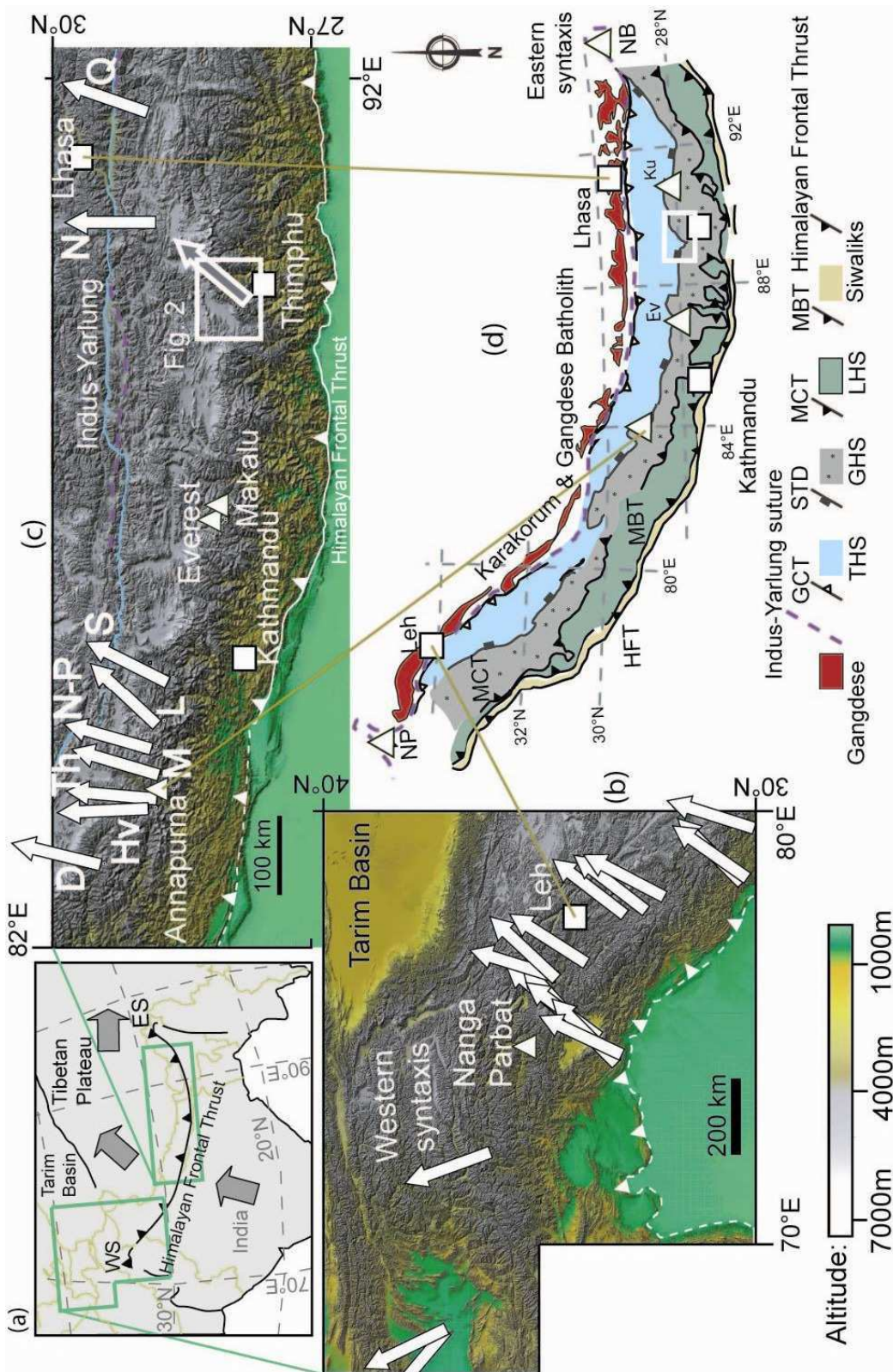
Among the general along-strike continuity of tectonometamorphic units in the Himalaya, the eastern Himalaya in Bhutan witnesses the existence of the southern extent of the Tethyan Himalaya sequence (THS) and the South Tibetan Detachment (STD), in form of tectonic windows, which have been only described in this part of the Himalayas. These tectonic windows represent snapshots of the deformation history in the THS just “in situ” on top of the Greater Himalayan Sequence (GHS). This study focuses on the Lingshi klippe, which is located in a cornerstone area within the orogen because three different major Himalayan

deformational events are superimposed within a small area (Figs. 1d & 2). These deformational events comprise regional N-S compression (e.g., Hodges et al., 2000; Yin, 2006), southward extrusion of midcrustal rocks of the GHS (e.g., Grujic et al., 2002; Carosi et al., 2006), and E-W extension of the upper crust in the THS along the Yadong-Gulu graben (e.g. Armijo et al., 1986; Cogan et al., 1998; Jessup et al., 2008) (Fig. 2).

The main goal of this paper is to characterize the rotation pattern of the Lingshi klippe and to increase the knowledge about the kinematic evolution of NW Bhutan and the eastern Himalaya by means of paleomagnetic analysis combined with structural and geochronological data. Furthermore this study deals with secondary magnetizations distributed along small circles to decipher deformation processes like flexural folding which occurred after remanence acquisition.

Figure 1: Paleomagnetic setting and study area location. (a) Himalaya-Tibetan Plateau system with location of the Western Syntaxis domain and Central-East Himalaya enlarged in Fig. 1b, c. Arrows are generalized GPS motions relative to Siberia (Tapponnier et al., 2001). (b) Digital topography (SRTM data) of the Western Syntaxis with selected paleomagnetic vertical-axis block rotations against India for remanence ages < 55 Ma (details in Klootwijk et al., 1985; Klootwijk et al., 1994; Appel et al., 1995; Schill et al., 2001; Thomas et al., 2002; with references therein). (c) Digital topography of the Central and Eastern Himalaya with block rotations in the Tethyan Himalayan sequence (D, Hv, Th, M, N-P, L, S details in Schill et al., 2004; N and Q in Antolín et al., submitted). Study area location within the white box and corresponding block rotation versus India, after this study. (d) Simplified geological map of the Himalayan Belt with location of the study area (modified after Pan et al., 2004; Yin, 2006). NP, Nanga Parbat; Ev, Everest; Ku, Khula Kangri; NB, Namche Barwa. GCT, Great Counter Thrust; THS, Tethyan Himalayan sequence; STD, South Tibetan Detachment; GHS, Greater Himalayan sequence; MCT, Main Central Thrust; LHS, Lesser Himalayan sequence; MBT, Main Boundary Thrust.

Chapter 5: Late orogenic deformation in the Lingshi klippe (NW Bhutan) deduced from paleomagnetic data: Consequences for extension and clockwise rotation in the eastern Himalaya



5.3 Geological framework

The study area belongs to the eastern Himalaya, NW of Thimphu (Figs. 1d & 2). The eastern Himalayan tectonostratigraphic units in Bhutan have key similarities with neighbouring areas in the central and western Himalayan fold-thrust belt (e.g., McQuarrie et al., 2008). The Lesser Himalayan Sequence (LHS) in the footwall of the Main Central Thrust (MCT) is characterized by duplex structures of Middle Miocene age (McQuarrie et al., 2008). The Greater Himalayan sequence has been probably exhumed during contemporaneous normal-sense ductile shearing along the STD and the south-vergent thrusting on the Main Central Thrust (MCT) (e.g., Burchfiel et al., 1992; Grujic et al., 1996; Carosi et al., 2006) at about 24-12 Ma for the whole Himalaya (Godin et al., 2006 and references therein). The younger limit of this time interval is mostly derived from geochronological data obtained in the STD and MCT zones of the eastern Himalaya. E.g., dating on granites cropping out in the STD footwall indicate that the STD was active at 12-10 Ma in the Khula Kangri massif and 15.5-11.0 Ma in the Masang Kang area, constrained by Th-Pb dating (Edwards and Harrison, 1997) and U-Pb geochronology of magmatic zircons (Kellett et al., 2009) (Fig. 2). In western Arunachal the MCT zone was active at ~10 Ma as shown by dating of monazite inclusions in garnet from the MCT zone (Yin et al., 2006). North of the STD, which coincides with the political border between Bhutan and China (Tibet), the Tethyan Himalayan sequence (THS) crops out over a N-S width of ~150 km until the Indus-Yarlung Tsangpo suture zone (Fig. 1d). The THS records the sedimentation on the passive northern margin of the Indian continent since Cambro-Ordovician to Eocene times (e.g., Willems et al., 1996).

One major difference in the eastern part of the Himalayan arc is the occurrence of klippen of low-grade sedimentary rocks (THS) atop the GHS (e.g., Gansser, 1983; Grujic et al., 1996). These klippen are remnants of the earlier and southern outline of the STD (Grujic et al., 2002; Kellett et al., 2009). Now removed by surface denudation, but to a shallower level than elsewhere in the Himalayan Belt so that the klippen are preserved (Grujic et al., 2002). The klippen occur as cores of open, upright synclines and they encompass ca. 10 % of the total surface of Bhutan.

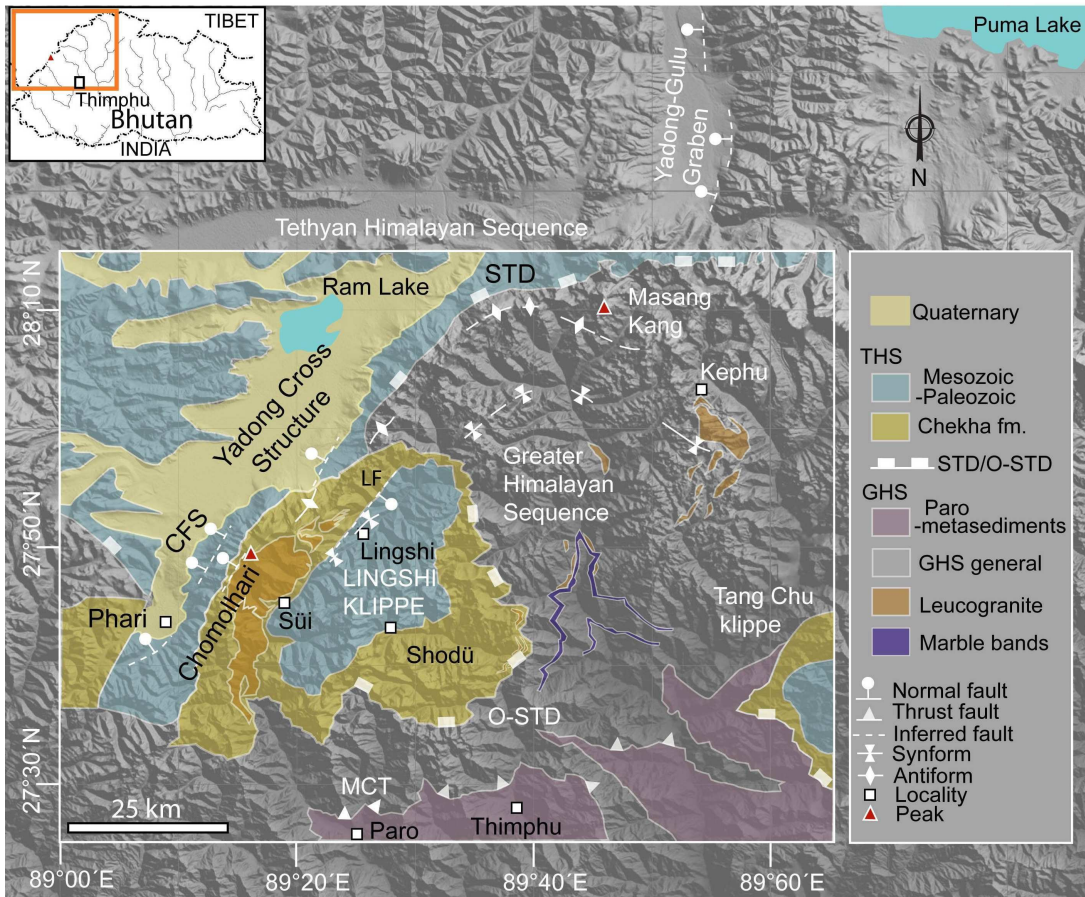


Figure 2: Simplified geological map of NW Bhutan after Gansser (1983), Grujic et al. (1996), Wu et al. (1998) and Kellet et al. (2009); overlapped with digital topography. Inset shows the geographic location of this geological map.

5.3.1 Stratigraphy and structural anatomy of the Lingshi klippe

The largest of these klippen is the Lingshi klippe with 1514 km². It is bounded to the west by the Chomolhari range and the Yadong cross structure (southern segment of the Yadong-Gulu graben) and to the north, south and east by high-grade metamorphic rocks of the GHS (Fig. 2). Here the GHS mainly consists of two-mica-garnet ± sillimanite gneiss and schist, and migmatites (Grujic et al., 2002). North of the Lingshi klippe and south of the Masang Kang peak (Fig. 2), NE-striking with top-down-to-SE sense, normal shear zones have been related to exhumation of the GHS and dated to ~17 Ma (Carosi et al., 2006). The klippe is defined by a diffuse normal sense shear zone which separates the GHS from the Chekha formation and the THS (e.g., Grujic et al., 1996). It was in ductile motion until 11 Ma and named outer-STD to differentiate it from the regionally described STD system (Kellett et al., 2009). The boundary between the Chekha formation and the THS might be also a normal fault with similar features as the STD (Fig. 3a; Grujic et al., 2002; Kellett et al., 2009). The existence of two close, sub-parallel detachments is at least geometrically similar to the structural situation

observed in the Mount Everest massif (Searle et al., 2003) and in the Annapurna-Manaslu region (Searle & Godin, 2003).

The stratigraphic succession from bottom to top comprehends the last facies of the Chekha Formation (Dando Gömpa formation) with pre-Cambrian age outcropping in the SW side of the Klippe (Fig. 3a). This facies is intruded by the Miocene Chung La leucogranite dikes (Kellett et al., 2009), and migmatites and granites of the Chomolhari massif. On top of the Dando Gömpa formation appears the Chekha formation (pre-Cambrian limestone facies) at the eastern and northern rim of the klippe (Fig. 3a; Gansser, 1983). The overlying Paleozoic and Mesozoic rocks of the THS can be subdivided into the tilloid greywacke zone with limestone lenses and crinoidal calc-schists of Permo-Carboniferous age, undifferentiated Paleozoic sediments, lower Mesozoic sediments and Cretaceous sediments. In the NW area the general distribution of the sediments outlines a broad irregular syncline with Cretaceous sediments in the core (Gansser, 1964, 1983; this study; Fig. 3a). The axial plane strikes ~NE within the klippe. South of this fold a second synclinal fold have been described in the geological map of Gansser (1964) which shows an ~ENE-trending axis. However this second synclinal has been poorly defined and constrained in the field until now. It is noteworthy that there is ~25° clockwise divergence in strike between the two synclines. East of the NW broad syncline and parallel to it a NNE-trending antiform outcrops affecting the GHS and Chekha formation north of the Chomolhari peak. The axial planes of the broad syncline and the antiform continue to the north within the GHS with a shift of the strike to E-directed, sub-parallel to the trace of the STD in the Masang Kang area (Fig. 2). McQuarrie et al. (2008) propose that the emplacement of north-dipping thrust sheets in the duplex systems of the LHS during ca. 10 Ma to present resulted in folding of the overlying GHS and THS rocks in the Kuru Chu valley, SE-Bhutan.

The two major folds described in the northern part of the klippe are separated by the sub-vertical and NNE-trending Lingshi normal fault (Gansser, 1983). Focal mechanisms of earthquakes (1937-2003) in Bhutan and in the neighbouring Sikkim close to the Lingshi fault indicate strike-slip deformation at midcrustal to deep crustal depths (Drukpa et al., 2006). The fault might be seismically active as suggested by focal solution mechanisms of earthquakes (Drukpa et al., 2006).

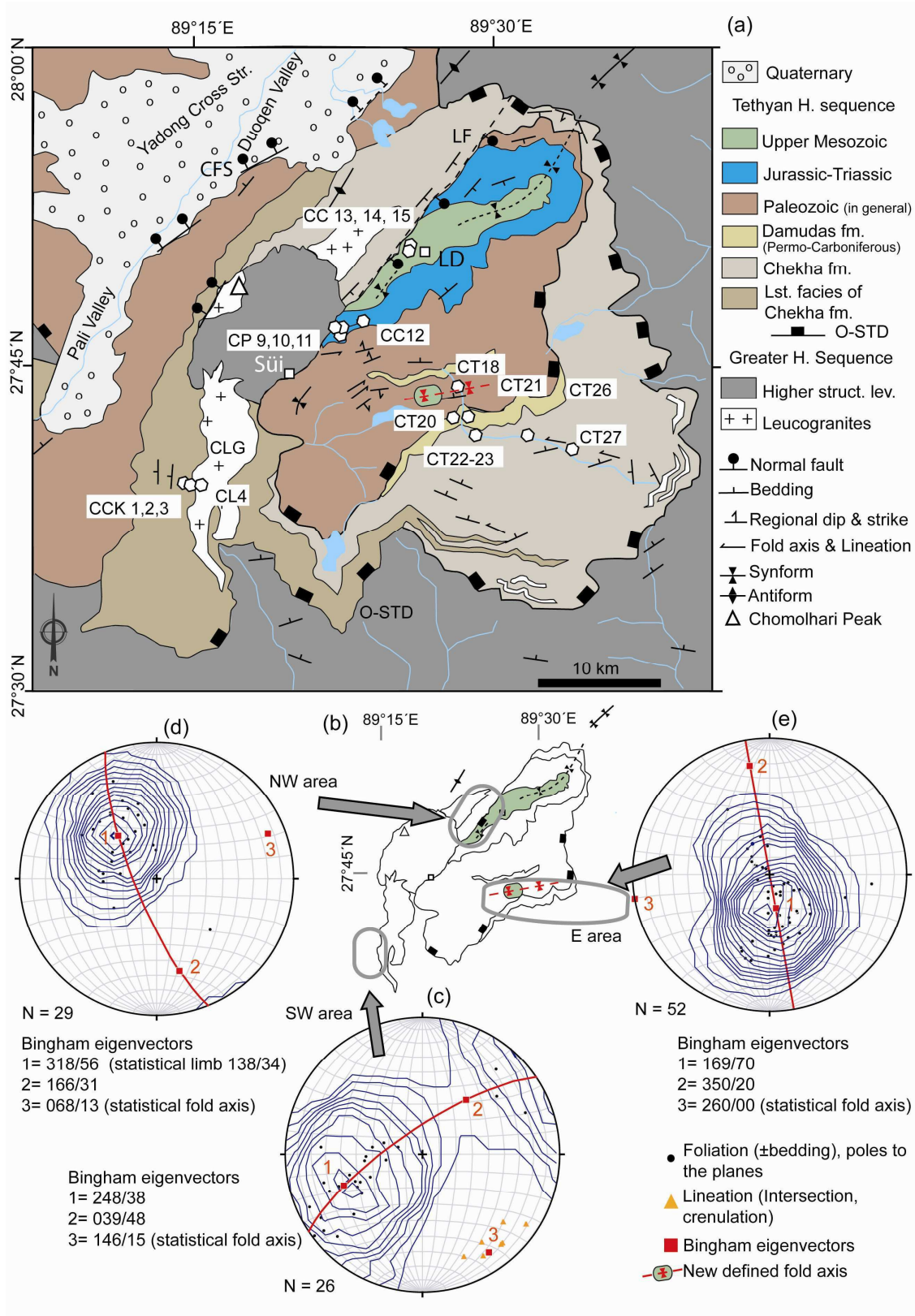
The Lingshi klippe is strongly tectonically bounded to the west by the Yadong-Gulu graben. It is one of the seven major Tibetan Grabens which were formed due to E-W extension since later-Miocene times (e.g. Armijo et al., 1986; Ratschbacher et al., 1994). To the south it is a half-graben named Yadong cross structure (Burchfiel et al., 1992) and encompasses the Duoqen and Pali valleys which are filled by Quaternary sediments (Figs. 2 & 3a). The half-

graben is defined in the east side by a set of high-angle normal faults dipping ~NW and named Chomolari fault system (CFS) (Figs. 2 & 3; Armijo et al., 1986; Wu et al., 1998).

Interpretation of the INDEPTH seismic data suggest that the Duoqen valley half-graben is a shallow extensional basin superimposed on a large monoclinial flexure in the underlying GHS/THS caused by southward motion along a lateral ramp in the Main Himalayan thrust (Cogan et al., 1998; Hauck et al., 1998). This may have caused the structures observed at the surface in the Chomolhari massif and at the western side of the Lingshi klippe (Fig. 3a).

Figure 3: (a) Redrawn geological map of the Lingshi klippe from Gansser (1983) and modified after Grujic et al. (1996), Wu et al. (1998), Kellet et al. (2009), and this study. LF, Lingshi fault; CFS, Chomolhari fault system; O-STD, outer-STD; LD, Lingshi village. Paleomagnetic sampling sites are indicated by white symbols and labels. (b) Outlined core of the klippe with the fold pattern and location of the three study areas. (c), (d), (e) equal area lower hemisphere projection of the poles of foliation/bedding with Bingham statistics for the different areas.

Chapter 5: Late orogenic deformation in the Lingshi klippe (NW Bhutan) deduced from paleomagnetic data: Consequences for extension and clockwise rotation in the eastern Himalaya



5.4 Structural investigations, finite deformation

In the SW area of the klippe (Fig. 3b) deformation is well documented by the foliation and lineation. Bingham fitting (Bingham, 1974) of the foliation poles reveal a maximum at 248° trend (T) and 38° plunge (P) (eigenvector 1) (Fig. 3c). Bingham distribution of the foliation poles suggests a statistical fold axis at $146^\circ/15^\circ$ (T/P) (eigenvector 3). Lineation of intersection and crenulation strike NW-SE with a shallow plunge toward SE and match the statistical fold axis (Fig. 3c). For the NW area covering the CP sites (Fig. 3b), the foliation is rather uniform representing the NW statistical fold limb of the NW broad syncline (eigenvector 1 = $318^\circ/56^\circ$) and attitude $132^\circ/34^\circ$ (dip direction/dip, Fig. 3d). The statistical fold axis, mostly defined with one of the flanks, have an axis T/P = $068^\circ/13^\circ$ (Fig. 3d). The foliation pattern in the eastern area of the klippe (Fig. 3b, sites CT) describes two fold limbs with a statistical horizontal fold axis trending 260° (Fig. 3e). This fold is the aforementioned described second syncline in agreement with Cretaceous K-Ar dated sediments in the fold core, sites CC20 and CC18 (Fig. 3b; details in the geochronology results).

5.5 Methodologies

5.5.1 Paleomagnetic sample treatment and analytical procedure

Paleomagnetic sampling has been carried out in 22 sites (Fig. 3a) within carbonate bearing sediments (shale, limestones, slates and quartzites) of the following stratigraphic units: Chekha formation (3 sites, CCK1-3 sites), last facies of Chekha formation (Dando Gömpa) (7 sites, CT18-27 sites), undifferentiated Paleozoic sediments (7 sites, CP5-10 sites), and Cretaceous/Jurassic (4 sites, CC12-17 sites) (Fig. 3a); furthermore, one site was drilled in the Chung La leucogranite (site CL4). In general, 10 cores, 2.5 cm in diameter, were drilled from each site using a gasoline-powered drill, oriented by magnetic compass, and cut into standard specimens (2.2 cm length). Because of poor outcrop quality block samples were taken from sites CC12 to CC17 and standard specimens were obtained in the laboratory. All magnetic measurements were carried out in the paleomagnetic laboratory of ETH Zürich (Switzerland). For two pilot samples from each site, the natural remanent magnetization (NRM) was progressively demagnetized in a magnetically shielded room. One sample was demagnetized by heating in an ASC Model TD48 furnace (ASC Scientific) and the other by alternating field (AF) treatment using a 2G600 automatic degaussing system (2G Enterprises). Remanence directions were measured with a 2G Enterprises SQUID magnetometer 755R (noise level $<0.01\text{mA/m}$ for a 10 cm^3 specimen). Low-field magnetic susceptibility was monitored after

each heating step to detect possible changes in the magnetic mineralogy. AF-demagnetized specimens were then subjected to isothermal remanence (IRM) acquisition employing an ASC Model IM-10 pulse magnetizer (ASC Scientific) with a maximum field of 2.5 T, and subsequent stepwise thermal demagnetization of composite IRM, where three different magnetic fields (hard 2.5 T, medium 0.7 T, and soft 0.3 T) are applied in three orthogonal axes prior to thermal demagnetization of the sample (Lowrie, 1990). The remaining specimens were thermally demagnetized in steps of 5-50 °C. Linear principle component analysis (PCA) was applied for separation of the remanence components. A maximum angular deviation (MAD) < 15° was accepted for further statistical processing. Site means directions have been determined using Fisher statistics (Fisher, 1953). Additionally we applied Bingham (1974) distribution analyses and the small circle method (Waldhör, 1999; Waldhör and Appel, 2006). A small circle distribution of remanence directions puts constraints on the determination of block rotations. Vertical-axis block rotation are determined using the intersection between the small circle fitting of the remanence directions and the small circle around the vertical axis defined by the expected inclination from APWP (e.g., Waldhör et al., 2001; Schill et al., 2002b).

5.5.2 ⁴⁰K-⁴⁰Ar and fission-track analytical procedures

Block samples for radiometric dating were taken from the leucogranites in the western part of the klippe and from the meta-sediments far from leucogranite intrusions.

The K-Ar analyses were carried out on the selected mineral fractions at the IDES laboratory, Université Paris-Sud 11, Orsay (France). K was measured by flame emission spectroscopy and was compared with reference values of MDO-G and ISH-G standards (Gillot et al., 1992). For argon analyses, samples were wrapped in Cu foil and fused for 15 minutes above 1500 °C using a high-frequency furnace. Before analysis, multiple-step gas cleaning was performed using Ti foam at 700 °C and SAES MP-10 getters at 400 °C. ⁴⁰Ar and ³⁶Ar were measured following the K-Ar Cassinot-Gillot technique (Cassinot & Gillot, 1982), which is based on a direct comparison between the unknown (sample) and an air pipette aliquot measured with the same ⁴⁰Ar signal conditions, with a mass spectrometer identical to the one described by Gillot & Cornette (1986). The interlaboratory standard GL-O, with the recommended value of 6.679 x 10¹⁴ atom/g of ⁴⁰Ar* (Odin et al., 1982), was used for ⁴⁰Ar signal calibration. Typical uncertainties of 1 % are achieved for the ⁴⁰Ar signal calibration (including GL-O standard uncertainty) and for the K determination. The uncertainty on the ⁴⁰Ar* determination is a function of the radiogenic content of the sample. The detection limit of the system is 0.1 % of ⁴⁰Ar (Quidelleur et al. 2001). The total age uncertainty for each

analysis is then given by the square root of the quadratic sum of the three sources of uncertainty mentioned above (e.g., Quidelleur et al., 1999). In order to take into account the systematic errors, the age uncertainty for each flow is conservatively calculated by simply weighing each duplicate uncertainty using the proportion of radiogenic argon, similarly to the mean flow age calculation. All uncertainties herein are quoted at the 1 sigma level. The decay constants and isotopic ratios of Steiger & Jäger (1977) have been used.

The K-Ar technique used here has also been shown to be a powerful tool to constrain the stage durations of the late Cretaceous from comparison with the astronomical time scale (Fiet et al., 2006), as well as the timing of large igneous provinces, such as the Deccan (Chenet et al., 2007) and the Ethiopian traps (Coulié et al., 2003). Finally, direct comparison with the $^{40}\text{Ar}/^{39}\text{Ar}$ technique has shown identical ages (Coulié et al., 2003), while dating of MMhb-1 standard, for instance, provided ages of 525 ± 2 Ma using the GL-O standard (Fiet et al., 2006), in perfect agreement with the values of 523 ± 2 Ma obtained by $^{40}\text{Ar}/^{39}\text{Ar}$ (Renne et al., 1998).

For apatite fission-track analyses, samples were processed by Alexander Grist at Dalhousie University and analyzed by I. Coutand (at University Lille, France). Standard magnetic and heavy liquid mineral separation procedures were used. Apatites were mounted in araldite epoxy, and afterwards sample surfaces were ground and polished. The apatite mounts were etched in 5M HNO_3 at 24°C for 20s. An "external detector", consisting of low-U (<5 ppb) muscovite, was used for each sample. Samples were irradiated at the Dalhousie University Slowpoke reactor. Following irradiation, the muscovites were etched in 48% HF for 30 min, at room temperature. Tracks were counted using a 100X dry lens and 1250X total magnification in crystals with well-etched, clearly visible tracks and sharp polishing scratches. A Kinetek stage and software were used for analyses. Standard and induced track densities were determined on external detectors (geometry factor = 0.5), and spontaneous track densities were determined on internal mineral surfaces. Ages were calculated using $\zeta = 369.5 \pm 5.1$ for dosimeter glass CN5.

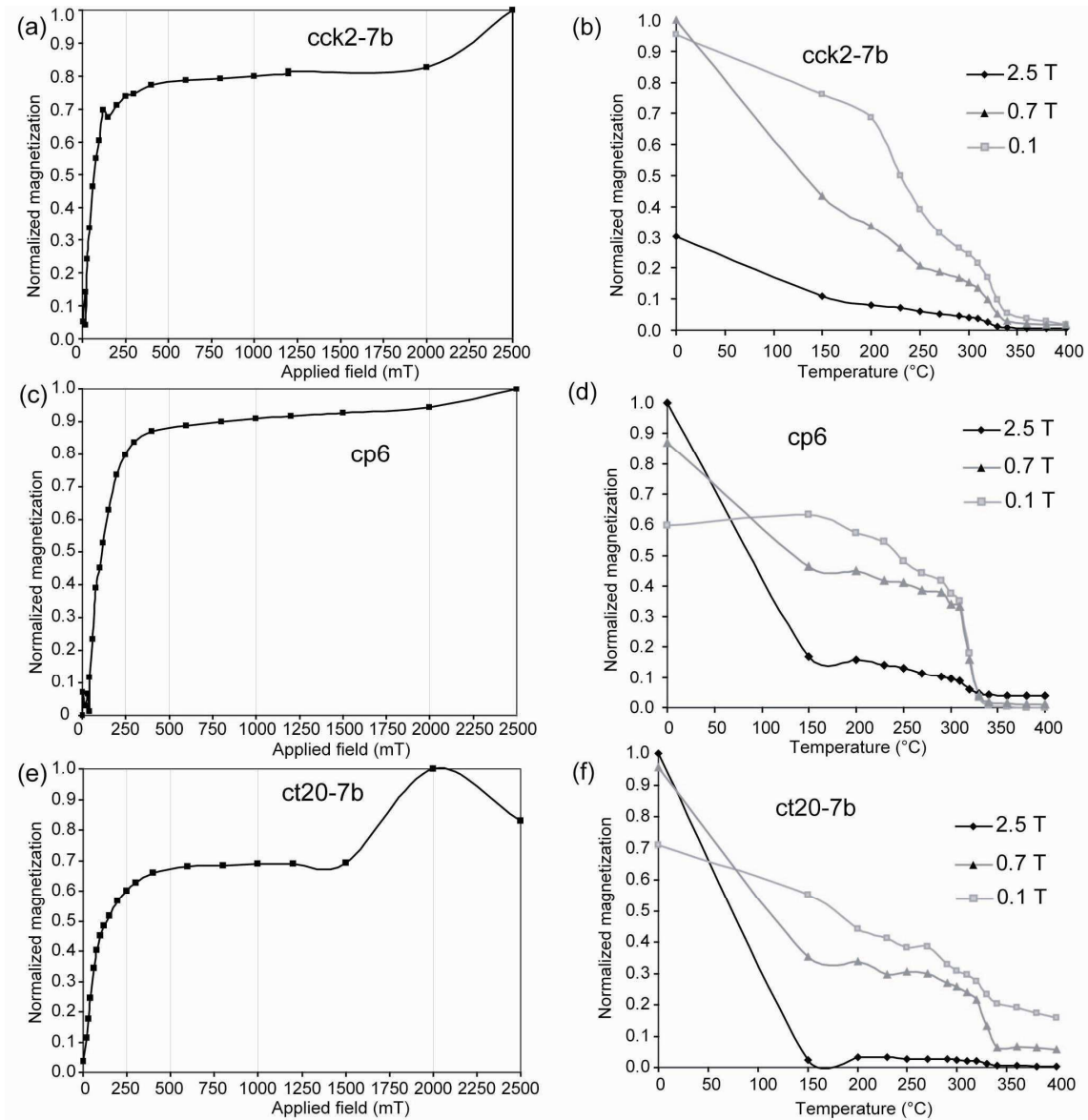
5.6 Results

5.6.1 Magnetic mineralogy and carriers of the remanence

Mainly Pyrrhotite (Curie temperature $T_c=325$ °C) and additionally magnetite ($T_c=580$ °C) have been identified as the carriers of the remanence by IRM acquisition (SIRM) and stepwise thermal demagnetization of composite IRM. We consider the steeper decays of the

intensity of NRM at unblocking temperatures (T_{ub}) of $270\text{ }^{\circ}\text{C} < T_{ub} < 325\text{ }^{\circ}\text{C}$ as related to pyrrhotite and the unblocking temperatures of $150\text{-}250\text{ }^{\circ}\text{C}$ and $360\text{-}580\text{ }^{\circ}\text{C}$ are attributed to a soft-magnetite-like phase or magnetite. In addition all samples reveal goethite ($T_{ub} < 150\text{ }^{\circ}\text{C}$) in the hard and medium coercivity spectrum, with a minor contribution to the total NRM (Fig. 4). According to the rock-magnetic experiments and the contribution of pyrrhotite and magnetite to the thermal demagnetization of the NRM three different groups of sites can be distinguished: (1) low-temperature magnetite-like phase and pyrrhotite dominated, (2) pyrrhotite dominated, and (3) pyrrhotite and high-temperature component dominated. For group (1), saturation in fields of ca. $>300\text{ mT}$ is indicative for pyrrhotite and magnetite (Fig. 4a). Most of the remanence (apart from the goethite component) is unblocked between 150 and $270\text{ }^{\circ}\text{C}$ pointing to thermally unstable magnetite-like phase (Fig. 4b). For group (2) saturation during IRM acquisition is reached at $>500\text{ mT}$ (Fig. 4c). This indicates a dominance of pyrrhotite over magnetite. It is noteworthy that the thermal demagnetization of IRM reveals dominant unblocking temperatures between 290 and $340\text{ }^{\circ}\text{C}$ for all applied fields, but particularly for the intermediate component (Fig. 4d). Group (3) is characterised by saturation at $>500\text{ mT}$ and unblocking temperatures between 290 and $340\text{ }^{\circ}\text{C}$ for the soft and intermediate component indicating pyrrhotite (Fig. 4e, f). Additionally a high-temperature unblocking magnetite component is present too as indicate the not completely demagnetized soft component before $400\text{ }^{\circ}\text{C}$.

Figure 4: Isothermal remanence acquisition with a maximum field of 2.5 T and subsequent thermal demagnetization of IRM imparted at 2.5 T, 0.7 T, and 0.3 T (after Lowrie, 1990) of representative samples of (a) the Chekha Formation (CCK site), (b) the Permian metacarbonates (CP site), and (c) the Cretaceous shales (CT site).



For samples with both, low and high contribution of pyrrhotite to the NRM, stable remanence directions were determined using linear PCA in a temperature range between 270 and 330 °C. Reliable pyrrhotite remanence directions were obtained in 19 of the 22 sampled sites. Figure 5 shows four representative examples of the thermal demagnetization behaviour (Fig. 5a,b,c,d). Remanence directions of the high-temperature magnetite component were determined in the temperature range of 400 to 580 °C in the sites CCK3, CC13, CC14 and CT18. The low temperature magnetite component generally reveals unstable directions ($MAD > 15^\circ$) different to the pyrrhotite component direction (Fig. 5c). Further analyses will focus on the pyrrhotite component as it dominates the stable remanence of the studied rocks.

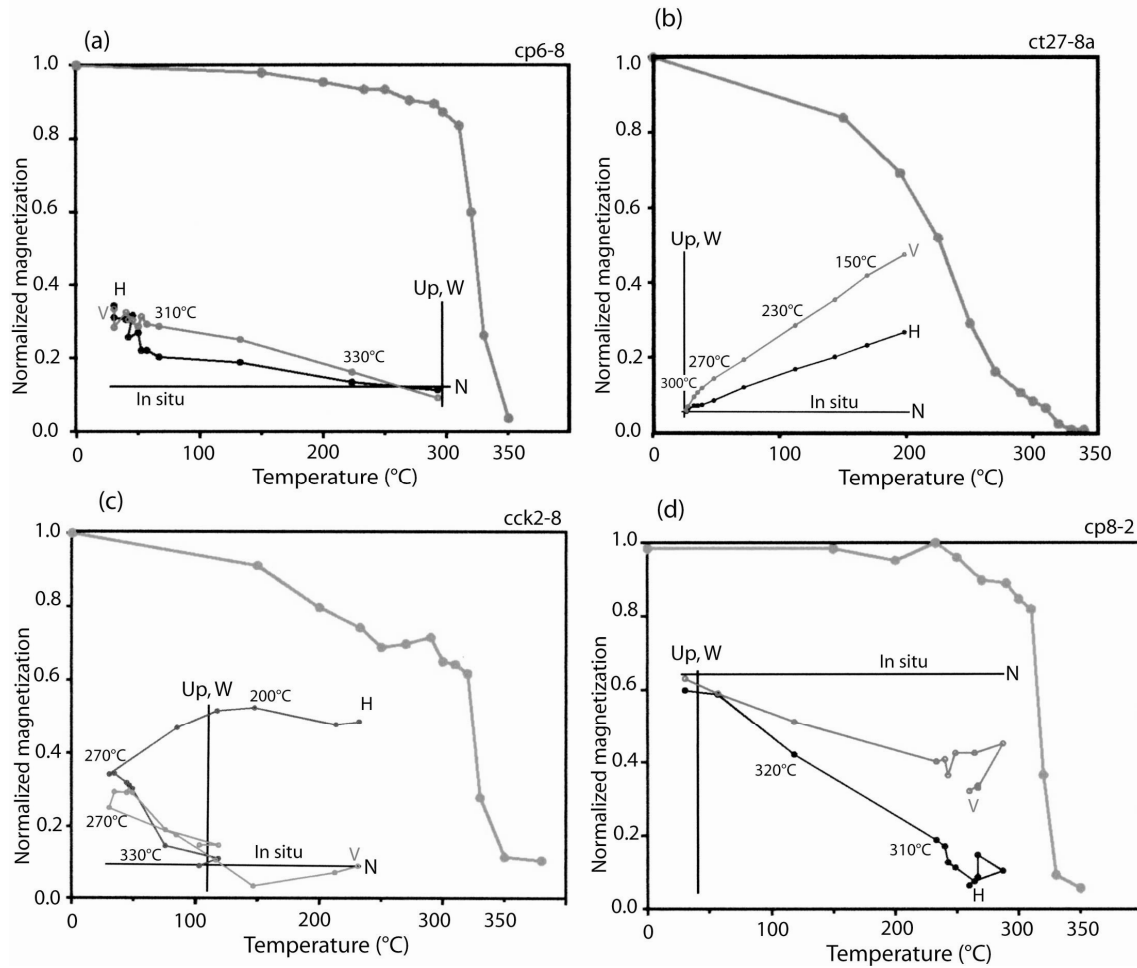


Figure 5: Thermal demagnetization of natural remanent magnetization (NRM) of characteristic specimens of the three study areas. Decay plot and orthogonal vector projection in geographic coordinates. Pyrrhotite dominate the stable remanence (a), (b), (c). (d) Soft-magnetite and pyrrhotite show different directions.

Table 1: List of paleomagnetic sites (CCK: Chekha Formation, CL: Leucogranite, CP: Permian metacarbonates, Cretaceous shales, CKL: Limestone facies of the Chekha Formation) with geographic latitudes and longitudes, altitude above sea level and geological bedding (dip and dip direction). Site mean directions for the pyrrhotite component in geographic (D_{geo} , I_{geo}) and stratigraphic (D_{str} , I_{str}) coordinates. S: number of samples included into the mean directions, N: number of measured samples, D: declination, I: inclination, k: precision value, α_{95} : confidence angle.

Site	Latitude (°N)	Longitude (°E)	Altitude (m)	Mean Dip Dir. (°)	Mean Dip (°)	S	(N)	D _{geo} (°)	I _{geo} (°)	k	α _{gs} (°)	D _{str} (°)	I _{str} (°)	k	α _{gs} (°)
CCK1	27°41.943'	089°17.560'		111.2	71.5	4	8	199.8	-8.1	11	29	181	-17.1	2.3	79.9
CCK2	27°41.957'	089°17.596		90.6	40.6	3	8	25.7	23.7	9.9	41.4	26.9	20.9	9.2	43.2
CCK3	27°41.944'	089°17.512'		68.5	45	4	8	28.8	12.1	8.3	33.9	7.4	-11.5	6.9	37.8
CL4	27°41.944'	089°17.512'		51.5	51	2	4	166.7	18.5	10.7		145	22.9	4.3	
CP5			4150	138.2	29.4	4	8	54.8	34.8	10.1	30.4	69.6	25.5	13	26.5
CP6	27°47.636'	089°21.050'	4210	13.5	53.8	9	11	189.5	-30.1	18.2	12.4	236.8	-48.3	10.2	17
CP7			4235	90.2	30.8	6	9	4.5	41.7	15	17.9	27.5	-31.6	13.4	19
CP8			<4200	158.6	44.3	7	8	26.4	0.8	7.7	23.2	36.6	29.1	9	21.2
CP9	27°47.483'	089°21.06'	4200	155.9	44.4	5	11	22.1	36.2	9.5	26.2	29.6	13.1	17.2	19
CP10	27°47.459'	089°21.632'	4190	236.4	38	7	8	49.9	26.6	9.2	21.2	36.8	22.3	14.4	16.6
CC12	27°49.708'	089°23.922'	4410	48	32										
CC14	27°51.584'	089°25.741'	4180	337.5	17	5	8	206.6	-28.2	28.3	14.6	201.5	-16.7	28.6	14.5
CC15	27°52.377'	089°26.717'		137.5	17.5										
CC17				341.5	21	4	8	193	-27.6	5.3	43.9	189.3	-1	5.3	43.9
CT18	27°44.986'	089°27.487'	4490	343.5	13.5	5	8	303.4	-6	6	34	301.8	-12.9	7.3	30.3
CT20	27°43.374'	089°27.452'	4250	316.3	19	5	8	34	-5	6.2	33.3	35	-6.7	6.4	32.7
CT21	27°43.263'	089°27.537'	4240	282.7	19.10	4	8	262.4	-20.1	16.5	23.3	259.4	-23.7	17	23
CT22	27°42.959'	089°27.838'	4155	286.4	36.6	7	11	209.4	-16.8	11.2	18.9	208.3	16.3	9	21.3
CT23	27°42.946'	089°27.824'	4118	233	21	7	8	214.7	-40.7	3.4	38.2	206.5	-23.9	3.4	38.2
CT26	27°42.534'	089°31.378'	3740	297.5	38.5	6	11	52.8	30.9	8.1	25.1	36.7	15.6	9.3	23.2
CT27	27°41.719'	089°35.463'	3780	206.6	39.7	6	8	247.6	-59.6	4.4	36.3	2.2	-62.2	5.5	31.6

5.6.2 Pyrrhotite component: distribution and directions

The pyrrhotite site mean directions obtained by Fisher statistics (1953) are shown in Figure 6 (data given in Table 1). Fourteen sites yield statistically significant site mean directions ($k > 7.7$). In the following, we will evaluate the site mean directions sorted by the SW, NW and eastern areas (Fig. 3b) in order to better access the deformation processes. The SW area, south of Chomolhari (CCK sites) yields a mean vector declination (D)/inclination (I)= $024.7^\circ/14.7^\circ$ ($n=3$; $k= 115.3$; $\alpha_{95}= 14.2^\circ$). The NW area (sites CP and CC) yields a mean vector D/I= $026.8^\circ/29.3^\circ$ ($n=8$; $k= 20.2$; $\alpha_{95}= 13.6^\circ$). However, the site means directions can be better fitted by Bingham statistics and small circle fitting as is described in the vertical-axis block rotation results. In the eastern area (CT sites) site mean directions indicate less grouping of the intra-site remanence directions. The seven sites do not represent a Gaussian distribution (Fig. 6) and can be better fitted by Bingham statistics. It yields eigenvector 1= $053.1^\circ/29.0^\circ$, eigenvector 2= $148.0^\circ/8.8^\circ$, eigenvector 3= $253.2^\circ/59.5^\circ$. For an approximate general view we calculated the overall mean vector of the 13 meta-sedimentary sites with $k > 7.7$ which yields $029.3^\circ/24.8^\circ$ ($k= 21$; $\alpha_{95}= 9.7$) (Fig. 6).

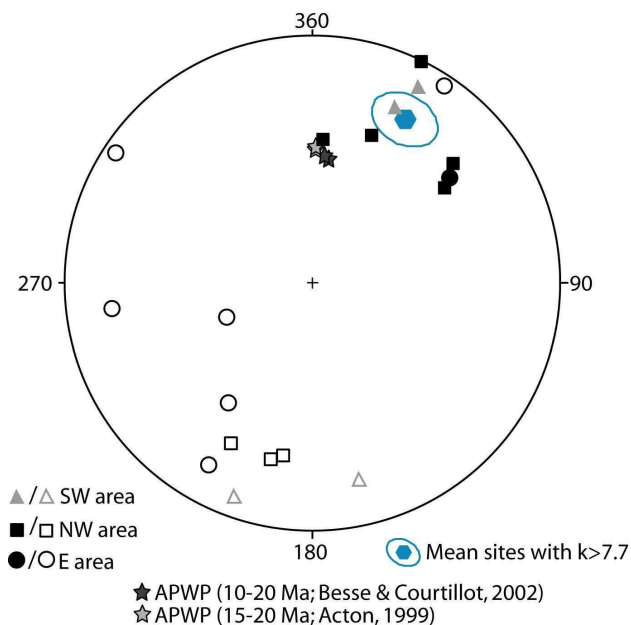


Figure 6: Equal area projection of the site mean directions carried by the pyrrhotite component of the Tethyan meta-sediments of the Lingshi klippe and expected direction from the APWPs. Solid symbols indicate normal polarity and open symbols indicate reversed polarity. Ellipse indicates the 95% confidence limit of the overall mean direction for sites with $k > 7.7$.

The origin and age of the pyrrhotite component will be evaluated further below the presentation of the K-Ar and fission-track results. These data are key points to distinguish

between different origins of the remanence (primary or secondary), the process of remanence acquisition (thermal or chemical) and the timing of the acquisition.

5.6.3 K-Ar and fission-track results

In the Lingshi klippe different lithologies and areas have been sampled for K-Ar dating and fission-track ages (Table 2; Fig. 7). The results are presented in geochronological order of the determined ages.

K-Ar age on illites of 64.1 Ma of the shale sample CC14-1, located in the core of the broad syncline in the NW area of the klippe (Fig. 7), corresponds to a Cretaceous sedimentary age as previously pointed out by Gansser (1983). Cretaceous ages of 79.8 Ma and 74.3 Ma are also obtained for the samples CC20-11 and CC18 from the central domain of the klippe, between two outcropping bands of Permo-Carboniferous rocks (Damudas group (Fig. 7). They confirm the presence of Cretaceous sediments within the core of the syncline located in the eastern area of the Lingshi klippe as previously noted Gansser (1964). Four samples have been analysed using the smallest possible fraction of illites. From a sample located in the paleomagnetic site CP9 (Fig. 3a) a metamorphic cooling age of 13.1 ± 0.2 Ma has been determined (Fig. 7). Cooling ages from the Tang Chu klippe (Schill et al., unpublished data) and cooling ages from the central Tethyan Himalaya, however, reveal similar ages. This is in agreement with ca. 11-16 Ma cooling ages on micas (Ar/Ar and Rb/Sr) from the GHS (Castelli & Lombardo, 1988; Maluski et al., 1988; Ferrara et al., 1991; Stüwe & Foster, 2001).

From the leucogranites intruded into the Chekha Formation an apatite fission-track central age of 4.4 ± 0.5 Ma is obtained (Fig. 7). Due to the few confined track length the thermal history cannot be modelled precisely. From a larger dataset in the vicinity an approximate mean exhumation rate of ~ 1.2 mm/a has been estimated for the western Bhutan area during Pliocene (Grujic et al., 2002).

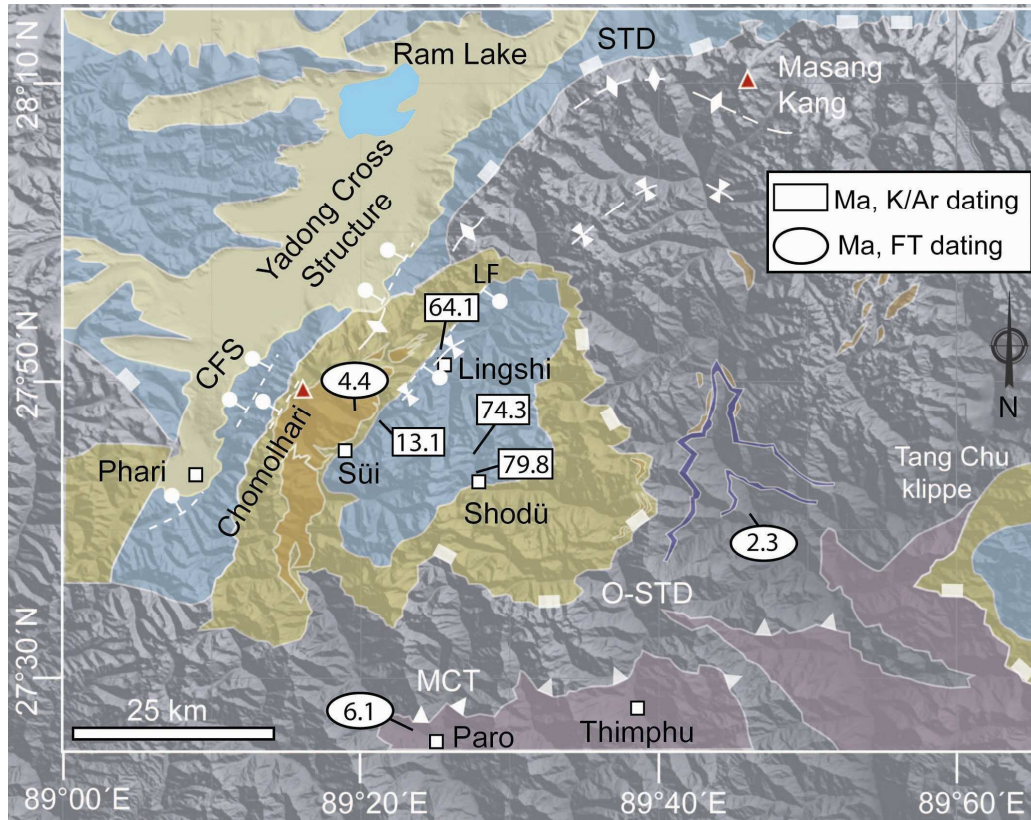


Figure 7: A, Geological map of the Lingshi klippe (Fig. 1c) with geochronology results. K-Ar dating on illites and Apatite fission-track central age dating (FT). See Table 3 for details of fission-track analyses.

Field code	Longitude	Latitude	Elevation	Number of grains	Spontaneous track density	Induced track density	Dosimeter	$P(\chi^2)$	Central age $\pm 1\sigma$
	[° E]	[° N]	[km]	(N)	$\rho_s \times 10^5 \text{ cm}^{-2}$	$\rho_i \times 10^5 \text{ cm}^{-2}$	$\rho_d \times 10^5 \text{ cm}^{-2}$	[%]	[Ma]
BH299					0.453	17.06	9.7284		
FT03-014	89.33608	27.79572	4.729	25	(99)	(3725)	(7938)	89.27	4.4 \pm 0.5
BH109	89.39972	27.44222	2.4	22	1.265	37.541	9.7661	78.55	6.1 \pm 0.4
BH171	89.77081	27.69294	1.44	23	0.13	10.113	9.7472	97.72	2.3 \pm 0.5

Table 2: Apatite fission track data. N, number of individual grains dated; ρ_s , spontaneous track density; Ns, number of spontaneous tracks counted; ρ_i , induced track density in external detector (muscovite); Ni, number of induced tracks counted; ρ_d , induced track density in external detector adjacent to dosimetry glass; Nd, number of tracks counted in determining ρ_d ; $P(\chi^2)$, chi-square probability.

5.7 Origin and age of the pyrrhotite component

Pyrrhotite forms during low-grade metamorphism in marly carbonates (Carpenter, 1974; Crerar et al., 1978). Among other processes pyrrhotite is formed on the expense of sedimentary magnetite and pyrite. This transformation occurs at temperatures of about >200 °C in presence of carbonate and water (e.g. Lambert et al., 1973). The process of remanence acquisition can be assumed to be chemical for peak metamorphic conditions with temperatures $T_p < 325$ °C and to be thermal for $T_p > 325$ °C (e.g., Crouzet et al., 2001). K-Ar dating on metamorphic illites with a closing temperature of ca. 350-425 °C (Hames and Bowring, 1994; Lister and Baldwin, 1996; Kellet et al., 2009) therefore reveals the approximate age of remanence acquisition.

Last peak temperature metamorphic conditions and cooling about 350 °C for the core of the Lingshi klippe occurred at ca. 13 Ma and point to a thermal secondary origin of the pyrrhotite remanence, post-dating the main Eohimalayan folding (Hodges, 2000). A fold test (McFadden, 1990) and partial unfolding of site CP9, where two limbs of a small scale fold have been sampled, reveal best grouping at 18 % of unfolding (Fig. 8), which indicates a post-folding origin of the pyrrhotite component.

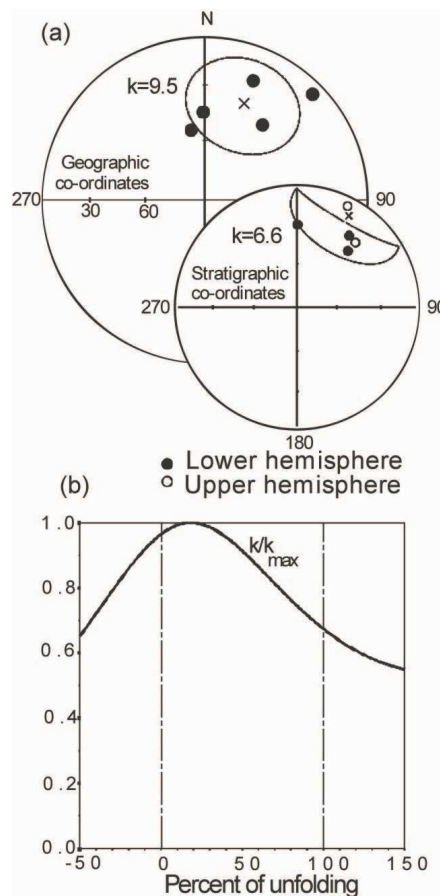


Figure 8: (a) Single specimen directions of the pyrrhotite component of site CP9 in geographic and stratigraphic coordinates. (b) Stepwise unfolding of the single specimen directions of site CP 9 indicating a best-grouping at 18% of unfolding.

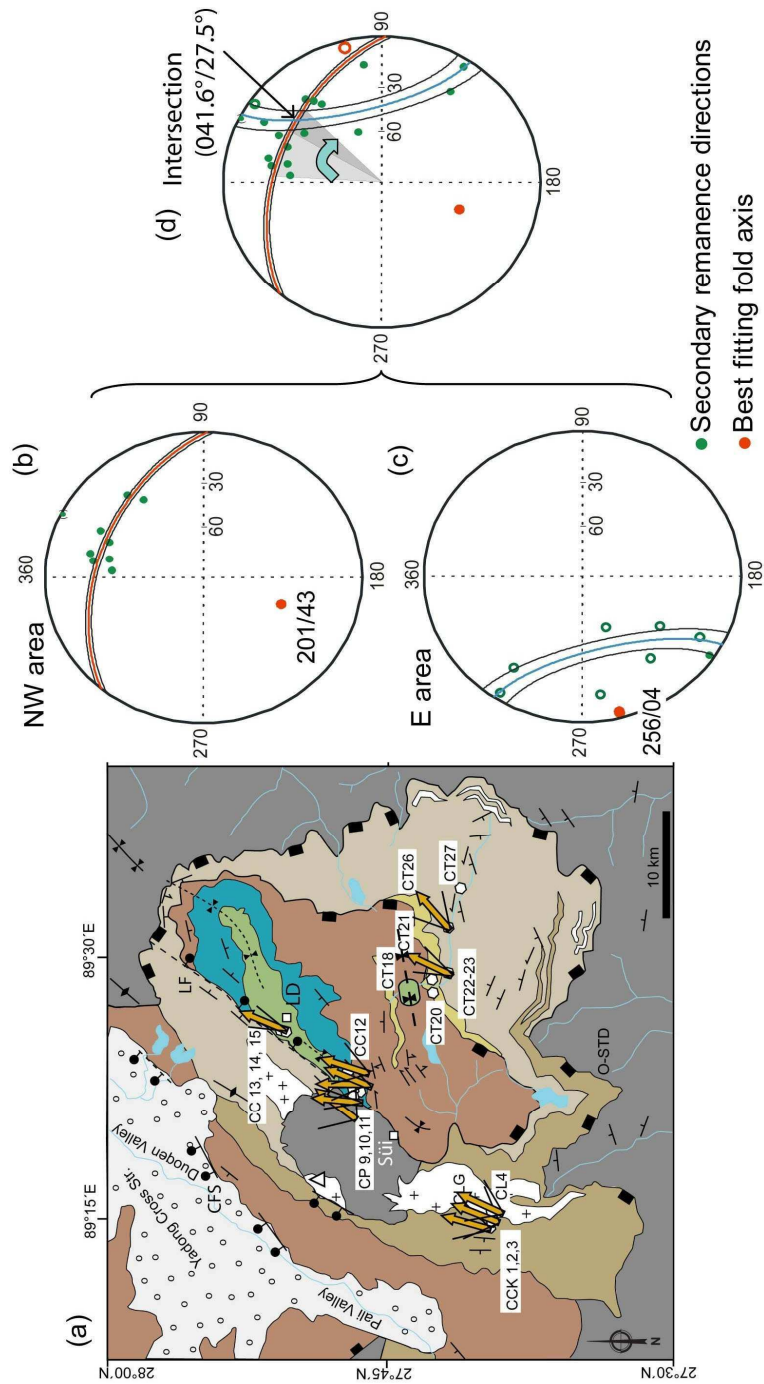
For the Cretaceous sites CC13, CC14, and CC18, the ratio between $k_{\text{stratigraphic}}/k_{\text{geographic}}$ is between 1 and 1.5 and favours a pre-folding remanence acquisition. However, fold tests and partial unfolding are statistically not significant. These results in conjunction with the Bingham distribution of the site mean directions suggest that the pyrrhotite component can be regarded as a record of the middle Miocene field after the Eohimalayan south-vergent folding phase (e.g., Hodges, 2000) and the extrusion of the GHS along the MCT and STD, but at the end or synchronous with the late orogenic folding events which might be related to the emplacement of the Lesser Himalayan duplex structures at ca. 10 Ma (McQuarrie et al., 2008).

5.8 Miocene clockwise vertical-axis block rotation

At temperatures between 325°C and 200°C pyrrhotite acquired its remanence with an expected remanence direction of $D/I = 004.0^\circ/40.5^\circ$ at 15 Ma related to the calculated ca. 13 Ma age of remanence acquisition. The paleomagnetic reference direction has been averaged from the APWPs of Acton (1999) and Besse & Courtillot (2002) from 10 to 20 Ma for stable India (Fig. 6). Additionally the expected inclination has been corrected regarding the N-S Greater India shortening budget since 15 Ma (Guillot et al., 2003), and consequently more southward latitudinal position of the study area at 15 Ma. Comparing the observed site mean directions with the expected yield vertical-axis block rotations at site scale as shown in Figure 9a. As a first approximation for the rotation of the whole area, the angle of vertical-axis block rotation from the Fisher mean direction of the 13 mean sites shows a 25.3° clockwise rotation of the klippe since 15 Ma. However, when analysing the site mean directions with Bingham statistics and the small circle method of Waldhör et al. (2001) a more accurately vertical-axis rotation can be obtained. This method is based on the fact that flexural folding distributes well-grouped remanence directions on a small-circle around the fold axis (e.g., Waldhör et al., 2001; Schill et al., 2002b; this study). The secondary remanence directions of the NW and eastern area are fitted by small circle (Fig. 9b, c). The pole of a least-squares fitted small circle through the secondary remanence directions describes the fold axis caused by the late-orogenic deformation occurring after remanence acquisition. In the NW and eastern areas fold axes of $201^\circ/43^\circ$ and $256^\circ/04^\circ$ were obtained respectively (Fig. 9b, c). The intersection of the two fitted small circles at $D/I = 041.6^\circ/27.5^\circ$ indicates the pre-large scale folding mean direction (Fig. 9d). Comparing this direction with the expected one at 15 Ma yields 37.6°

clockwise angle of vertical-axis block rotation since remanence acquisition. The observed remanence inclination is 13° shallower than expected, indicating 13° SSW tilting of the area since remanence acquisition. However it is not possible to address if the tilting was previous, during or after the vertical-axis rotation.

Figure 9: Vertical-axis block rotations. (a) Geological map of the Lingshi klippe with site mean rotations and respective rotation errors ($\alpha_{95}/\cos I$) against stable India at 15 Ma. Stereographic projection of site mean directions carried by pyrrhotite in the NW area (b) and E area (c) and their best-fitting small circle (red line and blue line respectively) and the 95% confidence of the small circles (thin lines) calculated after Schill et al. (2002b). The red dots represent the best-fitting fold axes around which the small circle distribution of the remanence directions occurs. (d) Intersection of the two small circle distributions of the NW and E areas. The angle between the expected remanence direction from APWP at 15 Ma (Acton et al., 1999; Besse and Courtillot, 2002) and the intersection between the two small circles marks the rotation prior to the late-orogenic folding (causing the small circle distribution). 95% confidence is given by the intersection of the individual confidence angles.



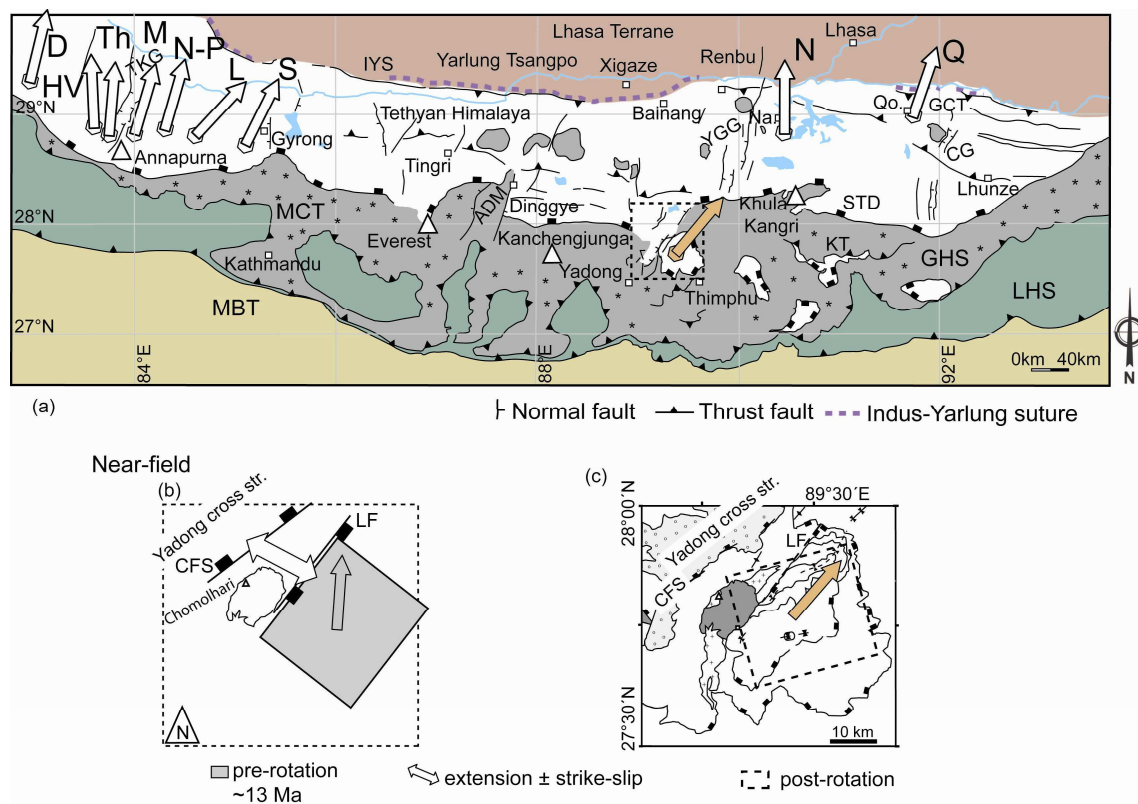
5.9 Late orogenic folding

The small circle evaluation of the secondary remanence directions distribution defines the axes of two large-scale folds affecting the Lingshi klippe (Fig. 9b, c). In the NW area a ca. N-trending axis has been obtained from the distribution of the pyrrhotite remanence directions (Fig. 9b). This axis is ca. parallel to the fold axis mapped by Gansser (1983). However, it presents an anomalous orientation in relation to the main N-S shortening regime. This orientation might be related to a surface manifestation of a lateral ramp in the Main Himalayan Thrust at the Yadong cross structure which produces the flexure of the GHS and THS strata in the Chomolhari range and at the western side of the klippe (Wu et al., 1998). The WSW-ENE trending fold axis in the eastern area (Fig. 9c) is in agreement with earlier geological map by Gansser (1964) and our structural, and geochronology data. The trend axis is in consonance with the general N-S shortening regime of the Himalayan fold-thrust belt (e.g., Hodges et al., 2000; Yin, 2006). Furthermore, 50 km to the east, a broad E-W trending syncline outcrops in the Tang Chu Klippe (Gansser, 1983; Grujic et al., 2002).

5.10 Discussion: consequences for eastward extrusion

Small circle method indicates a 37.6° clockwise vertical-axis rotation in the Lingshi klippe since remanence acquisition. We integrate this new study in the regional pattern of the Tethyan Himalaya block rotations (Fig. 10a). This rotation might witness a near-field imprint of the late Miocene to recent E-W extension around the Yadong cross structure. Taking into account ca. NNE orientation of normal faults related to the Yadong-Gulu half-graben at the Duoqen valley (Chomolhari fault system) and Lingshi fault. Extension along these faults could produce a clockwise rotation of the Lingshi fault hangingwall (Fig. 10b, c). This extension might be coupled or not with strike-slip displacements along new faults or along reactivated Eocene-Miocene structures or unconformities. Conjugate strike-slip faulting coeval with E-W extension has been observed in the interior of the Tibetan Plateau along the Bangong-Nujiang suture (Armijo et al., 1989; Taylor et al., 2003) (Fig. 10d). Onset of E-W extension of the Tibetan plateau started between 14 Ma and 4 Ma (e.g. Blisniuk et al. 2001; Mahéo et al., 2007). Strike-slip faults in the area of the Lingshi klippe are not documented in detail. However, Ratschbacher et al. (1994) proposed a left-lateral shear component in a $060^\circ \pm 23^\circ$ (minimum compressive stress orientation, σ_3) direction along the Yadong-Gulu Graben based on fault plane solutions, the right-stepping en-echelon Yadong-Gulu half-grabens and left-slip focal mechanism (at 42km depth; Ekstrom, 1987) from the 1980 earthquake near Yadong (Fig. 10d). This is in agreement with linear distribution of thermal anomalies inferred from the boiling spring distribution at the surface, which indicates deep

shear zones at mid-crustal depth related to the extrusion of the Tibetan plateau (Hochstein and Regenauer-Lieb, 1998). However present day GPS velocities in the study area point out that the present-day stress field corresponds to an E-W minimum stress axis with a right-lateral component increasing towards the north and east (Zhang et al., 2004; Van der Woerd et al., 2009). On a regional scale 37.6° clockwise rotation is in consonance with the SE extrusion of the Tibetan plateau around the eastern syntaxis as shown by GPS velocities data within the Himalaya-Tibet system (e.g., Zhang et al., 2004; Gan et al., 2007) (Fig. 10c). The rotation of the Lingshi klippe reinforces the idea that late-orogenic eastward rotations along the northern margin of the Indian plate might be triggered by strain partitioning between E-W extension and the eastward extrusion of the Tibetan plateau (Fig. 10a, d; Schill et al., 2004; Antolín et al., submitted). In contrast, an oroclinal bending model would expect no rotation or slightly counterclockwise rotations in the eastern Himalaya.



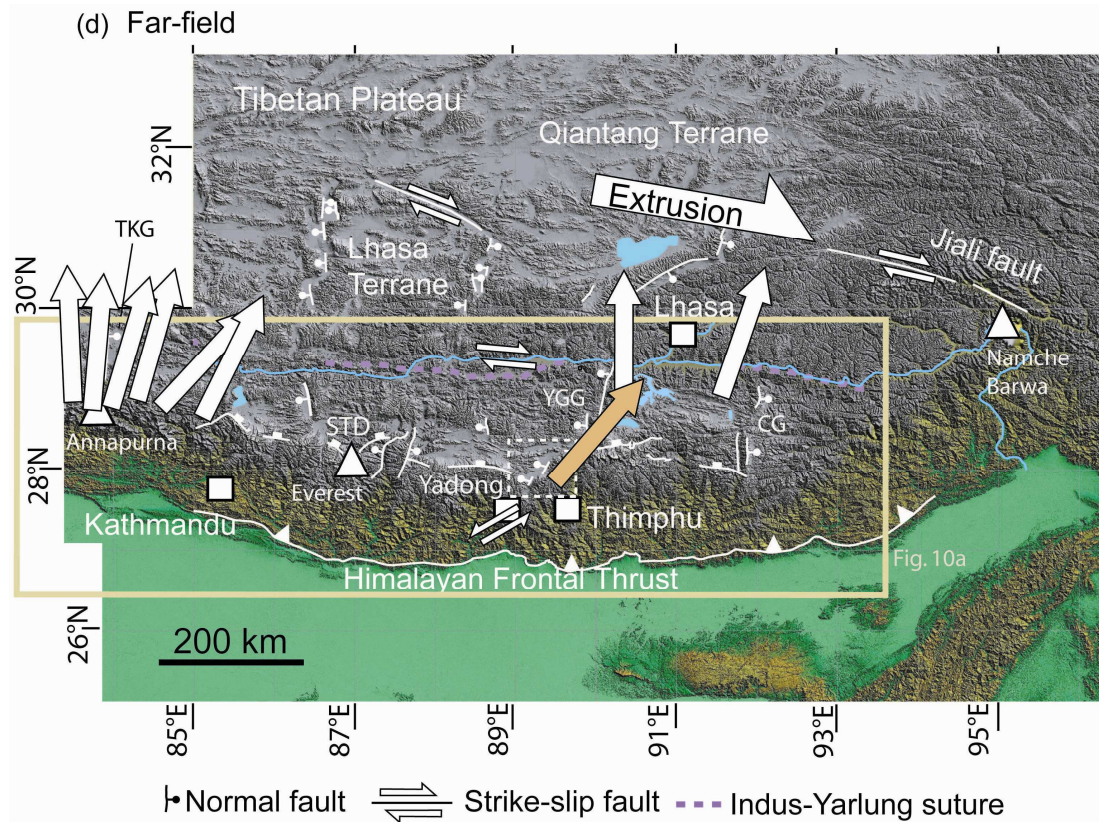


Figure 10: Explanation of the rotation pattern from near-field to far-field. (a) Geological map of the Central and Eastern Himalayan Belt after Lee et al. (2004), Pan et al. (2004), Kellet et al. (2009) and Antolín et al. (in press) with the published paleomagnetic block rotations in the Tethyan Himalaya: D, Dolpo ; HV, Hidden valley; Th, Thakkhola; M, Manang; N-P, Nar/Phu; L, Larkya; S, Shiar (Schill et al., 2004 and references therein), and N, Nagarze; Q, Qonggyai (Antolín et al., submitted). (b) Near-field setting during remanence acquisition. (c) Clockwise rotation after extension along the Chomolhari fault system (CFS) and Lingshi Fault (LF) normal faults. (d) Far-field tectonic scenario with the main extensional and strike-slip faults in the Central-East Himalaya and the Central Lhasa Terrane after Armijo et al. (1989), Kapp and Guynn (2004), and Pan et al. (2004). TKG, Thakkhola Graben; YGG, Yadong-Gulu Graben; CG, Cona Graben. Strike-slip sense at Yadong is from Drukpa et al. (2006).

5.11 Conclusions

This study contributes to the basic geological map of the Lingshi klippe by identifying Cretaceous sediments inside the cores of the two synclines i.e., depositional ages of 64.1 Ma in the northern syncline and 74.3 Ma and 79.8 Ma in the southern syncline, and the distribution and orientation of the main fold axes that govern the internal structure of the klippe.

Magnetic mineralogy analyses presented here indicate that pyrrhotite is the main carrier of the remanence in the Chekha formation and THS sampled rocks within the klippe, as pointed out by IRM saturation at >500mT and unblocking of the SIRM at ca. 325 °C. The remanence origin is secondary according to an intra-site fold test in site CP9 and is related to the last

metamorphic climax at ca. 13 Ma (K-Ar age) after the Eohimalayan tectonic phase (Hodges, 2000). Therefore the magnetization is of thermoremanent origin and witnesses the middle Miocene magnetic field. However, the site means remanence directions show small circle distributions suggesting that the remanence was acquired at the end or synchronous with folding deformation. By means of the small circle reconstruction method the pre-folding remanence direction was obtained, revealing a 37.6° clockwise rotation of the study area against stable India since 15 Ma. This new obtained vertical-axis rotation possibly developed as a response of local E-W extension and unclear strike-slip displacements of the upper-crust along the ca. NNE trending faults of the Chomolhari fault system (Yadong-Gulu graben) and the Lingshi fault, and to far-field tectonic stresses generated by the SE motion of the Tibetan plateau around the Namche Barwa syntaxis (Tapponnier et al., 2001; Royden et al., 2008). From a paleomagnetic point of view the eastern Himalaya can be regarded as one large internally deformed tectonic unit, which is characterized by the accommodation of E-W extension and SE extrusion of the Tibetan plateau, in contrast to the western part of the Himalayan arc, which is characterized by oroclinal bending around the Nanga Parbat syntaxis.

Acknowledgements

We thank K. S. Ghalley (Geological Survey of Bhutan) for the introduction into the local geology. Structural stereographic projections were produced with Allmendinger's Stereonet for Windows v.1.2. C. Jones kindly provided paleomagnetic software for calculating the Bingham statistics. Funding for this project has been provided by the Swiss National Science Foundation (SNF), grant 21-65085.01 and the NSERC.

References

- Acton, G.D., 1999. Apparent polar wander of India since the Cretaceous with implications for regional tectonics and true polar wander, in Radhakrishna, T., and Piper, J.D.A. (Eds.), *The Indian subcontinent and Gondwana; a paleomagnetic and rock magnetic perspective: Memoir-Geological Society of India*, vol, 44, pp. 129-175.
- Antolín, B., Appel, E., Montomoli, C., Dunkl, I., Ding, L., Gloaguen R., El Bay, R. In press. Kinematic evolution of the eastern Tethyan Himalaya: Constraints from magnetic fabric and structural properties of the Triassic flysch in SE Tibet. In: Poblet, J. and Lisle, R. (Eds.), *Kinematic Evolution and Structural Styles of Fold-and-Thrust Belts*. Geological Society, London, Special Publications.
- Antolín, B., Appel, E., Gloaguen, R., Dunkl, I., Ding, L., Montomoli, C., Liebke, U., Xu, Q. (submitted to Tectonophysics). Paleomagnetic evidence for clockwise rotation and tilting in the eastern Tethyan Himalaya (SE Tibet): Implications for the Miocene tectonic evolution of the NE Himalaya.
- Appel, E., Patzelt, A., Chouker, C., 1995. Secondary paleoremanence of Tethyan sediments from the Zaskar Range (NW Himalaya). *Geophys. J. Int.* 122, 227-242.
- Armijo, R., Tapponnier, P., Mercier, J.L., Tonglin, H., 1986. Quaternary extension in southern Tibet: field observations and tectonic implications. *J. Geophys. Res.* 91 (nB14), 13803-13872.
- Armijo, R., Tapponnier, P., Tonglin, H., 1989. Late Cenozoic Right-Lateral Strike-Slip Faulting in Southern Tibet. *J. Geophys. Res.* 94, 2787-2838.

- Beaumont, C., Jamieson, R.A., Nguyen, M.H., Lee, B., 2001. Himalayan tectonics explained by extrusion of a low-viscosity crustal channel coupled to focused surface denudation. *Nature*, 414, 738–742.
- Besse, J., Courtillot, V., 2002. Apparent and true polar wander and the geometry of the geomagnetic field over the last 200 Myr. *J. Geophys. Res.* 107 (B11), 2300.
- Bingham, C., 1974. An antipodally symmetric distribution on the sphere. *Annals of Statistics* 2, 1201–1225.
- Blisniuk, P.M., Hacker, B.R., Glodny, J., Ratschbacher, L., Bi, S., Wu, Z., McWilliams, M.O., Calvert, A., 2001. Extension in central Tibet since at least 13.5 Myr. *Nature* 412, 628–632.
- Burchfiel, B.C., Chen, Z., Hodges, K.V., Liu, Y., Royden, L.H., Deng, C., and Xu, J., 1992, The South Tibetan detachment system, Himalaya orogen: Extension contemporaneous with and parallel to shortening in a collisional mountain belt. *Geological Society of America Special Paper* 269, 41 p.
- Carosi, R., Montomoli, C., Rubatto, D., Visonà, D., 2006. Normal-sense shear zones in the core of the Higher Himalayan Crystallines (Bhutan Himalaya): evidence for extrusion?. In: Law, R.D., Searle, M.P., Godin, L. (Eds.), *Channel Flow, Ductile Extrusion and Exhumation in Continental Collision Zones*. *Geol. Soc. London, Spec. Pub.* 268, 425–444.
- Carpenter, R.H., 1974. Pyrrhotite Isograd in Southeastern Tennessee and Southwestern North Carolina. *GSA Bulletin*. 85-3, 451–456.
- Cassignol, C., Gillot, P.-Y., 1982. Range and effectiveness of unspiked potassium-argon dating: Experimental groundwork and applications, ed. Odin, G. S., John Wiley, New York.
- Castelli, D., Lombardo, B., 1988. The Gophu La and Western Lunana granites: Miocene muscovite leucogranites of the Bhutan Himalaya. *Lithos.* 21(3), S. 211–225.
- Chenet, A.L., Quidelleur, X., Fluteau, F., Courtillot, V. and Bajpai, S., 2007. 40K–40Ar dating of the Main Deccan large igneous province: Further evidence of KTB age and short duration. *EPSL*. 263, 1–15.
- Cogan, M.J., Nelson, K.D., Kidd, W.S.F., Wu, C., and Team, P.I., 1998. Shallow structure of the Yadong-Gulu rift, southern Tibet, from refraction analysis of Project INDEPTH common midpoint data. *Tectonics*. 17, 46–61.
- Coulié, E., Quidelleur, X., Gillot, P.-Y., Courtillot, V., Levèvre, J.-C. & Chiesa, S., 2003. Comparative K-Ar and Ar/Ar dating of Ethiopian and Yemenite Oligocene volcanism: Implications for timing and duration of the Ethiopian Traps. *EPSL*. 206, 477–492.
- Crerar, D.A., Susak, N.J., Borcsik, M. and Schwartz, S., 1978. Solubility of the buffer assemblage pyrite+pyrrhotite+magnetite in NaCl solutions from 200 to 350 degrees C. *Geochimica et Cosmochimica Acta*. 42, 1427–1438.
- Drukpa, D., Velasco, A. A., Doser, D. I., 2006 Seismicity in the Kingdom of Bhutan (1937–2003): Evidence for crustal transcurrent deformation, *J. Geophys. Res.* 111, B06301.
- Edwards, M.A., Harrison, T.M., 1997. When did the roof collapse? Late Miocene north-south extension in the High Himalaya revealed by Th–Pb monazite dating of the Khula Kangri granite. *Geology*. 25, 543–546.
- Ekstrom, G. A., 1987. A broad band method of earthquake analysis. Ph.D. thesis, Harvard Univ., Cambridge, Mass., 226 pp.
- Eldredge, S., Bachtadse, V., Van der Voo, R., 1985. Paleomagnetism and the orocline hypothesis. *Tectonophysics*. 119, 153–179.
- Ferrara, G., Lombardo, B., Tonarini, S., Turi, B., 1991. Sr, Nd and O isotopic characterisation of the Gophu La and Gumburanjun leucogranites (High Himalaya). *Schweiz. mineral. petrogr. Mitt.* 71, S. 35–51.
- Fiet, N., Quidelleur, X., Parize, O., Bulot, L. G. & Gillot, P.-Y., 2006. Lower Cretaceous stage durations combining radiometric data and orbital chronology: Towards a more stable relative time scale? *EPSL*. 246, 407–417.
- Fisher, R.A., 1953. Dispersion on a sphere. *Proc. R. Soc. London*. 217, 295–305.
- Gan, W., Zhang, P., Shen, Z.-K., Niu, Z., Wang, M., Wan, Y., Zhou, D., Cheng, J., 2007. Present-day crustal motion within the Tibetan Plateau inferred from GPS measurements. *J. Geophys. Res.* 112, B08416.
- Gansser, A., *The geology of the Himalayas*. Wiley, New York, 1964. 289 pp.
- Gansser, A., *Geology of the Bhutan Himalaya*. Schweizerische Naturforschende Gesellschaft, Zürich, 1983. 181 pp.

- Gillot, P.-Y. & Cornette, Y., 1986. The Cassinot technique for potassium-argon dating, precision and accuracy: examples from late Pleistocene to recent volcanics from southern Italy. *Chem. Geol.*, 59, 205-222.
- Gillot, P. Y., Cornette, Y., Max, N. & Floris, B., 1992. Two reference materials, trachytes MDO-G and ISH-G, for argon dating (K-Ar and $^{40}\text{Ar}/^{39}\text{Ar}$) of Pleistocene and Holocene rocks. *Geostandards Newsletter*, 16, 55-60.
- Godin, L., Grujic, D., Law, R.D., Searle, M.P. 2006. Channel flow, extrusion and exhumation in continental collision zones: an introduction. In: Law, R.D., Searle, M.P., Godin, L. (Eds.), *Channel Flow, Ductile Extrusion and Exhumation in Continental Collision Zones*. Geol. Soc. London, Spec. Pub. 268, 1-23.
- Grujic, D., Casey, M., Davidson, C., Hollister, L.S., Kundig, R., Pavlis, T., Schmid, S., 1996. Ductile extrusion of the Higher Himalayan Crystalline in Bhutan: evidence from quartz microfabrics. *Tectonophysics*. 260, 21-43.
- Grujic, D., Hollister, L.S., Parrish, R.R., 2002. Himalayan metamorphic sequence as an orogenic channel: insight from Bhutan. *EPSL*. 198, 177-191.
- Hames, W.E., and Bowering, S.A., 1994. An empirical evaluation of the argon diffusion geometry in muscovite. *EPSL*. 124, 161-169.
- Hauck, M.L., Nelson, K.D., Brown, L.D., Zhao, W.J., Ross, A.R., 1998. Crustal structure of the Himalayan orogen at similar to 90 degrees east longitude from Project INDEPTH deep reflection profiles. *Tectonics*. 17, 481- 500.
- Hochstein, M.P., Regenauer-Lieb, K. 1998. Heat generation associated with collision of two plates: the Himalayan geothermal belt. *J. Volc. Geoth. Res.* 83. (75-92).
- Hodges, K.V., 2000. Tectonics of the Himalaya and southern Tibet from two perspectives. *Geol. Soc. Amer. Bull.* 112, 324-350.
- Jessup, M.J., Newell, D.L., Cottle, J.M., Berger, A.L., Spotila, J.A., 2008. Orogen-parallel extension and exhumation enhanced by focused denudation in the Arun River gorge, Ama Drime Massif, Tibet-Nepal. *Geology*. 36, 587-590.
- Jones, C. H., 2002. User-driven Integrated Software Lives: "PaleoMag" Paleomagnetism Analysis on the Macintosh. *Computers and Geosciences*. 28 (10), 1145-1151.
- Kellett, D.A., Grujic, D., Erdmann, S., 2009. Miocene structural reorganization of the South Tibetan detachment, eastern Himalaya: Implications for continental collision. *Lithosphere*. 1, 5, 259-281.
- Klootwijk, C.T., Conaghan, P.J., Powell, C.McA. 1985. The Himalayan Arc: Large scale continental subduction, oroclinal bending and back-arc spreading. *EPSL*. 75, 167-183.
- Lambert, I.B., 1973. Post-depositional availability of sulphur and metals and formation of secondary textures and structures in stratiform sedimentary sulfide deposits. *J. Geol. Soc. Aus.* 20, 205-215.
- Lister, G.S., Baldwin, S.L., 1996. Modelling the effect of arbitrary P-T-t histories on argon diffusion in minerals using the MacArgon program for the Apple Macintosh. *Tectonophysics*. 253, 83-109.
- Lowrie, W., 1990. Identification of ferromagnetic minerals in a rock by coercivity and unblocking temperature properties, *Geophys. Res. Lett.* 17(2), 159 - 162.
- McFadden, P. L. 1990. A new fold test for palaeomagnetic studies. *Geophys. J. Int.* 103, 163-169.
- Mahéo, G., Leloup, P.H., Valli, F., Lacassin, R., Arnaud, N., Paquette, J.-L., Fernandez, A., Haibing, L., Farley, K.A., Tapponnier, P., 2007. Post 4 Ma initiation of normal faulting in southern Tibet. Constraints from the Kung Co half graben. *EPSL*. 256, 233-243.
- McQuarrie, N., Robinson, D., Long, S., Tobgay, T., Grujic, D., Gehrels, G., Ducea M., 2008. Preliminary stratigraphic and structural architecture of Bhutan: Implications for the along strike architecture of the Himalayan system. *EPSL*, 272, 105-117.
- Maluski, H., Matte, P. & Brunel, M., 1988. Argon 39 - Argon 40 dating of metamorphic and plutonic events in the north and high Himalaya belts (southern Tibet - China). *Tectonics*. 7(2), S. 299-326.
- Odin, G. S. et al., 1982. in *Numerical dating in stratigraphy*, 123-150, ed. Odin, G. S. John Wiley and Sons, Chichester.
- Pan, G., Ding, J., Yao, D., Wang, L., 2004. Geological map of Qinghai-Xizang (Tibet) Plateau and Adjacent Areas (1:1,500,000). Chengdu Institute of Geology and Mineral Resources, China Geological Survey. Chengdu Cartographic Publishing House.
- Quidelleur, X., Gillot, P.-Y., Carlot, J. & Courtillot, V., 1999. Link between excursions and paleointensity inferred from abnormal field directions recorded at La Palma around 600 ka. *EPSL*. 168, 233-242.

- Quidelleur, X., Gillot, P. Y., Soler, V. & Lefèvre, J. C., 2001. K/Ar dating extended into the last millennium: Application to the youngest effusive episode of the Teide volcano (Spain), *Geophys. Res. Lett.* 28, 3067-3070.
- Ratschbacher, L., Frisch, W., Liu, G., Chen, C., 1994. Distributed deformation in southern and western Tibet during and after the India-Asia collision. *J. Geophys. Res.- Solid Earth* 99, 19917-19945.
- Renne, P. R., Swisher, C. C., Deino, A. L., Karner, D. B., Owens, T. L. & DePaolo, D. J., 1998. Intercalibration of standards, absolute ages and uncertainties in $^{40}\text{Ar}/^{39}\text{Ar}$ dating. *Chem. Geol.*, 145, 117-152.
- Royden, L.H., Burchfiel, B.C., Van der Hilst, R.D., 2008. The Geological Evolution of the Tibetan Plateau. *Science*. 321, 1054-1058.
- Schill, E., Appel, E., Zeh, O., Singh, V.K., Gautam, P., 2001. Coupling of late-orogenic tectonics and secondary pyrrhotite remanences: Towards a separation of different rotation processes and quantification of rotational underthrusting in the western Himalayas (N-India). *Tectonophysics*. 337, 1-21.
- Schill, E., Crouzet, C., Gautam, P., Singh, V.K., Appel E., 2002a. Where did rotational shortening occur in the Himalayas? - Inferences from palaeomagnetic analyses of remagnetisations. *EPSL*. 203(1), 45-57.
- Schill E., Appel E., Gautam P., Dietrich P., 2002b. Thermo-tectonic history of the Tethyan Himalayas deduced from palaeomagnetic record of metacarbonates from Shiar Khola (central Nepal). *J. Asian Earth Sci.* 20, 203-210.
- Schill, E., Appel, E., Godin, L., Crouzet, C., Gautam, P., Regmi, K., 2003. Record of deformation by secondary magnetic remanences and magnetic anisotropy in the Nar/Phu valley (central Himalaya). *Tectonophysics*. 377, 197-209.
- Schill, E. and Holt, W.E., 2004. 20 Ma of lateral mass transfer around the western Himalayan syntaxis. Extended abstracts: 19th Himalaya-Karakoram-Tibet Workshop, Niseko, Japan. 19th Himalaya-Karakoram-Tibet workshop extended abstracts. *Himalayan J. Sci.* 2, 4, 244-245.
- Schill, E., Appel, E., Crouzet, C., Gautam, P., Wehland, F., Staiger, M., 2004. Oroclinal bending versus regional significant clockwise rotations in the Himalayan arc-Constrains from secondary pyrrhotite remanences. In: Sussman, A.J. and Weil, A.B. (Eds.), *Orogenic Curvature: Integrating Paleomagnetic and Structural Analyses*. *Spec. Pap. Geol. Soc. Am.* 383, 73-85.
- Searle, M.P., Simpson, R.L., Law, R.D., Parrish, R.R., Waters, D.J., 2003. The structural geometry, metamorphic and magmatic evolution of the Everest massif, High Himalaya of Nepal-South Tibet. *J. Geol. Soc. London*. 160, 345- 366.
- Searle, M.P., Godin, L., 2003. The South Tibetan Detachment and the Manaslu Leucogranite: A Structural Reinterpretation and Restoration of the Annapurna-Manaslu Himalaya, Nepal. *The Journal of Geology*. 111, 505-523
- Steiger, R. H. & Jäger, E., 1977. Subcommittee on Geochronology: convention on the use of decay constants in Geo and Cosmochronology. *EPSL*. 36, 359-362.
- Stüwe, K., and Foster, D., 2001. $^{40}\text{Ar}/^{39}\text{Ar}$, pressure, temperature and fission track constraints on the age and nature of metamorphism around the Main Central thrust in the eastern Bhutan Himalaya: *J. Asian Earth Sci.* 19, 85-95.
- Tapponnier, P., Peltzer, G., Le Dain, A.Y., Armijo, R and Cobbold, P., 1982. Propagating extrusion tectonics in Asia: New insights from simple experiments with plasticine. *Geology*. 10, 611-616.
- Taylor, M., Yin, A., Ryerson, J.F., Kapp, P., Ding, L., 2003. Conjugate strike-slip faulting along the Bangong-Nujiang suture zone accommodates coeval east-west extension and north-south shortening in the interior of the Tibetan Plateau. *Tectonics*. 22(4), 1044.
- Thiede, R.C., Arrowsmith, J.R., Bookhagen, B., McWilliams, M.O., Sobel, E.R., Strecker, M.R., 2005. From tectonically to erosionally controlled development of the Himalayan orogen. *Geology*. 33, 689-692.
- Van der Woerd, J., Leloup, Ph.-H., Liu-Zeng, J., Lacassin, R., Tapponnier, P., 2009. A comment on "Orogen-parallel, active left-slip faults in the eastern Himalaya: Implications for the growth mechanism of the Himalayan arc" by Li and Yin *EPSL*, 278 (2008) 258-267. *EPSL*. 285, 217-222.
- Waldhör, M., 1999. The small circle reconstruction in palaeomagnetism and its application to palaeomagnetic data from the Pamirs. PhD thesis. Tübingen University. p. 99
- Waldhör, M., Appel, E., Frisch, W., Patzelt, A., 2001. Paleomagnetic investigation in the Pamirs and its tectonic implications. *J. Asian Earth Sci.* 19, 429-451.

- Waldhör, M., Appel, E., 2006. Intersections of remanence small circles: new tools to improve data processing and interpretation in palaeomagnetism. *Geophys. J. Int.* 166, 33-45.
- Willems, H., Zhou, Z., Zhang, B., Gräfe, K. U., 1996. Stratigraphy of the Upper Cretaceous and Lower Tertiary strata in the Tethyan Himalayas of Tibet (Tingri area, China). *Geol. Rundsch.* 85, 723-754.
- Wu, C., Nelson, K. D., Wortman, G., Samson, S.D., Yue, Y., Li, J., Kidd, W. S. F., Edwards, M.A., 1998. Yadong cross structure and South Tibetan Detachment in the east central Himalaya (89°-90°E). *Tectonics*, 17-1, 28-45.
- Yin, A. 2006. Cenozoic evolution of the Himalayan Orogen as constrained by along strike variations of structural geometry, exhumation history, and foreland sedimentation. 2006. *Earth-Science Rev.* 76, 1-131.
- Yin, A., Dubey, C. S., Kelty, T. K., Gehrels, G. E., Chou, C. Y., Grove, M. & Lovera, O. 2006. Structural evolution of the Arunachal Himalaya and implications for asymmetric development of the Himalayan orogen. *Current Science.* 90, 195-206.
- Zeitler, P.K., Koons, P.O., Bishop, M.P., Chamberlain, C.P., Craw, D., Edwards, M.A., Hamidullah, S., Jan, M.Q., Khan, M.A., Khattak, M.U.K., Kidd, W.S.F., Mackie, R.L., Meltzer, A.S., Park, S.K., Pecher, A., Poage, M.A., Sarker, G., Schneider, D.A., Seeber, L., and Shroder, J.F., 2001. Crustal reworking at Nanga Parbat, Pakistan: Metamorphic consequences of thermal-mechanical coupling facilitated by erosion. *Tectonics.* 20, 712-728.
- Zhang, P.Z., Shen, Z., Wang, M., Gan, W., Bürgmann, R., Molnar, P., Wang, Q., Niu, Z., Sun, J., Wu, J., Hanrong, S., Xinzhaio, Y., 2004. Continuous deformation of the Tibetan Plateau from global positioning system data. *Geology.* 32, 809-812.

World Wide Web references

Digital topography, SRTM data, is from the Consortium for Spatial Information (CGIAR/CSI):
<http://srtm.csi.cgiar.org>

6

Conclusions and open research questions

The results of the studies presented in this thesis provide detailed insights into the tectonometamorphic evolution of the eastern Tethyan Himalayan sequence. Furthermore, first paleomagnetic block rotation pattern of SE-Tibet is described and interpreted. The three main questions posed in the first chapter of this work:

- 1) What is the kinematic and metamorphic evolution of the eastern Tethyan Himalayan flysch?
- 2) How is the vertical-axis block rotation pattern in the eastern Tethyan Himalaya?
- 3) Which mechanism has produced the block rotation pattern?

have been answered through the chapters and are summarized, and inter-linked below.

6.1 Kinematic and metamorphic evolution of the Tethyan Triassic flysch in SE Tibet

A 4-phase deformation and metamorphic history is described after quantifying the magnetic fabric related to the sheet silicate preferred orientation, degree of metamorphism and age of cooling (K/Ar dating). The last orogenic phase (D4) is constrained from the paleomagnetic study in SE-Tibet and NW Bhutan.

D1 (Early Eocene - Late Eocene?)

During the Eohimalayan or D1 phase (Hodges, 2000; Godin, 2003; Carosi et al., 2007) the collision of India and Asia produced the development of E-W trending south facing isoclinal folds with related axial planar foliation (S1). South of the locality of Qonggyai where D1 phase controls the orientation of the structures, the magnetic lineation is interpreted as the direction of stretching lineation of the phyllosilicates, under the prevailing stress field, during thrust sheet emplacement. The N-S trend and northward plunge of the magnetic lineation is in agreement with the north-dipping Lhunze fault and likely thrust emplacement towards the Himalayan foreland (Aikman et al., 2008). Same studied sites indicate diagenetic to low-anchizonal metamorphism and K/Ar ages older than the Neohimalayan phase (Hodges, 2000). The D1 deformation phase described here is responsible for crustal thickening of the THS and Himalayan Belt during most probably Eocene times.

D2 (Late Eocene/Early Oligocene - ca. 22 Ma)

Continuous N-S shortening in the flysch thrust-wedge derived in a change of the fold vergence and magnetic (tectonic) foliation dipping. This has been observed in the studied profiles from the Indus Yarlung Suture until ca. 20 km south of it. However from an E-W strike point of view this was observed east of Zetang and from Gyaca to ~30 km east of Gyaca. North-vergent deformation starts with the incipient development of the north-vergent F2 folds and related S2 crenulation cleavage. The incipient development of a new planar feature (S2 foliation) is recorded in the magnetic fabric by a subtle prolate ellipsoid with K_{\min}

axes distributed on a semicircle. This composite fabric is detected in between the D1 and D2 domains and witnesses the combination of the S1 and the younger S2 foliation. K_{max} axes strike E-W with gentle plunge, parallel to the intersection lineation between S1 and S2, and perpendicular to the shortening direction. As the foliation S2 becomes pervasive it transposes the older S1 and K_{min} cluster parallel to the pole of the S2 tectonic foliation in the northern areas. The S2 foliation has E-W to WNW-ESE direction and dips to the south, opposite to the main vergence of the Himalayan Belt. Interestingly, east of the Cona Graben the D1 and D2 tectonic domains defined by opposite sense of vergence are likely separated by a fault (Qusum Thrust) noted by Pan et al. (2004). The southern domain is structurally dominated by north-dipping S1 tectonic foliation and the northern domain by south-dipping S2 foliation. Kübler Index and vitrinite reflectance data indicate a wide range of thermal overprint from high anchizone to epizone during the D2 phase. Looking at the K/Ar geochronology it is generalized that the northern (S2) domains from Zetang to Gyaca present Early Miocene K/Ar ages younger than the southern domain controlled by supposed Eohimalayan F1 folds and S1 foliation. The northern analyzed samples, which shown higher metamorphic degree (lower KI values), present ca. 24-22 Ma K/Ar ages similar in the two analyzed fractions $<2 \mu\text{m}$ and $<0.2 \mu\text{m}$, suggesting equilibrium conditions dominated by newly formed illite. In this sense 24-22 Ma is related to the cessation of authigenic illite growth during S2 foliation development.

D3 (ca. 22 - ca. 13 Ma)

Continuation of backward deformation towards higher structural levels was probably responsible for the formation of the north-directed Great Counter backthrust at around 18 Ma to 10 Ma (Quidelleur et al. 1997; Harrison et al. 2000) which placed the Triassic flysch over the mélangé complex and the Cretaceous rocks. This event is recorded in the N-S trending and steep southward plunge of the magnetic lineation parallel with the stretching lineation east of Gyaca and close to the GCT.

In the central part of the study area, the Yala Xiangbo north Himalayan dome was emplaced at ca. 18 Ma, and cooled below the muscovite closure window at ca. 13.5 Ma (Aikman et al. 2004, this study). In the surroundings of the dome the base of the THS experienced greenschist-facies overprint.

6.2 D4 phase (after Middle-Late Miocene) and paleomagnetic block rotation pattern in SE-Tibet and NW-Bhutan

E-W extension is witnessed by N-S trending kilometric normal faults, Yadong-Gulu and Cona Grabens, outcropping in the THS and southern Tibet (Armijo et al., 1986), which were

active since 14 Ma or 4 Ma ago (Blisniuk et al. 2001; Mahéo et al., 2007). In central Tibet E-W extension is coupled with strike-slip faults, which finally have been associated with the eastward extrusion of the Tibetan Plateau (Armijo et al., 1989; Taylor et al., 2003).

Neotectonic analyses demonstrate the existence of small scale and kilometric ca. N-S striking normal faults related to the Cona Graben which cross-cut all the previous structures and affect the Yarlung Tsangpo river equilibrium as noted by a knick-point at the Cona Graben area. The channel network pattern is controlled by the Cona Graben in its surroundings.

Our paleomagnetic study in the Cretaceous dykes intruding the Triassic flysch of SE-Tibet indicates the presence of a stable secondary pyrrhotite magnetization. This has been ca. 20° clockwise rotated in the Qonggyai valley, west of the Cona Graben after remanence acquisition at ca. 22 Ma and in comparison with stable India. A lack of rotation has been quantified in Nagarze area, where the last peak metamorphism might be older than in Qonggyai, but without consequences for the estimated vertical-axis rotation. To the south ca. 37° clockwise rotation occurred in the Lingshi klippe (NW-Bhutan) close to the eastern side of the south termination of the Yadong-Gulu Graben after ca. 13 Ma. However, more areas should be analyzed to rely on this interpretation. Our data suggest that local E-W extension combined with strike-slip along reactivated Tertiary structures or unconformities in an eastward regional motion of the upper crust (like show the GPS and rigid rotation velocity field; Gan et al., 2007) around the eastern syntaxis could have been accommodated by the obtained clockwise rotation pattern.

Additionally, the observed pattern of tilting around horizontal axis in the Qonggyai valley may reflect concealed North Himalayan doming.

6.3 Open research questions

The development of this study has generated new data, ideas and questions to be explored which are summarized herein:

- 1) It might be interesting to determine the anisotropy of the ferrimagnetic pyrrhotite sub-fabric in the slates of the Triassic flysch by measurements of the anisotropy of anhysteretic remanence magnetization (AARM) to decipher if the phyllosilicates sub-fabric orientation is enhanced by the ferrimagnetic sub-fabric.
- 2) An intra-site comparison between illite crystallinity (Kübler Index), the degree of anisotropy and the shape parameter of the AMS, could improve the understanding of the relationship between fabric acquisition and metamorphic evolution. The AMS study in SE-Tibet indicates well established stages during the evolution of the magnetic fabric and a wide number of illite crystallinity measurements were performed on.

3) The presented paleomagnetic study in this thesis answers some questions about the Miocene tectonics and metamorphism in SE-Tibet and NW-Bhutan. It can be extended to other areas like south of the Lhunze fault, at both sides of the Cona Graben (close to Comai and south of Lhunze localities). Here marine limestones outcrop (Pan et al., 2004) and might contain pyrrhotite as it has intensively been demonstrated in western and central Nepal limestones. This would give a constraint about the vertical-axis rotation of the two sides of the southern segment of the Cona Graben. Furthermore, east of Lhunze the STDS shift from E-W direction to NE-SW (eastern flank of the Namche Barwa syntaxis; from Pan et al., 2004 geological map). This change in the plane of slip along the STDS might be a potential area to record vertical-axis block rotations.

5) The paleomagnetic study in the diorite dykes demonstrate the presence of stable remanence directions carried by pyrrhotite. A possible origin of the sulphur for the pyrrhotite growth is to come by migration from the organic matter of the Triassic slates. However this mechanism needs to be analyzed in detail through study of the variation in the pyrrhotite content and quality of the Zijderveld diagrams from the slates to the margin and inner core of the dyke. This can be done parallel to analyses in the sulphur content of the analyzed rocks.

6) Further geological mapping and structural studies combined with thermo-geochronology analyses around the Lhunze fault and Cona Graben faults would be useful to determine the timing of these faults and their structural importance.

7) A N-S cross section of the eastern Tethyan Himalaya and its restoration could be used to estimate the shortening magnitude, and to compare it with other Himalayan sections.

References

- Aikman, A., Harrison, T.M., Lin, D., 2004. Preliminary results from the Yala-Xiangbo Leucogranite dome, SE Tibet. 19th Himalaya-Karakoram-Tibet workshop extended abstracts. *Himalayan J. Sci.* 2, 91.
- Aikman, A., Harrison, T.M., Ding, L., 2008. Evidence for Early (>44 Ma) Himalayan Crustal Thickening, Tethyan Himalaya, southeastern Tibet. *EPSL.* 274, 14-23.
- Armijo, R., Tapponnier, P., Mercier, J.L., Tonglin, H., 1986. Quaternary extension in southern Tibet: field observations and tectonic implications. *J. Geophys. Res.* 91 (nB14), 13803-13872.
- Armijo, R., Tapponnier, P., Tonglin, H., 1989. Late Cenozoic Right-Lateral Strike-Slip Faulting in Southern Tibet. *J. Geophys. Res.* 94, 2787-2838.
- Blisniuk, P.M., Hacker, B.R., Glodny, J., Ratschbacher, L., Bi, S., Wu, Z., McWilliams, M.O., Calvert, A., 2001. Extension in central Tibet since at least 13.5 Myr. *Nature.* 412, 628-632.
- Carosi, R., Montomoli, C., Visonà, D., 2007. A structural transect in the Lower Dolpo: Insights on the tectonic evolution of Western Nepal. *J. Asian Earth Sci.*, 29, 407-423.
- Gan, W., Zhang, P., Shen, Z-K., Niu, Z., Wang, M., Wan, Y., Zhou, D., Cheng, J., 2007. Present-day crustal motion within the Tibetan Plateau inferred from GPS measurements. *J. Geophys. Res.* 112, B08416.
- Godin, L., 2003. Structural evolution of the Tethyan sedimentary sequence in the Annapurna area, central Nepal Himalaya. *J. Asian Earth Sci.* 22, 307-328.

- Harrison, T.M., Yin, A., Grove, M., Lovera, O.M., 2000. The Zedong Window: A record of superposed Tertiary convergence in southeastern Tibet. *J. Geophys. Res.* 105, 19,211-19,320.
- Hodges, K.V., 2000. Tectonics of the Himalaya and southern Tibet from two perspectives. *Geol. Soc. Amer. Bull.* 112, 324-350.
- Mahéo, G., Leloup, P.H., Valli, F., Lacassin, R., Arnaud, N., Paquette, J.-L., Fernandez, A., Haibing, L., Farley, K.A., Tapponnier, P., 2007. Post 4 Ma initiation of normal faulting in southern Tibet. Constraints from the Kung Co half graben. *EPSL.* 256, 233-243.
- Pan, G., Ding, J., Yao, D., Wang, L., 2004. Geological map of Qinghai-Xizang (Tibet) Plateau and Adjacent Areas (1:1,500,000). Chengdu Institute of Geology and Mineral Resources, China Geological Survey. Chengdu Cartographic Publishing House.
- Quidelleur, X., Grove, M., Lovera, O.M., Harrison, T.M., Yin, A., 1997. Thermal evolution and slip history of the Renbu-Zedong Thrust, southeastern Tibet. *J. Geophys. Res.* 102, 2659-2679.
- Taylor, M., Yin, A., Ryerson, J.F., Kapp, P., Ding, L., 2003. Conjugate strike-slip faulting along the Bangong-Nujiang suture zone accommodates coeval east-west extension and north-south shortening in the interior of the Tibetan Plateau. *Tectonics.* 22(4), 1044.